ATOMIC AND MOLECULAR ADSORPTIONS OF HYDROGEN AND OXYGEN ON SILICON NANOTUBES: AN *AB INITIO* STUDY

by

HAOLIANG CHEN

Presented to the Faculty of the Graduate School of

The University of Texas at Arlington in Partial Fulfillment

of the Requirements

for the Degree of

DOCTOR OF PHILOSOPHY

THE UNIVERSITY OF TEXAS AT ARLINGTON

May 2013

ACKNOWLEDGEMENTS

I would like to express my gratitude to my advisor, Dr. Asok K. Ray for his guidance through the course of my study and research. I also would like to extend my thanks to my committee members, Dr. Nail Fazleev, Dr. Samarendra Mohanty, Dr. Zdzislaw Musielak, and Dr. Qiming Zhang, for their interest in my research work.

I would also like to thank members of our research groups, Kapil Adhikari, Sarah Hernandez, Megan Lee, Dayla Morrison, Shafaq Moten, Sarah Duesman, Prabath Wanaguru, Raymond Atta-Fynn, Jianguang Wang and Ma Li for being very helpful throughout my research work. Their valuable suggestions during our regular research meetings have enriched my research experience. I am very grateful to Dr. Kapil Adhikari for being helpful in the very beginning of my research work.

I am very grateful to my parents for providing me an encouraging environment during my undergraduate and graduate studies. Special thanks go to my girlfriend Yao Lin for her continuous support and care.

Finally I would like to acknowledge the support from the Welch Foundation, Houston, Texas.

April 15th, 2013

ABSTRACT

ATOMIC AND MOLECULAR ADSORPTIONS OF HYDROGEN

AND OXYGEN ON SILICON NANOTUBES:

AN *AB INITIO* STUDY

Haoliang Chen, PhD

The University of Texas at Arlington, 2013

Supervising Professor: Asok K. Ray

A systematic *ab initio* study of silicon nanotubes (SiNTs) in single-walled, double-walled armchair and zigzag configurations will be presented. Electronic and structural properties of all these nanostructures have been calculated using hybrid density functional B3LYP and 3-21G* basis set as implemented in the *GAUSSIAN 03/09* suite of software. The binding energy increases as diameter of the nanotube increases generally for both armchair and zigzag SiNTs. The HOMO-LUMO gaps of the armchair and zigzag SiNTs are in the range from 0.20 to 1.81 eV and do not show any metallic behavior. Radial buckling calculations indicate that the armchair SiNTs all have smooth tubular structure presenting the character of sp^2 hybridization, and the zigzag SiNTs have a "puckered" structure presenting the character of sp^3 hybridization. Double-walled armchair SiNTs with small interlayer separations, called meshed tubes, do not hold the coaxial cylindrical structure after optimization. The SiNTs (n, n)@(n+3, n+3) are found to have large formation energies and binding energies per atom. All Si nanotubes are found to be semiconductors. However, the band gap, in general, is observed to decrease from single-walled nanotubes to double-walled nanotubes.

Atomic, molecular and co-adsorption of hydrogen and oxygen in nanotubes have also been studied by optimizing the distances of the adatoms or admolecules from both inside and outside the tube. The adatom or admolecule is initially placed in four adsorption sites-normal (or parallel for zigzag SiNTs) bridge, zigzag bridge, hollow and on-top sites. For single H atom adsorption, the on-top site is the most preferred site, either from the outside or the inside of the nanotubes. The O atom prefers bridge sites breaking the Si-Si covalent bond. The admolecule is originally placed perpendicular and parallel to the tube axis. Hydrogen molecule does not dissociate while oxygen molecule dissociates after optimization. The on-top site is the only preferred site for hydrogen molecule. For oxygen, the most preferred sites are the two bridge sites. Complete dissociation, partial dissociation and non-dissociation were observed for adsorption of two oxygen molecules. Peroxide structure has also been observed in adsorption of two oxygen molecules with smaller adsorption energies than complete dissociation. For the co-adsorption of one hydrogen molecule and one oxygen molecule, the oxygen molecule dissociated into two oxygen atoms and moved to bridge sites. The hydrogen molecule does not dissociate. The suppression effect on the HOMO-LUMO gap has been observed for co-adsorption of hydrogen and oxygen molecules on zigzag SiNTs.

TABLE OF CONTENTS

LIST OF ILLUSTRATIONS

LIST OF TABLES

CHAPTER 1

INTRODUCTION

1.1 Overview of Silicon Nanotubes

The discovery of carbon nanotube (CNT) by Iijima [1] has evolved into new areas of research, namely nanoscience and nanotechnology. The first CNTs discovered were made of several concentric cylindrical-like shells regularly spaced by an amount of about 3.4 Å. Shortly after the discovery of multi-walled carbon nanotubes (MWCNTs), single-walled carbon nanotubes (SWCNTs) were synthesized in abundance using arc-discharge methods with transition-metal catalysts [2,3]. Carbon nanotubes have unique characteristics in that they can behave either as metals or semiconductors, depending on their diameter and chirality. They are also mechanically very stable and strong, and their carrier mobility is equivalent to that of good metals, suggesting that they would make ideal interconnects in nanosized devices. Carbon nanotubes have attracted significant academic and industrial interest due to their outstanding and unique mechanical, electronic and optical properties. The extraordinary success in fabricating CNTs and in their applications has motivated remarkable experimental and theoretical research on nanotubes of other elements [4-11]. An obvious extension of carbon nanotubes is in the area of silicon nanotubes (SiNTs), specifically since carbon and silicon belong to the same column of the periodic table, with identical valence electronic structure.

Silicon has been widely recognized as the most important material of the 20th century. This is largely due to its role as the fundamental component in integrated circuits and consequently in the microelectronic revolution. Silicon nanomaterials are particularly important in nanotechnology because Si-based nanoelectronics are compatible with Si-based microelectronics. It is widely believed that silicon nanotubes (SiNTs) and nanoforms will be the next most compatible and miscible materials with the current micro and nanoelectronics

devices [12-17]. Thus progressively increasing research is currently being pursued in the area of single- and multi-walled SiNTs and interactions of atomic and molecular systems with these tubes.

The properties of silicon and carbon are a direct consequence of the arrangement of electrons around the nucleus of the atom. One distinguishing feature of carbon is that it can participate in either sp^2 or sp^3 bond configurations and can form a variety of phases, such as diamond, graphite, fullerenes and nanotubes [18]. The four valence electrons of carbon, involved in chemical bonding, occupy both the 2s and 2p orbitals. Covalent bonds are formed by promotion of the 2s electrons to one or more 2p orbitals. The resulting hybridized orbitals are the sum of the original orbitals. Depending on how many p orbitals are involved, this can happen in three different ways. In the first type of hybridization, the 2s orbital pairs with one of the 2p orbitals, forming two hybridized sp orbitals in a linear geometry. The second type of hybridization involves the 2s orbitals hybridizing with two 2p orbitals. As a result, three sp^2 orbitals are formed. These are on the same plane separated by an angle of 120°. In the third hybridization, one 2s orbital hybridizes with the three 2p orbitals, yielding four sp^3 orbitals separated by an angle of 109.5°; sp^3 hybridization yields the characteristic tetrahedral arrangements of the bonds. Compared to carbon, silicon tends to utilize all three of its valence p orbitals, resulting in sp^3hybridization.The bonds involving silicon are, in general, weaker because it has a larger atomic radius (which means larger orbital size and weaker π-type overlaps). There is also smaller energy difference between the valence s and the p orbitals of silicon, and hence hybridization energies are lower.

A single-walled nanotube (SWNT) is constructed by wrapping one single layer of the graphite-like sheet to form a cylindrical shape. The structure of such nanotubes can be described in terms of chirality and length. Chirality and diameter are specified in terms of the magnitude of the components of chiral vector. The chiral vector C_h which maps an atom from the left hand border onto an atom on the right border line is an integer multiple of the two basis

vectors a_1 and a_2 , i.e., $C_h=na_1+ma_2$ with integers n and m. Thus the geometry of any nanotube can be described by the integer pair (n, m) which determines the chiral vector. Depending upon how the sheet is rolled we have three types of tubes. For armchair m=n, for zigzag m=0 and for chiral nanotubes m≠n. The crystalline structure of 3D bulk silicon is cubic diamond, similar to that of carbon diamond. However, unlike the carbon counterpart, a 1D single-walled silicon nanotube has not been found in nature yet, largely because silicon prefers sp^3 bonds rather than sp^2 bond. The cubic diamond silicon is known as a semiconductor with an energy band gap of 1.17eV. At high pressures, however, the cubic-diamond structured silicon can undergo a phase transformation to highly coordinated (six-fold or above) metallic phases such as the β-tin and hexagonal closed-packed structures. Forming tubular structures of Si was initially considered to be hypothetical at best because Si prefers sp^3 hybridization. Considerable theoretical and experimental efforts have been carried out over the past and recent years to investigate the existence and fabrication of SiNTs.

The synthesis of SiNTs has been demonstrated by various groups. Sha *et al.*[19] reported the synthesis of large diameter SiNTs (≈50nm) by chemical vapor deposition (CVD), in which the hollow tubular structure consisted mostly of crystalline silicon and some amorphous silicon. These SiNT structures are grown in combination with silicon nanowires and have been characterized using selected area electron diffraction (SAED) and high-energy transmission electron microscopy (HRTEM). Jeong *et al.*[20] reported the growth of SiNTs by molecular beam epitaxy on porous alumina covered with a thick layer of silicon oxide (≈10nm). The pore size of the nanotube is about 40nm with a wall thickness of 4-5 nm, and they claimed it could be polycrystalline Si. De Crescenzi *et al.*[21] reported the synthesis of SiNTs (diameter ranges between 2-35 nm) exhibiting the characteristic of polycrystalline material by the dc-arc plasma method. Those nanotubes were found to be organized in a puckered lattice and can assume several chiralities showing metallic as well as semiconducting character. The structural properties of the fabricated SiNTs are different to those of CNTs. The thickness of shells of the

SiNTs was more than several nanometers with the shells consisting mostly of crystalline silicon and a little amorphous silicon. The tube wall consists mostly of crystalline silicon and a little amorphous silicon embedded in amorphous SiO_2 layers. This atomic arrangement bears no resemblance to the theoretical models of either SWSiNTs or multi-walled SiNTs. The synthesis of SWSiNTs still remains an open challenge. The wide gap between the hypothetical structures and the real materials makes a novel model of SiNTs beyond cylindrical configurations highly desirable, which is obviously needed for experimental progress toward understanding the atomic structures and growth mechanisms of these nanomaterials.

Even if SWSiNTs has never been observed, theoretical predictions have been performed for various kinds of Si tubes. Menon and Richter[14] proposed novel quasi-one-dimensional (QOD) structures of Si, characterized by a core of bulk like fourfold-coordinated atoms whose surfaces closely resemble the crystalline Si. On the basis of silicon's inability to adopt the sp^2 coordination, Seifert *et al*.[22] argued that the existence of SiNTs is doubtful. Alternatively, these authors proposed that Si-based silicide and SiH nanotubes are theoretically stable and energetically viable and could thus be considered as sources of silicon nanotubes, particularly in view of the existence of many layered silicides. Fagan *et al*.[23] showed that there is a significant cost in producing graphite-like sheets of silicon, but once they are formed, the extra cost to produce the tubes is lower than that in carbon. Zhang *et al*.[17] discussed that silicon tubular structures are much less stable due to the strong tendency of silicon to undergo sp^3 hybridization, thereby favoring the formation of tetrahedral diamond-like structure, rather than the tubular one. However, they suggested that, under appropriate conditions, silicon nanotubes with puckered surface structures may be formed. Kumar *et al*.[24] found that there was a mixed sp^2-sp^3 bonding character between Si atoms. The sp^2 bonding gives rise to π conjugation of neighbor silicon atoms. Zhang *et al*.[25] proposed that single-walled silicon nanotubes can adopt a number of distorted tubular structures such as “gearlike” structures. The “gearlike” structures contain alternating sp^3-like and sp^2-like silicon local configuration. Yan *et*

al.[26] studied the structural characteristics and electronic properties of single-crystalline silicon nanotubes. Si atoms in the tubes are all fourfold coordinated and their chemical bonding originates from sp^3 hybridization. The band gap increases as the tube-wall thickness decreases and is insensitive to the external diameter. Rathi and Ray[27] have studied the electronic and geometric structures of zigzag and chiral silicon nanotubes. The Si-Si bond length alternation in SiNTs is more pronounced than in CNTs, indicating a strong tendency for bond delocalization in SiNTs. The zigzag SiNTs has predominantly ionic bonding while armchair and some chiral SiNTs are covalently bonded.

Depending on the exact way CNTs are wrapped, they are either metallic or semiconducting. In principle, only armchair CNTs are intrinsically metallic. If n-m is a multiple of 3, then the CNT is semiconducting with a very small band gap, otherwise the nanotube is a moderate semiconductor. Fagan *et al*.[28] reported that the electronic properties of single-walled SiNTs are very similar to the equivalent CNTs. As happen to CNTs, they may also present metallic(armchair) or semiconductor(zigzag or chiral) behaviors. The gap was found to increase in proportion to the inverse of the diameter. Zhang *et al*.[29] argued that all small diameter SiNTs are metallic regardless of their chiralities. Compared with zigzag nanotubes, armchair nanotubes of silicon are the most reasonable structures due to the efficient overlapping of p orbitals and delocalized π bonds. Zhang *et al*.[25] pointed out that the energetics and the structures of gearlike SiNTs are shown to depend primarily on the diameter of the tube, irrespective of the type. The energy gap is very sensitive to both the diameter and the type of the nanotube. All three types of SWSiNTs are semiconductors with rather small band gaps(<1 eV). Only the armchair (n, n) show a discernible trend and the energy gap of an armchair SiNT is linearly proportional to the inverse of the diameter of the tube. Durgun *et al*.[30] found that single-walled SiNTs with small radius are unstable and are clustered either at T=0K or at finite temperatures. Zigzag SWSiNTs (n, 0) are metallic for $6 \leq n \leq 11$, but become semiconducting for $n \geq 12$.Seifert *et al*.[22] conclude that, silicide and SiH nanotubes have semi-

conducting gaps, independent of chirality, which converged rapidly with increasing diameter. Pradhan and Ray[7] have used finite cluster approach to study armchair Si and Ge nanotubes. The silicon nanotubes do not appear to be metallic.

Although SiNTs have been successfully synthesized, there is no doubt that they are possibly metastable structures due to the presence of sp^3hybridization.There is a definite "cost" associated with the forming of a SiNT. Barnard and Russo[31] proposed that the atomic heat of formation of a silicon nanotube is dependent of the chiral structure of the tube and the individual cohesive and strain energies are dependent on both the diameter and chirality. Ponomarenko *et al*.[32] investigated the energetics and relative stability of clean and hydrogenated silicon nanotubes. Their results suggest that the strain energy of infinite Si tubes can be reduced by the chemisorption of atomic hydrogen onto the surfaces of the tubes. Also the energetics of finite, clean and hydrogenated Si tubes can be described as interplay between the strain energy due to the curvature of the tube, and the chemical energy arising from the presence of dangling bonds at the open ends of the tubes. They suggested that the balance between the strain and chemical energy can be controlled by the chemisorption of atomic hydrogen onto the walls of finite, open-ended silicon nanotubes. Kang *et al.*[33,34] studied the thermal behavior and the structure of hypothetic silicon nanotubes using classical molecular dynamics simulations based on the Tersoff potential.

In order to stabilize single-walled SiNTs, foreign atoms, such as hydrogen, oxygen or transition metal (TM) atoms, were incorporated into SiNTs in different ways, forming hydrogenated, polygon stacked, or TM-encapsulated SiNTs. Andriotis *et al.*[35] found out that the encapsulation of metal (M= Ni and V) could stabilize SiNTs, and these metal encapsulated SiNTs which had narrow energy gaps were metallic at infinite length with tight-binding molecular dynamics methodology. Menon *et al*.[36] have studied nanotubes of Si with pentagonal rings stabilized with Ni doping. They obtained an icosahedral cluster with the stoichiometry $Si_{12}Ni$ to be stable from first-principles calculations. Singh *et al.*[37] have investigated the stability of finite

and infinite hexagonal prismatic structures of Si with 3d magnetic elements and predicted that such structures can be stabilized through doping by the transition metal (TM) elements.

The structure of SiNTs is still an open question of fundamental physical and chemical importance, which clearly requires concerted efforts. It is well known that the physical properties of the nanotubes depend much on their geometric structures, and so can be easily changed by an applied pressure of strain, which could be used to fabricate the nanoscale devices and transducers. Due to the experimental surroundings, the SWSiNTs may be subjected to various mechanical deformations. The effects of deformations, especially uniaxial tensile and torsional strainsm on the energy bands and electronic properties of SWSiNTs are of great interest, offering the potential applications in nanoelectronic devices, and have attracted much attention. Kang *et al.*[34] studied the response of silicon nanotubes under axial compression, and determined Young's modulus for the SiNTs was constant irrespective of the SiNTs' diameter. As the SiNTs' diameter increased, the collapse pressure decreased linearly. Shan *et al.*[38] showed that the band gap properties are very sensitive to the deformation degree and the helicity of the SWSiNTs.

SiNTs can be classified into two types: One is multi-walled SiNTs and the other single-walled SiNT. Although multi-walled nanotubes (MWNTs) have been synthesized and investigated first, there are very few *ab initio* studies on MWNTs compared to single-walled nanotubes (SWNTs), partly because of the complexity of MWNTs compared to SWNTs. The first logical step towards the study of MWNTs would obviously be double-wall nanotubes (DWNTs) constructed from inserting one nanotube inside another one. Two coaxial SWNTs (n_1, m_1) and (n_2, m_2) make a DWNT (n_1,m_1)@(n_2,m_2) where (n_1,m_1) and (n_2,m_2) represent the inner and outer tubes, respectively. Some *ab initio* studies of DWNTs have shown that DWNTs have lower band gaps than those of SWNTs [27-28].Zhao *et al.*[39] reported the favorable configurations of double-walled silicon nanotubes with faceted wall surfaces. These tubes have

higher energetic favorability than the conventionally adopted cylindrical configurations of single-walled silicon nanotubes.

Adsorptions of atoms and molecules in fine pores have been recognized to have fundamental interest in both applied and fundamental research, because of the reduced dimensionality, and technological importance, for many reasons, including separation of mixtures, hydrogen storage[40-42], *etc*. In particular, there has been considerable interest in evaluating the capability of nanotubes as a hydrogen-storage material for clean energy sources[43-45].Large empty space inside the single-walled nanotubes provides a possibility to be applied for fuel cell vehicles. Hydrogen has been recognized as a clean source of energy and is often referred to as the fuel of the future. Hydrogen produces only water as a byproduct when it is used in a fuel cell. One problem associated with hydrogen is storage, requiring either very low temperature or very high pressure. Both storage requirements are neither practical nor cost effective. This has simulated worldwide research to find effective materials and structures for hydrogen storage. The problem associated with conventional storage mediums like metals and intermetallics is the limitation on the storage capacity or the reversibility of stored hydrogen under normal conditions.[46-49] A light weight nanostructure with a large surface-to-bulk ratio is ideal for hydrogen storage.

The U.S. Department of Energy (DOE) has set up an objective of developing and verifying on-board hydrogen storage systems having a storage capacity of 5.5 wt% by 2015[50], and thus the hydrogen storage capacity of single walled nanostructures has become extremely important. A number of publications are devoted to the experimental and theoretical study of gas adsorption on different adsorbent structures. Dillon *et al*.[51]have reported that carbon nanotubes (CNTs) can be used for hydrogen storage and measured the H_2 adsorption capacity of single-walled carbon nanotubes (SWCNT) and the gravimetric storage capacity ranging between 5-10 wt%. Darkrim and Levesque[52] studied the influence of the distance between the nearest neighbors SWNT's on adsorption using the Lennard-Jones potential. A detailed

study[53] on hydrogen adsorption and storage in SWNTs and multi-walled nanotubes using density-functional-based tight-binding calculations has shown that many hydrogen atoms can be stored in the interior and adsorbed to the outer wall of carbon nanotubes, and that the hydrogen storage capacity is limited by the repulsive interactions between H_2 molecules and also those with carbon atoms. In 2000, the storage capacities of silicon carbide nanotubes were reported to be 7%[54]. Mukherjee and Ray[55] have investigated, in detail, the feasibilities of using silicon carbide (SiC) nanotubes as hydrogen storage media. The relatively promising results led to the development of many works on adsorption of hydrogen in nanotubes by molecular simulations and by experiments. Notwithstanding the simulations and experiments, there are no existing adsorbents that satisfy the DOE target to date. Hence, there is still a need to develop highly efficient adsorbents that are specifically designed for hydrogen storage. Silicon nanotubes have been intensively studied in anticipation of their application in novel nanoscale materials and device structures, as well as for their fundamental physics.

Also, as is known, hydrogen greatly affects the electronic and structural properties of many materials. It can bind to defects or impurities, therefore changing their electrical activity by passivation effects[56-58], which is essential for the performance of many photovoltaic and electronic devices. Particularly, hydrogen is a common impurity in silicon to saturate dangling bonds. The interaction between hydrogen and silicon surface has been extensively studied, many groups have reported the identification of a molecular form of hydrogen in Si[59-61]. For clean silicon surfaces, hydrogen interaction is shown to greatly change their structure and properties. Hydrogen is the simplest adsorbate but the adsorption of hydrogen on Si material is complex. The adsorption and desorption of hydrogen molecules on silicon is a subject of countless research.[62-64].

In this context, we note that the electronic properties of single-wall nanotubes (SWNTs) can be appreciably altered by the presence of other adsorbed molecules.[65]Upon exposure to gaseous molecules, the electrical resistance of a semiconducting SWNT is found to dramatically

increase or decrease. This has important ramifications for device applications involving SWNTs, and it has led to considerable interest in the possible use of SWNT's as the basis of chemical sensors.[66] Oxygen, in particular, has been found to influence electronic properties of SWNTs, with the electrical resistance, the thermoelectric power, and the local density of states all depending on oxygen exposure.[67] Oxygen and silicon are two common substances on earth. The behavior of oxygen in silicon has been a subject of considerable interest and controversy. The favorable formation of sp^3 hybridization in Si atoms promotes the growth of Si nanowires and multi-walled Si nanotubes, which have been fabricated using different methods. The oxidation of silicon surface has been an important research subject in surface science and a key process in the fabrication of semiconductor devices. Similar to hydrogen, oxygen has the capacity to passivate silicon dangling bonds. However, unlike hydrogen, each oxygen atom would passivate two silicon bonds, as in silicon dioxide. The interaction of oxygen with silicon plays a very important role in both the bulk- and surface- governed electronic properties of semiconductors[68,69]. Plans *et al.*[68] have studied how oxygen breaks the covalent silicon-silicon bond forming a local configuration similar to that of SiO_2. Theoretical studies have shown that oxygen molecule is not stable in the Si lattice[70,71]. Zhao *et al.*[72] have studied surface structures and electronic states of silicon nanotubes stabilized by oxygen atoms. Moreover, in silicon oxides, the Si-O-Si bond angles can vary widely in different phases. For example, the Si-O-Si bond angles in α cristobaliteare 146° but become 180° in β cristobalite. Surface relaxations *may* modify the electronic state hybridization and the electrical and optical properties of nanotubes. More strikingly, it has been reported that small-gap semiconducting nanotubes can be made metallic upon exposure to a small amount of oxygen.[65] The increased electrical conductivity induced by oxygen adsorption has been attributed to an increase in the local density of states and a shrinking of the band gap of the nanotube. Zhao *et al.*[73] have reported that the incorporation of oxygen atoms as silicon monoxides in (8, 0) single-walled silicon nanotube stabilizes the nanotube and can tailor the electronic structure from semiconducting to

metallic. It is expected that the well-established silicon based industry will be attracted towards nano-structures of silicon to explore further applications in nanoelectronics.

This dissertation is organized as follows: Chapter 1 gives an overview of silicon nanotubes and introduction of density functional theory. Chapter 2 describes the structure and properties of single-walled and double-walled silicon nanotubes. Chapter 3 is devoted to the atomic hydrogen and oxygen adsorption in silicon nanotubes. Chapter 4 extends the discussion to the molecular hydrogen and oxygen adsorption in silicon nanotubes. In addition, alkali metal adsorptions in silicon nanotubes are discussed in Chapter 5. Chapter 6 summarizes the conclusions and suggestions for future research.

There has been no groundwork here for the work that has been done in this dissertation. As discussed above, several research groups have explored the adsorption capacity of tubular materials under different conditions to try to reach the DOE target for H_2 storage and transportation. However, most of the experimental and theoretical efforts in this area so far have failed to approach the proposed target. In addition, their results are sometimes controversial and cannot be applied in practice, in the sense that they were not confirmed or reproduced by other research groups. As a result, the theoretical and experimental studies so far show that the problem of hydrogen adsorption in nanotubes still remains quite challenging, and much more has to be done to obtain an eventual answer to the question of whether such systems are suitable for efficient H_2 storage. Silicon is more polarizable than carbon due to the presence of more electrons in its outer shells. Therefore, we anticipate that SiNTs can be tailored to achieve a stronger van der Waals attraction to adsorbed molecules than CNTs. The nature of the interaction between hydrogen and the host nanomaterials, as revealed through theoretical modeling, helps us understand the basic mechanisms of hydrogen storage. We have carried out a systematic study on adsorption of atomic and molecular hydrogen in several types of silicon nanotubes. The adsorption of atomic and molecular hydrogen has various influences on the electronic and structural properties of silicon nanotubes with different chiralities. We

expect to gain a comprehensive understanding of the adsorption behavior of hydrogen upon silicon nanotubes.

1.2 Density Functional Theory

Electronic structure calculations are today an important tool for investigating the physics and chemistry of new molecules and materials. An important factor for the success of these techniques is development of first principles methods that make reliable modeling of a wide range of systems possible without introducing system dependent parameters. Density functional theory (DFT)[74] is a quantum mechanical modeling method used to investigate the electronic structure of many-body systems, in particular atoms, molecules, and the condensed phases. Within this theory, the properties of a many-electron system can be determined by using functionals, i.e. function of another function, which in this case is the spatially dependent electron density. DFT is among the most popular and versatile methods available in condensed-matter physics, computational physics and computational chemistry.

To understand behavior of any electronic system such as an atom, molecule, nano-cluster, or solid, we have to first know the fundamental properties of the system. The ground state properties like total energy, atomization energy, vibrational frequency, equilibrium geometry etc. of the system can be calculated by solving the N-electron Schrödinger equation for the N-electron ground state wavefunctions. This method of solving Schrödinger equation is exact in principle but not useful for any practical purpose, especially for large N.DFT methods are efficient and practical methods to solve any electronic system with large N. DFT is in principle an exact formulation for the ground state of many-electron systems and it maps an N electron-system to a single variable, the electron-density, which reduces the computational cost significantly.

DFT provides an elegant way to solve a many-electron problem with improvable compromise between accuracy and efficiency. It attempts to address both the inaccuracy of HF and the high computational demands of post-HF methods by replacing the many-body

electronic wavefunction with the electronic density as the basic quantity. Whereas the wavefunction of an N electron system is dependent on 3N variables, the density is a function of only three variables and is a simpler quantity to deal with both conceptually and practically, while electron correlation is included in an indirect way from the outside. The orbital-free formulation of N-electron problem started with Thomas-Fermi theory[75,76] in 1920s. In Thomas-Fermi model of an electronic system, the total energy is expressed as the functional of the electron density and the energy functional is minimized keeping fixed electron number. This model gives the total energy of electronic systems with an error of about 10%. However, this model is not good enough to estimate most properties of interest. Because of the crude formulation and absence of exchange-correlation energy, atoms do not bind together to form molecules and solids in Thomas-Fermi theory[77].The electron exchange energy was included into the Thomas-Fermi functional by Dirac in 1930[78].

Although density functional theory has its conceptual roots in the Thomas-Fermi model, DFT was put on a firm theoretical footing by the two Hohenberg-Kohn theorems. The use of electron-density as the basic variable in many electron systems was re-established by two Hohenberg-Kohn theorems published in 1964[79] and Kohn-Sham theorems published in 1965 [80].These theorems, often regarded as twin pillars of modern density functional theory, are exact in principle. There has been a significant amount of theoretical and computational research works based on this theory in past forty years[81-87].

Despite recent improvements, there are still difficulties in using density functional theory to properly describe intermolecular interactions, especially van der Waals forces, charge transfer excitations, transition states, global potential energy surfaces and some other strongly correlated systems. The introduction of hybrid functionals, which mix LDA and GGA with exact Hartree-Fock exchange, has shown good performance for a truly wide variety of chemical systems and properties.

1.2.1 Theoretical Formalism

To appreciate the special place of DFT in the modern quantum chemical methods, it is useful first to have a look into the more traditional wavefunction-based approaches. These approaches attempt to provide approximate solutions to the Schrödinger equation, the fundamental equation of quantum mechanics that describes any given chemical system.

The Hamiltonian for an N-electron and M-nuclei system is given by

$$H = -\sum_{i=1}^{N}\frac{\hbar^2}{2m}\nabla_i^2 - \sum_{I=1}^{M}\frac{\hbar^2}{2M_I}\nabla_I^2 - \frac{1}{4\pi\epsilon_0}\sum_{I=1}^{M}\sum_{i=1}^{N}\frac{Ze^2}{r_{iI}} + \frac{1}{4\pi\epsilon_0}\sum_{i<j}^{N}\frac{e^2}{r_{ij}} + \frac{1}{4\pi\epsilon_0}\sum_{I<J}^{M}\frac{Z_I Z_J e^2}{R_{IJ}} \quad (1.1)$$

where the first and second terms give the kinetic energies of electrons, and nuclei respectively, the third term gives electrons-nuclei interaction energy, the fourth term gives the electron-electron interaction energy and the last term gives the nuclei-nuclei interaction energy.

In Born-Oppenheimer approximation, the electrons in a molecule are considered to be moving in the field of fixed nuclei. The second term of the equation (1.1) is therefore can be neglected and the last term can be taken as a constant. Any constant added to an operator only adds to the operator eigenvalues and has no effect on the eigenfunctions. The equation (1.1) then can be written as

$$H = -\sum_{i=1}^{N}\frac{\hbar^2}{2m}\nabla_i^2 - \frac{1}{4\pi\epsilon_0}\sum_{I=1}^{M}\sum_{i=1}^{N}\frac{Ze^2}{r_{iI}} + \frac{1}{4\pi\epsilon_0}\sum_{i<j}^{N}\frac{e^2}{r_{ij}} \quad (1.2)$$

In atomic unit equation (1.2) has the form

$$H = \sum_{i=1}^{N}\left(-\frac{1}{2}\nabla_i^2\right) + \sum_{i=1}^{N}v(r_i) + \sum_{i<j}^{N}\frac{1}{r_{ij}} \quad (1.3)$$

In many cases the problems related to electronic structures can be studied by the time-independent Schrödinger equation

$$H\Psi = E\Psi \quad (1.4)$$

where H is the Hamiltonian given by equation (1.3), E is the electronic energy and $\Psi = \Psi\ (x_1, x_2, x_3, \ldots, x_N)$ is the many-electron wave function where x_i's are the electron coordinates and spins. One of the methods to solve the many electron problems is to solve equation (1.4) to find this

many-electron wave function and then calculate the properties of the system by taking this many-electron wave function a basic variable.

In Hartree approximation[88], this many electron wavefunction is taken as the product of single electron wavefunctions,

$$\Psi(x_1, x_2, x_3, \dots \dots x_N) = \Psi_1(x_1)\Psi_2(x_2)\Psi_3(x_3) \dots \dots \Psi_N(x_N) \quad (1.5)$$

the single-electron wave functions $\Psi_i(x_i)$ satisfy one-electron Schrödinger equation

$$\left[-\frac{1}{2}\nabla^2 + v(r_i) + \varphi_i\right]\Psi_i(r) = \varepsilon_i\Psi_i(r) \quad (1.6)$$

where $v(r_i)$ is the potential due to nuclei and the Coulomb potential$\varphi_i$is determined by the equation

$$\nabla^2\varphi_i = -4\pi\sum_{j=1,i\neq j}^{N}\left|\Psi_j\right|^2 \quad (1.7)$$

The equation (1.5) takes no account of indistinguishability of electrons since it assigns a specific state to a specific electrons. Therefore, even if we consider the electrons to be independent particles (which is not the case) the equation (1.5) has a fundamental problem. Accroding to Pauli's exclusion principle a many-electron wave function must be antisymmetric with respect to the interchange of space and spin coordinates of any two electrons.

The Hartree product does not satisfy the antisymmetry principle. A correct antisymmetrized wave function can be represented by a single determinantal functions called Slater determinant.This Slater determinant has N electrons occupying N spin orbitals without specifying which electron is in which orbital. Interchanging the coordinates of two electrons corresponds to interchanging two rows of the Slater determinant, which changes the sign of the determinant. Thus Slater determinants meet the requirement of the antisymmetry principle.

The HF method [88,89] assumes that the exact N-body wavefunction of the system can be approximated by a single Slater determinant of N spin orbitals. By invoking the variational principle, one can derive a set of N-coupled equations for the N spin orbitals. Solution of these equations yields the Hartree-Fock wavefunction and energy of the system, which are upper-bound approximations of the exact ones. The main shortcoming of the HF method is that it

treats electrons as if they were moving independently of each other; in other words, it neglects electron correlation.

Use of the Slater determinant introduces a nonlocal exchage effect in the Schrödinger equation and this improves the total energy calculation but the single particle picture, with the wave function described in terms of orbital with particular spins and occupation numbers is unchanged. It has been noted that a single Slater determinant wave function must inevitably lead to a poor energy since the lowest-lying configuration is generally only one of very many with comparable energies, and a better approximation would result from taking a linear combination [90]. This approach known as “configuration interaction” (CI) includes the correlation effects beyond Hartree-Fock approximation by improving the many-particle wave functions. In principle, CI provides an exact solution of the many-electron problems. In practice, however, the explosive increase in the number of configurations with increasing electron number limits its application to only small systems with relatively few electrons. Furthermore, the complexity of the resulting solutions means that a simple interpretation of the results is often difficult.

The predecessor to density functional theory was the Thomas-Fermi model. Thomas-Fermi model [75,76] represented the total energy of a many-electron system as the functional of electron-density,

$$\rho(r) = N \int \Psi^*(r, r_2, r_3, \dots r_N)\Psi(r, r_2, r_3, \dots r_N) dr_2 dr_3 \dots dr_N \tag{1.8}$$

the total energy is given by,

$$E_{TF}[\rho] = T_{TF}[\rho] + E_{ne}[\rho] + J[\rho] \tag{1.9}$$

where the first term is the kinetic energy, second term is the nuclei-electron interaction energy and the third term is the Coulombic electron-electron interaction energy. The kinetic energy is calculated by assuming that the motions of the electrons are uncorrelated. The Thomas-Fermi model is entirely a local approximation in which the kinetic energy is calculated based on the results for uniform electron-gas. Also, the Thomas-Fermi model does not require the

antisymmetrized wave function with respect to permutation of any pair of electrons. Therefore the exchange effect is not taken into account. Dirac added an exchange term to the Thomas-Fermi model by incorporating a term derived from the exchange energy density in a homogenous system. As discussed in introduction the Thomas-Fermi model is too crude to estimate general characteristics of an electronic system. The most important deficiency of this model is that it fails to explain the formation of bonds between atoms in a molecule. Hohenberg and Kohn [79] provided the fundamental theorems showing that for ground states the Thomas-Fermi model may be regarded as an approximation to an exact theory, the density functional theory.

Modern DFT rests on two theorems by Hohenberg and Kohn. The first theorem states that the ground-state electron density uniquely determines the electronic wavefunction and hence all ground-state properties of an electronic system. The second theorem establishes that the energy of an electron distribution can be described as a functional of the electron density, and this functional is a minimum for the ground-state density. Thus, the problem of solving the many-body Schrödinger equation is bypassed, and now the objective becomes to minimize a density functional.

The Hohenberg-Kohn theorems establish that one can use electron-density as the basic variable and get rigorously accurate results for any many-electron system. It states that *the external potential can be determined, within a trivial additive constant, by the electron-density*.

If $\rho(r)$ is the electron density for the non-degenerate ground state of some N-electron system, then,

$$\int \rho(r)dr = N \tag{1.10}$$

the external potential $v(r)$can be determined from $\rho(r)$. Hence the ground-state wave function Ψ can be determined from $\rho(r)$. Similarly, other electronic properties can also be determined from $\rho(r)$.

If there were two external potentials v and v' each giving the same electron density $\rho(r)$ for its ground state, we would have two Hamiltonians H and H' whose ground state densities were the same although the normalized wave functions Ψ and Ψ' would be different

$$H\Psi = E\Psi \tag{1.11}$$

$$H'\Psi' = E'\Psi' \tag{1.12}$$

H and H' have the ground-state energies E and E' respectively.

now taking Ψ' as the trial function for H problem,

$$E < \langle\Psi'|H|\Psi'\rangle$$

$$=\langle\Psi'|H'|\Psi'\rangle + \langle\Psi'|H - H'|\Psi'\rangle$$

$$=E' + \langle\Psi'|v(r) - v'(r)|\Psi'\rangle$$

$$=E' + \int\big(v(r) - v'(r)\big)\rho(r)dr \tag{1.13}$$

similarly, taking Ψ as the trial function for H' problem,

$$E' < \langle\Psi|H'|\Psi\rangle$$

$$=\langle\Psi|H|\Psi\rangle + \langle\Psi|H' - H|\Psi\rangle$$

$$=E + \langle\Psi|v'(r) - v(r)|\Psi\rangle$$

$$=E - \int\big(v(r) - v'(r)\big)\rho(r)dr \tag{1.14}$$

adding inequalities (1.13) and (1.14) we get,

$$E + E' < E' + E \tag{1.15}$$

this is a contradiction. Therefore the initial assumption that there are two different potential for the same electron-density is wrong. Thus, the density must uniquely determine the external potential, and hence the Hamiltonian and the ground state energy of the system. The ground state total energy can be written as a functional of the electron density,

$$E_v[\rho] = T[\rho] + V_{ne}[\rho] + V_{ee}[\rho] = \int \rho(r)v(r)dr + F_{HK}[\rho] \tag{1.16}$$

where $T[\rho]$ is the kinetic energy, $V_{ne}[\rho]$ is the nuclei-electron interaction energy and $V_{ee}[\rho]$ is the electron-electron Coulomb interaction energy and $F_{HK}[\rho]$= $T[\rho]$+$V_{ee}[\rho]$ is a universal functional of $\rho(r)$ in a sense that $F_{HK}[\rho]$ is defined independently of the external potential $v(r)$.

The second Hohenberg-Kohn theorem states: *For a trial density $\rho_1(r)$, such that $\rho_1(r) \geq 0$ and $\int \rho_1(r)dr$=N*

$$E_0 \leq E[\rho_1] \tag{1.17}$$

where E_0 is the ground state energy and $E[\rho_1]$ is the energy functional of (1.16).

The energy variational principle can be obtained from this theorem. It means that the ground-state electron density is the density that minimizes $E[\rho]$. The first theorem assures that $\rho_1(r)$ determines its own v_1, Hamiltonian H_1, and wave function Ψ_1. Let us take Ψ_1 as a trial function for the Hamiltonian H of interest with external potential v. The variational principle asserts that,

$$\langle \Psi_1 | \hat{H} | \Psi_1 \rangle \geq \langle \Psi | \hat{H} | \Psi \rangle \tag{1.18}$$

To prove,

$$\langle \Psi_1 | \hat{H} | \Psi_1 \rangle = \int \rho_1(r) v(r) dr + F_{HK}[\rho_1] = E_v[\rho_1] \geq \langle \Psi | \hat{H} | \Psi \rangle = E_v[\rho] \tag{1.19}$$

Assuming differentiability of $E[\rho]$ the variational principle requires that the ground state density satisfies the stationary principle

$$\delta\{E_v[\rho] - \mu(\int \rho(r)dr - N)\} = 0 \tag{1.20}$$

which gives the Euler-Lagrange equation

$$\mu = \frac{\delta E_v[\rho]}{\delta \rho(\boldsymbol{r})} = v(r) + \frac{\delta F_{HK}[\rho]}{\delta \rho(\boldsymbol{r})} \tag{1.21}$$

where μ is the Lagrange multiplier associated with the constraint $\int \rho(r)dr$=N.

The functional $F_{HK}[\rho]$known as Hohenberg-Kohn functional or the universal functional is very important in the formulation of density functional theory. Once the functional $F_{HK}[\rho]$=$T[\rho]$+$V_{ee}[\rho]$ is known exactly we would have exact solution of any many-electron problem. The functional $F_{HK}[\rho]$ contains the functional for kinetic energy and that for electron-electron interaction energy. The exact form for both of these is not known. The classical part of the electron-electron interaction is known exactly, but the explicit and exact forms for non-classical effects are still unknown. The non-classical contribution the electron-electron interaction contains all the effects of self-interaction correction, and exchange-correlation.

Although the Hohenberg-Kohn theorems do not give insights of actual methods of calculation, and it is usually *v(r)* rather than *ρ(r)*that is known, they provide confidence that it is sensible to seek solutions of many-body problems based on the density rather than the wave functions.

The second major work on density functional theory appeared in 1965. In this work the Kohn and Sham proposed a systematic way of approaching the unknown universal functional. It was in fact very important step towards implementing density functional theory in practical computational calculations. Early attempts to approximate the universal functional $F_{HK}[\rho]$used the Thomas-Fermi approximation for the kinetic component $T[\rho]$. It was soon realized that only very crude answers can be obtained with this local functional for the kinetic energy, no matter how sophisticated the approximation for the $V_{ee}[\rho]$ component is. Kohn and Sham therefore proposed a functional giving the major part of the kinetic energy and the scheme makes the density functional theory practical. Kohn and Sham assumed that the kinetic energy term has a component that is independent of the electron-electron interaction and that the electron-electron potential term has a component that is described as a classical Coulomb potential. Therefore the universal functional is given by,

$$F_{HK}[\rho] = T[\rho] + V_{ee}[\rho] = T_s[\rho] + J[\rho] + E_{xc}[\rho] \quad (1.22)$$

where the first term is the kinetic energy term which is independent of electron-electron interaction, the second term is the classical Coulomb potential and the third term is the exchange-correlation energy defined by the equation

$$E_{xc}[\rho] \equiv T[\rho] - T_s[\rho] + V_{ee}[\rho] - J[\rho] \quad (1.23)$$

Kohn-Sham method invokes a non-interacting reference system, with the Hamiltonian,

$$\hat{H}_s = \sum_i^N \left(-\frac{1}{2}\nabla^2\right) + \sum_i^N v_s(r_i) \quad (1.24)$$

for which the ground-state electron density is exactly *ρ(r)*.For a non-interacting system, the many electron wavefunction is a single Slater determinant

$$\Psi_s = \frac{1}{\sqrt{N!}}\det[\psi_1\psi_2\cdots\psi_N] \quad (1.25)$$

where the Ψ_i are the N lowest eigenstates of the one-electron Hamiltonian h_s:

$$\hat{h}_s\psi_i = \left[-\frac{1}{2}\nabla^2 + v_s(r)\right]\psi_i = \varepsilon_i\psi_i \quad (1.26)$$

$$\rho(r) = \sum_i^N \sum_s |\psi_i(r,s)|^2 \quad (1.27)$$

The kinetic energy is then given by,

$$T_s[\rho] = \left\langle \Psi_s \middle| \sum_i^N \left(-\frac{1}{2}\nabla_i^2\right) \middle| \Psi_s \right\rangle = \sum_i^N \left\langle \psi_i \middle| -\frac{1}{2}\nabla^2 \middle| \psi_i \right\rangle \quad (1.28)$$

It is to be noted that $T_s[\rho]$ here is not the true kinetic energy of the interacting system whose ground state density is *ρ(r)*, but is in fact much closer to the kinetic energy $T[\rho]$, in the final optimized description, than it is to the Thomas-Fermi kinetic energy. There are two parts of contributions to the exchange correlation energy $E_{xc}[\rho]$: one is from the non-classical effects of the electron-electron interactions and the other is from the kinetic energy. The Euler equation now becomes

$$\mu = v_{eff}(r) + \frac{\delta T_s[\rho]}{\delta \rho(\boldsymbol{r})} \quad (1.29)$$

where the Kohn-Sham effective potential is defined by

$$v_{eff}(r) = v(r) + \frac{\delta J[\rho]}{\delta \rho(r)} + \frac{\delta E_{xc}[\rho]}{\delta \rho(r)} = v(r) + \int \frac{\rho(r')}{|r-r'|} dr' + v_{xc}(r) \quad (1.30)$$

which the exchange-correlation potential

$$v_{xc}(r) = \frac{\delta E_{xc}[\rho]}{\delta \rho(\boldsymbol{r})} \quad (1.31)$$

Equations 1.26 to 1.31 are the four essential Kohn-Sham equations. The effective potential V_{eff} as we see from equation (1.30) is also a functional of the electron density. Therefore, the Kohn-Sham equations have to be solved self-consistently. Figure 1.1 shows the flowchart for the standard DFT calculations.

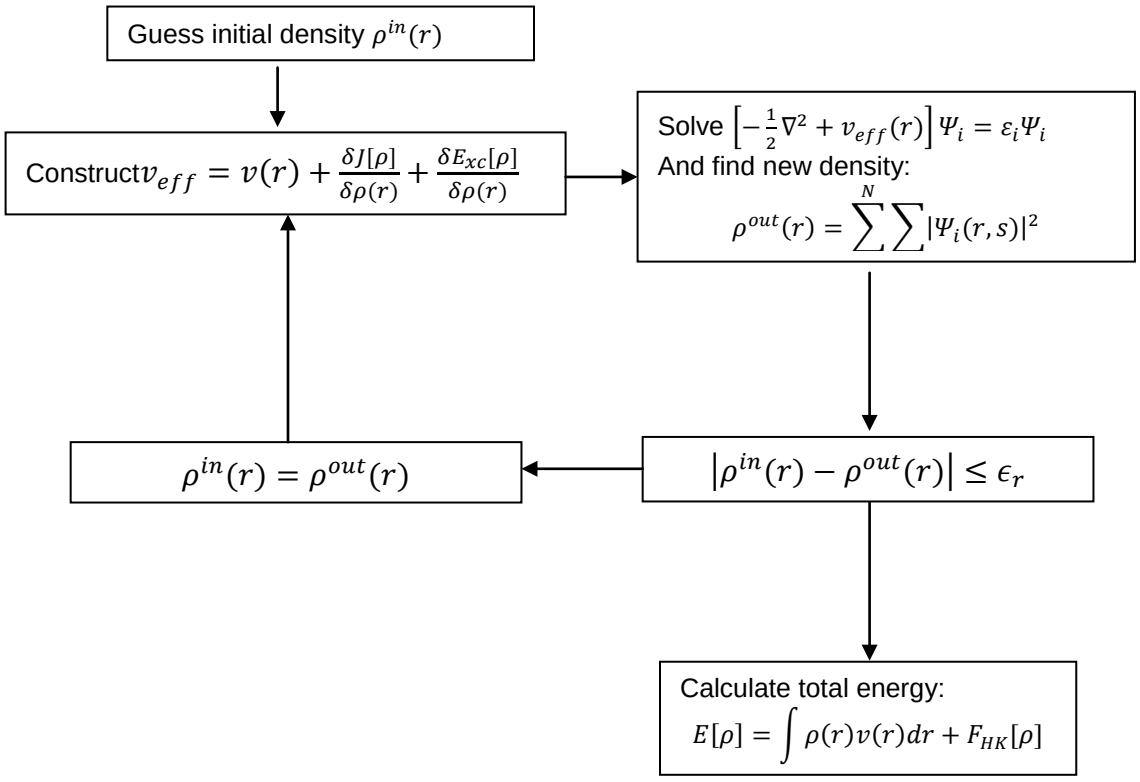

Figure 1.1 Flowchart for DFT calculations

The Kohn-Sham scheme provides a simple but rigorous way to compute the electronic properties within density functional theory. In principle, the Kohn-Sham equations will yield exact ground state properties if an exact exchange correlation potential is given. However, the Kohn-Sham scheme does not provide methods to obtain the explicit exchange and correlation functionals and therefore, approximations have to be considered.

Kohn-Sham formalism exactly incorporates most of the contributions to the electronic energy of an atomic or molecular system. All the unknown quantities are collectively put in the term called exchange-correlation functional. As discussed above, this functional contains non-classical contribution of the electron-electron interactions and the kinetic energy not covered by the non-interacting reference system. An explicit form for this exchange-correlation functional is

needed to specify Kohn-Sham equations. Finding the explicit form for this functional the greatest challenge in density functional theory.

Within the framework of Kohn-Sham DFT, the intractable many-body problem of interacting electrons in a static external potential is reduced to a tractable problem of non-interacting electrons moving in an effective potential. The effective potential includes the external potential and the effects of the Coulomb interactions between the electrons, e.g., the exchange and correlation interaction. Non-interacting systems are relatively easy to solve as the wavefunction can be represented as a Slater determinant of orbitals. Further, the kinetic energy functional of such a system is known exactly. The exchange-correlation part of the total-energy functional remains unknown and must be approximated. In fact, the accuracy of the approximate exchange-correlation functional determines the quality of any DFT calculation.

The most fundamental and simplest approximation is the local-density approximation (LDA), in which the energy depends only on the density at the point where the functional is evaluated. It is based upon exact exchange energy for a uniform electron gas, which can be obtained from the Thomas-Fermi model, and from fits to the correlation energy for a uniform electron gas. LDA, which in essence assumes that the density corresponds to that of a homogeneous electron gas, proved to be an improvement over HF

Local density approximation (LDA) was first proposed by Kohn and Sham. LDA is a fairly good model for simple metals like sodium. For any system with very slowly varying densities this approximation is reasonably good but for the systems characterized by rapidly varying densities it is not good enough. However, LDA has a prominent role in DFT because uniform electron gas is the only system for which we know the form of exchange and correlation energy functionals exactly or at least to vary high accuracy and this represents the bedrock of almost all current functionals.

The total exchange-correlation energy of a system with very slowly varying density can be given by,

$$E_{xc}^{LDA}[\rho] = \int \rho(r)\varepsilon_{xc}(\rho)dr \quad (1.32)$$

where $\varepsilon_{xc}(\rho)$ is the exchange and correlation energy per particle of a uniform electron gas of density$\rho(r)$. The functional derivative of the total exchange-correlation gives the local approximation to the Kohn-Sham exchange-correlation potential

$$v_{xc}^{LDA}[r] = \frac{\delta E_{xc}^{LDA}}{\delta \rho(\mathbf{r})} = \varepsilon_{xc}(\rho(r)) = \rho(r)\frac{\delta \varepsilon_{xc}(\rho)}{\delta \rho} \quad (1.33)$$

The Kohn-Sham equation becomes

$$\left[-\frac{1}{2}\nabla^2 + v(r) + \int \frac{\rho(r')}{|r-r'|}dr' + v_{xc}^{LDA}(r)\right]\Psi_i = \varepsilon_i \Psi_i \quad (1.34)$$

The local exchange-correlation energy is the sum of correlation and exchange effects,

$$\varepsilon_{xc}(\rho) = \varepsilon_x(\rho) + \varepsilon_c(\rho) \quad (1.35)$$

where $\varepsilon_x(\rho)$ is the exchange energy per particle of a homogenous electron gas. The analytical expression of this term for homogeneous electron gas is known exactly and is given by,

$$\varepsilon_x(\rho) = -\frac{3}{4}\left(\frac{3}{\pi}\right)^{\frac{1}{3}}\rho(r)^{\frac{1}{3}} = -\frac{0.4582}{r_s} \quad (1.36)$$

Here r_s is the Wigner-Seitz radius,

$$\frac{4}{3}\pi r_s^3 = \frac{1}{\rho} \quad (1.37)$$

There is no simple analytical formula for the correlation energy$\varepsilon_c(\rho)$. Only some limiting cases are found to have analytic form. For example, in high-density limit the correlation energy is given by[91, 92],

$$\varepsilon_c = 0.0311\ln r_s - 0.048 + r_s(A\ln r_s + C), \qquad r_s \ll 1 \quad (1.38)$$

And in low-density limit the correlation energy is given by [106, 107],

$$\varepsilon_c = \frac{1}{2}\left(\frac{g_0}{r_s} + \frac{g_1}{r_s^{3/2}} + \frac{g_2}{r_s^2} + \cdots\right), \qquad r_s \gg 1 \quad (1.39)$$

In practice, the common current realization of DFT is through the Kohn-Sham (KS) approach. The KS method is operationally a variant of the HF approach, on the basis of the construction of a non-interacting system yielding the same density as the original problem. Non-interacting systems are relatively easy to solve because the wavefunction can be exactly

represented as a Slater determinant of orbitals, in the setting often referred to as a Kohn-Sham determinant. The form of the kinetic energy functional of such a system is known exactly and the only unknown term is the exchange-correlation functional. Here lies the major problem of DFT: the exact functionals for exchange and correlation are not known except for the free electron gas. However, many approximations exist which permit the calculation of molecular properties at various levels of accuracy..

The Kohn-Sham-LDA is further extended to the spin dependent case by replacing the scalar external potential $v(r)$ by a spin dependent potential $v_{\alpha\beta}(r)$ and replacing the charge density $\rho(r)$ by the density matrix $\rho_{\alpha\beta}(r)$[93-95]. The electron densities with spin projection up $\rho_{\alpha}(r)$ and down $\rho_{\beta}(r)$ are treated separately. Similarly, one can deal with $\rho(r) = \rho_{\alpha}(r) + \rho_{\beta}(r)$, along with the polarization $\zeta(r) = \left[\rho_{\alpha}(r) - \rho_{\beta}(r)\right]/\rho(r)$. ζ takes values between -1 (fully polarized downwards) and +1 (fully polarized upwards). The spin-up and spin-down densities are generated from the spin-up and spin-down Kohn-Sham wave functions. This so-called local spin density (LSD) approximation improved LDA for atomic and molecular systems with unpaired spins. Most of the modern LDA functional are very similar having the difference only in how the correlation energy is fitted into the functional. Vosko-Wilk-Nusair (VWN) [95], Cole-Perdew (CP) [96], Perdew-Zunger(PZ81) [97] and Perdew-Wang (PW92) [98] functionals are commonly used in modern LDA.

LDA and its spin generalization LSD allow one to use the knowledge of the uniform electron gas to predict properties of the in homogenous electron gases occurring in atoms, molecules and solids. Specifically, LSD usually has moderate accuracy for most systems of interest, making errors of order 5-10%. Its most remarkable feature is its reliability, making the same kinds of errors on every system it's applied to. The success of LDA is due to the systematic error cancellation in its formulation. In general, LDA underestimate correlation but overestimates exchange in inhomogeneous systems. This error cancellation is due to the fact that the exchange-correlation hole $\rho_{xc}^{LDA}(r_1, r_2)$ is spherically symmetric and it obeys the sum rule

[99-101] which corresponds to the fact that, if an electron has been found at r_1 , then there is one less electron left to find elsewhere (i.e. , by integral over all r_2),

$$\int \rho_{xc}^{LDA}(r_1, r_2)\, dr_2 = -1 \tag{1.40}$$

where the exchange-correlation hole $\rho_{xc}^{LDA}(r_1, r_2)$ is defined by

$$V_{ee} = \iint \frac{1}{r_{12}} \rho_2(r_1, r_2) dr_1 dr_2 = J[\rho] + \frac{1}{2} \iint \frac{1}{r_{12}} \rho(r_1) \rho_{xc}^{LDA}(r_1, r_2) dr_1 dr_2 \tag{1.41}$$

with $J[\rho]$ being the classical Coulomb interaction. This is true because for everyr_1, $\rho_{xc}^{LDA}(r_1, r_2)$ is the exact exchange-correlation hole of a homogenous electron gas with density$\rho(r_1)$. Hence, the LDA and LSD describe the total charge of $\rho_{xc}^{LDA}(r_1, r_2)$ correctly.

Since the LDA formula for E_{xc} is formally justified for systems with slow varying densities, the logical first step ahead is the suggestion of using not only the information about $\rho(r)$ but to supplement this with information about the gradient of charge density $\nabla\rho(r)$ in order to account for the non-homogeneity of the true electron density[54]. The exchange correlation functional is expanded in a Taylor series in the gradient of density.

$$E_{xc}^{GEA} = \int \rho(r) \varepsilon_{xc}(\rho) \mathrm{dr} + \int C_{xc}(\rho) \frac{\nabla\rho}{\rho^{2/3}} \mathrm{dr} + \cdots \tag{1.42}$$

This approximation is called gradient expansion approximation (GEA). As we can see in the above equation, the first term of this expansion is LDA. It is expected that this gradient expansion should be a better approximation. However, GEA does not make significant correction to the LDA. The GEA was even worse than LDA. This is because the LDA has much more 'first-principles character' than GEA.LDA preserves the properties of exchange correlation holes but GEA does not. GEA exchange-correlation hole improves the LDA hole only at short separations, but is poorly damped and oscillatory at large separations, and GEA violates the sum rule of the exchange-correlation hole [102,103].

Perdew and others introduced the so-called generalized gradient approximation [104-109] such that the exchange correlation energy can be written as a functional of both the density and its gradient:

$$E_{xc}^{GGA}\left[\rho_\alpha \rho_\beta\right] = \int d^3 r\, f(\rho_\alpha(r), \rho_\beta(r), \nabla\rho_\alpha(r), \nabla\rho_\beta(r)) \tag{1.43}$$

While LDA remains a major workhorse in solid state physics, its success in chemistry is at best moderate due to its strong tendency for overbinding. The first real breakthrough came with the creation of functionals belonging to the so-called generalized gradient approximation (GGA) that incorporates dependence not only on the electron density but also on its gradient, thus being able to better describe the inhomogeneous nature of molecular densities. The next major step in the development of DFT was the introduction of hybrid functionals, which mix GGA with exact Hartree-Fock exchange. This method has shown good performance for a truly wide variety of chemical systems and properties.

The first modern GGA was that of Langreth and Mehl, who proposed the idea of truncating the gradient expansion for the exchange-correlation hole. Considering the problems encountered by GEA, Perdew *et al.* proposed several versions of GGA functional by introducing the real-space cutoff procedure on the hole, which restores the sum rule or the normalization and negativity conditions on the GGA hole and generates a short-ranged hole whose angular and system average was much closer to the true hole. The Perdew-Wang 1991 (PW91) GGA functional incorporates no free parameters and is entirely determined from uniform electron gas properties and extract constraints. The Perdew-Burke-Ernzerhof [110] functional is a simplified and refined version of the PW91 functional. Becke derived an exchange functional known as B88 incorporating the known behavior of the exchange hole at large distances outside a finite system. Lee, Yang and Parr obtained the correlation energy as an explicit functional of the density and its gradient and Laplacian, now generally known as the “LYP” functional.

The well-known GGA functionals systematically improve the LDA and, in some calculations, approach the accuracy of traditional quantum chemical (e.g. Configuration Interaction) methods, at much less computational cost. However, according to the quasi local nature of GGA, the dispersion or long-ranged van der Waals interaction arising from long-ranged correlated electronic density fluctuations in the weak bonding systems such as noble gas dimmers could not be accurately described by either LDA or GGA. On the other hand,

similar to LDA, GGA has the difficulty to describe the hole centered far from the electron causing the hole.

Considering the local or semi local nature of LDA and GGA, Becke proposed the so-called Hybrid Density Functional method which incorporates the exact treatment of exchange by Hartree-Fock theory with DFT approximations for dynamical correlation. This idea was motivated by re-examination of the adiabatic connection,

$$H_\lambda = T + \lambda V_{ee} + \sum_i v_\lambda(r_i) \tag{1.44}$$

where λ is an inter-electronic coupling-strength parameter that "switches on" the $\frac{1}{r_{12}}$ Coulomb repulsion between electrons. $\lambda = 0$ corresponds to the non-interacting Kohn-Sham reference system, while $\lambda = 1$ corresponds to the fully interacting real system, with $\rho(r)$ being fixed as the exact ground state density of H_λ. The $E_{xc}[\rho]$ can be written as

$$E_{xc}[\rho] = \int_0^1 d\,\lambda U_{xc}^\lambda[\rho] \tag{1.45}$$

where,

$$U_{xc}^\lambda[\rho] = \langle \Psi_n^\lambda | V_{ee} | \Psi_n^\lambda \rangle - J[\rho] \tag{1.46}$$

The obvious first approximation for the λ dependence of the integrated in equation (1.45) is a linear interpolation, resulting in the Becke's half-and-half functional:

$$E_{xc}^{h\&h}[\rho] = \frac{1}{2}(U_{xc}^0 + U_{xc}^1) \tag{1.47}$$

where U_{xc}^0 is the exact exchange energy of the KS determinant and U_{xc}^1 is the potential energy contribution to the exchange-correlation energy of the fully interacting system. This half and half functional has the merit of having a finite slope as $\lambda \to 0$, and becomes exact if $E_{xc,\lambda=1}^{DFT}$ is exact and the system has high density. However, it does not provide a good quality of the total energy and the uniform gas limit is not obtained. Due to this Becke proposed the semi-empirical generalization of 3-parameter hybrid exchange-correlation functional

$$E_{xc}^{B3} = E_{xc}^{LSDA} + a_0(E_x^{exact} - E_x^{LSDA}) + a_x \Delta E_x^{GGA} + a_c \Delta E_c^{GGA} \tag{1.48}$$

where a_0, a_x and a_c are semiempirical coefficients to be determined by an appropriate fit to experimental data. E_x^{exact} is the exchange energy of the Slater determinant of the Kohn-Sham orbitals. ΔE_x^{GGA} is the gradient correction for the exchange and ΔE_c^{GGA} is the gradient correction for the correlation.

Whatever be the approximation for the exchange correlation functional we have to solve for a set of one-electron equation of type

$$\left[-\frac{1}{2}\nabla^2 + v_{eff}(r)\right]\Psi_i = \varepsilon_i \Psi_i \tag{1.49}$$

To solve this equation we need to find the coefficients c_i required to express Ψ_i in a given basis set φ_i^b:

$$\Psi_i = \sum_{i=1}^{N} c_i \varphi_i^b \tag{1.50}$$

N is in principle infinite but is practice one works with a limited set of basis functions. The types of basis functions are chosen according to the system under study. Generally, plane-wave basis sets are used in periodic calculations and Gaussian basis sets are used in cluster calculations.

A general expression for a basis function is given by,

$$f = N \times e^{-\alpha r} \tag{1.51}$$

Where N is the normalization constant, α is the orbital exponent and r is the radius. In 1950, S.F. Boys[111] suggested to use Gaussian type of function in molecular calculation. The Gaussian type functions contain the exponential $e^{-\beta r^2}$ rather than$e^{-\alpha r}$. The use of Gaussian type functions, being very easy to evaluate, significantly reduces the computational cost of molecular calculations. There are a significant number of basis sets which use such Gaussian-type orbitals (GTOs) [112-114]. Most commonly used basis sets are minimal basis sets, double-, triple- quadruple- zeta basis sets, split-valence basis sets, polarized basis sets and diffuse basis sets. The minimal basis set has a single basis function for each orbital. In double triple or quadruple zeta basis set there are multiple basis functions corresponding to each valence atomic orbitals. The split-valence basis set often denoted in the form X-YZg have X number of

primitive Gaussians comprising each core atomic orbitals. The valence orbitals are composed of two basis functions, one composed of a linear combination of Y primitive Gaussian and the other composed of a linear combination of Z primitive Gaussians. For example the basis set 3-21G splits each valence orbital into two parts, an inner shell and an outer shell. The basis function of the inner shell is represented by two Gaussians, and that of the outer shell by one Gaussian; the core orbitals are each represented by one basis function, each composed of three Gaussians. The 3-21G basis set supplemented with d-functions called polarization functions is designated 3-21G*.

1.2.2 Computational Formalism

Both methods based on Hartree-Fock (HF) theory and density functional theory (DFT) have their advantages and disadvantages. For example, DFT within the local spin density approximation (LSDA) calculations underestimate the band gaps of semiconductors. The discontinuity of exchange-correlation Kohn-Sham potential results in this discrepancy between theoretical and experimental band gaps. On the other hand, hybrid density functional theory incorporating HF exchange with DFT exchange-correlation has proved to be an efficient method for many systems. It has been verified that hybrid functionals can reproduce the band gaps of semiconductors and insulators quite well.

Though different DFT functionals may produce slightly different quantitatively but not qualitatively different results, studies on semi-conducting materials have shown that, hybrid functionals, in particular B3LYP, is one of the most efficient and computationally inexpensive among all the DFT functionals available for calculation of electronic and structural properties of the semiconducting materials. Hybrid functionals are in general found to be efficient in reproducing the band gaps of semiconductors and insulators [115,116] by treating the exchange part of the interactions better. Muscat *et al.*[115] have shown that the hybrid functional B3LYP reproduces the observed band gaps reliably in a wide variety of materials including semiconductors, ionic and semi-ionic oxides, sulphides and the transition metal oxides.

Bauschlicher [117] has studied the geometries, zero-point energies, and atomization energies of molecules containing first and second row atoms for several levels of theory, including Hartree-Fock theory, second order Moller-Plesset perturbation theory, and density functional theory with five different functionals, including two hybrid functionals and found that B3LYP yielded the best results. Studies by Tomic *et al.*[118,119] have shown that that the B3LYP functional provides better agreements with experimentally derived band gaps compared with results obtained with PBE0, correlated calculations, perturbation theories, and screened exchange functionals for a wide class of zinc-blend and wurtzite structured III-V materials. Similarly, calculations of properties such as ionization energies, electron affinities, electronegativities, hardnesses, fundamental frequencies, and zero-point energies of a wide range of molecules have shown that the hybrid functionals such as B3LYP represent a significant improvement over local and non-local density functional [120,121].

We have carried out here first-principles calculations on silicon nanotubes using hybrid density functional theory. In particular, we have used B3LYP (Becke's 3-parameter and the Lee-Yang-Parr exchange-correlation hybrid functional) and the 3-21G* basis set as implemented in the GAUSSIAN 03/09 suite of programs for full geometry optimizations without any symmetry constraints of the nanotube structures.[122, 123]

Our approach for construction of the nanotubes is based on single-walled carbon nanotubes. Here we have used finite cluster approach with dangling bonds terminated by hydrogen atoms to simulate the effect of infinite nanotubes. The easiest way to visualize how nanotubes are built is to start with graphite-like sheet of silicon. Then a single-walled nanotube (SWNT) is constructed by wrapping one single layer of the graphite-like sheet to form a cylindrical shape. The structure of such nanotubes can be described in terms of chirality and length. Chirality and diameter are specified in terms of the magnitude of the components of chiral vector. The chiral vector C_h which maps an atom from the left hand border onto an atom on the right border line is an integer multiple of the two basis vectors a_1 and a_2, i.e., $C_h=na_1+ma_2$

with integers n and m. Thus the geometry of any nanotube can be described by the integer pair (n, m) which determines the chiral vector. Depending upon how the sheet is rolled we have three types of tubes. For armchair m=n, for zigzag m=0 and for chiral nanotubes m≠n.

CHAPTER 2

AB INITIO STUDY OF SILICON NANOTUBES

In Section 2.1, the structural and electronic properties of single- and double-walled armchair silicon nanotubes will be discussed. Section 2.2 discusses the special geometric properties and electronic properties of single-walled zigzag silicon nanotubes.

2.1 Armchair Silicon Nanotubes

We have used the finite cluster approximation, using six unit cells of each nanotube with the dangling bonds at both ends of the tube saturated by hydrogen atoms to simulate the effect of infinite nanotubes. The presence of the hydrogen energy levels will not affect the band gaps of the nanotubes. Nanotubes are categorized as single-walled nanotubes(SWNTs) and multi-walled nanotubes(MWNTs). In this section, we focus on the structural and electronic properties of single-walled and double-walled armchair SiNTs.

2.1.1 Single-Walled Armchair Silicon Nanotubes

Single-walled nanotubes are quasi-one-dimensional structures composed of a single graphite-like layer rolled into a tubular structure. We have carried out calculations for SWSiNTs from (4, 4) to (12, 12). Full geometry and spin optimizations have been performed without any symmetry constraints with an all electron 3-21G* basis set and the B3LYP functional.

The binding energy or the binding energy per atom for each system was computed as the following formula:

$$E_b = \{[mE\,(\mathrm{Si}) + nE\,(\mathrm{H})] - E\,(\mathrm{Si}_m\mathrm{H}_n)\}/\,(m+n) \qquad (2.1)$$

Where m is the number of silicon atoms and n is the number of hydrogen atoms in the nanotube, and E(Si) and E(H) are the ground state total energies of the silicon and hydrogen atoms, respectively and $E(\mathrm{Si}_m\mathrm{H}_n)$ total energy of the optimized clusters representing the

nanotubes. All of our nanotubes are hydrogen terminated at the two ends to saturate the dangling bonds and to simulate the effect of infinity long tubes.

Table 2.1 shows the variations of the binding energies per atom versus the number of atoms in the SiNTs and variation of HOMO-LUMO gaps with the tube diameter. As the number of atoms increases the binding energy of SiNT increases. The largest SiNT studied here, (12, 12) has a binding energy of 3.465 eV/atom, about 75% of the bulk binding energy of 4.63 eV/atom. One of the central questions in the theory and applications of nanotubes is the possible metallic or semi-conducting properties of these tubes. To examine this we calculated the highest-occupied-molecular-orbital to lowest-unoccupied-molecular-orbital (HOMO-LUMO) gap. These can provide a measure of the band gap for the infinite solid as the number of atoms in the cluster increases and also helps to analyze the conductivity of the nanotube. The gaps for the SiNTs are in the range of 0.43 to 1.01 eV. These gaps are smaller than the bulk silicon gap of 1.1 eV but still not indicate any metallic behavior of silicon nanotubes even for the largest nanotube studied. We do note that as we go beyond the Si (6, 6) nanotube, with the tube diameter increasing, the gap decreases and tends to be saturated at 0.94eV. This feature is different from that observed in case of CNTs, which were found to be metallic in armchair configuration. Radial buckling is also calculated for the armchair SiNTs. Small nanotubes (Si (4, 4) and Si (5, 5)) have high buckling with a puckered "gear-like" structure[25] (the gear-like structure is that of a deformed tubular shape) and nanotubes from Si (6, 6) to Si (12, 12) have very small buckling with a smooth CNT-like tube (Fig.2.1).

Table 2.1 Binding energy per atom (eV), HOMO-LUMO gaps (eV), diameter (Å) and radial buckling* (Å) for armchair SiNTs.

Nanotube	Stoichiometry	Total No. of atoms	B. E. per atom (eV)	HOMO-LUMO gap (eV)	Diameter (Å)	Radial buckling(Å)
Si (4,4)	$Si_{80}H_{16}$	96	3.407	0.43	8.556	0.2724
Si (5,5)	$Si_{100}H_{20}$	120	3.431	0.52	10.666	0.2509
Si (6,6)	$Si_{120}H_{24}$	144	3.429	0.98	12.918	0.0386
Si (7,7)	$Si_{140}H_{28}$	168	3.441	1.01	14.588	0.0329
Si (8,8)	$Si_{160}H_{32}$	192	3.450	1.00	17.180	0.0305
Si (9,9)	$Si_{180}H_{36}$	216	3.455	0.98	19.312	0.0361
Si (10,10)	$Si_{200}H_{40}$	240	3.460	0.96	21.452	0.0317
Si (11,11)	$Si_{220}H_{44}$	264	3.463	0.94	23.580	0.0336
Si (12,12)	$Si_{240}H_{48}$	288	3.465	0.94	25.718	0.0342

*Radial buckling is determined by calculating the standard deviation of the radius of the nanotubes.

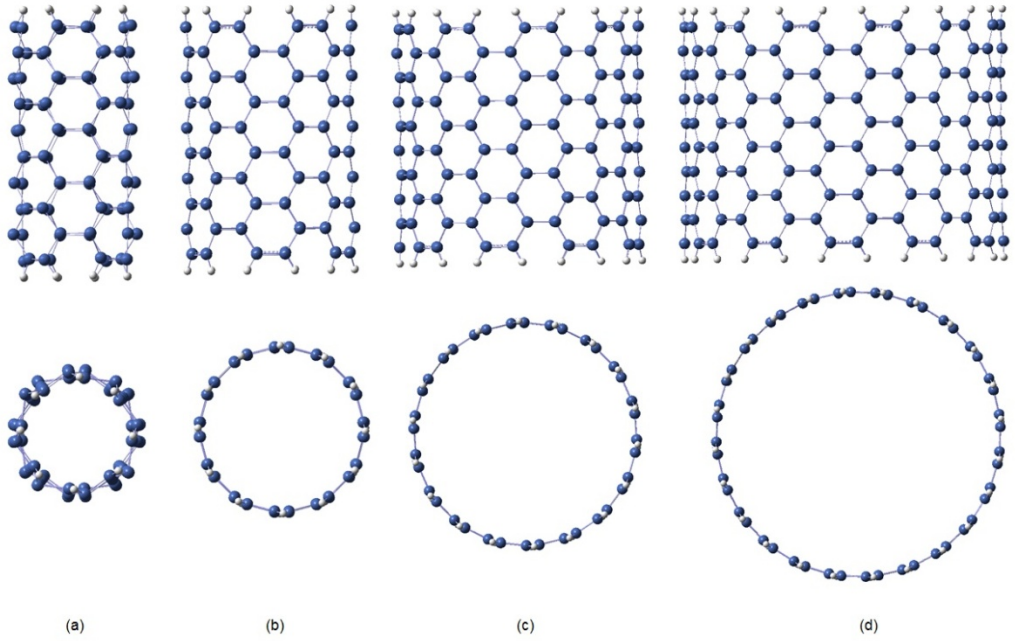

Figure 2.1 The optimized structure of the armchair (a) Si (4, 4); (b) Si (6, 6); (c) Si (9, 9); (d) Si (12, 12) nanotubes.

To explore the sensitivity of the results with respect to the basis set used, we compared our results with the results reported by Pradhan and Ray[7]. They have used B3LYP and the Los Alamos pseudopotential LANL2DZ[124] with the associated basis set to perform atomistic simulations of SiNTs. In Fig. 2.2, as the number of atoms increase the binding energy of silicon nanotubes increases with basis set of LANL2DZ and the binding energies from our result are commonly higher than theirs. Their largest SiNT studied, Si (9, 9) has a cohesive energy of 3.138 eV/atom, about 68% of the bulk binding energy of 4.63 eV/atom. As a comparison, the Si (9, 9) nanotube in our case has a cohesive energy of 3.455 eV/atom, about 74.6% of the bulk binding energy of 4.63 eV/atom. Pradhan and Ray also calculated the HOMO-LUMO gaps of the tubes. Beyond the Si (6, 6) nanotube with the tube diameter increasing, the gap decreases (Fig. 2.3). The HOMO-LUMO gaps from our results are smaller than theirs and as the tube diameter increases, the HOMO-LUMO gaps with the two basis sets tend to merge together and saturate at around 0.94 eV. In pseudopotential basis set, the small-core approximation assumes that there is no significant overlap between core and valence wave-function, resulting in a larger HOMO-LUMO gap than that of an all electron basis set. As the size of the nanotube increases, the total number of electrons gets larger, increasing the overlap of the orbitals, leading to a smaller gap difference between the two basis sets.

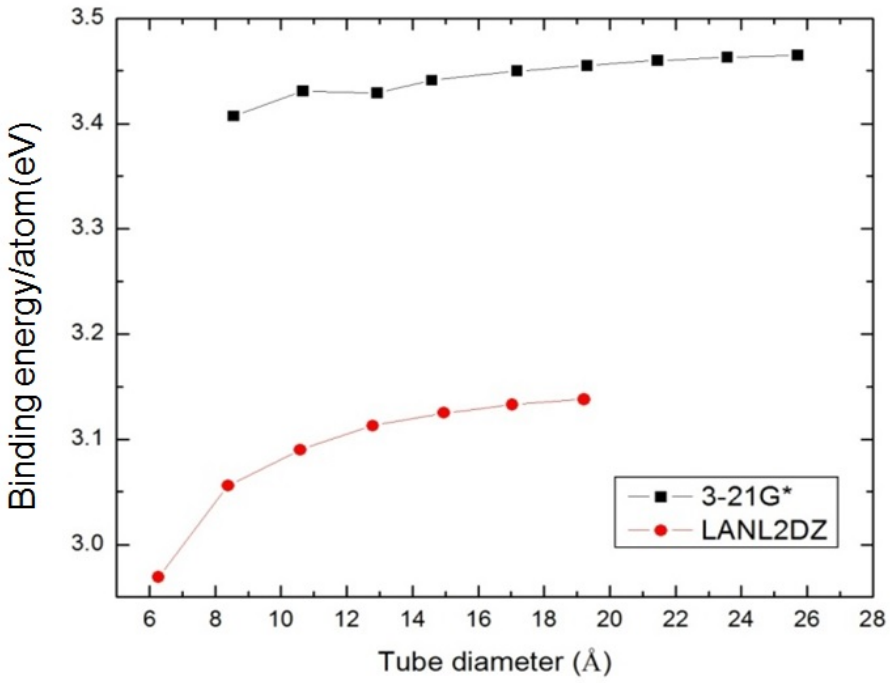

Figure 2.2 Binding energy/atom versus tube diameter for armchair SiNTs with basis set of 3-21G*and LANL2DZ.

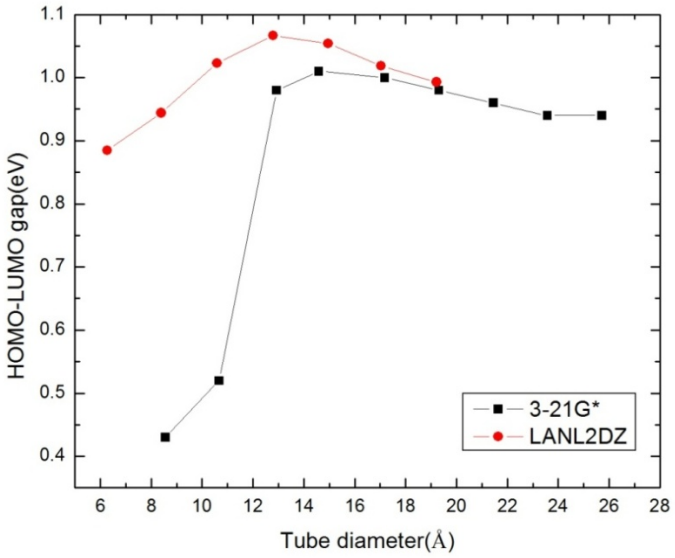

Figure 2.3 HOMO-LUMO gap versus tube diameter for armchair SiNTs with basis sets of 3-21G* and LANL2DZ.

2.1.2 Double-Walled Armchair Silicon Nanotubes

Although multi-walled nanotubes (MWNTs) have been synthesized and investigated first, there are very few *ab initio* studies on MWNTs compared to single-walled nanotubes (SWNTs), partly because of the complexity of MWNTs compared to SWNTs. A first step to study MWNTs is to study double-walled silicon nanotubes. A double-walled nanotube (DWNT) has inner concentric tube with smaller diameter inside its hollow. A cylindrical DWSiNT is built simply by assembling the two single-walled SiNTs in a coaxial configuration. The binding energy per atom was calculated using the same equation for SWSiNTs.

The formation energy for each DWNT is given by:

$$\Delta E = E(m, m) + E(n, n) - E[(m. m) @ (n, n)] \quad (2.2)$$

whereE(m, m) and E (n, n) are the optimized ground state total energies of SWSiNTs (m, m) and (n, n), respectively and E[(m, m)@(n, n)] is the optimized ground state total energy of a DWSiNT (m, m)@(n, n). Thus, a positive binding energy per atom represents the stability of a

nanotube (single- or double-walled) in the separated atom limit and positive formation energy of a double-walled nanotube is a measure of the stability of a double-walled nanotube relative to the constituent single-walled nanotubes.

Table 2.2: Tube diameter (in Å), radial buckling (in Å), B.E./Atom (in eV), and HOMO-LUMO gap (in eV) for SWSiNTs.

Nanotube	Stoichiometry	No. of atoms	Tube diameter (Å)	Radial buckling (Å)	B.E./atom (eV)	HOMO-LUMO gap (eV)	B.E./atom (eV) †	HOMO-LUMO Gap(eV) †
(3,3)	$Si_{60}H_{12}$	72	6.126	0.472	3.494	1.81	3.235	1.82
(4,4)	$Si_{80}H_{16}$	96	8.556	0.272	3.407	0.43	3.164	0.33
(5,5)	$Si_{100}H_{20}$	120	10.666	0.251	3.431	0.52	3.191	0.53
(6,6)	$Si_{120}H_{24}$	144	12.918	0.039	3.429	0.98	3.187	0.99
(7,7)	$Si_{140}H_{28}$	168	14.588	0.033	3.441	1.01	3.198	1.01
(8,8)	$Si_{160}H_{32}$	192	17.180	0.031	3.450	1.00	3.205	1.00
(9,9)	$Si_{180}H_{36}$	216	19.312	0.036	3.455	0.98	3.210	0.97
(10,10)	$Si_{200}H_{40}$	240	21.452	0.032	3.460	0.96	3.214	0.95
(11,11)	$Si_{220}H_{44}$	264	23.580	0.034	3.463	0.94	3.216	0.94
(12,12)	$Si_{240}H_{48}$	288	25.718	0.034	3.465	0.94	3.218	0.93

† single point run with basis set 6-311G* using the optimized structure from 3-21G*

Table 2.2 shows the results from Si(3, 3) to Si(12, 12) SWSiNTs, including the tube diameter, radial buckling, binding energy per atom, and HOMO-LUMO gap. The basis set 3-21G* was used initially for the optimizations of SWNTs followed by single point self-consistent-field energy computations with the 6-311G* basis set [125]. We note here that geometries are fairly insensitive to the choice of the basis set and optimizations of large nanotubes with a large basis set such as 6-311G* can be rather demanding computationally. This procedure also has the added advantage to gauge the effects of basis sets on the properties of the nanotubes studied. After some initial oscillations, as shown in Fig.2.4, the binding energy increases monotonically saturating to a value of around 3.46eV. The trend is consistent with the results obtained with the basis set 6-311G*, the major difference being the saturated binding energy value of 3.22eV. Thus, a larger basis set, though producing lower total energy values, yields a

lower saturated binding energy per atom value by about 0.24eV. We note here that the nanotube Si(3,3) has the highest binding energy per atom with the largest buckling associated with puckered structure and sp^3-type bonding. Fig. 2.5 shows the HOMO-LUMO gaps of the SWSiNTs using both 3-21G* and 6-311G* basis sets and the gaps appear to be fairly insensitive to the choice of the basis set except for Si(4,4). For example, the largest gap obtained was 1.81eV and the smallest is 0.94 eV for Si(3, 3) and Si(12, 12) tubes with a 3-21G* set. The corresponding values are 1.82eV and 0.93eV with the larger 6-311G* set. We note also that the gaps are characteristic of "band gaps" for a typical semiconductor in that the experimental value of the band gap of Si is 1.11eV at 300K. Also, the nanotube Si(3, 3) with the highest binding energy per atom has the largest buckling associated with a more puckered structure and sp^3-type bonding. The only exception, as mentioned before, is the Si(4, 4) tube, where the gaps are 0.43 and 0.33eV, with the smaller and larger basis sets respectively. This can be attributed to several factors, such as the dependence of finite basis sets to a "more puckered" structure and the centrally localized natures of the HOMO and the LUMO compared to the delocalized nature of these orbitals for other tubes. Specifically, we have plotted the HOMOs and the LUMOs for some single-walled SiNTs (Fig. 2.6). The HOMO and LUMO for Si (4, 4) are localized in the middle of the nanotube but delocalized for other SiNTs such as Si (6, 6). We note here that finite basis sets do not necessarily have a systematic influence on HOMO-LUMO gaps, indicating that a uniform pattern for the change of HOMO-LUMO gap may not be obtained when we change the size of the basis set.

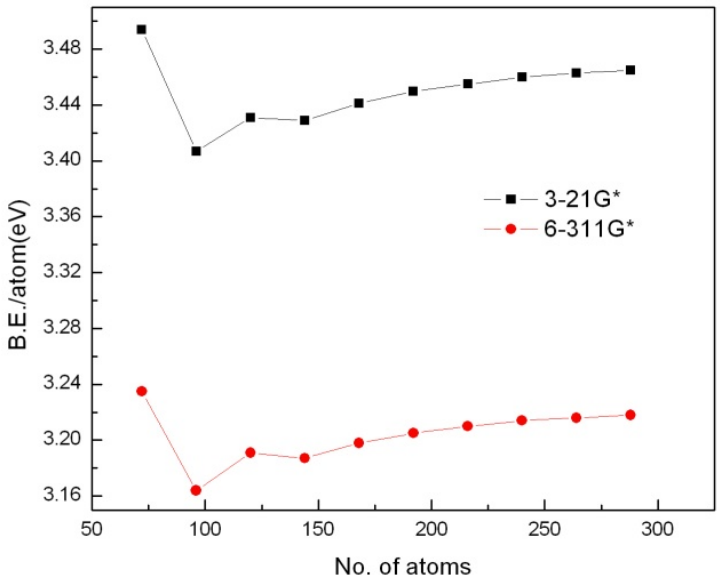

Figure 2.4 Variation of B.E./atom (eV) *versus* the number of atoms.(for SWSiNTs)

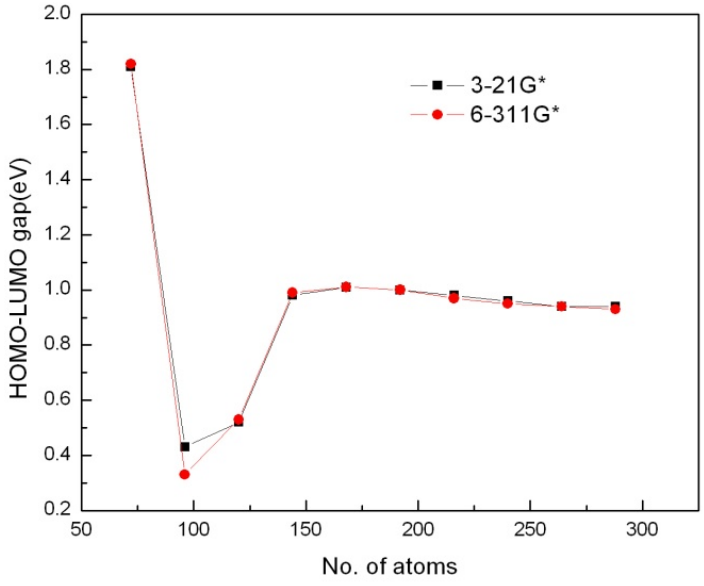

Figure 2.5 HOMO-LUMO gap *versus* the number of of atoms.(for SWSiNTs)

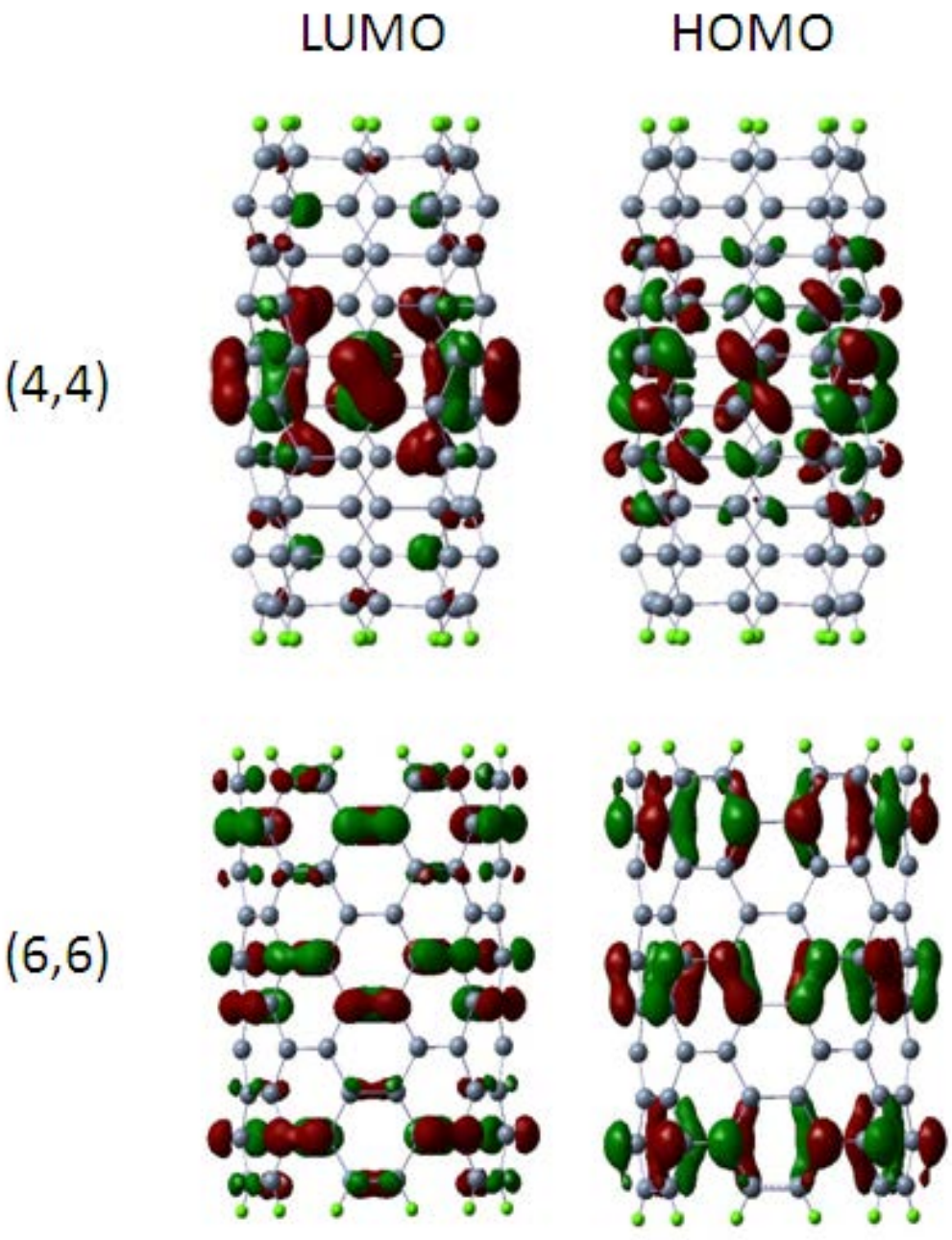

Figure 2.6 HOMO and LUMO plots for Si(4,4) and Si(6,6).

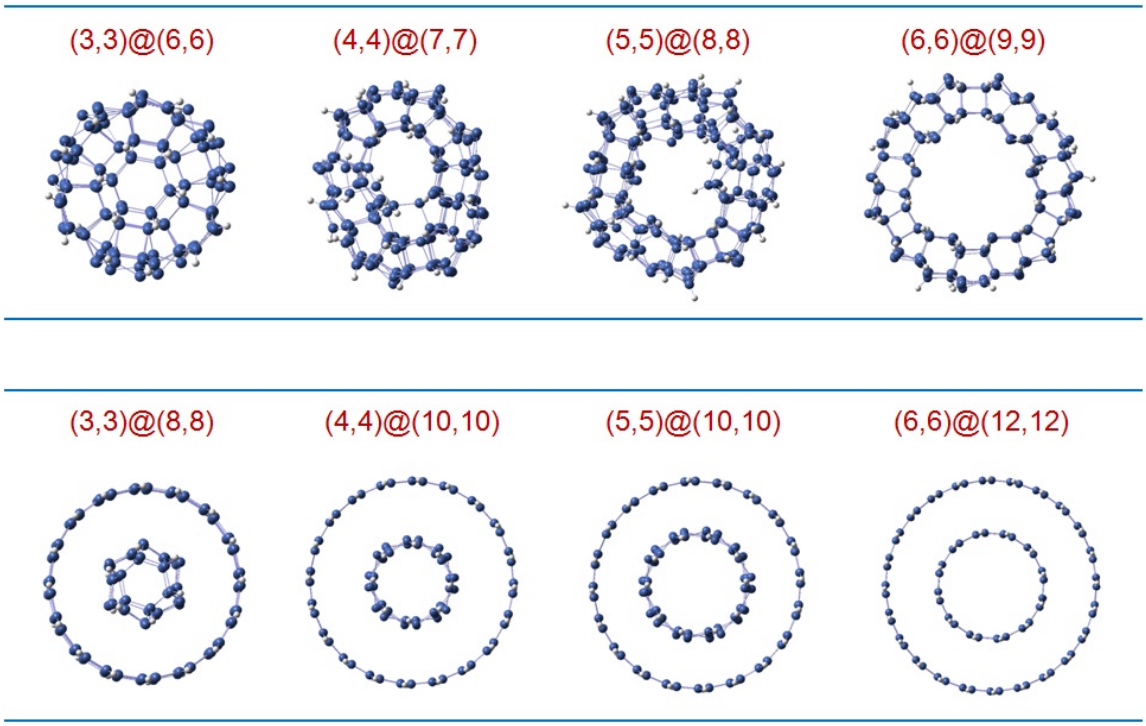

Figure 2.7 Top view of (3,3)@(6,6), (4,4)@(7,7), (5,5)@(8,8), (6,6)@(9,9), (3,3)@(8,8), (4,4)@(10,10), (5,5)@(10,10), (6,6)@(12,12) double-walled SiNTs. Two examples incorporating one “meshed” and one non- “meshed” nanotube for each group are shown.(Four groups:(3,3)@(n,n),(4,4)@(n,n),(5,5)@(n,n),(6,6)@(n,n))

As mentioned before, the DWNTs were constructed by inserting optimized SWNTs inside one another and re-optimizing. Fig. 2.7 shows the top views of optimized geometries of several double-walled SiNTs. As should be noted, discussed below in detail, some DWNTs maintain the double-walled cylindrical structure after optimiztion while others do not. We call the second set “meshed” DWSiNTs. Fig. 2.8 and Table 2.3 show the variations of binding energies per atom with respect to the total number of atoms in the separated atom limit for 22 double walled SiNTs. For (3, 3) @ (n, n) (n =6-12), (4, 4) @ (n, n) (n =7-12) and (5, 5) @ (n, n) (n =8-12), the binding energy first decreases and then shows an increasing pattern. For the (6, 6) @ (n, n) (n =9-12), the binding energy per atom shows a monotonically decreasing pattern. We also note from Tables 2.2 and 2.3 that the stabilities of DWSiNTs are of the same order as

those of SWSiNTs. The largest value of the binding energy of a SWSiNT obtained in this study is 3.494 eV/atom for the (3, 3) tube whereas the largest value of a DWSiNT is 3.702 eV/atom for the (5,5)@(8,8) tube, both with the 3-21G* basis set. The results from 6-311G* shows the same trend as the results we get from 3-21G*. In Figure 2.8, the binding energies per atom from 6-311G* are commonly lower than those from 3-21G* with a difference of 0.24eV approximately, which is the same as what has been observed for the armchair SWSiNTs. Though not directly comparable, we note here that the experimental value of the binding energy of Si is approximately 4.7eV/atom. The effects of the basis sets on the binding energies have been estimated by calculating the basis set superposition error (BSSE) energy [126-128] for a typical system Si(6, 6) @ (9, 9) and the constituent tubes Si (6,6) and Si (9, 9). The BSSE energy for Si(6, 6) is 0.003eV/atom and for Si(9, 9) is 0.002eV/atom, for (6 ,6)@(9, 9) is 0.001eV/atom, all computed with the 3-21G* basis set. As can be inferred from the data in Table2.2 and 2.3, these energies are negligible compared to the binding energy per atom for the single- and double-walled SiNTs and the trends are expected to be same for all other tubes with no significant effects on the conclusions of this study.

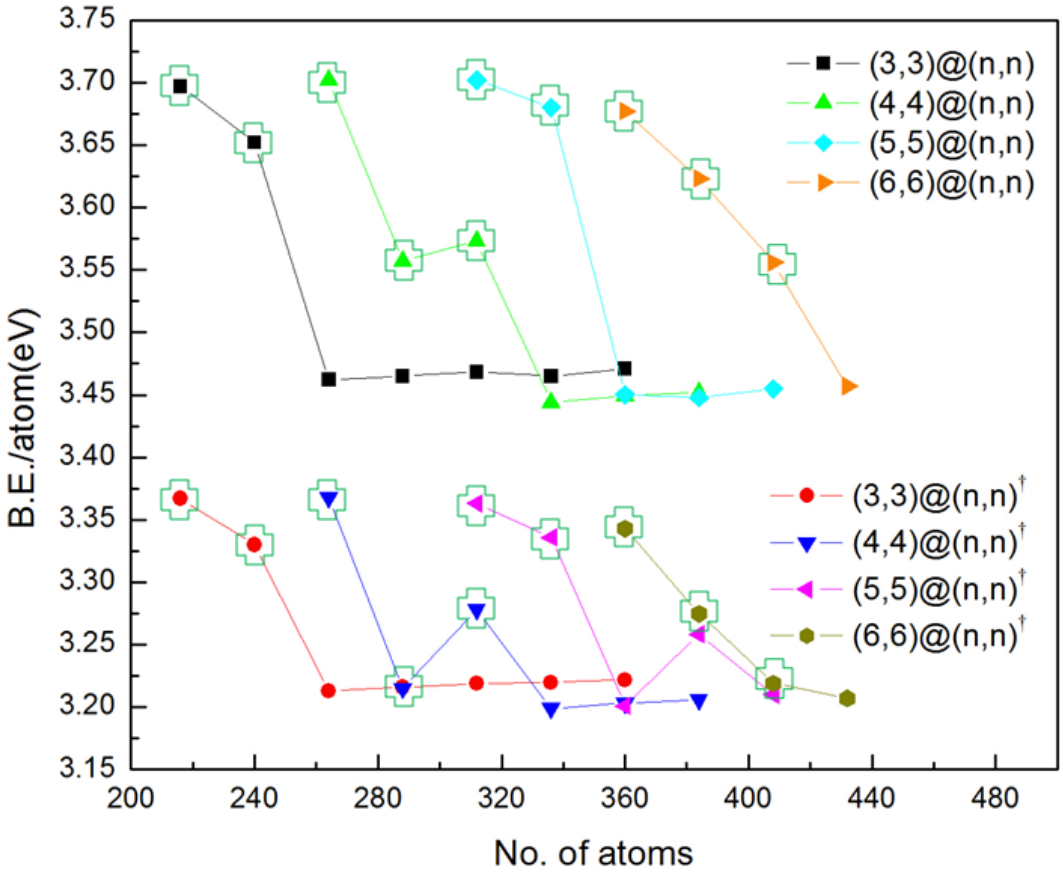

Figure 2.8 Variation of B.E./atom (eV) *versus* the number of atoms for (3,3)@(n,n) (6≤n≤12),(4,4)@(n,n) (7≤n≤12), (5,5)@(n,n) (8≤n≤12) and (6,6)@(n,n) (9≤n≤12). (†computation with 6-311G*, the data points within hollow green cross are “meshed” nanotubes.)

Table 2.3 Interlayer separation (in (Å), binding energy per atom (in eV), formation energy (in eV) and HOMO-LUMO gap (in eV) for Si DWNTs.

Nanotube	Stoichiometry	No. of atoms	Interlayer separation (Å)	B.E./ atom (eV)	Formation energy ΔE(eV)	HOMO-LUMO gap(eV)	B.E./ atom (eV)†	Formation energy ΔE(eV) †	HOMO-LUMO gap (eV)†
(3,3)@(6,6) *	$Si_{180}H_{36}$	216	3.054	3.697	53.28	1.23	3.367	35.44	1.22
(3,3)@(7,7) *	$Si_{200}H_{40}$	240	3.442	3.652	46.83	1.16	3.330	29.20	1.15
(3,3)@(8,8)	$Si_{220}H_{44}$	264	5.521	3.462	0.171	0.99	3.213	-0.220	0.99
(3,3)@(9,9)	$Si_{240}H_{48}$	288	6.597	3.465	-0.131	0.97	3.216	-0.153	0.97
(3,3)@(10,10)	$Si_{260}H_{52}$	312	7.662	3.468	-0.041	0.96	3.219	-0.049	0.95
(3,3)@(11,11)	$Si_{280}H_{56}$	336	8.725	3.465	-0.024	0.94	3.220	-0.023	0.94
(3,3)@(12,12)	$Si_{300}H_{60}$	360	9.524	3.471	-0.024	0.93	3.222	-0.022	0.93
(4,4)@(7,7) *	$Si_{220}H_{44}$	264	2.923	3.702	73.03	0.64	3.368	48.0	0.65
(4,4)@(8,8) *	$Si_{240}H_{48}$	288	3.953	3.557	33.79	0.34	3.215	16.81	0.33
(4,4)@(9,9) *	$Si_{260}H_{52}$	312	4.821	3.573	39.74	0.27	3.278	22.36	0.28
(4,4)@(10,10)	$Si_{280}H_{56}$	336	6.509	3.444	0.188	0.43	3.199	-0.134	0.44
(4,4)@(11,11)	$Si_{300}H_{60}$	360	7.595	3.449	0.454	0.85	3.203	0.364	0.94
(4,4)@(12,12)	$Si_{320}H_{64}$	384	8.663	3.452	0.484	0.87	3.206	0.408	0.93
(5,5)@(8,8) *	$Si_{260}H_{52}$	312	2.988	3.702	79.52	0.59	3.363	50.99	0.60
(5,5)@(9,9) *	$Si_{280}H_{56}$	336	3.090	3.680	76.92	0.54	3.336	44.71	0.76
(5,5)@(10,10)	$Si_{300}H_{60}$	360	5.388	3.450	-0.029	0.48	3.201	-0.099	0.51
(5,5)@(11,11)	$Si_{320}H_{64}$	384	6.522	3.448	-0.132	0.51	3.258	-0.192	0.23
(5,5)@(12,12)	$Si_{340}H_{68}$	408	7.583	3.455	-0.106	0.52	3.210	-0.134	0.53
(6,6)@(9,9) *	$Si_{300}H_{60}$	360	3.064	3.677	81.87	0.39	3.343	51.17	0.43
(6,6)@(10,10) *	$Si_{320}H_{64}$	384	3.207	3.623	65.43	0.33	3.275	27.32	0.65
(6,6)@(11,11) *	$Si_{340}H_{68}$	408	4.599	3.556	41.14	0.28	3.219	20.54	0.44
(6,6)@(12,12)	$Si_{360}H_{72}$	432	6.409	3.457	-0.327	0.66	3.207	-0.393	0.78

* "meshed" double walled SiNT
† single point run with basis set 6-311G* using the optimized structure from 3-21G*
The "interlayer separation" of the "meshed" nanotube is calculated by taking the difference between the average radius of the Si atoms on the inner wall and on the outer wall.

Fig.2.9 and 2.10 show the variation of the formation energy with respect to the interlayer separation of all DWSiNTs, both coaxial and "meshed" tubes. The formation energy gives a measure of the stability of a DWSiNT with respect to the individual SWSiNTs. The variation of the formation energy with respect to the interlayer separation, as studied in some

earlier computational works on DWSiNTs, have shown that there is a most favorable interlayer separation of a DWSiNT depending on the constituent atoms of the nanotubes. For DWNTs with Si(3, 3) as inner tube, the maximum formation energy is 53.28eV for an interlayer separation of 3.054 Å with the 3-21G* basis set and 35.44eV with the 6-311G* set. With Si(4, 4) as inner tube, the corresponding numbers are 73.03eV and 2.923 Å with the 3-21G* set and 48.00eV with the 6-311G* set. We note here the existence of a peak, characterized by a separation point of the “meshed” tubes and the co-axial tubes, in the formation energy of (4,4) @ (n,n) for both basis sets. The interlayer separation was calculated by taking the difference of average diameters of inner and outer tube, and then divided by two. The same method was used to calculate the interlayer separation for both “meshed” nanotubes and co-axial double-walled SiNTs. However, due to the non-coaxial nature of “meshed” tubes, the interlayer separation measure should be exercised with caution. We have included them in the plots and in the discussions below for the sake of completeness(Fig. 2.11 and 2.12).

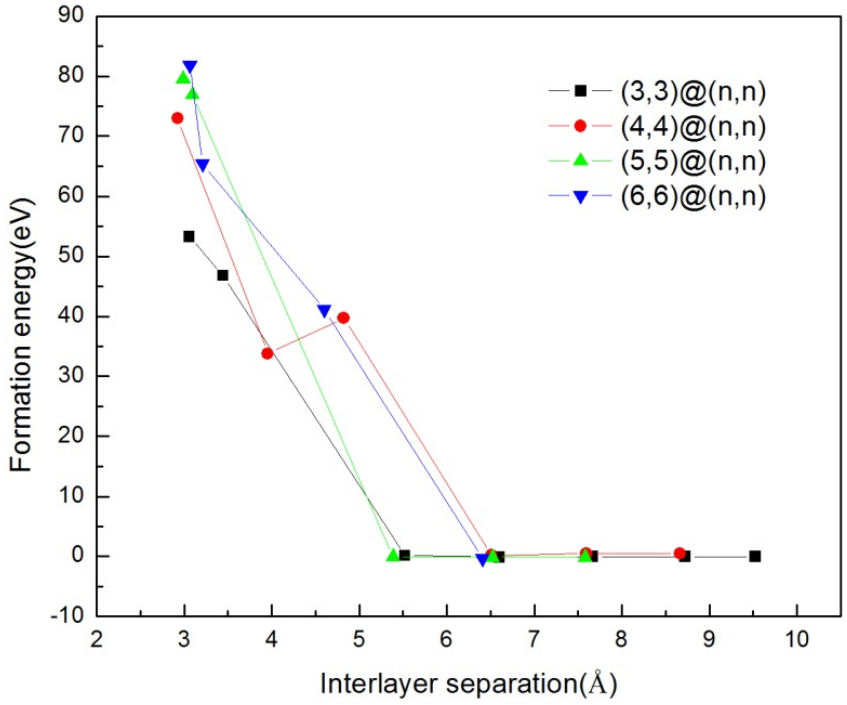

Figure 2.9 Variation of formation energy (eV) *versus* the interlayer separation (Å) with 3-21G*.(for DWSiNTs)

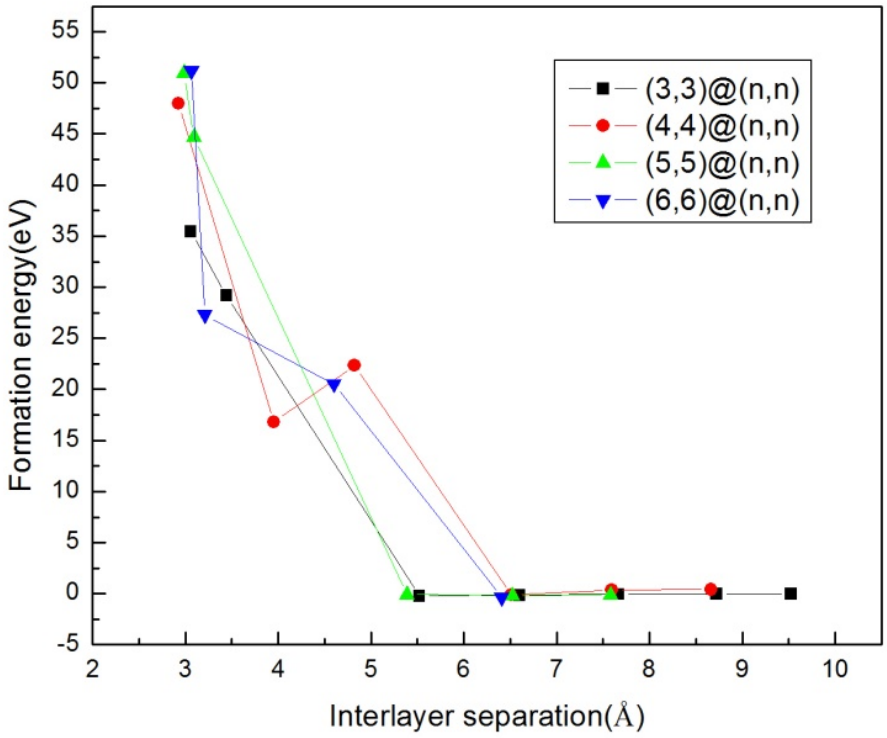

Figure2.10 Variation of formation energy (eV) *versus* the interlayer separation (Å) with 6-311G*.(for DWSiNTs)

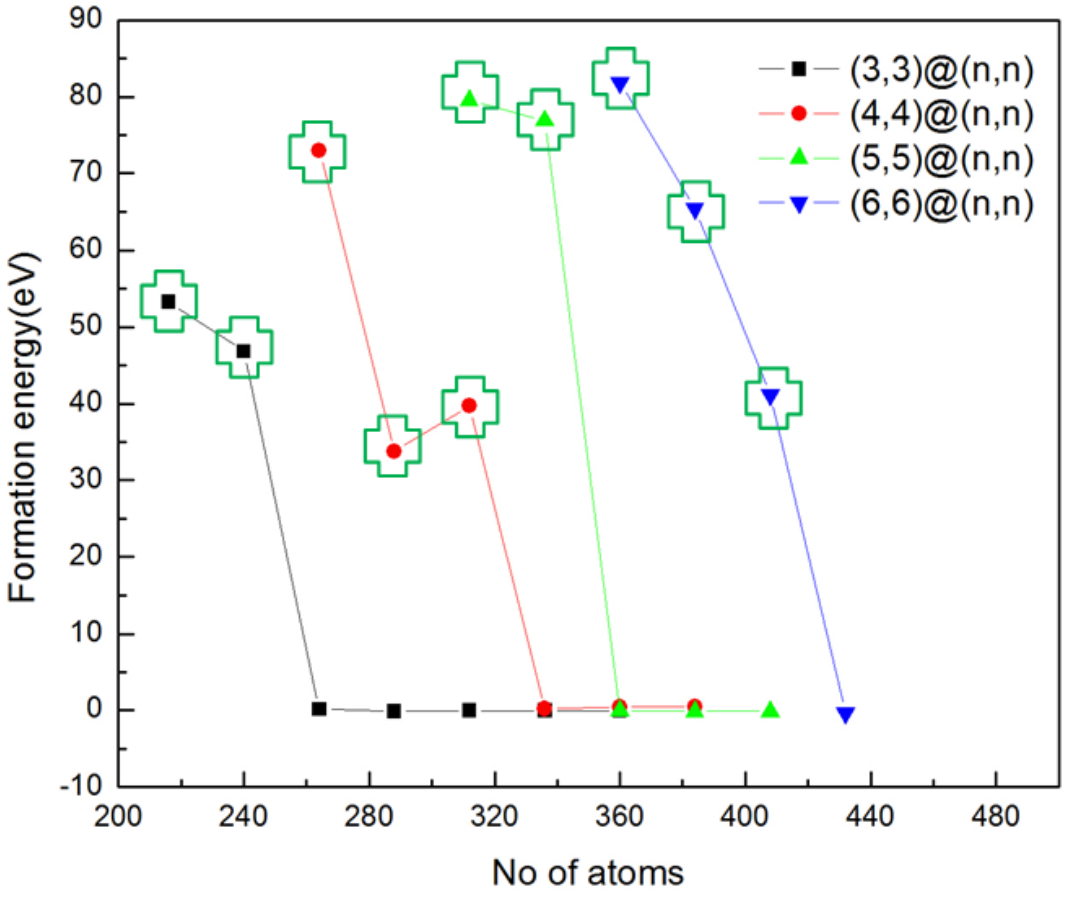

Figure 2.11 Variation of formation energy (eV) *versus* the number of atoms with 3-21G*. (for DWSiNTs)

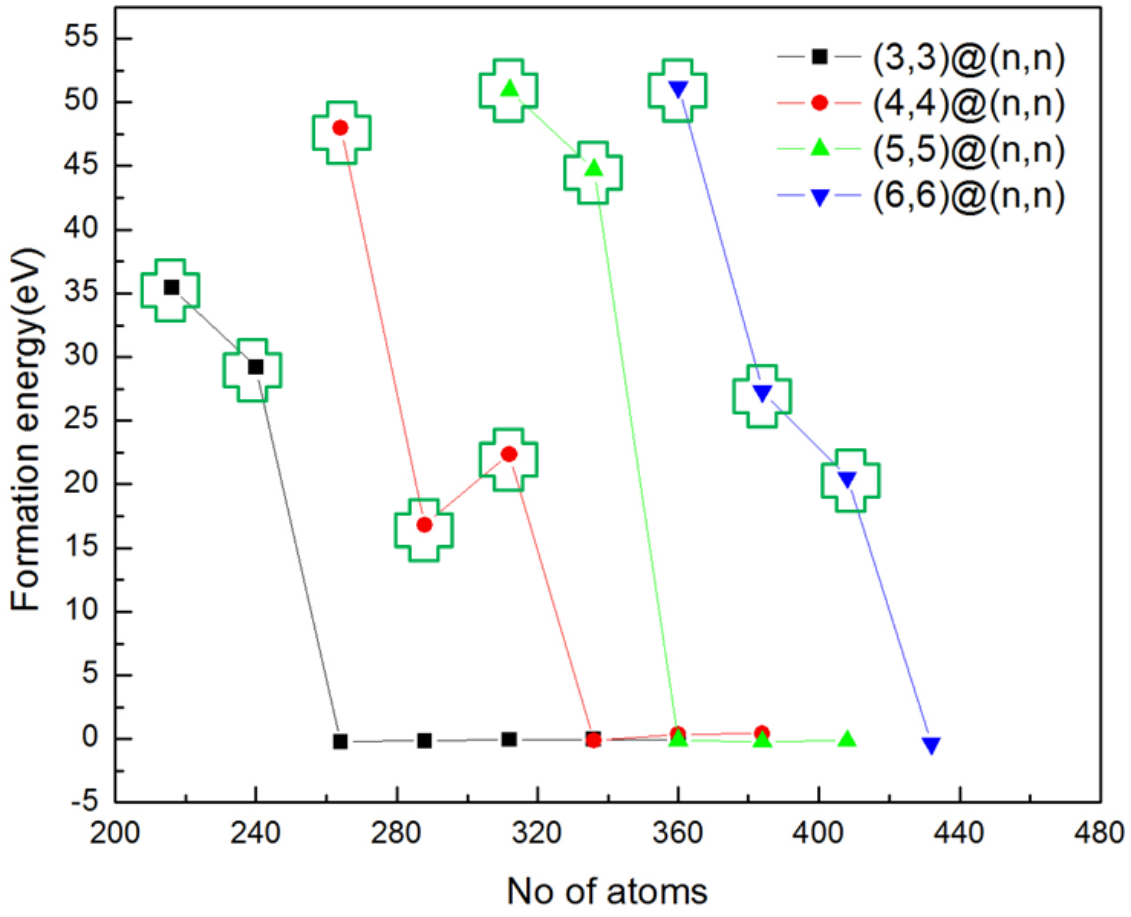

Figure 2.12 Variation of formation energy (eV) *versus* the number of atoms with 6-311G*. (for DWSiNTs)

For Si(5, 5) as the inner tube, with the smaller basis set, the maximum formation energy was found to be 79.52eV with an interlayer separation of 2.988 Å when the outer tube is Si(8, 8) and the maximum formation energy is 50.99eV with the larger basis set. For Si(6, 6) as the inner tube, the corresponding values are 81.87eV and 3.064 Å, and 51.17eV. Thus the formation energy of DWSiNTs is found to have a maximum around an interlayer separation of about 3.0 Å. This has been observed before in our studies of SiC double-walled nanotubes [129, 130]. We also note that these smaller nanotubes are no longer co-axial tubes with two separate walls. Fig.2.7 shows the top view of these nanotubes (the upper four nanotubes). The nearest Si-Si distance between the inner and the outer walls is 2.43 Å which is close to the bond length of the Si dimer, indicating the formation of Si-Si covalent bonds. Cylindrical DWSiNTs containing coaxial SWSiNTs are unlikely to be synthesized owing to their high energetic disadvantage. We do note that the structures of a number of theoretically proposed DWSiNTs with faceted wall surfaces have been calculated from first-principles calculations [39]. Tang *et al*. demonstrated the self-organized growth of small-diameter (13nm) SiNTs [131]. The structures of the silicon nanotubes reported are hollow inner pore, crystalline silicon wall layers with a 0.31 nm inter-planar spacing. Therefore, the interlayer spacing obtained in our models agrees well with experimental result. These can be called “meshed” double walled SiNTs (the upper four nanotubes in Fig.2.7) because one tube is like a gear meshed with another tube from top view. We note that (6,6)@(9,9) is a particularly stable DWSiNT, with the second highest binding energy and the highest formation energy among all the tubes studied here. The large nanotubes do not deform like small nanotubes (i.e. the lower four nanotubes in Fig. 2.7) and the nearest Si-Si distance between the inner and the outer walls is 5.11 Å, which means that the Si-Si bonds are not particularly strong between the inner and the outer walls. These double walled SiNTs, although with coaxial two separate walls configuration, have small formation energies, several of them being negative, indicating they are not stable compared to SWSiNTs. The results on formation energies from the larger basis set 6-311G* basis set do not indicate any

discernibly different behavior. It should be noted that some tubes in Table 2.3 have negative formation energies. The negative formation energies and relatively larger interlayer separation indicate that there is no interaction between the inner and outer tubes, and the constituent single-walled nanotubes are more stable individually than the double-walled nanotubes, as mentioned before in the definition of the formation energy.

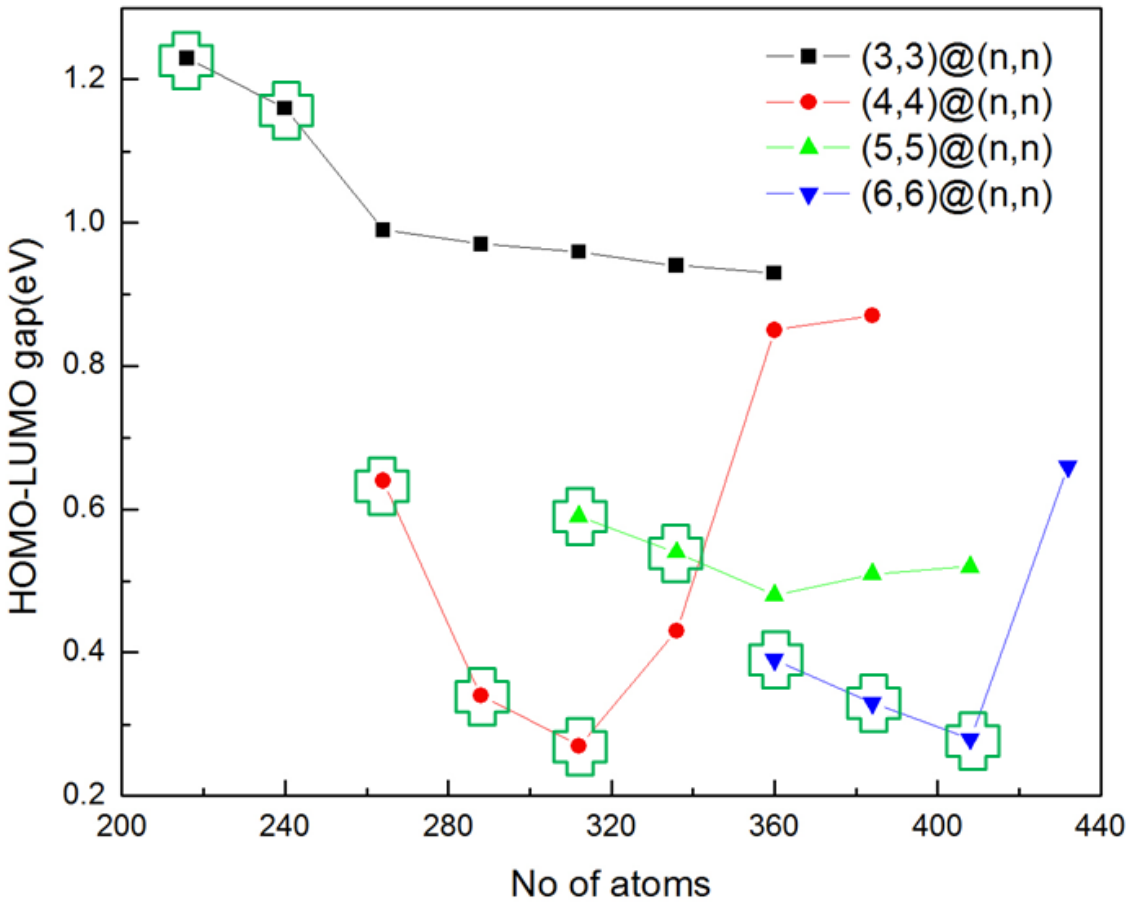

Figure 2.13 HOMO-LUMO gap *versus* the number of atoms at the 3-21G* level. (for DWSiNTs)

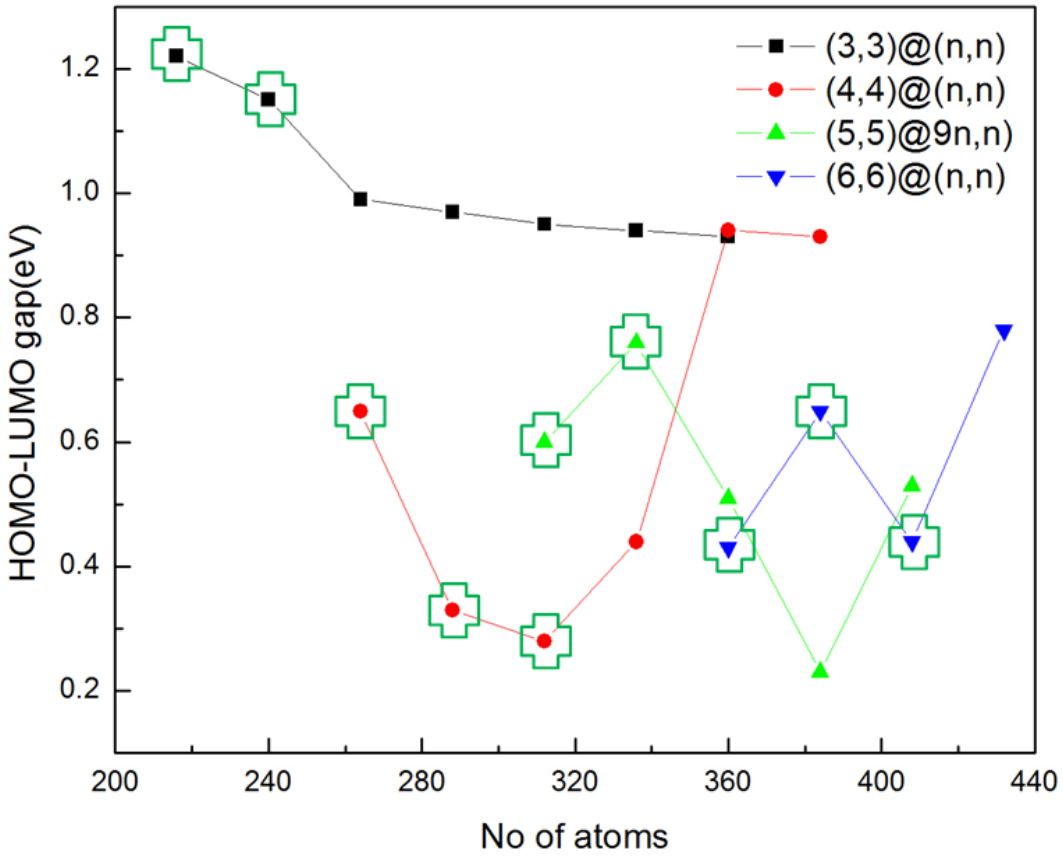

Figure 2.14 HOMO-LUMO gap *versus* the number of atoms at the 6-311G* level. (for DWSiNTs)

The energy differences between HOMO and LUMO give a measure of the "band gap" for the "infinite" nanotubes. This measure is qualitative in the sense that the tubes studied here are finite in length and any extrapolation to infinite tubes should be viewed with caution. Fig. 2.13 and 2.14 show the variation of the band gaps of the DWNTs with respect to the number of atoms at the levels of the two basis sets. At the 3-21G* level, all the DWSiNTs are narrow band gap semiconductors with the band gap varying from 0.28 to 1.23eV. The corresponding numbers are 0.23 and 1.22eV at the 6-311G* level, indicating the same semiconducting characteristic. These gaps are, in general, smaller than the gaps obtained for the SWSiNTs. We also note that, at the 3-21G* level, the band gap decreases first and then increases as the size

of the DWSiNT increases for(4, 4) @ (n, n) (n =7-12), (5, 5) @ (n, n) (n =8-12)and(6, 6) @ (n, n) (n =9-12). But for (3, 3) @ (n, n) (n =6-12), the band gap shows a monotonically decreasing trend. The HOMO-LUMO gaps from 6-311G* are very close to those from 3-21G*, specifically for the nanotubes (3,3)@(n,n) (n=6-12) and (4,4)@(n,n) (n=7-12). For (5,5)@(n,n) (n=8-12) and (6,6)@(n,n) (n=9-12), we observe a different trend when we change the basis set from 3-21G* to 6-311G*. For the larger basis set, the gaps oscillate, indicating different ionization behavior. Guided by our results for the SWSiNTs, we plotted the HOMOs and the LUMOs for the DWSiNTs and some of the results are shown in Fig.2.15, We note that the orbitals are non-centrally localized, for example, for (5,5)@(9,9) and (6,6)@(10,10) but delocalized for (6,6)@(9,9). The nature of the localizations and possible lack of hybridizations can result in an increase of the HOMO-LUMO gap, resulting in oscillatory behaviors. Clearly, the localization features of the orbitals have a direct influence on gaps for both SWNTs and DWNTs. It is also worth noting that both (5,5)@(9,9) and (6,6)@(10,10) have relatively higher buckling and charge transfer. Although DWSiNTs and SWSiNTs have very close binding energy per atom, their electronic structures are quite different. For example, the band gaps of (6,6) and (9,9) are all 0.98eV, however the band gap of (6,6)@(9,9) decreases to 0.39eV. This is clearly illustrated in the density-of-states plot of (6,6), (9,9), and (6,6)@(9,9) tubes in Fig. 2.16. Fig.2.17 shows the HOMO and LUMO plots of (6,6), (9,9) and (6,6)@(9,9) nanotubes.

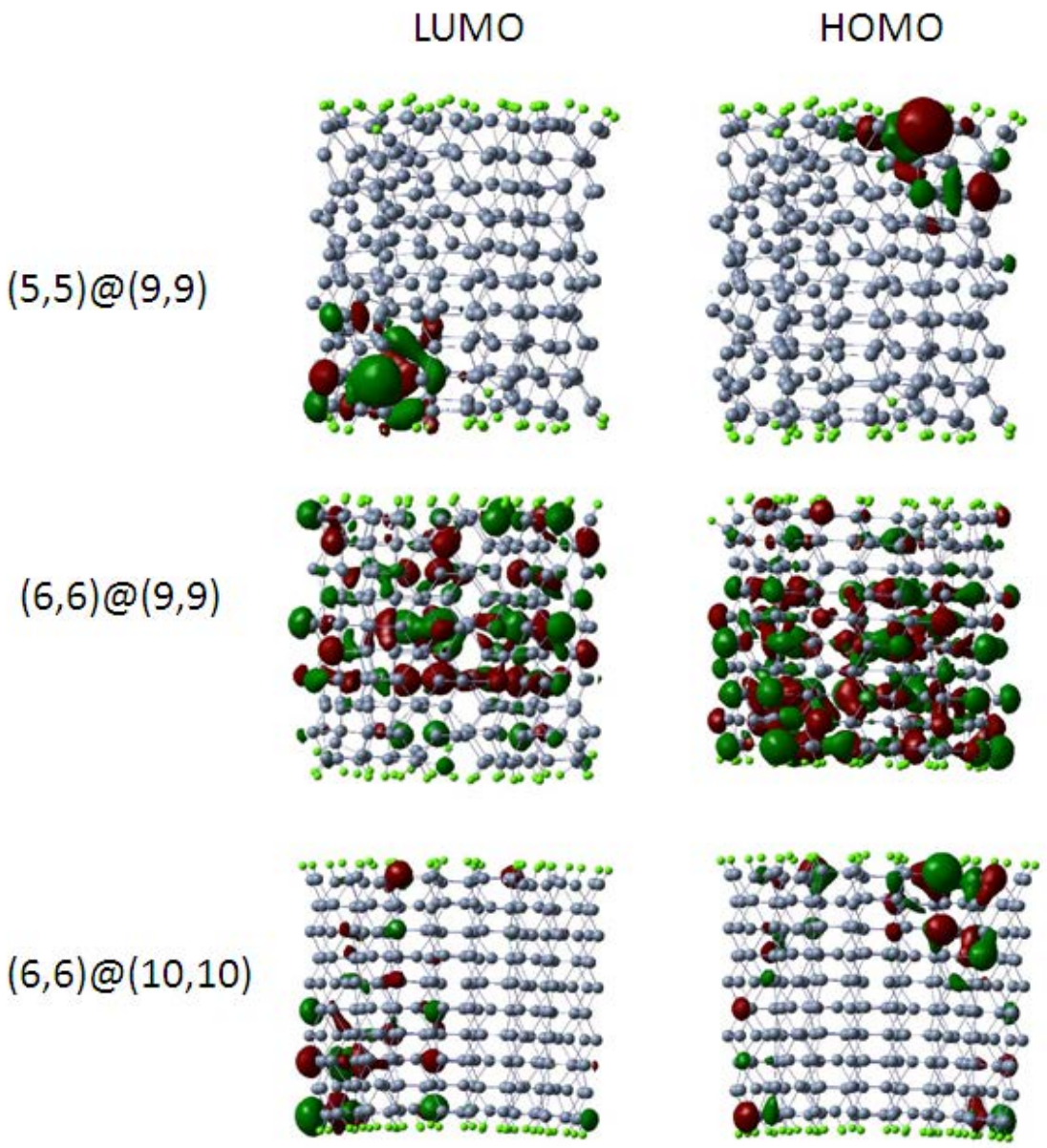

Figure 2.15 HOMO and LUMO plot for three double-walled nanotubes: (5,5)@(9,9),(6,6)@(9,9) and (6,6)@(10,10).

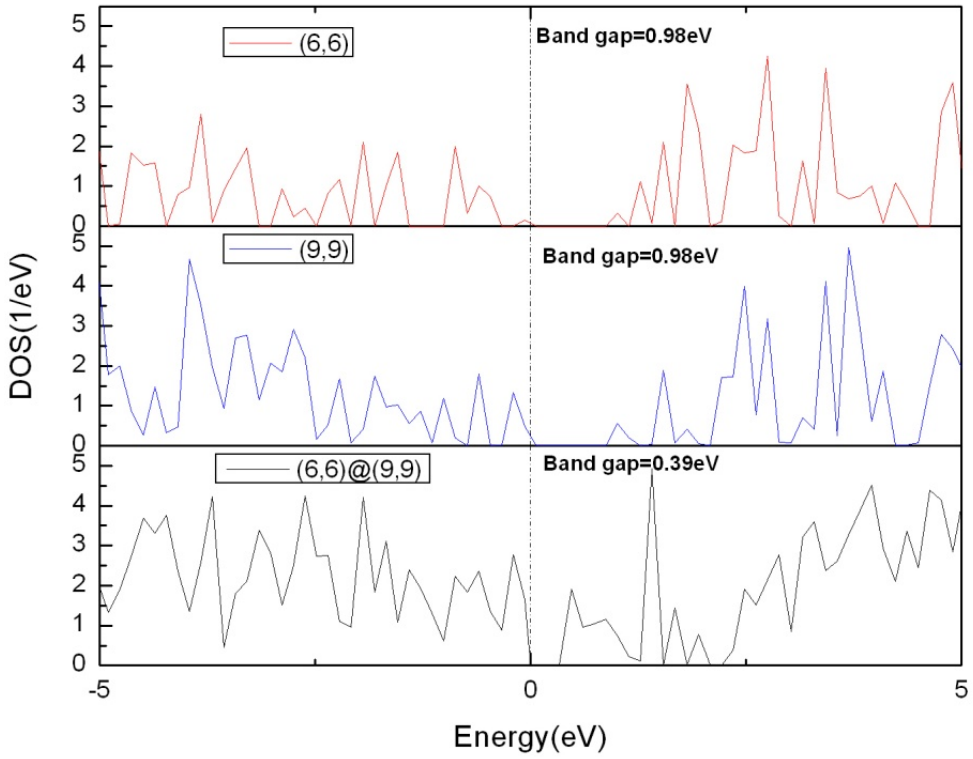

Figure 2.16 Density of states (DOS) of (6,6), (9,9) and (6,6)@(9,9) Si nanotubes.

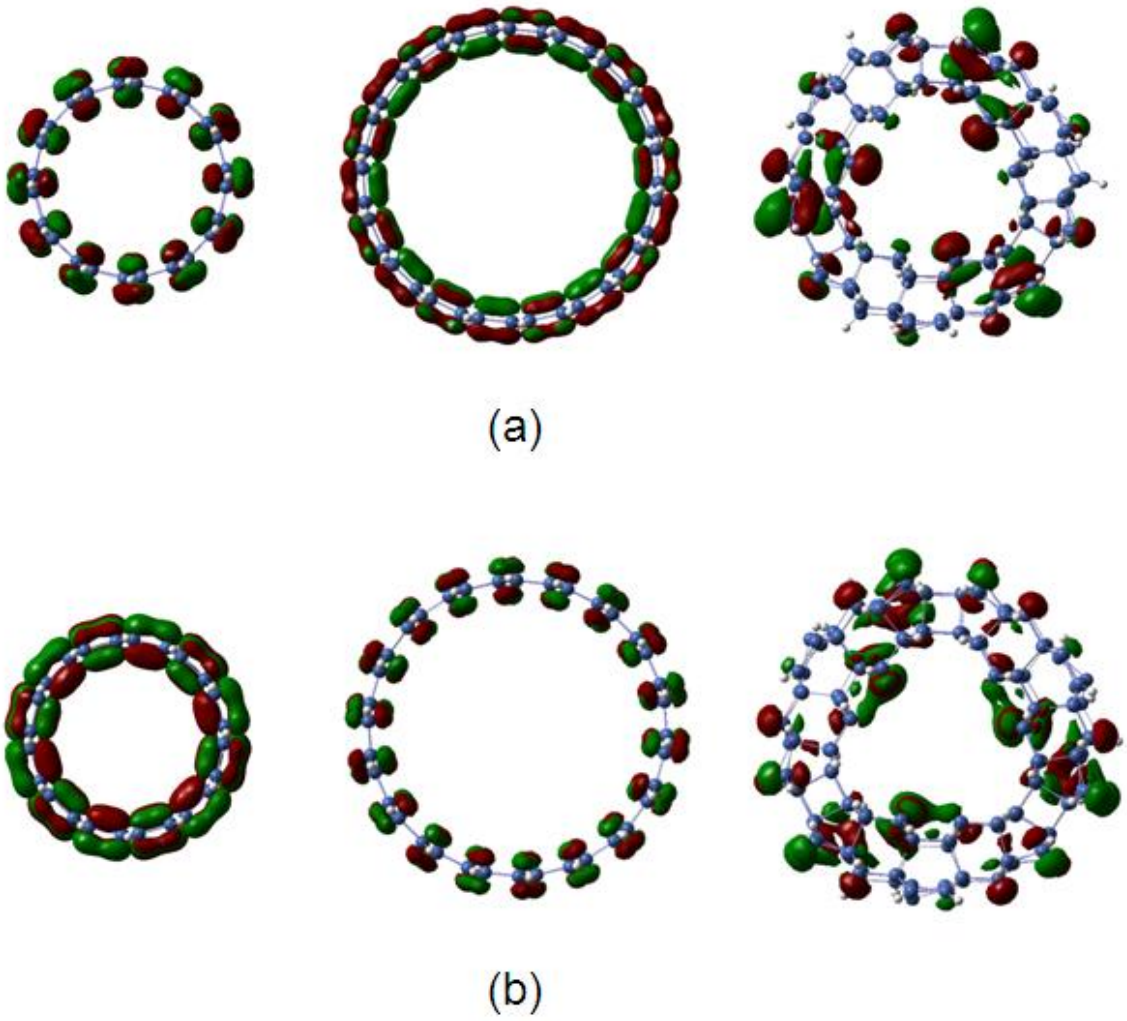

Figure 2.17 (a)HOMO of (6,6),(9,9) and (6,6)@(9,9) and (b) LUMO of (6,6), (9,9) and (6,6)@(9,9).

After optimization, the nanotube surfaces were found to be slightly rippled. Nearly half of the Si atoms display the characters of sp^3-type bonding, whereas others have more sp^2-typebonding. The radial buckling β is determined by calculating the standard deviation of the radius of the Si atoms. Table 2.4 shows the variation of buckling of inner and outer walls with respect to the diameters of the inner and outer tubes. The buckling of the inner tubes is, in general, larger than the buckling of the tubes in single-walled geometry. As the interlayer separation increases, the buckling of the inner tube decreases and approaches its

corresponding value in single-walled configuration. For example, buckling of the Si nanotube (3, 3) is calculated to be 0.472 Å in single-walled configuration. In double-walled configuration (3,3)@(6,6), the buckling of inner tube (3,3) is 0.485 Å, which decreases to 0.473 Å in (3,3)@(12,12). Buckling of the outer tubes in DWNTs is greater than the buckling of the tubes in single-walled configuration.

The Mulliken charge analysis shows there is charge transfer between Si atoms. This analysis also shows that there is charge transfer between two walls in a DWSiNT. Table 2.5 shows the Mulliken charges in the inner and outer tubes of the DWSiNTs. The charge transfer is significant when the inter layer separation is small. When the interlayer separation is smaller, the interaction between the two nanotubes is stronger and the buckling of the constituent SW nanotube is larger. The interlayer interaction is not only due to van der Waals force but also due to Coulomb force. As the inter layer separation increases van der Waals interaction dominates over the Coulomb interaction. Fig. 2.18 shows the Mulliken charge distribution in a DWSiNT (6,6)@(9,9). We also note that the charge analysis is rather strongly dependent on the basis set.

Table 2.4 Diameter (D) and buckling(β) of inner and outer tube (in Å) in DWSiNTs

Nanotubes	D_{in}	D_{out}	β_{in}	β_{out}
(3,3)@(6,6)	6.577	12.684	0.485	0.469
(3,3)@(7,7)	6.640	13.524	0.846	1.080
(3,3)@(8,8)	6.129	17.170	0.474	0.032
(3,3)@(9,9)	6.126	19.319	0.473	0.036
(3,3)@(10,10)	6.127	21.451	0.472	0.032
(3,3)@(11,11)	6.126	23.578	0.474	0.034
(3,3)@(12,12)	6.126	25.175	0.473	0.037
(4,4)@(7,7)	8.599	14.445	0.910	0.834
(4,4)@(8,8)	8.759	16.665	1.117	1.183
(4,4)@(9,9)	8.473	18.114	0.951	1.479
(4,4)@(10,10)	8.482	21.50	0.262	0.062
(4,4)@(11,11)	8.441	23.63	0.297	0.063
(4,4)@(12,12)	8.440	25.766	0.297	0.064
(5,5)@(8,8)	10.619	16.594	0.918	0.915
(5,5)@(9,9)	11.299	17.479	0.980	0.985
(5,5)@(10,10)	10.665	21.441	0.252	0.032
(5,5)@(11,11)	10.632	23.675	0.246	0.041
(5,5)@(12,12)	10.596	25.762	0.242	0.058
(6,6)@(9,9)	12.779	18.906	0.468	0.483
(6,6)@(10,10)	13.219	19.233	0.532	0.567
(6,6)@(11,11)	12.408	21.607	0.241	0.192
(6,6)@(12,12)	12.960	25.778	0.065	0.067

The study of double-walled silicon nanotube in armchair configuration revealed the evolution of electronic properties with the size of the nanotubes. It is shown that the stabilities of the double-walled Si nanotubes are of the same order as those of single-walled Si nanotube. The formation energy of the nanotubes reaches high values when interlayer separation is about 3.0 Å. In particular, (6,6)@(9,9) DWNT is the most stable tube with also the largest formation energy of 81.87eV. All Si nanotubes are semiconductors. However, the band gap, in general, is observed to decrease from single walled nanotubes to double walled nanotubes.It should be possible to experimentally synthesis both single-walled and double-walled Si nanotubes. The binding energy per atom or the binding energy of the nanotubes depends not only on the

number of atoms but also on the coupling of the constituent single-walled nanotubes. Nanotubes with small interlayer separations, called meshed tubes, do not hold the coaxial cylindrical structure after optimization. The SiNTs (n, n)@(n+3, n+3) are found to have large formation energies and binding energies per atom. For example, (3,3)@(6,6), (4,4)@(7,7), (5,5)@(8,8), and (6,6)@(9,9) all have large binding energies per atom, around 3.7eV/atom.

Table 2.5 Mulliken charges in inner tube (n_i) and outer tube (n_o)

Nanotube	n_i	n_o	$n_i^{\dagger}$	$n_o^{\dagger}$
(3,3)@(6,6)	0.720	-0.720	-0.902	0.902
(3,3)@(7,7)	1.089	-1.089	-0.128	0.128
(3,3)@(8,8)	-0.045	0.045	0.078	-0.078
(3,3)@(9,9)	-0.013	0.013	0.025	-0.025
(3,3)@(10,10)	-0.001	0.001	0.0	0.0
(3,3)@(11,11)	0.0	0.0	0.0	0.0
(3,3)@(12,12)	0.0	0.0	0.0	0.0
(4,4)@(7,7)	0.766	-0.766	-1.112	1.112
(4,4)@(8,8)	0.879	-0.879	-1.615	1.615
(4,4)@(9,9)	0.346	-0.346	0.154	-0.154
(4,4)@(10,10)	-0.015	0.015	0.014	-0.014
(4,4)@(11,11)	-0.001	0.001	0.0	0.0
(4,4)@(12,12)	0.0	0.0	0.0	0.0
(5,5)@(8,8)	0.694	-0.694	-0.995	0.995
(5,5)@(9,9)	1.747	-1.747	1.618	-1.618
(5,5)@(10,10)	-0.093	0.093	-0.028	0.028
(5,5)@(11,11)	0.198	-0.198	-1.141	1.141
(5,5)@(12,12)	-0.001	0.001	0.0	0.0
(6,6)@(9,9)	1.295	-1.295	1.510	-1.510
(6,6)@(10,10)	2.266	-2.266	2.858	-2.858
(6,6)@(11,11)	-0.190	0.190	-0.026	0.026
(6,6)@(12,12)	-0.007	0.007	0.010	-0.010

† single point run with basis set 6-311G* using the optimized structure from 3-21G*

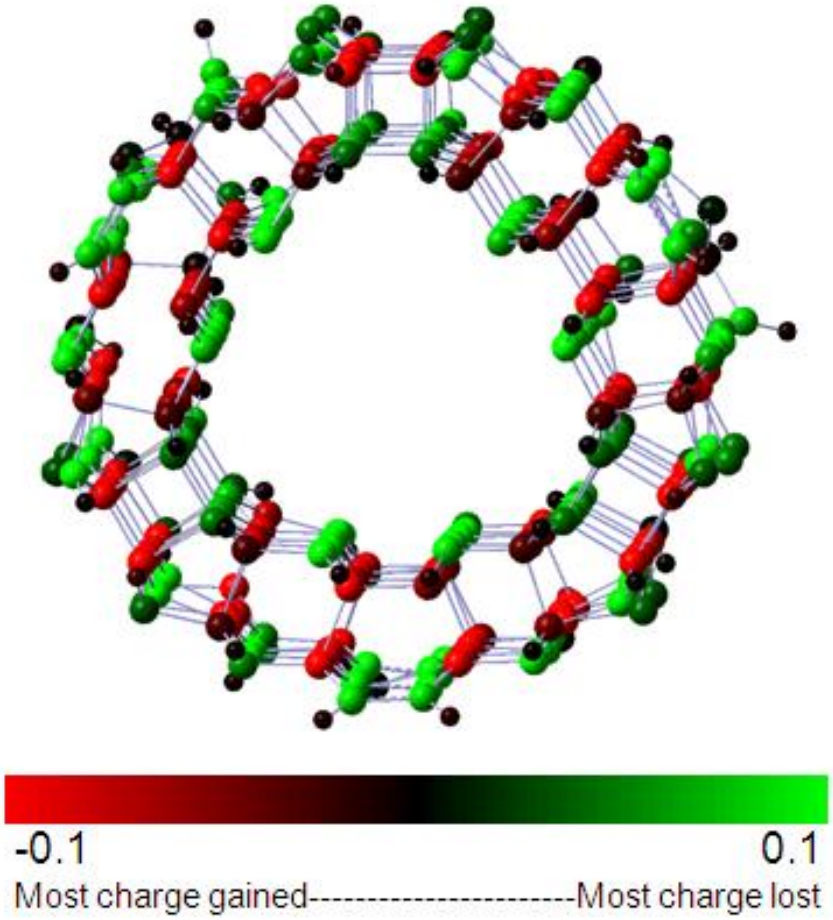

Figure 2.18 Mulliken charge distributions for (6,6)@(9,9) nanotube. Hydrogen atoms at dangling bonds remain almost neutral.

2.2 Zigzag Silicon Nanotubes

One of the central questions for SiNTs is whether SiNTs based on sp^2 hybridization exist or not. It is shown that a slightly distorted structure of single-walled SiNTs where the Si-Si bonds have a somewhat enhanced sp^3 character is more stable than the pristine CNT-like structure. The structure of SiNTs is still an open question of fundamental physical and chemical importance. Apart from the sp^2-like character of armchair SiNTs, in this section we discuss the special sp^3-like geometry and electronic properties of single-walled zigzag SiNTs.

Table 2.6 Binding energies per atom, HOMO-LUMO gaps in eV and radial buckling in Å for zigzag silicon nanotubes.

Nanotube	Stoichiometry	Total No. of atoms	B. E. per atom (eV)	HOMO-LUMO gap (eV)	Diameter (Å)	Radial buckling(Å)
Si (3,0)	$Si_{66}H_6$	72	3.441	0.42	3.90	0.411
Si (4,0)	$Si_{88}H_8$	96	3.497	0.50	4.93	0.386
Si (5,0)	$Si_{110}H_{10}$	120	3.511	0.61	6.15	0.352
Si (6,0)	$Si_{132}H_{12}$	144	3.534	0.38	6.92	0.338
Si (7,0)	$Si_{154}H_{14}$	168	3.542	0.55	8.61	0.305
Si (8,0)	$Si_{176}H_{16}$	192	3.556	0.26	9.83	0.266
Si (9,0)	$Si_{198}H_{18}$	216	3.567	0.58	11.05	0.253
Si (10,0)	$Si_{220}H_{20}$	240	3.573	0.25	12.28	0.265
Si (11,0)	$Si_{242}H_{22}$	264	3.579	0.22	13.50	0.263
Si (12,0)	$Si_{264}H_{24}$	288	3.584	0.20	14.71	0.269

Table 2.6 lists the variations of the binding energies per atom versus the number of atoms in the SiNTs and variation of HOMO-LUMO gaps with the tube diameter, as well as the radial buckling. The optimized geometries of zigzag SiNT (n, 0) ($3 \leq n \leq 12$) is rendered in Fig. 2.19. As the number of atoms and diameter increases the binding energy per atom of SiNTs also increases and tends to be saturated (Fig. 2.20 and Fig. 2.21). The largest zigzag SiNT studied, (12, 0), has a binding energy of 3.584 eV per atom. Compared with the data of armchair SiNTs, the binding energy of zigzag SiNTs are slightly higher than the binding energy of armchair SiNTs (the largest armchair SiNT studied, (12, 12) has a binding energy of 3.465 eV per atom). A higher binding energy indicates that zigzag SiNTs are more stable than armchair SiNTs. It is noted that zigzag SiNTs have "wrinkled" surfaces rather than smooth tubular structure like armchair SiNTs. In order to determine how much the nanotubes have deviated from a smooth tubular structure, we plot the amount of radial buckling of the tube versus tube diameter (Fig. 2.22). Calculated by taking the standard deviation of distance between Si atoms and the tube axis, the radial buckling first decreases and then tends to saturate at tube (9, 0). The larger the radial buckling is, the smoother the nanotube is. The zigzag nanotube (9, 0) with diameter of 11.05 Å has a buckling of 0.253 Å, compared with the armchair nanotube (6, 6) with

diameter of 12.92 Å has a buckling of 0.039 Å. The "wrinkled" surface of zigzag SiNTs *may* indicate that the Si atom in zigzag SiNTs are sp^3 hybridized, otherwise they will have similar smooth surfaces due to sp^2 hybridization in armchair SiNTs. Since Si prefers sp^3 hybridization than sp^2 hybridization, the zigzag SiNTs with sp^3 character are more stable than armchair SiNTs. To further investigate the sp^3 character of zigzag SiNTs, we carried out the bond length measurement for zigzag SiNTs. The bond length of these nanotubes is in the range from 2.26 Å to 2.29 Å. In our previous study on armchair SiNTs, the bond length is in the range from 2.23 Å to 2.25 Å. Therefore there is an increase of the bond length of approximately 0.03 Å going from armchair SiNTs to zigzag SiNTs. Going from sp^2 to sp^3hybridization, there is a decrease of s character. Therefore the sigma bond of sp^3 orbital is weaker than the bond of sp^2 orbitals resulting in a longer bond length of sp^3 orbital bonding. Since the zigzag SiNTs have longer bond length than armchair SiNTs, it is reasonable to assume the zigzag SiNTs have some sp^3 character.

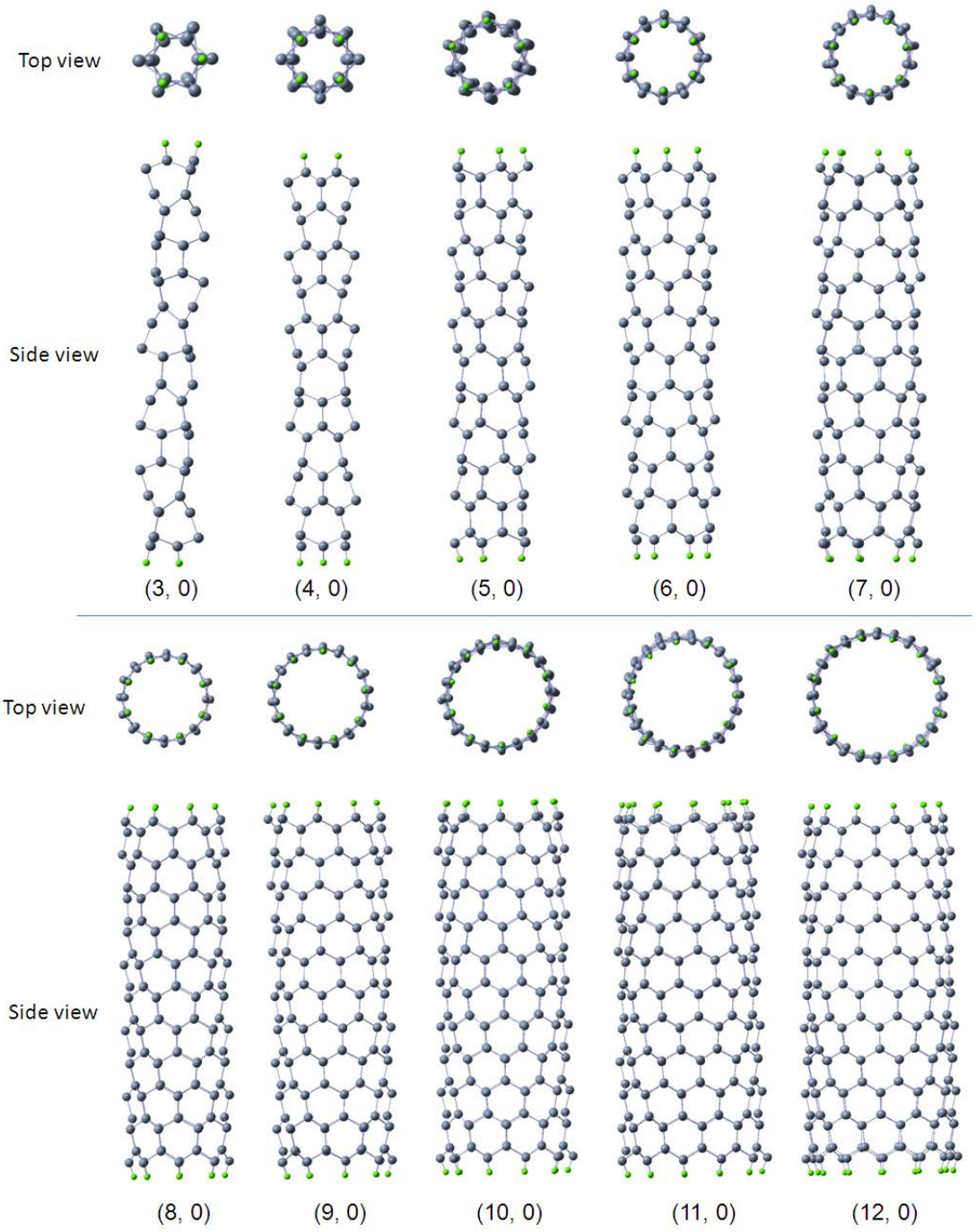

Figure 2.19 Optimized geometries of zigzag SiNTs (n, 0) (3≤n≤12). (Green atoms are hydrogen atoms and grey atoms are silicon atoms)

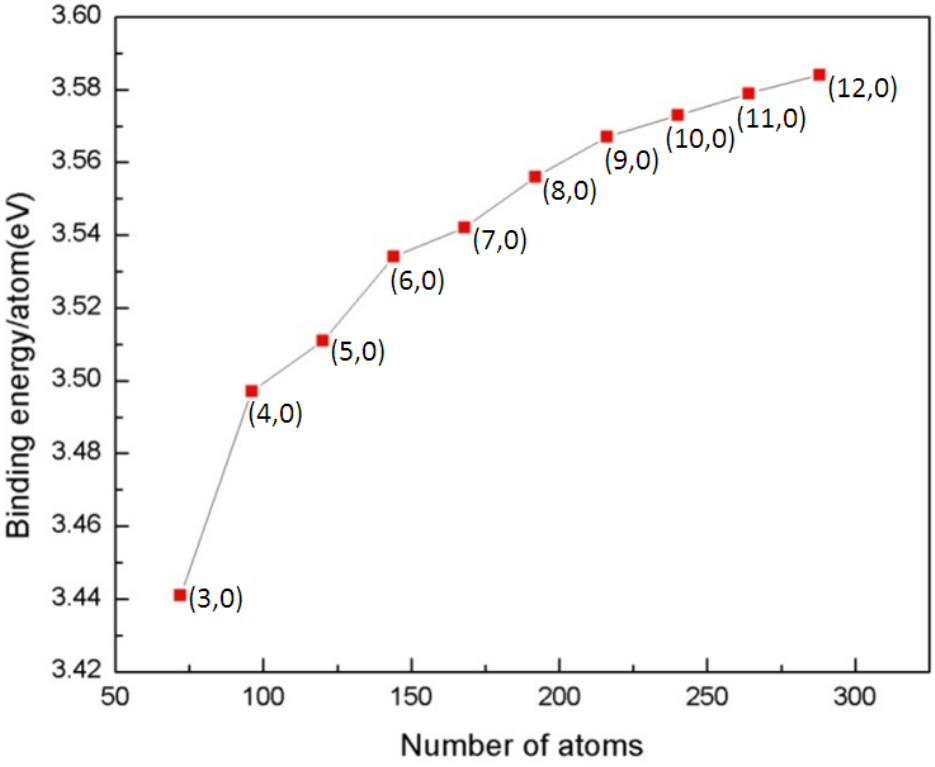

Figure 2.20 Binding energy per atom(eV) versus number of atoms for zigzag SiNTs.

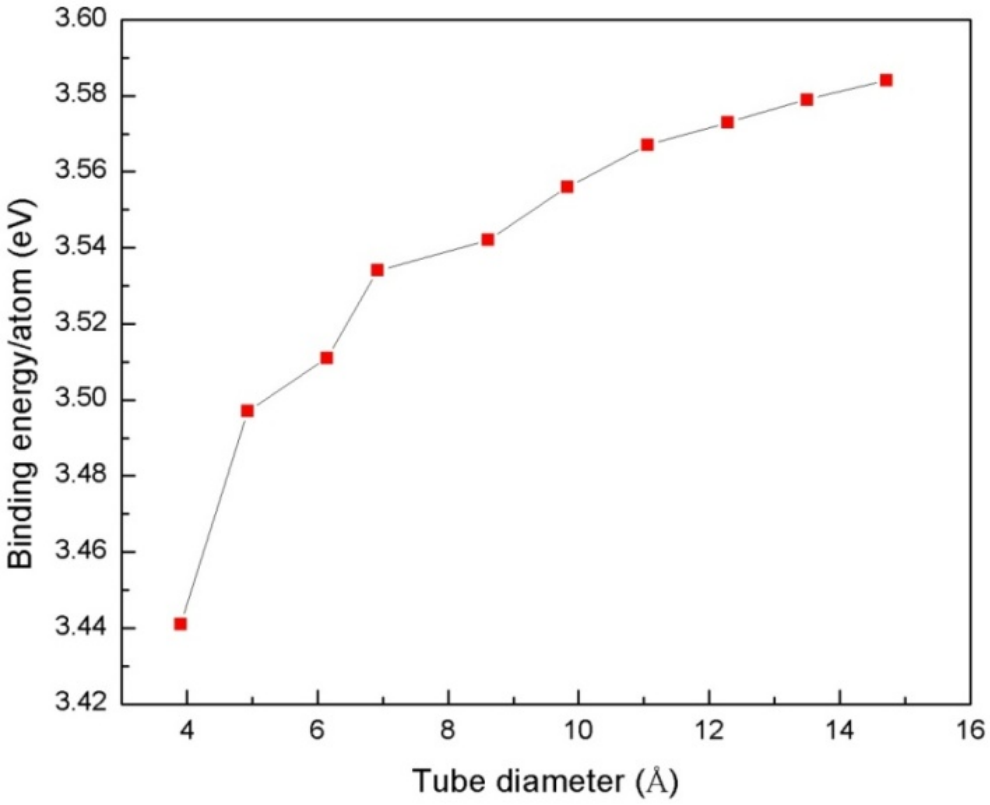

Figure 2.21 Binding energy per atom(eV) versus tube diameter(Å) for zigzag SiNTs.

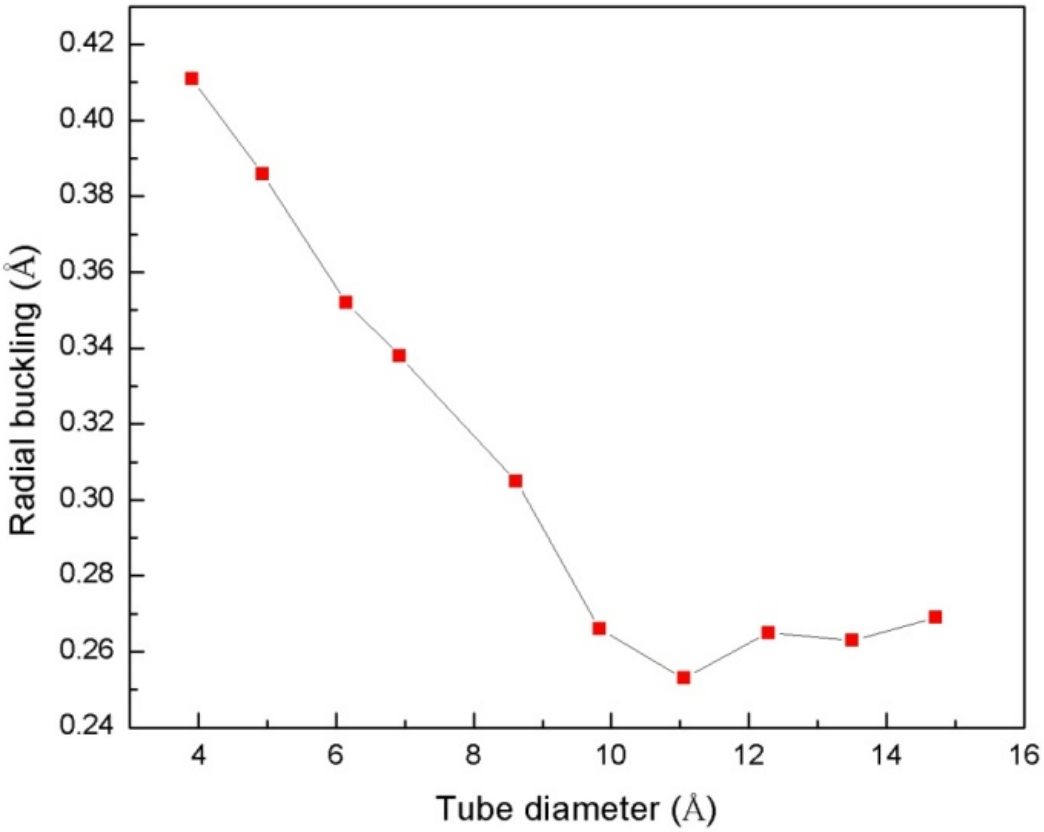

Figure 2.22 Radial buckling(Å) versus tube diameter(Å) for zigzag SiNTs.

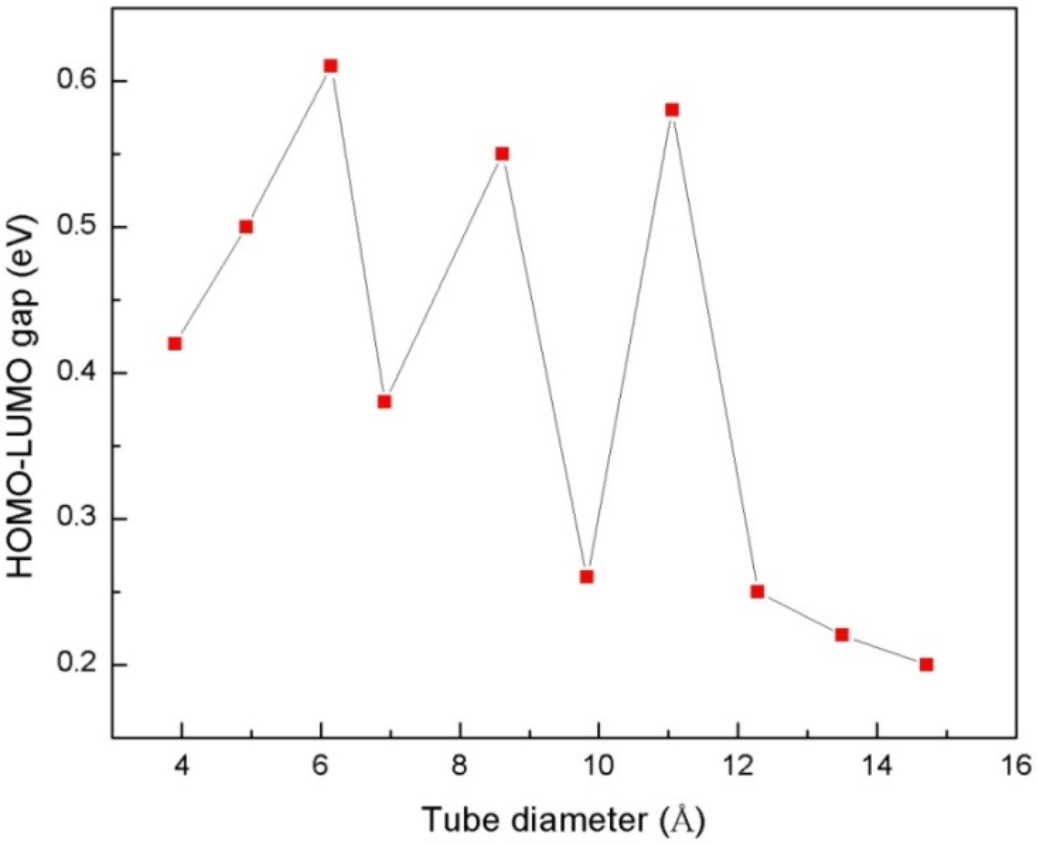

Figure 2.23 HOMO-LUMO gap(eV) versus tube diameter(Å) for zigzag SiNTs.

The HOMO-LUMO gaps of the zigzag SiNTs are in the range of 0.20 eV to 0.61 eV and showing an oscillating pattern (Fig. 2.23). These gaps are smaller than the bulk Si gap of 1.1 eV but still do not indicate any metallic behavior of SiNTs even for the largest nanotube studied. Fig. 2.24 shows the HOMO-LUMO plots for zigzag SiNTs (3, 0), (6, 0), (9, 0), (10, 0) and (12, 0). The HOMO and LUMO are delocalized through the tube body for (3, 0), but delocalized at the center or at the ends of the other nanotubes. (3, 0), (6, 0) and (9, 0) all have HOMO and LUMO at the center of their body, and their HOMO-LUMO gaps are relatively larger than (10, 0) and (12, 0), in which HOMO and LUMO only lie at the ends of the nanotube.

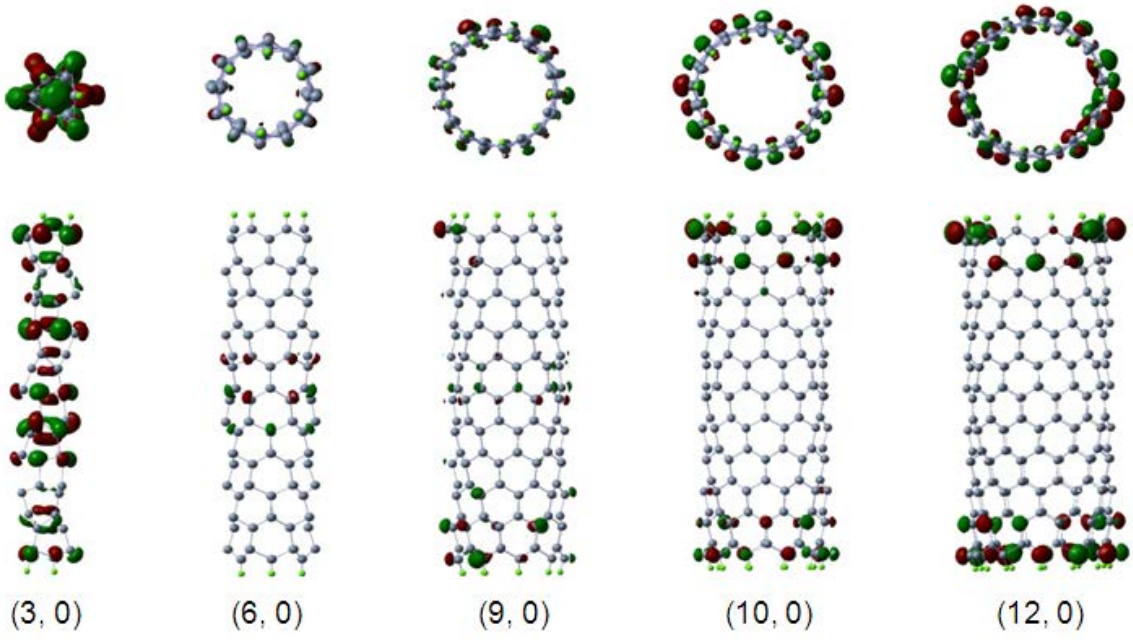

Figure 2.24 HOMO-LUMO plot for (3, 0), (6, 0), (9, 0), (10, 0) and (12, 0) SiNTs.

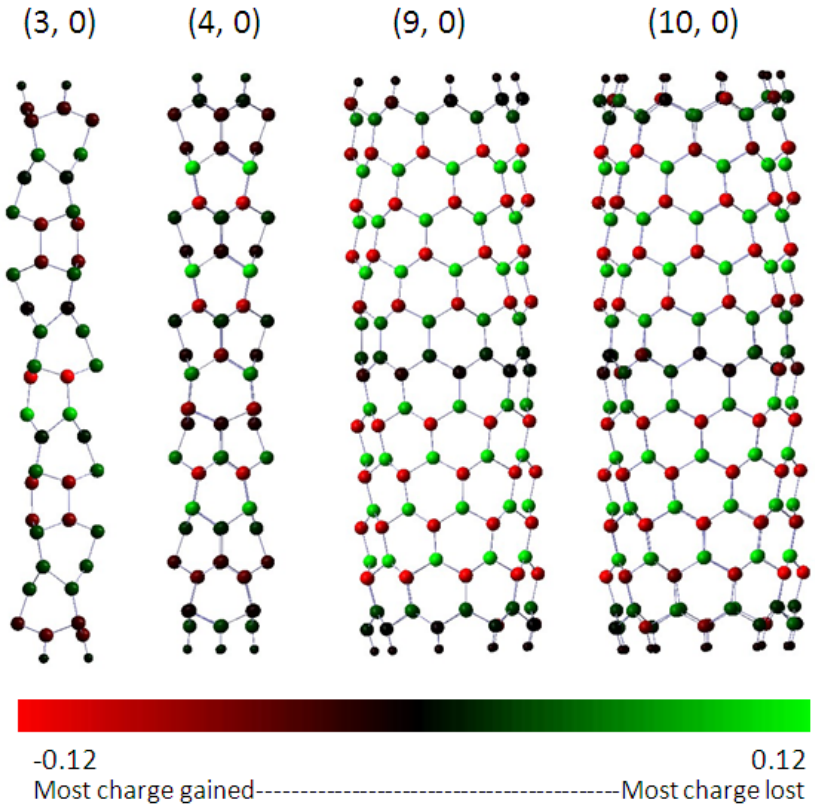

Figure 2.25 Mulliken charge distributions on four SiNTs.

In order to investigate the charge distribution on zigzag SiNTs, we have done the Mulliken charge analysis. Fig. 2.25 plots the Mulliken charge distribution on zigzag SiNTs (3, 0),(4, 0), (9, 0) and (10, 0). It is noted that there is a pattern of charge transfer between Si atoms in Si (9, 0) and Si (10, 0). A negatively charged Si atom is surrounded by three positively charged Si atoms and a positively charged Si is surrounded by three negatively charged Si atoms. This pattern occurs to (9, 0) and (10, 0) along the tube body except at the center and two ends of the nanotubes. The charge at center and two ends are nearly neutral. We also noted that there are two types of configurations through these nanotubes, one being pyramidal ($\sum\alpha \approx 328°$) and the other being planar ($\sum\beta \approx 360°$) (Fig. 2.26). This pattern of alternating pyramidal and planar configuration occurs in every zigzag SiNT studied here. Fig. 2.27 plots $\sum\alpha$

and ∑β for zigzag SiNTs. As the tube diameter increases, ∑α increases monotonically and tends to saturate at (8, 0) (Fig. 8). However, ∑β changes very slightly as the tube diameter increases. Table 2.7 lists the values of ∑α and ∑β from (3, 0) to (12, 0). In the smallest zigzag SiNT studied here (3, 0), ∑α is 274.59° and ∑β is 357.96°. For the largest zigzag SiNT (12, 0), ∑α is 336.36° and ∑β is 356.74°. The most favorite sum of angles slightly deviates from that of standard sp^3 hybridization (328°), due to the charge distribution and curvature effect. It is reasonable to believe that for any zigzag SiNTs larger than Si (12, 0) the alternating pattern of pyramidal and planar structure will still hold. It is intriguing that, the Si atoms which form a pyramidal structure with three surrounding Si atoms, are gaining charge. The Si atoms, which form a planar structure with three surrounding Si atoms, are losing charge. Recalling sp^2 hybridization gives a planar arrangement and sp^3 hybridization gives a tetrahedral arrangement, also Si atom with more p orbital character has more attraction to valence electrons (In sp^3 hybridized Si atom, a 3s electron is moved to 3p orbital and will increase the influence of the silicon nucleus on the valence electrons by increasing the effective potential), so the sp^3 hybridized Si atoms are gaining charge when bonded to sp^2 hybridized Si atoms.

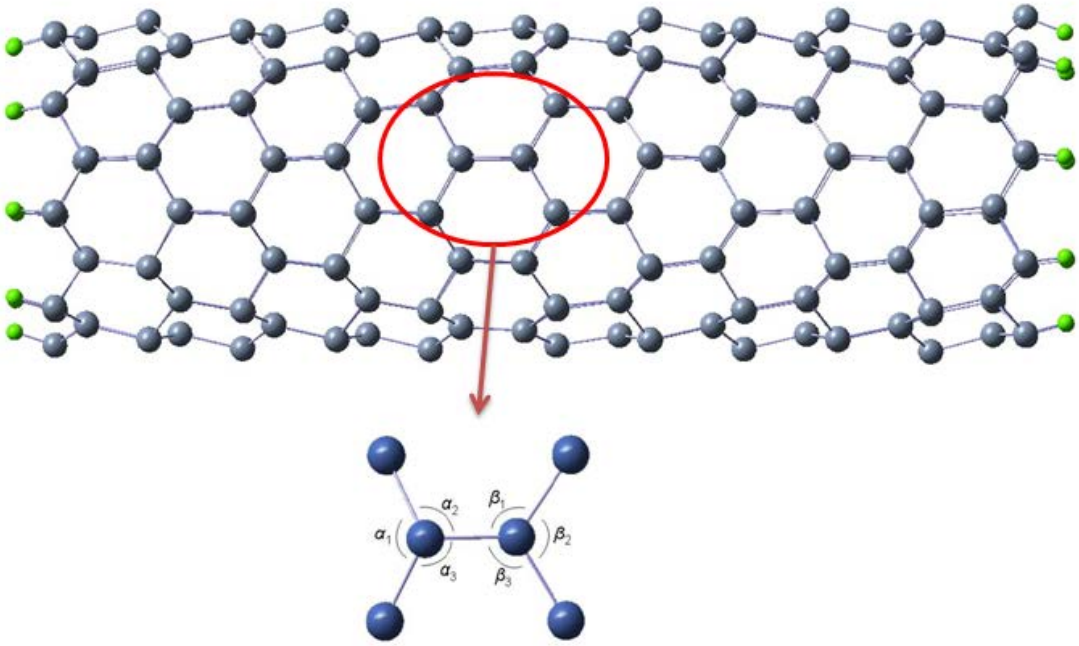

Figure 2.26 Local configurations in zigzag SiNTs.

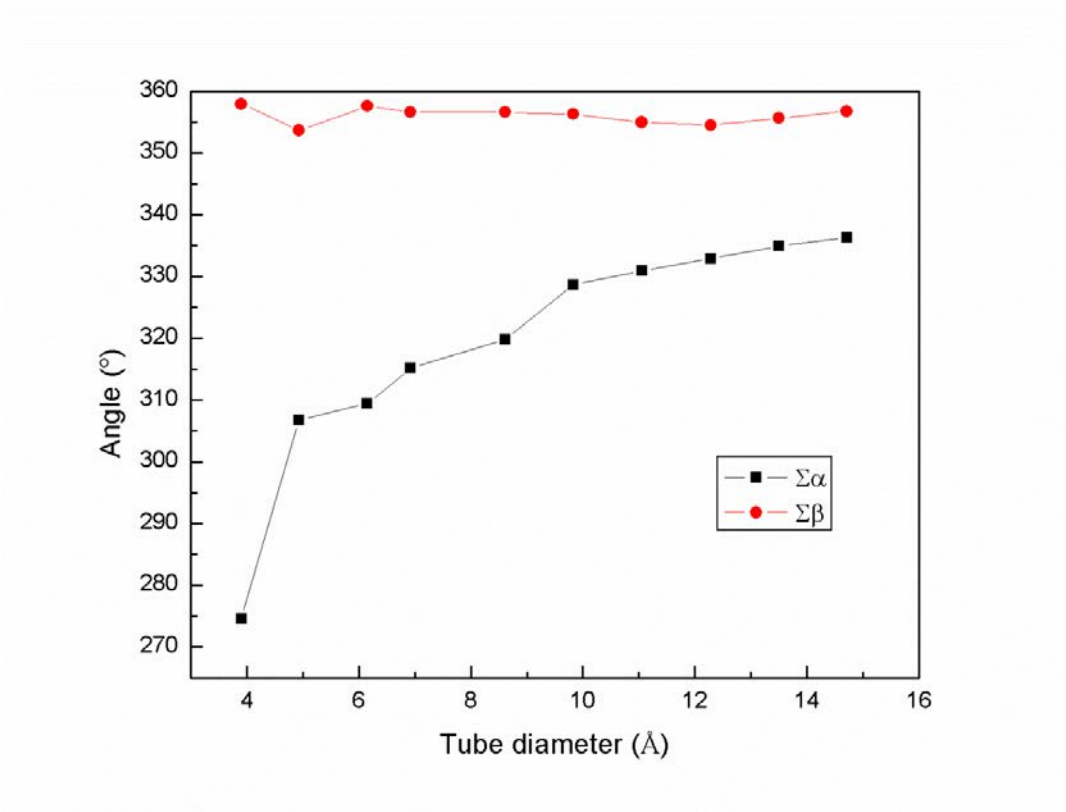

Figure 2.27 Sum of angles α and β(degrees) versus tube diameter(Å).

Table 2.7 Sum of angles α and β(degrees) for two types of local configurations.(∑α is the sum of the angles for Si atoms forming pyramidal structure and ∑β is the sum of angles for Si atoms forming planar structure)

Nanotube	∑α(deg)	∑β(deg)
(3, 0)	274.59	357.96
(4, 0)	306.76	353.67
(5, 0)	309.44	357.61
(6, 0)	315.16	356.66
(7, 0)	319.79	356.62
(8, 0)	328.70	356.31
(9, 0)	330.95	354.97
(10, 0)	332.91	354.49
(11, 0)	334.91	355.66
(12, 0)	336.36	356.74

Compared to armchair SiNTs, zigzag SiNTs all have large buckling and they do not show any metallic behavior although some nanotubes have small HOMO-LUMO gaps. The binding energy per atom for zigzag SiNTs increases monotonically as the tube diameter increase. The radial buckling first decrease and then tend to saturate at (9, 0) as the tube diameter increases. For large zigzag SiNTs there could still exist alternating pyramidal and planar structure, which has not been observed in our study on armchair SiNTs.

CHAPTER 3

ATOMIC HYDROGEN AND OXYGEN ADSORPTIONS IN SILICON NANOTUBES

Single-walled nanotubes (SWNTs) have unique mechanical and electronic properties, which make them promising building blocks for atomic and molecular electronics. A major critical issue toward their widespread application in nanotechnology is the control of their electronic properties. Foreign atoms, such as hydrogen, oxygen or transition metal (TM) atoms, can be incorporated into SiNTs in different ways, to change the electronic structure of SiNTs. This chapter is intended to outline both the adsorption of hydrogen and oxygen atoms in silicon nanotubes. In Section 3.1 we describe the adsorption of atomic hydrogen and oxygen in armchair silicon nanotubes. Subsequently, the adsorption of atomic hydrogen and oxygen in zigzag silicon nanotubes are discussed in Section 3.2.

3.1 Adsorptions of Atomic Hydrogen and Oxygen in Armchair Silicon Nanotubes

In Chapter 2 we have discussed the armchair single-walled silicon nanotubes. From Fig. 2.2 and 2.3, for tubes Si (6, 6) to Si (12, 12), the HOMO-LUMO gaps, the cohesive energies per atom and the radial buckling all tend to converge, the largest differences being 0.04eV, 0.036eV, and 0.0044 A, respectively. Thus, we believe that results obtained on atomic adsorptions using any of these tubes will not differ significantly and will not provide new chemical and physical insights. However, the computations time will increase significantly in proceeding from a (6, 6) tube to a (12, 12) tube. Thus we have opted to use Si (6, 6) to perform the atomic hydrogen and oxygen adsorption studies. The hydrogen atom can approach the nanotube wall from outside as well as inside. The adsorption energy (A.E.) is obtained by comparing the total energy of the spin-optimized composite system (SiNT + H) with the total energy of the optimized separated systems, namely SiNT and H with the 3-21G* basis set:

A.E. = E (SiNT) +E (H)-E (SiNT+H) (3.1)

For SiNT, there is only one type of bond and we have four different sites available (Fig. 3.1). There are two sites available at the center of the Si-Si bond. One is the normal bridge site and the other the zigzag bridge site. The third site, called hollow site, lies at the center of the hexagon. The last case is the hydrogen atom approaching the nanotube vertically on top of the silicon atom.

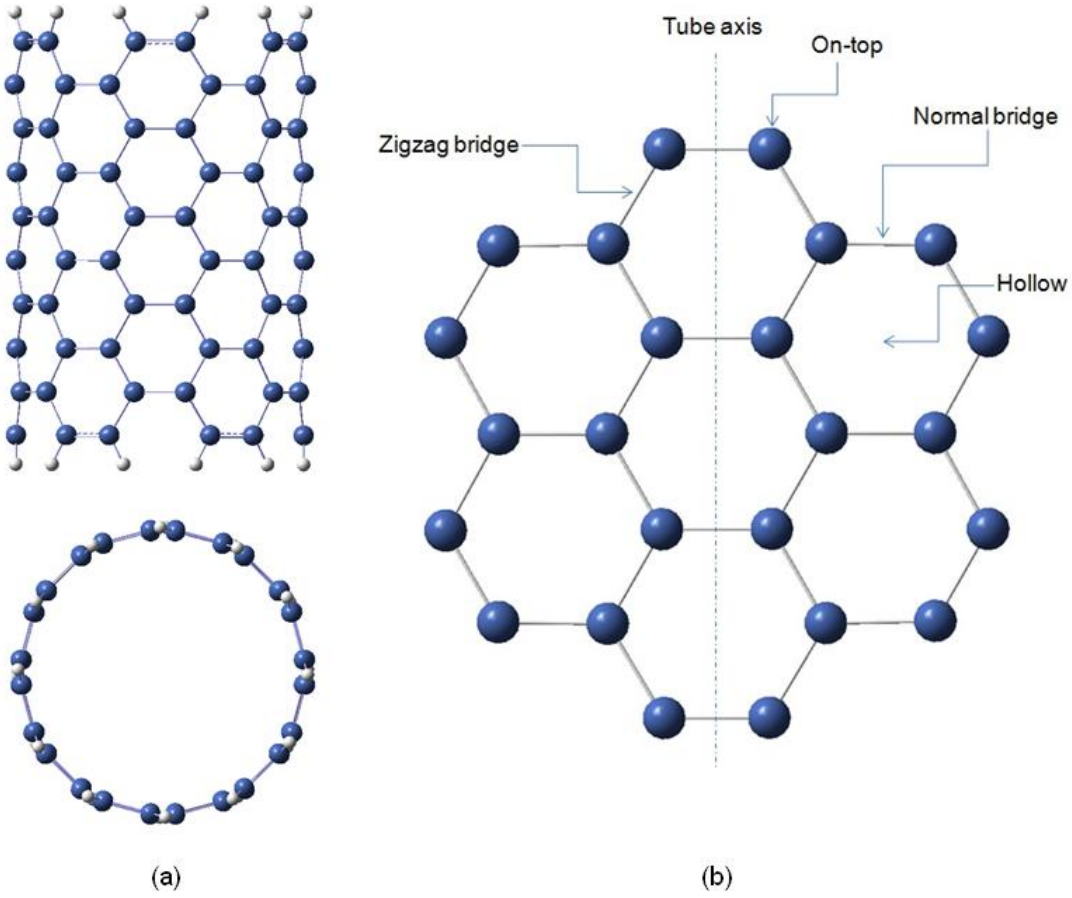

Figure 3.1 (a) Armchair Si (6, 6) nanotube; (b) Different sites for Si (6, 6) nanotube.

When the hydrogen atom approaches the tube wall from outside, after optimization we observed that the hydrogen atoms all moved to the on-top site for the four cases. It indicates

that on-top site is the most preferred site for external adsorption. Table 3.1 shows the adsorption energy and the distance of the hydrogen atom to the nearest silicon atom after optimization. The distance is identical (1.50 Å) for all four cases and the adsorption energy is also the same (5.97 eV) except for the initially hollow site with a very small difference of 0.03 eV from the other three sites. When the hydrogen atom approaches the tube wall from inside, after optimization we also observed that the hydrogen atoms all moved to the on-top site for the four cases. So that indicates on-top site is also the most preferred site for internal adsorption. In Table 3.2, we see that the distance from the hydrogen atom to the nearest silicon atom is also the same of 1.50 Å as in the cases of external adsorption. However, the adsorption energies are slightly lower (about 0.1 eV) than the cases of external adsorption. Also the radial buckling of the nanotubes increases significantly after adsorption of H atom. This may suggest that a sp^3 bonding environment is more pronounced in the nanotubes when introducing H atom.

Table 3.1 Adsorption energy in eV for different external adsorption sites and the corresponding optimized distance from the adsorbed hydrogen atom to the nearest silicon atom in Å, HOMO-LUMO gap in eV and radial buckling in Å.

Initial site	Final site	$D_{H\text{-}Si}$ (Å)	Adsorption energy (eV)	HOMO-LUMO gap (eV)	Radial buckling (Å)
Normal B.	On-top	1.50	5.97	0.53	0.298
Zigzag B.	On-top	1.50	5.97	0.53	0.298
Hollow	On-top	1.50	6.00	0.88	0.267
On-top	On-top	1.50	5.97	0.53	0.298

Table 3.2 Adsorption energy in eV for different internal adsorption sites and the corresponding optimized distance from the adsorbed hydrogen atom to the nearest silicon atom in Å, HOMO-LUMO gap in eV and radial buckling in Å.

Initial site	Final site	$D_{H\text{-}Si}$ (Å)	Adsorption energy (eV)	HOMO-LUMO gap (eV)	Radial buckling (Å)
Normal B.	On-top	1.50	5.87	0.63	0.264
Zigzag B.	On-top	1.50	5.87	0.63	0.264
Hollow	On-top	1.50	5.87	0.63	0.264
On-top	On-top	1.50	5.87	0.63	0.264

We have examined the HOMO-LUMO gaps for the external and internal adsorption of H atom on Si (6, 6) nanotube. We do note that the gaps varied from 0.53 eV to 0.88 eV suggesting a semiconductor behavior. Also the gaps are smaller than the bare armchair (6, 6) SiNT with gap of 0.98 eV which possibly suggests that increasing the number of adsorbed hydrogen atoms the tube *may* show some metallic behavior. To further study the stability of the nanotubes after H atom adsorption, we examined their HOMO distributions. Fig. 3.2 shows the HOMO plot for the bare Si (6, 6) nanotube, the external (initially normal bridge site) and internal hydrogen adsorption (initially normal bridge site). The electrons all delocalize on the whole system either before or after H atom adsorption. Fig. 3.3 shows the density of states (DOS) for armchair (6, 6) nanotube, external and internal H atom adsorption.

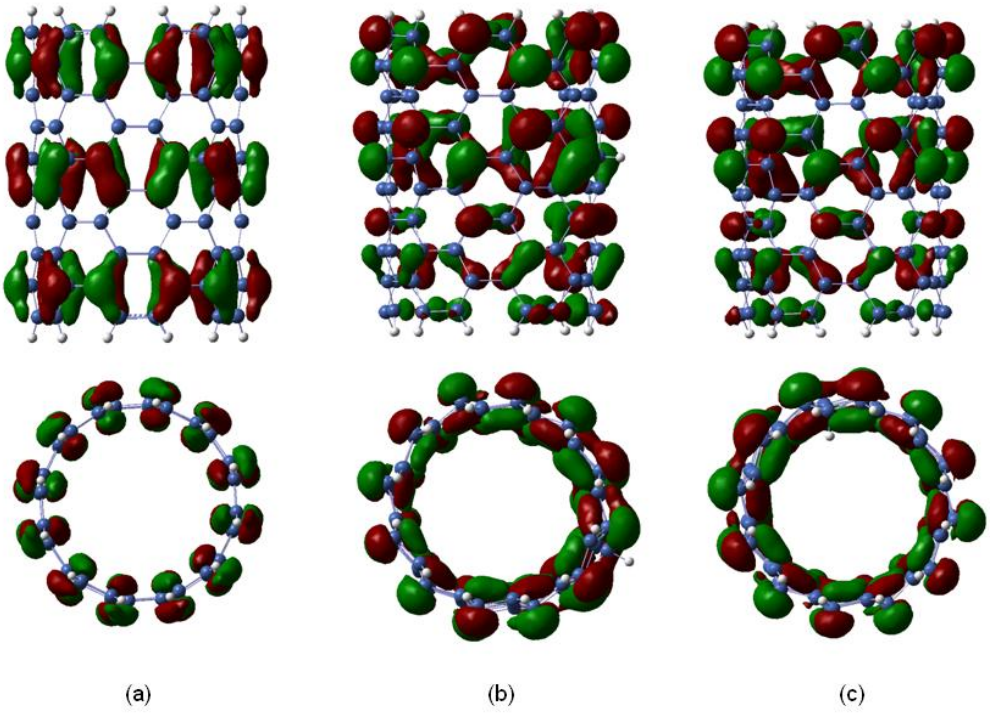

Figure 3.2 HOMO distribution of (a) bare Si (6, 6) nanotube; (b) the external H adsorption on Si (6, 6) nanotube (initially normal bridge site); (c) the internal H adsorption on Si (6, 6) nanotube (initially normal bridge site).

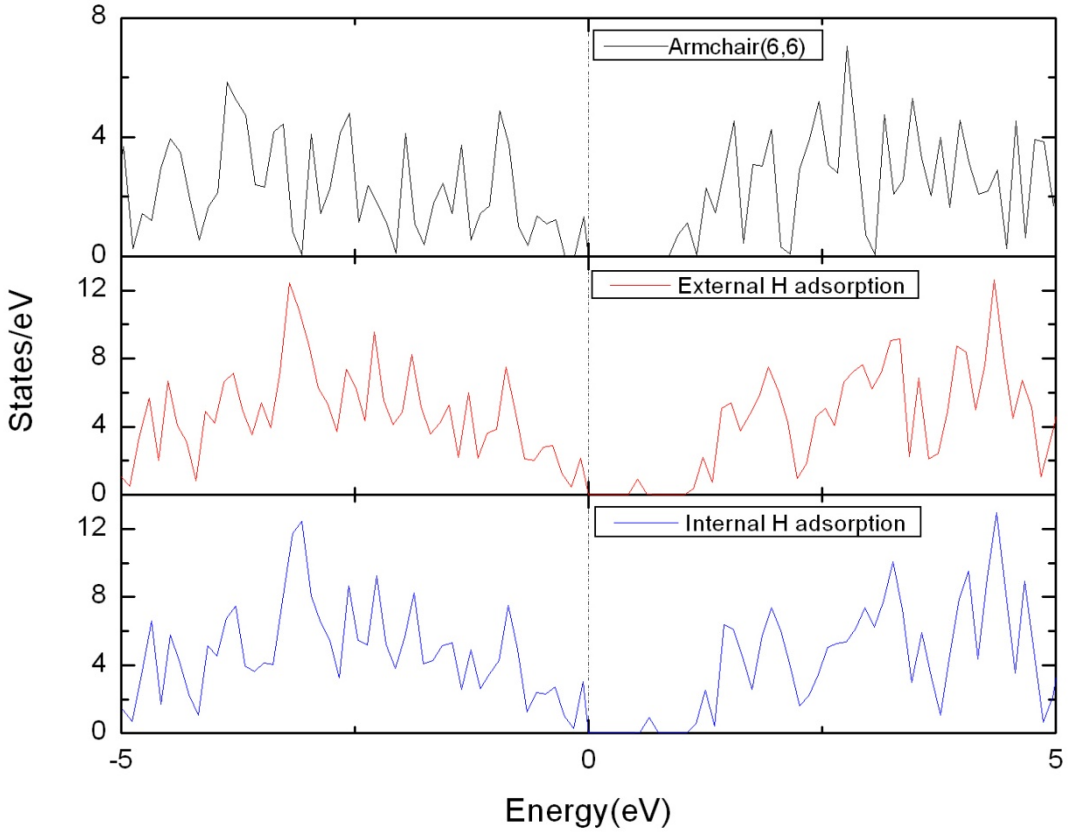

Figure 3.3 Density of states for bare Si (6, 6) nanotube, external H adsorption (initially nomal bridge) and internal H adsorption (initially normal bridge). E=0 is the HOMO.

We also examined the external and internal oxygen adsorption for armchair (6, 6) SiNT. The sites chosen for the oxygen atom are the same as those for hydrogen atom. Table 3.3 and 3.4 show the preferred sites of adsorption, optimized distance of the adsorbed oxygen from nearest silicon atom, adsorption energies of the adsorbed oxygen to the silicon nanotube and HOMO-LUMO gap of the cluster for all initial external and internal adsorption sites. It is evident

from the table that the adsorption energies for internal and external oxygen atom adsorptions with a silicon nanotube are approximately twice those of the hydrogen atom and the corresponding nanotube. The most preferable outer adsorption site for the oxygen atom is the normal bridge site with adsorption energy 9.68eV for external adsorption and 8.82eV for internal adsorption. The oxygen atom initially put at the external hollow site eventually goes to the external normal bridge site, whereas it moves to zigzag bridge site from initial hollow site when the oxygen atom is absorbed from inside the nanotube. Oxygen atom at external zigzag-bridge and external on-top sites has approximately similar binding energies with the nanotube. HOMO-LUMO gap of the nanotube with oxygen atom adsorbed in it varies from 0.58eV for internal normal bridge to 1.15eV for external normal bridge. The HOMO-LUMO gap depends very much on the site of adsorption. The gap of a SiNT is significantly lowered when oxygen is attached to the SiNT at the internal normal bridge site whereas for all other adsorption sites the gap is similar or slightly different than that of bare SiNT. Fig. 3.4 shows the HOMO plots for the external (initially hollow) and internal oxygen adsorption (initially on-top site). The electrons all delocalize on the whole system either before or after O adsorption. Fig. 3.5 shows the density of states for external and internal O adsorption. Also the radial buckling of the nanotubes increases significantly after adsorption of O which may suggest that incorporation of O atoms helps to form the sp^3 silicon nanotube.

Table 3.3 Adsorption energy in eV for different external adsorption sites and the corresponding optimized distance from the adsorbed oxygen atom to the nearest silicon atom in Å, HOMO-LUMO gap in eV and radial buckling in Å.

Initial site	Final site	$D_{O\text{-}Si}$ (Å)	Adsorption energy (eV)	HOMO-LUMO gap (eV)	Radial buckling (Å)
Normal B.	Normal B.	1.65	8.79	1.02	0.312
Zigzag B.	Zigzag B.	1.71	8.10	0.89	0.271
Hollow	Normal B.	1.66	9.68	1.15	0.314
On-top	On-top	1.57	7.79	0.92	0.290

Table 3.4 Adsorption energy in eV for different internal adsorption sites and the corresponding optimized distance from the adsorbed oxygen atom to the nearest silicon atom in Å, HOMO-LUMO gap in eV and radial buckling in Å.

Initial site	Final site	$D_{O\text{-}Si}$ (Å)	Adsorption energy (eV)	HOMO-LUMO gap (eV)	Radial buckling (Å)
Normal B.	Normal B.	1.73	7.87	0.58	0.360
Zigzag B.	Zigzag B.	1.72	8.17	0.99	0.322
Hollow	Zigzag B.	1.72	8.16	1.00	0.323
On-top	Normal B.	1.71	8.82	1.04	0.285

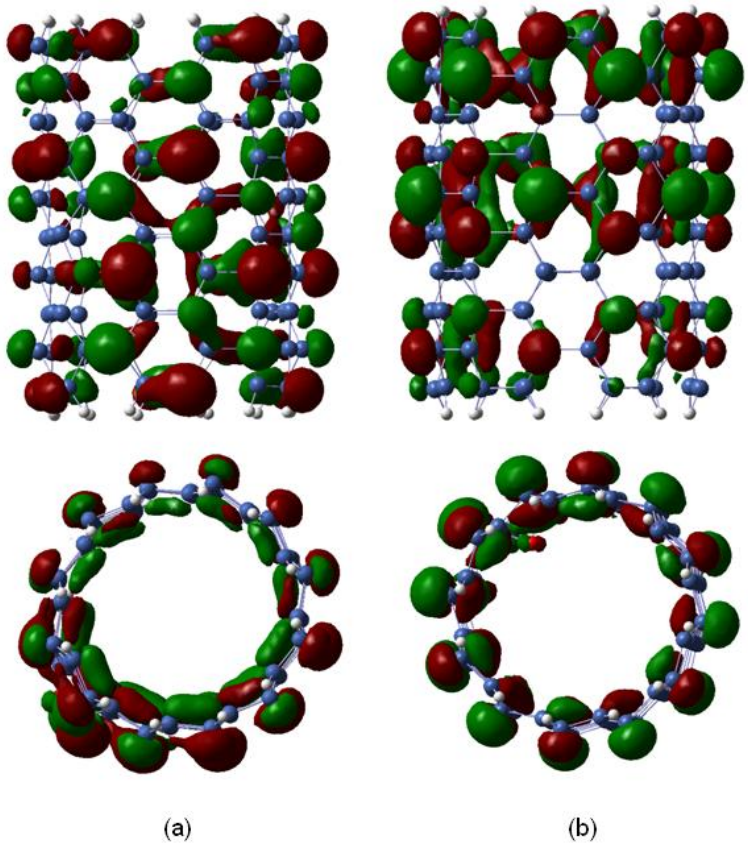

Figure 3.4 HOMO distribution of (a) the external O adsorption on Si (6, 6) nanotube (initially hollow site); (b) the internal O adsorption on Si (6, 6) nanotube (initially on-top site).

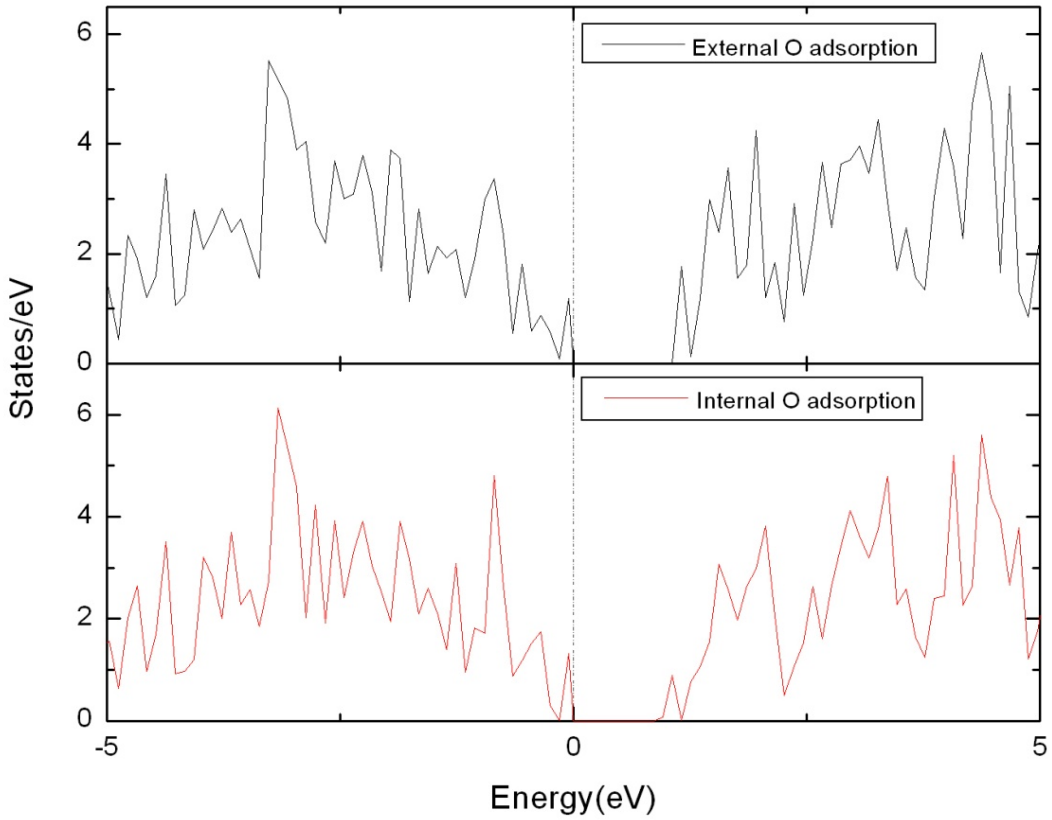

Figure 3.5 Density of states for external O adsorption (initially hollow site) and internal H adsorption (initially on-top site). E=0 is the HOMO.

For both H and O adsorption, we do notice that the radial buckling increases significantly after adsorption which means introducing H and O atoms will provide a more puckered structure (Fig.3.6). After we examined carefully the structure of the nanotubes, we found that there are basically two kinds of local configurations for the Si atoms, one being close to tetrahedral and the other planar. Some nanotubes (Si (4, 4), Si (5, 5), H and O adsorption) contain both structures alternating while others only contain planar structure. We have calculated the sums of angles surrounding two adjacent Si atoms (Fig.3.7). From Table 3.5, we

can see that in the nanotubes with high buckling (Si (4, 4), H and O adsorption on Si (6, 6)), the sums of angles $\sum\alpha$ obtained are close to the ideal value of 328.4° for a tetrahedral structure (sp^3 hybridization) and the sums of angles $\sum\beta$ obtained are all very close to the ideal value of 360° for a planar structure (sp^2hybridization). In the nanotubes with small buckling (bare Si (6, 6), Si (9, 9) and Si (12, 12)), the sums of angles $\sum\alpha$ and $\sum\beta$ are almost the same being close to the ideal value of 360° for a planar structure. We also examined the Mulliken charge distribution on these nanotubes (Fig 3.8 and 3.9). It is intriguing that the nanotubes with alternating tetrahedral and planar structure are polarized but the nanotubes with pure planar structure shows predominantly covalent character without charge polarization. It could be explained by the orbital hybridization that sp^3 hybridized (tetrahedral structure) Si atom has more p orbital character than sp^2 hybridized (planar structure) Si atom. Assume an excitation occurs to a Si atom, moving a 3s electron to 3p orbital. This will however increase the influence of the silicon nucleus on the valence electrons by increasing the effective potential (the amount of charge the nucleus exerts on a given electron=charge of core-charge of all electrons closer to the nucleus). Therefore, the Si atom with more p orbital character would have more attraction on the valence electrons than that with more s character. In Fig.3.10, we see that in bare Si (6, 6) nanotube (has only planar structure), the charges on Si atoms are all very close to zero which mean there is hardly any charge polarization. And in the cases of external H and O adsorption, the sp^3 hybridized (tetrahedral structure) Si atoms are gaining charge while the sp^2 hybridized (planar structure) Si atoms are losing charge. This is in good agreement with our theory above.

The study on armchair SWSiNTs indicates that the atomic hydrogen is adsorbed on the armchair silicon nanotube only on the top site with binding energy of about 6.0 eV. Attaching atomic hydrogen to the silicon nanotube decreases the band gap of the silicon nanotube. Oxygen atom is adsorbed in the silicon nanotube in various sites with binding energy more than that for hydrogen adsorption. Increasing the number of absorbed H and O atoms may change

the geometry and electronic structure significantly and provide a more stable puckered sp^3-sp^2 structure.

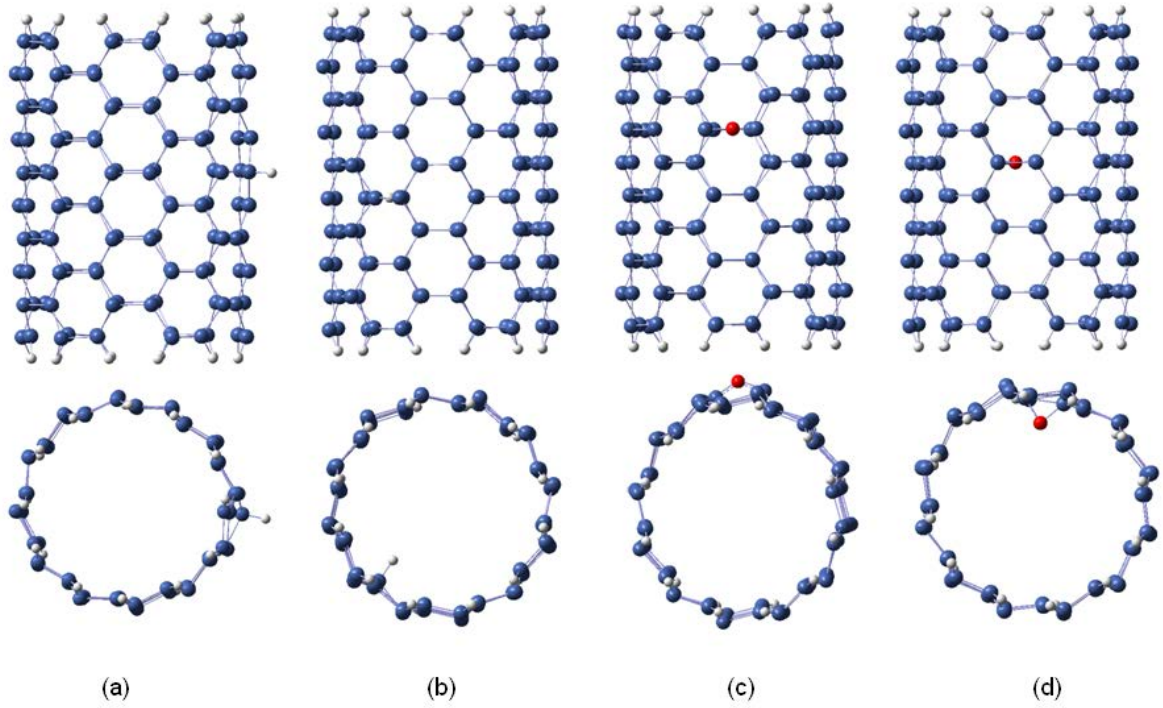

Figure 3.6 The optimized structure of (a) the external H adsorption on Si (6, 6) nanotube (initially normal bridge site); (b) the internal H adsorption on Si (6, 6) nanotube (initially normal bridge site); (c) the external O adsorption on Si (6, 6) nanotube (initially hollow site); (d) the internal O adsorption on Si (6, 6) nanotube (initially on-top site).

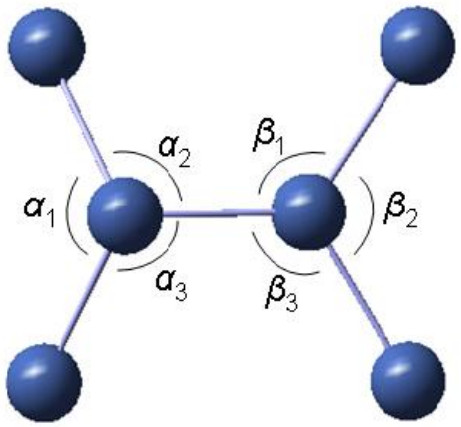

Figure 3.7 The angles surrounding two adjacent Si atoms in nanotubes.

Table 3.5 The sums of angles surrounding two adjacent Si atoms in the nanotubes and the corresponding buckling.

Nanotube	$\Sigma\alpha$(deg)	$\Sigma\beta$(deg)	Buckling(Å)
Si (4,4)	322.5	356.2	0.272
Si (6,6)	357.9	357.8	0.039
Si (9,9)	359.1	359.1	0.036
Si (12,12)	359.4	359.4	0.034
External H[1]	338.9	354.9	0.298
Internal H[2]	334.2	354.8	0.264
External O[3]	336.6	354.2	0.314
Internal O[4]	334.5	354.8	0.285

1. Initially normal bridge site; 2. Initially normal bridge site; 3.Initially hollow site; 4.Initially on-top site.

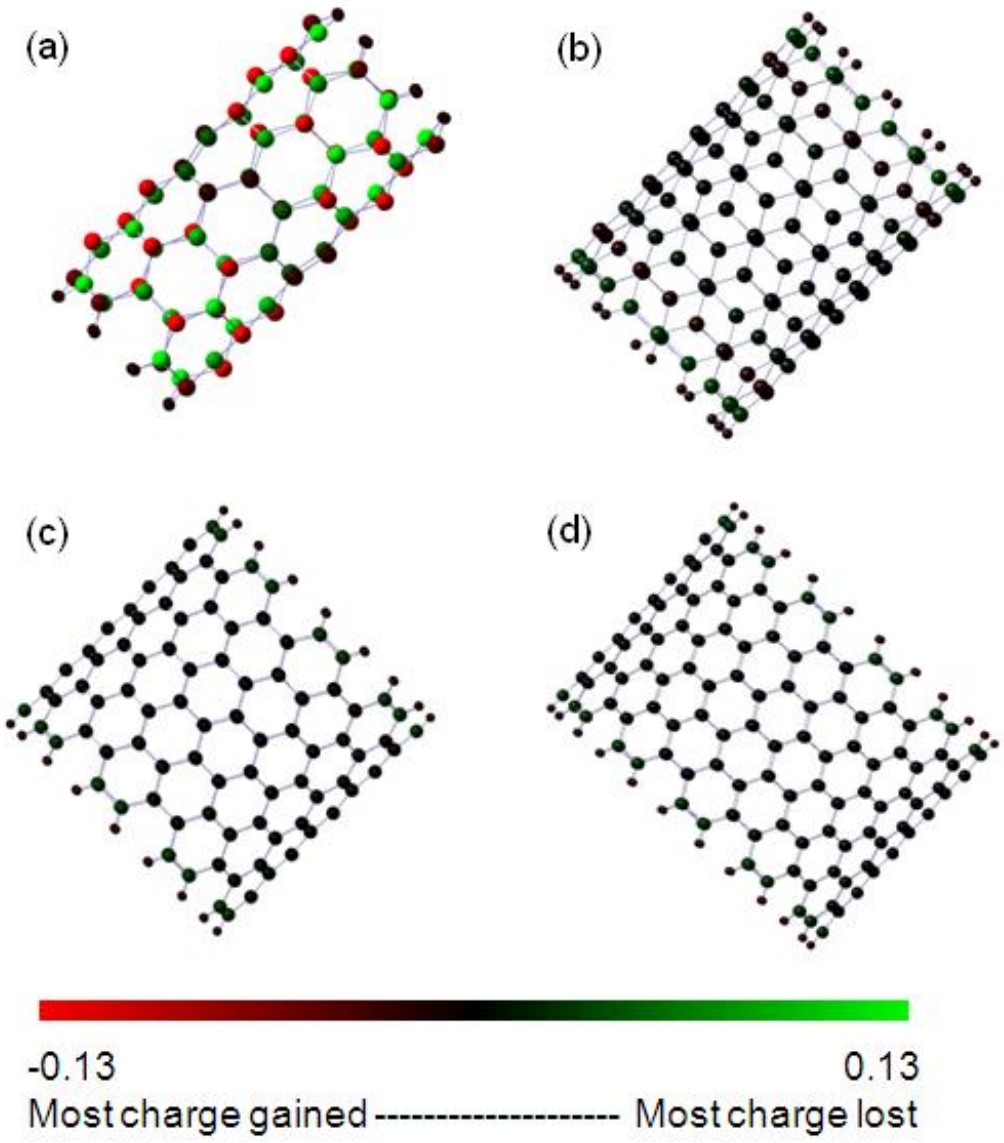

Figure 3.8 Mulliken charge distribution of (a) Si (4, 4) nanotube; (b) Si (6, 6) nanotube; (c) Si (9, 9) nanotube; (d) Si (12, 12) nanotube.

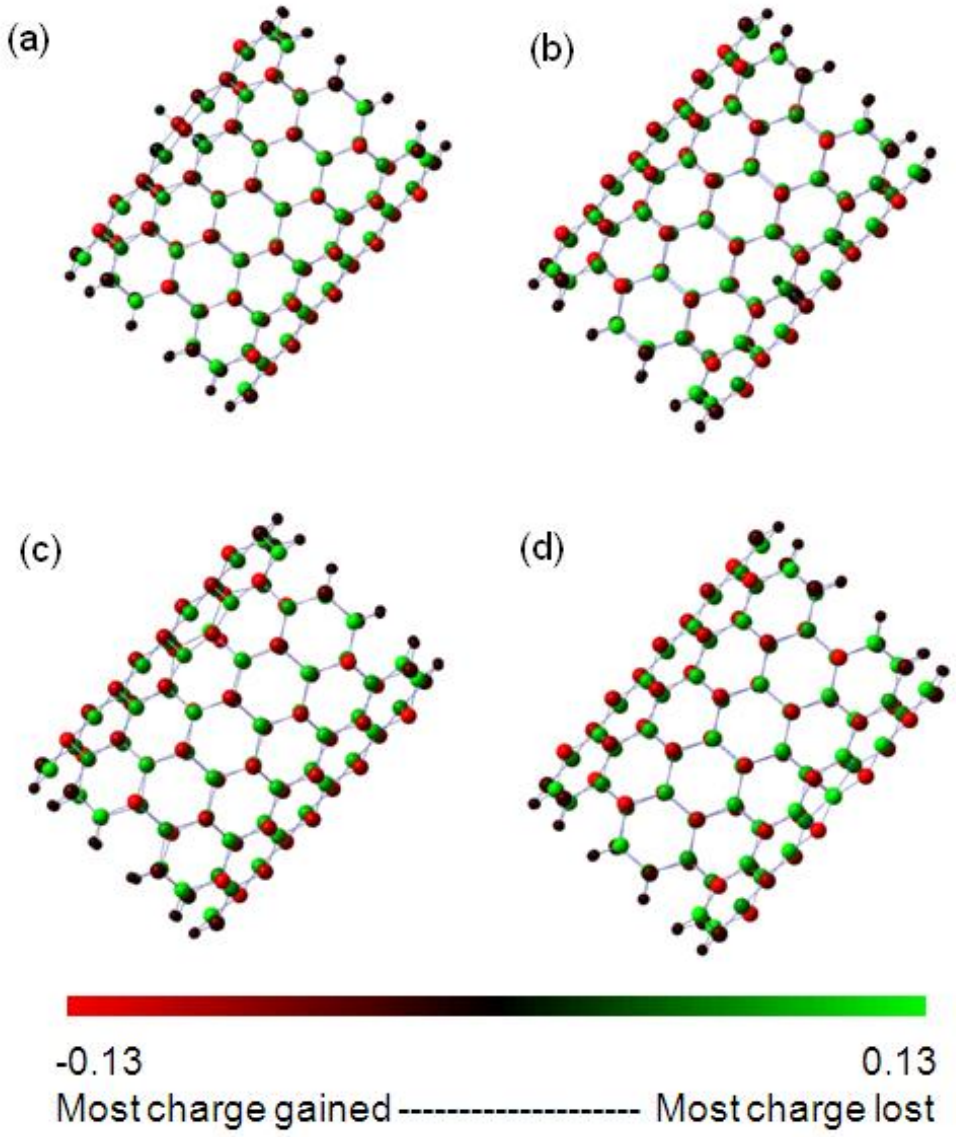

Figure 3.9 Mulliken charge distribution of (a) the external H adsorption on Si (6, 6) nanotube (initially normal bridge site); (b) the internal H adsorption on Si (6, 6) nanotube (initially normal bridge site); (c) the external O adsorption on Si (6, 6) nanotube (initially hollow site); (d) the internal O adsorption on Si (6, 6) nanotube (initially on-top site).

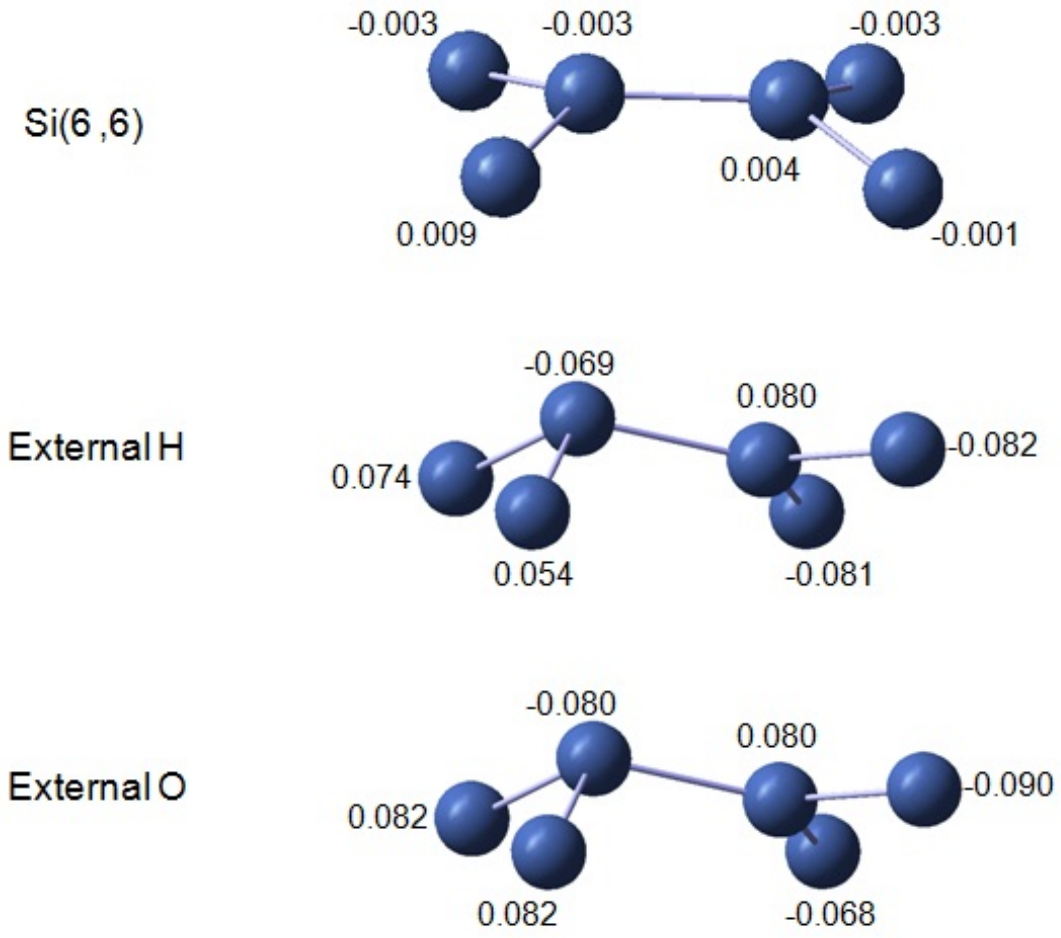

Figure 3.10 Mulliken charge distribution on Si atoms surrounding two adjacent Si atoms for Si (6, 6) nanotube, external H adsorption (initially normal bridge site) and external O adsorption (initially hollow site) on Si (6, 6) nanotube.

3.2 Adsorptions of Atomic Hydrogen and Oxygen in Zigzag Silicon Nanotubes

In Chapter 2, we have also described the geometric and electronic properties of single-walled zigzag silicon nanotubes. The zigzag SiNTs have a more puckered structure and sp^2-type bonding. From Si (9, 0), both the binding energy and radial buckling tend to saturate but the HOMO-LUMO gaps are oscillating. For the sake of comparison and since any larger zigzag SiNT is not expected to provide any more insight into the chemistry and physics of the

adsorption process and the computational cost obviously rises significantly with the size of the nanotube, both (9, 0) and (10, 0) tubes were chosen as the adsorbents for adsorption of hydrogen and oxygen atoms.

We describe the interaction of atoms with SiNTs for (1) adsorption from the outside of the nanotubes (2) adsorption from the inside of the nanotubes. To find the most stable configuration, several adsorption sites, shown in Fig. 3.11, have been considered, depending on the position of the adatom. The atom can be located at the top of Si atom, parallel bridge (PB) site, zigzag bridge (ZB) site, and the center of the Si hexagon (hollow site).

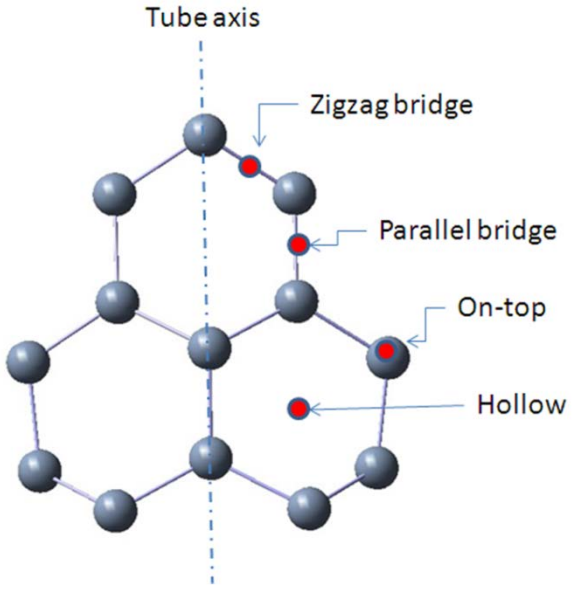

Figure 3.11 Four adsorption sites in zigzag silicon nanotubes.

Table 3.6 shows the adsorption of H atom in Si (9, 0) from the outside of the nanotube. The most preferred site is the on-top site with adsorption energy of 3.004 eV when the H atom was initially placed in on-top site (Fig. 3.12). When the H atom was initially placed in other sites, after optimization it moved to on-top site. Although the final sites are all on-top sites, the binding energy, HOMO-LUMO gap and radial buckling vary from case to case. This is because not all adatoms are exactly in the same on-top site after optimization. The shortest distance between H

atom and Si atoms is 1.49 Å. The HOMO-LUMO gaps are in the range from 0.44 eV to 0.57 eV indicating there is a decrease of the gap after adsorption of H atom, considering the energy gap of bare Si (9, 0) is 0.58 eV. Table 3.7shows the adsorption of H atom in Si (9, 0) nanotube from the inside of the nanotube. The most preferred site is also on-top site with adsorption energy of 2.788 eV when the H atom was initially placed in on-top site. When the H atom was initially place in other sites inside of the nanotube, after optimization H atom moved to on-top site. The HOMO-LUMO gaps decrease slightly in some cases. In general, the HOMO-LUMO gaps decrease after adsorption of H atom. It is noted that the H atom is adsorbed at where the HOMO and LUMO of Si (9, 0) are localized. The HOMO and LUMO of the H atom *may* have interacted with the HOMO and LUMO of Si (9, 0). The overlap of HOMO and LUMO from H and Si atoms has shrank the energy gap thus the HOMO-LUMO gap decreases after adsorption of H atom in Si (9, 0). Also the nanotubes still have a "wrinkled" surface after adsorption. However, the bond length measurement indicates there is a slight stretch of the bond length (approximately 0.10 Å) in the area close to the adsorbed H atom. Therefore, the adsorption of H atom could lower the bond strength of nearby Si atoms. We measured the angles for the nearest Si atom close to the H atom. Before adsorption the sum of angles was 356.3º (almost a planar arrangement) and after adsorption it became 338.13º (a pyramidal structure). This means there could be a transition from sp^2 to sp^3 character on the Si atom. Since the bond strength of sp^3 is weaker than sp^2 orbitals, the bond length is stretched.

Table 3.6 External H adsorption on Si(9, 0).

Initial site	Final site	$D_{H\text{-}Si}$ (Å)	Adsorption energy (eV)	HOMO-LUMO gap (eV)
Parallel B.	On-top	1.49	2.898	0.52
Zigzag B.	On-top	1.49	2.922	0.49
Hollow	On-top	1.52	2.892	0.57
On-top	On-top	1.49	3.004	0.44

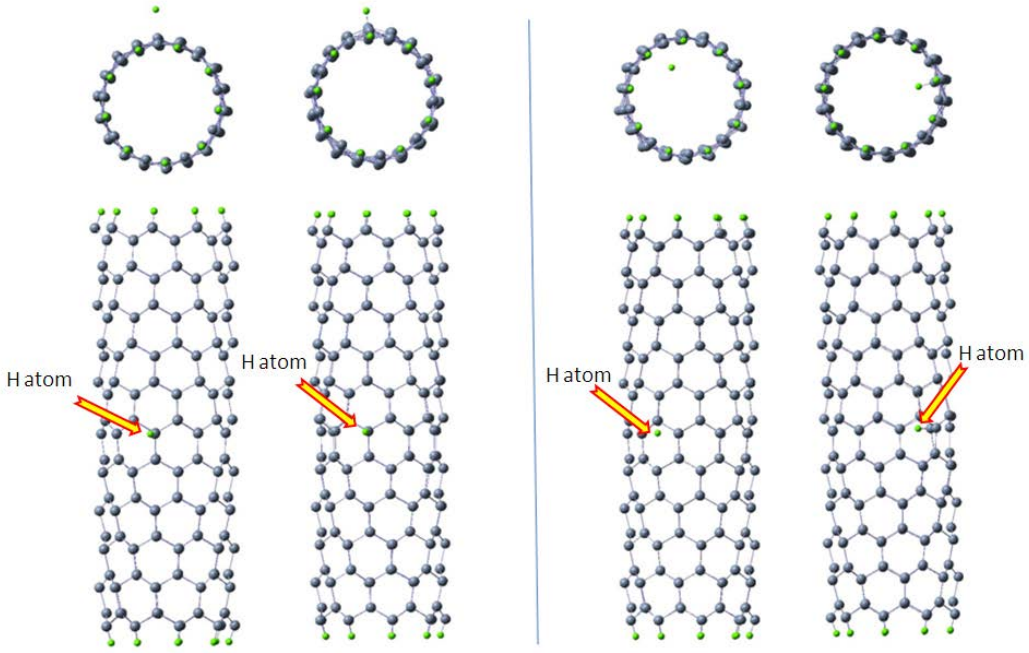

Figure 3.12 (a) H atom is initially placed in top site outside of nanotube (9, 0) (b) H atom is still in top site after optimization (c) H atom is initially placed in top site inside of nanotube (9, 0) (d) H atom is still in top site after optimization.

Table 3.7 Internal H adsorption on Si (9, 0).

Initial site	Final site	$D_{H\text{-}Si}$ (Å)	Adsorption energy (eV)	HOMO-LUMO gap (eV)
Parallel B.	On-top	1.49	2.768	0.58
Zigzag B.	On-top	1.49	2.605	0.53
Hollow	On-top	1.49	2.586	0.56
On-top	On-top	1.50	2.788	0.58

Table 3.8 shows the adsorption of O atom in Si (9, 0) from the outside of the nanotube. The most preferred site is zigzag bridge site with adsorption energy of 5.987 eV when the O atom was initially placed in hollow site (Fig. 3.13). When initially placed in other sites, the O

atom will move to zigzag bridge site or parallel bridge site. The O atom will not move to either hollow site or on-top site. The HOMO-LUMO gaps are in the range from 0.41 eV to 0.44 eV, so there is a decrease of the energy gap after adsorption of O atom. Similar to the adsorption of H atom, the shrink of the energy gap could also be attributed to the overlap of HOMO and LUMO from O and Si atoms. The shortest distance between O atom and Si atom is 1.72 Å. Table 3.9 shows the adsorption of O atom in Si (9, 0) from inside of the nanotube. The most preferred site is parallel bridge site with adsorption energy of 5.60 eV when the O atom was initially placed in hollow site. The O atom will also move to zigzag bridge site or parallel bridge site when initially placed in other sites. This is similar to the adsorption of O atom from outside of the nanotube. The energy difference between the adsorption energies of O atom in PB site and ZB site is not significant (less than 7%) so we believe that there is no such preference between PB and ZB sites. The HOMO-LUMO gaps also decreases after adsorption of O atom. Generally, whether the adsorption takes place inside or outside of the nanotube, the O atom prefers to go into the bridge sites.

Table 3.8 External O adsorption on Si (9, 0).

Initial site	Final site	$D_{O\text{-}Si}$ (Å)	Adsorption energy (eV)	HOMO-LUMO gap (eV)
Parallel B.	PB	1.72	5.524	0.42
Zigzag B.	ZB	1.72	5.850	0.44
Hollow	ZB	1.72	5.987	0.44
On-top	PB	1.72	5.527	0.41

Table 3.9 Internal O adsorption on Si (9, 0).

Initial site	Final site	$D_{O\text{-}Si}$ (Å)	Adsorption energy (eV)	HOMO-LUMO gap (eV)
Parallel B.	PB	1.73	5.460	0.47
Zigzag B.	ZB	1.73	5.415	0.45
Hollow	PB	1.73	5.600	0.46
On-top	ZB	1.72	5.428	0.45

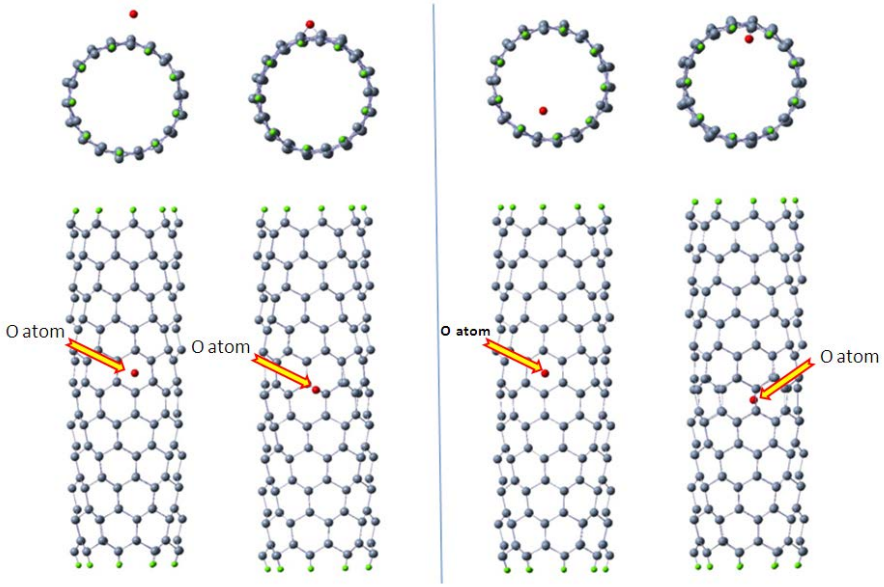

Figure 3.13 (a) O atom is initially placed in hollow site outside of nanotube (9, 0) (b) O atom is in zigzag bridge site after optimization (c) O atom is initially placed in hollow site inside of nanotube (9, 0) (d) O atom is in parallel bridge site after optimization.

We have also carried Mulliken charge analysis of adsorption on (9, 0). For H atom adsorption in on-top site, the Mulliken charge on H atom is 0.017|e| and the nearest Si atom has a charge of -0.052|e| (Fig. 3.14). Before adsorption this Si had a charge of 0.012|e| so there is a charge transfer from H atom to Si atom. For O atom adsorption in zigzag bridge site, the Mulliken charge on O atom is -0.488|e| and the two adjacent Si atoms have charge of 0.343|e| and 0.346|e|. Before adsorption these two Si atoms have charge of 0.012|e| and 0.007|e|, respectively. Therefore there is a significant charge transfer from the neighboring Si atoms to the O atom. The significant charge transfer from Si atoms to O atom is attributed to the large difference in the electronegativity of Si (χ=1.9) and O (χ=3.44). Although H (χ=2.2) is more electronegative than Si, the Si-H bond is not polarized such that H is negatively charged and Si atom is positively charged. This is because the hybridized Si atom with sp^3 character has more attraction to valence electrons than H atom. The difference between the electronegativities of Si

and H is not significant so that the hybridization plays a more important role in determining the polarization of Si-H bond.

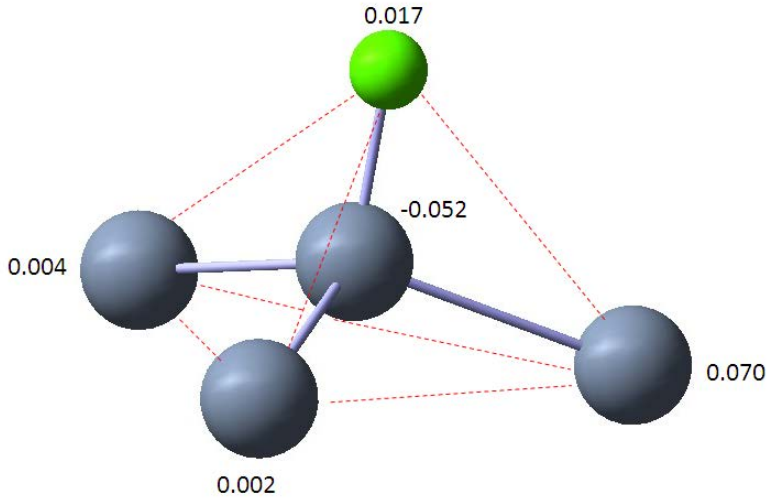

Figure 3.14 Mulliken charge on H atom and the nearest four Si atoms in Si (9, 0).

Table 3.10 and 3.11 show the adsorption of H atom in Si (10, 0) nanotube. Like the H adsorption in Si (9, 0), the most preferred site for hydrogen atom in Si (10, 0) is also on-top site (Fig. 3.15). The shortest distance between H atom and Si atom is 1.49 Å, which is the same as the adsorption in Si (9, 0). The adsorption energy range between 2.698 eV and 3.174 eV. The HOMO-LUMO gaps are in the range from 0.43 eV to 0.49 eV. Since the HOMO-LUMO gap of bare Si (10, 0) is 0.25 eV, there is an increase of the energy gap after the adsorption of H atom. Since in Si (10, 0) there is no localized HOMO and LUMO at the center of the tube body, the HOMO and LUMO of H and Si atoms do not overlap here. This may have increased the energy gap for the adsorption of H atom in Si (10, 0).

Table 3.10 External H adsorption on Si (10, 0).

Initial site	Final site	$D_{H\text{-}Si}$ (Å)	Adsorption energy (eV)	HOMO-LUMO gap (eV)
Parallel B.	On-top	1.50	2.698	0.44
Zigzag B.	On-top	1.49	3.174	0.49
Hollow	On-top	1.49	2.758	0.46
On-top	On-top	1.49	2.796	0.45

Table 3.11 Internal H adsorption on Si (10,0).

Initial site	Final site	$D_{H\text{-}Si}$ (Å)	Adsorption energy (eV)	HOMO-LUMO gap (eV)
Parallel B.	On-top	1.50	2.815	0.48
Zigzag B.	On-Top	1.50	2.897	0.45
Hollow	On-Top	1.50	2.961	0.43
On-top	On-Top	1.50	2.989	0.47

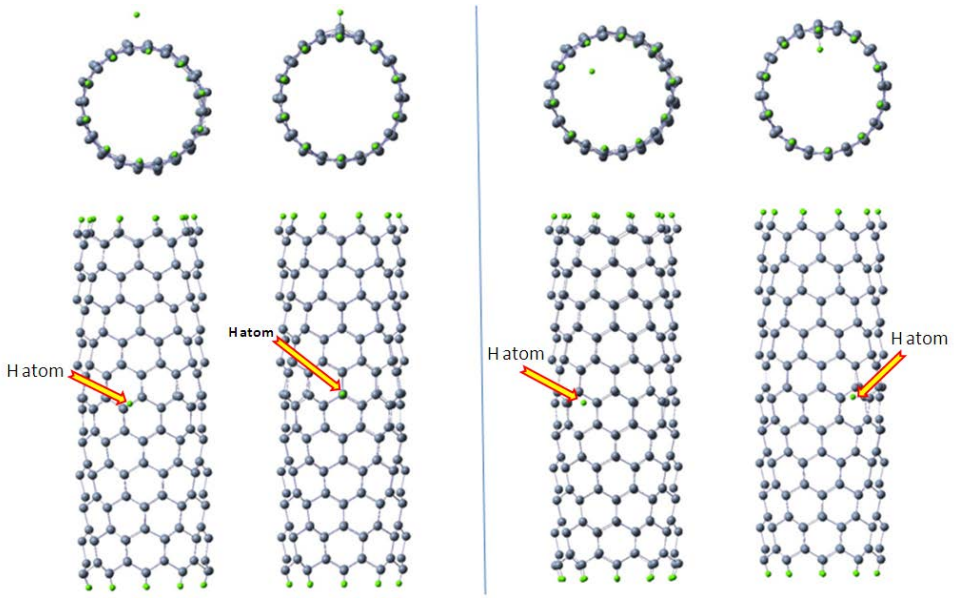

Figure 3.15 (a) H atom is initially placed in zigzag bridge site outside of nanotube (10, 0) (b) H atom is in top site after optimization (c) H atom is initially placed in top site inside of nanotube (10, 0) (d) H atom is in top site after optimization.

Table 3.12 External O adsorption on Si (10, 0).

Initial site	Final site	D_{O-Si} (Å)	Adsorption energy (eV)	HOMO-LUMO gap (eV)
Parallel B.	PB	1.72	6.275	0.60
Zigzag B.	ZB	1.72	6.183	0.60
Hollow	PB	1.71	6.149	0.59
On-top	PB	1.72	6.271	0.59

Table 3.13 Internal O adsorption on Si (10, 0).

Initial site	Final site	D_{O-Si} (Å)	Adsorption energy (eV)	HOMO-LUMO gap (eV)
Parallel B.	PB	1.73	6.053	0.60
Zigzag B.	ZB	1.72	6.027	0.58
Hollow	PB	1.71	6.306	0.59
On-top	ZB	1.72	5.980	0.52

Table 3.12 and Table 3.13 show the adsorption of oxygen atom in Si (10, 0) nanotube. The O atom shows a similar behavior of adsorption in (10, 0) compared to adsorption in (9, 0). The O breaks the Si-Si covalent bond and form Si-O-Si structure (Fig. 3.16). The adsorption energies range between 5.980 eV and 6.306 eV. The HOMO-LUMO gaps increase significantly compared to the bare nanotube, for an amount between 0.52 eV and 0.60 eV. This could be attributed to the same reason that adsorption of H atom increase the energy gap of (10, 0).

The Mulliken charge analysis of adsorption on Si (10, 0) is similar to the adsorption on (9, 0). The adsorption of H in top site on (10, 0) results in charge transfer from H atom to the nearest Si atom. The Mulliken charge on H atom is 0.033|e| and the nearest Si atom has charge of -0.126|e|. Before adsorption of H atom, this Si atom had charge of 0.003|e|. Similar to the adsorption on (9, 0), charge transfer from H to Si atom also occurred to (10, 0). For O adsorption in parallel bridge site on (10, 0), the Mulliken charge on O atom is -0.531|e| and the nearest two Si atoms have charge of 0.367|e| and 0.370|e|. Before adsorption of O, the two Si atoms had charge of 0.053|e| and 0.060|e|.

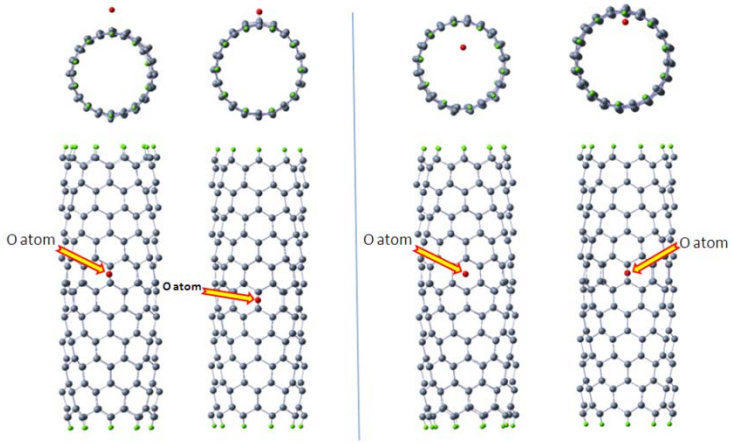

(a) (b) (c) (d)

Figure 3.16 (a) O atom is initially placed in parallel bridge site outside of nanotube (10, 0) (b) O atom is in parallel bridge site after optimization (c) O atom is initially placed in hollow site inside of nanotube (10, 0) (d) O atom is in parallel bridge site after optimization.

For the adsorption of H atom in both (9, 0) and (10, 0), the on-top site is the most preferred site. For the adsorption of O atom in (9, 0) and (10, 0), zigzag bridge site and parallel bridge sites are more preferred. This behavior is the same as the adsorption of H and O atoms in armchair SiNTs. After the adsorption of H and O atoms, Si (9, 0) has a slighted reduced energy gap. However after the adsorption of H and O atoms, Si (10, 0) has a significantly increased energy gap. As mentioned before, this could be attributed to the localization of the HOMO and LUMO in the nanotube. Further study on the band structure may explain the opposite behavior of change in the energy gap upon the adsorption of H and O atoms in Si (9, 0) and Si (10, 0).

CHAPTER 4

MOLECULAR HYDROGEN AND OXYGEN ADSORPTIONS IN SILICON NANOTUBES

Oxygen and silicon are very common substances in our lives. The behavior of oxygen in silicon has been a subject of interest and controversy for some time. Like hydrogen, oxygen has the capacity to passivate silicon dangling bonds. However, unlike hydrogen, each oxygen atom would passivate two silicon bonds, as it does in silicon dioxide. The interaction of atomic oxygen with silicon plays a very important role in both the bulk- and surface- governed electronic properties of semiconductors. The behavior of oxygen in silicon has been a subject of considerable interest and controversy. The favorable formation of sp^3 hybridization in Si atoms promotes the growth of Si nanowires and multi-walled Si nanotubes, which have been fabricated using different methods. The oxidation of silicon surface has been an important research subject in surface science and a key process in the fabrication of semiconductor devices. Hydrogen molecule adsorption in SiNTs plays an important role in storage of hydrogen. The adsorption energy of hydrogen molecule determines the storage capacity of hydrogen in SiNTs. Hydrogen greatly affects the electronic and structural properties of many materials. The question whether hydrogen in their molecular form can also affect the electronic and structural properties is also important. In Section 4.1, we describe the single molecule and co-adsorptions of hydrogen and oxygen in armchair SiNTs. In Section 4.2 the adsorption in zigzag SiNTs will be also discussed.

4.1 Single Molecule and Co-Adsorptions of Hydrogen and Oxygen Molecules in Armchair Silicon Nanotubes

First, we discuss the interaction between single hydrogen/oxygen molecule and armchair SiNTs. The adsorption energies, HOMO-LUMO gaps and charge distribution will be investigated thoroughly. The adsorption energy for each system was computed from:

E_a= {[E (SiNT) + E (X_2)]-E (SiNT+X_2)} , if the molecule does not dissociate (4.1)

or

E_a= {[E (SiNT) + 2E (X)]-E (SiNT+2X)}/2 , if the molecule dissociates (4.2)

Where E(SiNT) is the ground state total energy of the bare silicon nanotube, E (X_2) and E (X) are the ground state energies of the X molecule and atom, respectively. E (SiNT+X_2) and E (SiNT+2X) are the total energies of the optimized clusters incorporating SiNT and the adsorbed molecule or atom. All nanotubes are hydrogen terminated at two ends to saturate the dangling bonds and to simulate the effect of “infinite” tubes. The radial buckling was calculated by taking the standard deviation of the distance from the Si atoms to the tube axis.

We describe the interaction of molecules with SiNTs for (1) adsorption from outside of nanotube, (2) adsorption from inside of nanotube, (3) molecular axis perpendicular to the tube axis, (4) molecular axis parallel to the tube axis. To find the most stable configuration, several adsorption sites have been considered, depending on the position and orientation of molecular bond. The molecule can be located at the top of Si atom, the bridge of Si-Si bond (normal bridge site and the zigzag bridge site), and the center of the Si hexagon (hollow site).

Adsorptions of single hydrogen molecule

The study of single hydrogen molecule adsorption has been performed with two orientations for the hydrogen molecule, one being perpendicular and the other being parallel to the tube axis. For both perpendicular and parallel adsorptions, the hydrogen molecule could be placed outside or inside of the nanotube initially. We first investigate the molecular adsorption from outside of the nanotube. When the hydrogen molecule approached the SiNT from outside

the nanotube, after optimization we note that for all of the four initial sites of perpendicular adsorption, the optimized structure of the nanotube and the hydrogen molecule has a H-H distance of 0.75 Å. Since in our calculation, the optimized H_2distance without the nanotube was also 0.75 Å (the experimental bond length is 0.74 Å), it is reasonable to assume that the molecule did not dissociate and, in fact, maintained the original diatomic linear structure. In addition, for all four different initial sites, after optimization the hydrogen molecule moved to on-top site. For example, when the hydrogen molecule was placed in normal bridge site initially perpendicular to the tube axis (Fig. 4.1), after optimization the hydrogen molecule moved to the on-top site.In the case of parallel adsorption, the hydrogen molecule moved to various sites, still holding a molecular form. But the most stable site is still the on-top site. However, the hydrogen molecule changed its orientation from parallel to perpendicular to the tube axis. For example, in Fig. 4.1, the hydrogen molecule was placed initially in an on-top site with the hydrogen molecule parallel to the tube axis. After optimization, the hydrogen molecule is still in an on-top site but realigns itself perpendicular to the tube axis. Hydrogen molecules, most likely, orient themselves perpendicular to the tubes if adsorbed in on-top site.

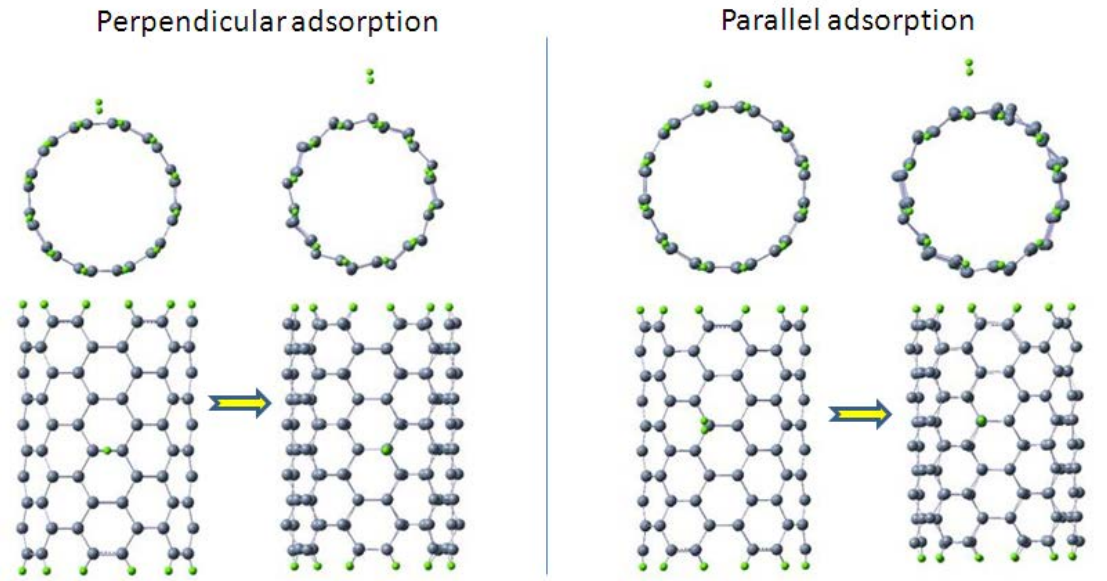

Figure 4.1 Perpendicular and parallel adsorption of H_2molecule from outside of the nanotube Si (6, 6).

As is well known, silicon, in stable form, favors a sp^3 configuration as opposed to a sp^2 configuration favored by carbon**.** In this study, the adsorbent is a bare Si (6, 6) nanotube with a smooth tube wall presenting a planar sp^2-like structure. After adsorption of the hydrogen molecule, the surface of the nanotube becomes more puckered, indicating the possibility of the existence of sp^3-like hybridization. To determine the possibility of any transition from sp^2 to sp^3, we performed a natural bond orbital (NBO) analysis. The bare Si (6, 6) nanotube only has sp^2-like bonds which can be confirmed from the Gaussian NBO analysis[132]. The hybridization of silicon atoms on Si (6, 6) is around $sp^{2.01}$ on average. For bare nanotube, each silicon atom forms three sp^2-sp^2 σ bonds and one π bond with three neighboring Si atoms. After adsorption of hydrogen molecule from outside of the nanotube, the hybridization of the silicon atoms increased to, on the average, to about around $sp^{2.41}$. It is evident that the transition from sp^2-like to sp^3-like hybridization among silicon atoms occurred after hydrogen adsorption. This tendency for sp^2-sp^3 hybridization upon H_2 adsorption is strong for Si (6, 6), because highly bent sp^2 bonding of the nanotube is favored for the transition to sp^3-like bonding. It should be noted that

although there is a tendency for the sp^2-to-sp^3 transition, we do not see pure sp^3 hybridization of Si atoms on the tube. Fig.4.2 shows NBO plot of one Si atom on the Si (6, 6) nanotube after external adsorption of the hydrogen molecule with three σ bonds and one π bond again instead of four sp^3-sp^3 bonds. A careful examination of the structure of the nanotubes reveals that there are basically two kinds of local geometrical configurations for the Si atoms, one being pyramidal (the sum of the angles between one Si atom and other three Si atoms surrounding it is approximately 338°) and the other planar (approximately 355°) (Fig. 4.3). There is an alternation of these two kinds of structures throughout the nanotube, attributed to the existence of possible geometrical frustration effect.[133] The geometrical frustration is revealed in that a certain type of local order favored by physical interactions cannot propagate throughout space. However, in the case of Si nanotubes, the frustration effect resulted in the co-existence of two different local structures. In Fig. 4.4, we note that the hexagonal ring in our study has a chair-like ring structure, with the “chair seat” flattened to some extent. This "flattened chair seat" effect could be more pronounced in silicon nanotubes with small diameters. It can be noted that there is an outward and inward local structural distortion along the radial direction which is consistent with significant increase of the radial buckling from 0.039 to 0.26Å. The large adsorption energy of hydrogen molecule on Si (6, 6) could also be mostly from the "frustration" of the local structure on the surface induced by the adsorption of hydrogen molecule.

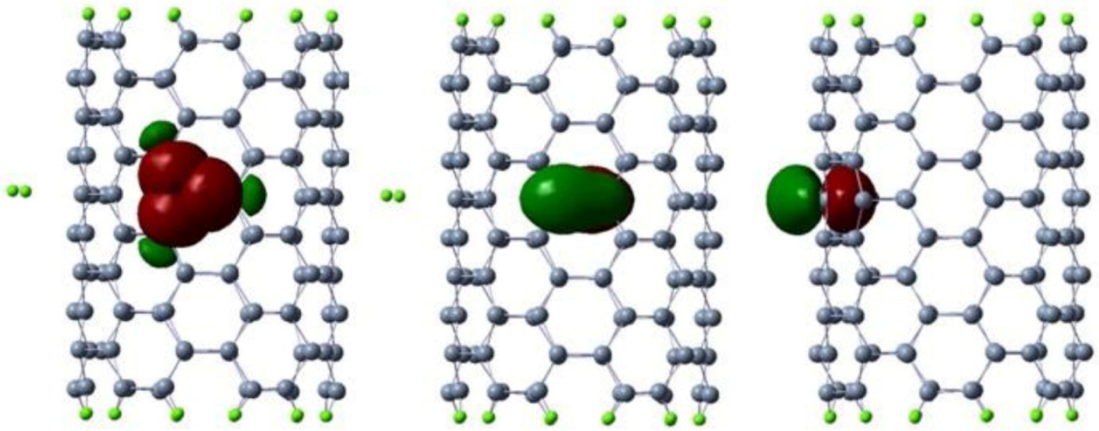

Figure 4.2 NBO plot of a Si atom on Si (6, 6) after external adsorption of single hydrogen molecule (a) the three sp^2-sp^2 like bonding, (b) and (c) the π bond.

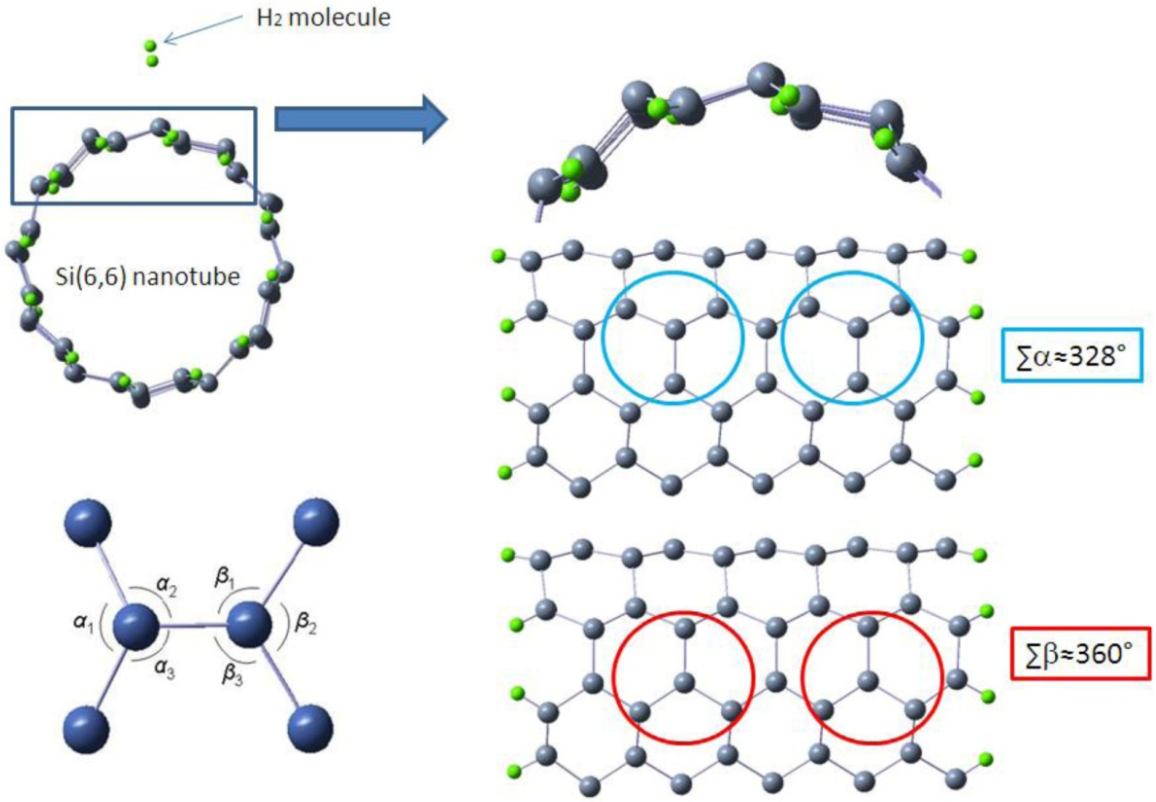

Figure 4.3 Two types of local configurations on Si(6,6) nanotube after molecular hydrogen adsorption.

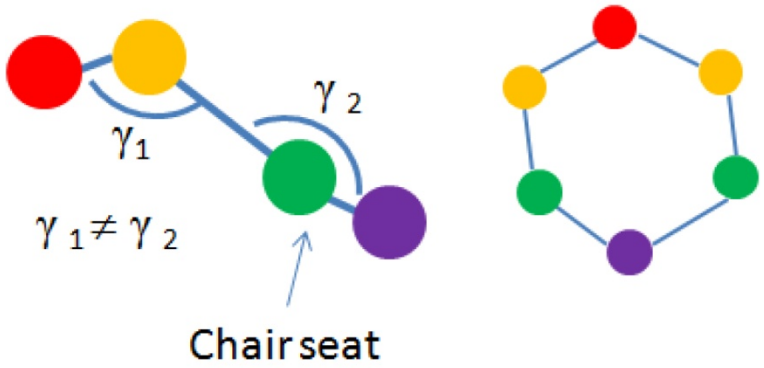

Figure 4.4 Side and top views of "chair-like" hexagonal ring after molecular adsorption on Si(6,6) nanotube.(Two yellow and two green Si atoms are overlapping each other so we only see one atom from side view)

As far as bond lengths are concerned, the bare Si (6, 6) nanotube before adsorption had an average bond length of 2.240 Å. After adsorption, the average bond length increased to 2.269 Å. The bond-length measurements showed that the frustration effect is mainly caused by the local strain because a change in bond lengths occurs only for Si-Si bonds. We also examined the HOMO-LUMO gaps (Tables 4.1 and 4.2) and the Mulliken charge distribution (Fig.4.5) on the nanotubes. The bare Si (6, 6) nanotube has a HOMO-LUMO gap of 0.98eV and the charges on Si atoms are all very close to zero which means the absence of any charge polarization. The HOMO-LUMO gap increased from 0.98 to 1.26eV for the most stable on-top site after adsorption of hydrogen molecule and significant charge polarization was observed on the nanotubes. In Figure 4.1, after optimization the Mulliken charge is -0.007|e| and 0.009|e| on the two hydrogen atoms. The hydrogen atom with Mulliken charge of 0.009|e| is closer to nanotube than the other. The nearest Si atom has a Mulliken charge of -0.097|e|. The hydrogen molecule is slightly polarized and attracted to the nanotube by the negatively charged Si atom. Each negatively charged Si atom is surrounded by three positively charged Si atoms and vice versa. The negatively charged Si atoms are displaced away from the surface forming the tip of

the pyramid. The driving force for such surface reconstruction effect is the attempt of the surface to lower its energy. This effect is similar as the relaxation at the (100) surface of sodium chloride while the negative chloride ions are displaced away from the bulk and the positive sodium cations are displaced inwards.[134] Since the HOMO-LUMO gap gives an indirect estimate of the electrical conductivity of the nanotube, the increase of the gap upon adsorption of hydrogen molecule implies a possible decrease of the electrical conductivity.

Table 4.1 Initial and final sites for external adsorption of onehydrogen molecule perpendicular to the tube axis, the shortest H-Si distance, adsorption energy and HOMO-LUMO gap.

Initial site	Final site	D_{H-Si} (Å)	D_{H-H} (Å)	Adsorption energy (eV)	HOMO-LUMO gap (eV)	Radial buckling (Å)
Normal B.	On-top	3.31	0.75	3.71	1.26	0.261
Zigzag B.	On-top	3.31	0.75	3.71	1.26	0.261
Hollow	On-top	3.31	0.75	3.71	1.26	0.261
On-top	On-top	3.31	0.75	3.71	1.26	0.261

Table 4.2 Initial and final sites for external adsorption of onehydrogen molecule parallel to the tube axis, the shortest H-Si distance, adsorption energy and HOMO-LUMO gap.

Initial site	Final site	D_{H-Si} (Å)	D_{H-H} (Å)	Adsorption energy (eV)	HOMO-LUMO gap (eV)	Radial buckling (Å)
Normal B.	Normal B.	4.99	0.75	1.80	0.37	0.247
Zigzag B.	Zigzag B.	3.97	0.75	2.50	0.56	0.254
Hollow	Hollow	3.99	0.75	2.64	0.96	0.341
On-top	On-top	3.67	0.75	3.69	1.26	0.264

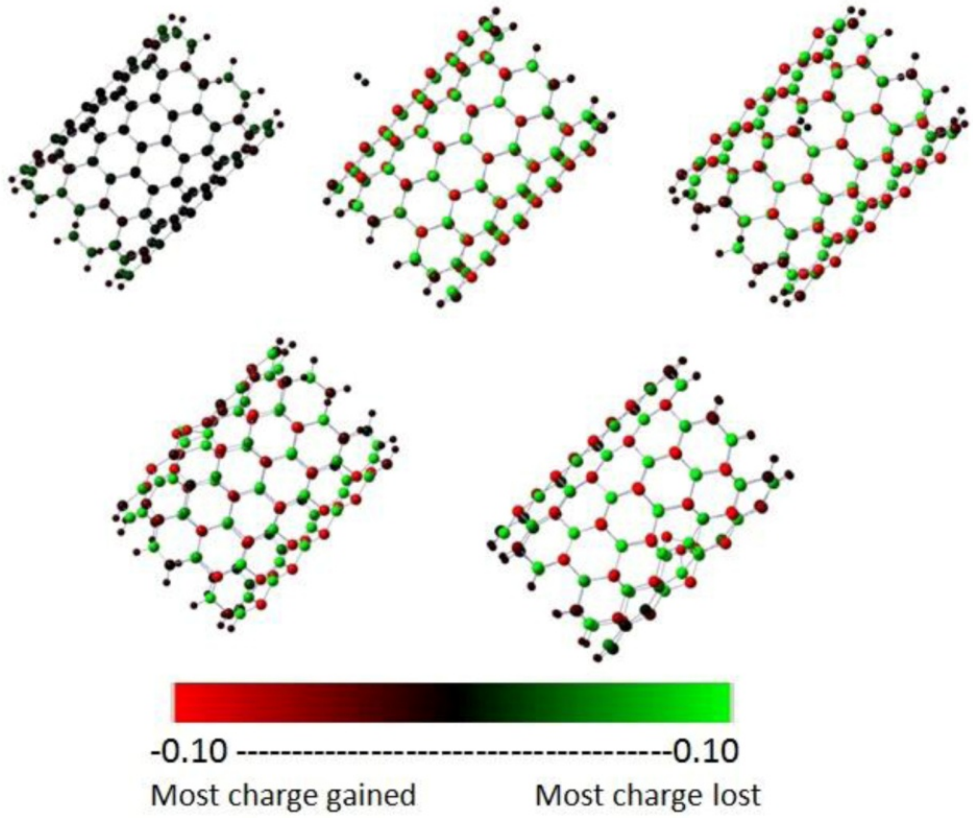

Figure 4.5 Mulliken charge distributions for Si nanotubes. Hydrogen atoms at dangling bonds remain almost neutral.(The first row from left to right: bare Si(6,6) nanotube, external adsorption of H_2 and Internal adsorption of H_2, the second row from left to right: external adsorption of O_2, internal adsorption on O_2)

The internal adsorption of hydrogen molecule showed similar trends as external adsorption. The parallel adsorption tends to be, in general, less favorable because after optimization the hydrogen molecule changed its orientation from parallel to perpendicular to the tube axis. In both perpendicular and parallel cases, the hydrogen molecule did not dissociate, with a bond length of 0.75 Å. In perpendicular adsorption, on-top site is the only preferred site whereas in the parallel adsorption on-top site is the most preferred site, in agreement with the most stable site for the external adsorption. Fig. 4.6 shows a typical example of the hydrogen molecule placed initially in normal bridge site perpendicular to the tube axis and moving to the on-top site with the molecular axis perpendicular to the tube axis after optimization. Fig. 4.6

shows a similar example of the hydrogen molecule placed initially in zigzag bridge site parallel to the tube axis and moving to the on-top site perpendicular to the tube axis after optimization. However, for perpendicular adsorption, although the on-top site is the only preferred site, the adsorption energies for the four different initial sites are not the same. It should be noted that, in general, as the distance between the hydrogen molecule and the nearest Si atom increases, the adsorption energy decreases as a result of weaker interaction (Tables 4.3 and 4.4). Similar to external adsorption, the HOMO-LUMO gap increases for the on-top site, accompanied also by increases in radial buckling and the average Si-Si bond length. NBO and geometrical analysis also yield similar results as for the external adsorption of hydrogen molecule. (Fig.4.7) There is sp^2-to-sp^3 transition occurring throughout the tube and also alternate pyramidal and planar configurations are observed throughout the nanotube. The stretch of Si-Si bond length was also observed for internal adsorption, resulting in effects similar to applications of mechanical stress.[135] The adsorption of the hydrogen molecule on the on-top site results in an increase of the band gap. This may be explained by the more sp^3 character contribution to the decrease of the band gap (i.e. sp^2 graphite is conductor while sp^3 diamond is insulator) in the case of the adsorption at the on-top site. We should stress here that the combined contributions of the sp^3 character and bond stretch effects on the band gap requires further investigation.

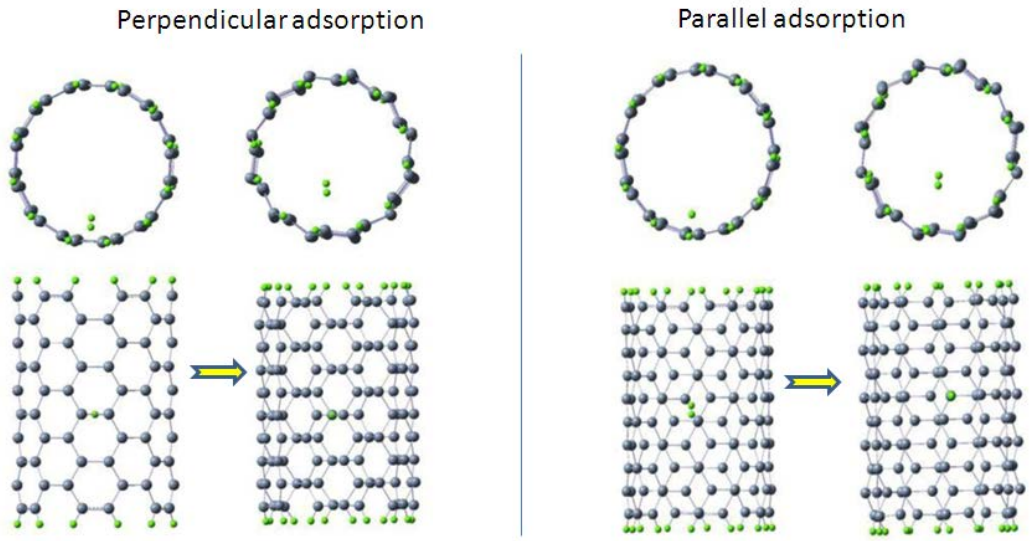

Figure 4.6 Perpendicular and parallel and adsorption of H_2 from inside of the nanotube.

Table 4.3 Initial and final sites for internal adsorption of onehydrogen molecule perpendicular to the tube axis, the shortest O-Si distance, adsorption energy and HOMO-LUMO gap.

Initial site	Final site	D_{H-Si} (Å)	D_{H-H} (Å)	Adsorption energy (eV)	HOMO-LUMO gap (eV)	Radial buckling (Å)
Normal B.	On-top	3.18	0.75	3.70	1.26	0.261
Zigzag B.	On-top	3.44	0.75	2.11	0.79	0.246
Hollow	On-top	3.27	0.75	2.66	0.99	0.356
On-top	On-top	3.21	0.75	3.70	1.26	0.261

Table 4.4 Initial and final sites for internal adsorption of onehydrogen molecule parallel to the tube axis, the shortest O-Si distance, adsorption energy and HOMO-LUMO gap.

Initial site	Final site	D_{H-Si} (Å)	D_{H-H} (Å)	Adsorption energy (eV)	HOMO-LUMO gap (eV)	Radial buckling (Å)
Normal B.	Normal B.	4.83	0.75	2.65	0.95	0.362
Zigzag B.	On-top	3.77	0.75	3.69	1.26	0.261
Hollow	Hollow	3.65	0.75	2.70	0.99	0.244
On-top	On-top	3.82	0.75	3.69	1.26	0.264

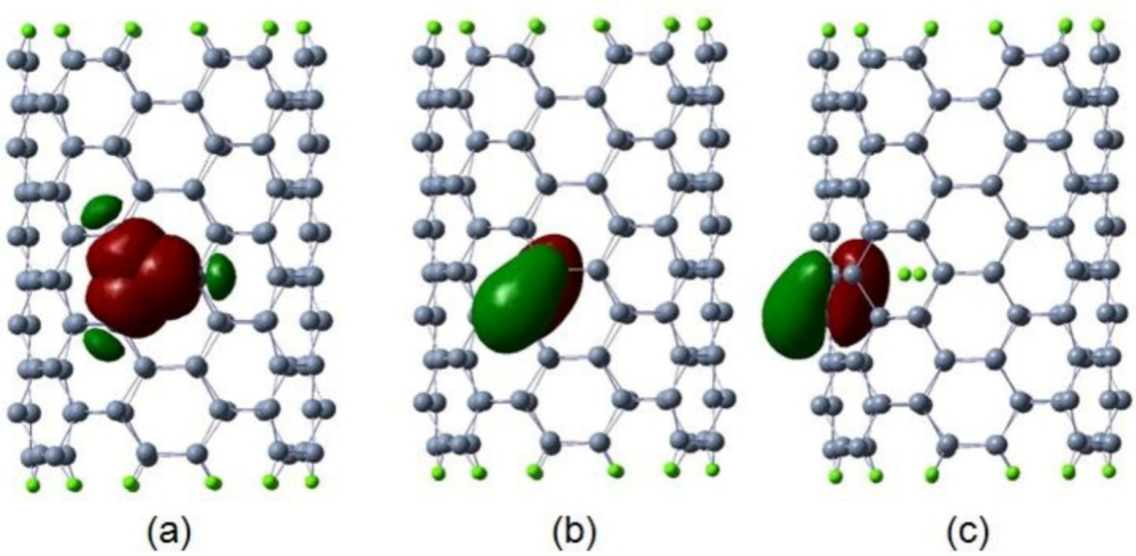

Figure 4.7 NBO plot of a Si atom on Si (6, 6) after internal adsorption of single hydrogen molecule : (a) the three sp^2-sp^2 like bonding (b) and (c) the π bond.)

Adsorptions of single oxygen molecule

The study of oxygen molecule adsorption was performed using the same set of structures and same adsorption sites as was used for adsorption of hydrogen molecule. In the external perpendicular adsorption of oxygen molecule, the molecule dissociated into two atoms, and the two oxygen atoms moved to two sites in most cases (Table 4.5). The most stable sites are the two bridge sites. For example, when an oxygen molecule was placed in the normal bridge site initially perpendicular to the tube axis, after optimization the oxygen molecule dissociated into two oxygen atoms. One oxygen atom moved to normal bridge site and the other moved to zigzag bridge site. (Fig.4.8)In three cases of perpendicular adsorption, the two oxygen atoms are in normal bridge site and zigzag bridge site with the largest adsorption energy of 9.64eV. Mulliken charge analysis shows that there is significant charge transfer between two oxygen atoms and the neighboring silicon atoms due to the difference in the electronegativities between O and Si atoms (Fig.4.9). The electronegativity of oxygen is larger than silicon and

thus there is charge transfer from Si to O which can be confirmed from Fig. 4.9. Although in three cases the oxygen atoms are all at the normal bridge and zigzag bridge sites, their adsorption energies, HOMO-LUMO gap, as well as distance between the two dissociated oxygen atoms differ from case to case. The oxygen molecule did not dissociate when we placed the molecule at the on-top site initially perpendicular to the tube axis. The O-O distance is 1.58 Å indicating a slightly stretched O-O molecular bond, and the bond is parallel to the Si-Si bond bridge. The oxygen molecule and the neighboring Si atoms form a Si-O-O-Si structure (Fig.4.9(b)) thus giving rise to a charge-transfer complex (CT complex). In this charge-transfer complex, a fraction of electronic charge is transferred between the oxygen molecule and the single-walled SiNT. The resulting electrostatic attraction provides a stabilizing force for the complex. This nature of attraction in a charge-transfer complex is not a stable chemical bond and is much weaker than covalent bond. The total energy of this complex is higher than the three dissociative cases indicating this structure may be an intermediate or transition state.

Table 4.5 Initial and final sites for external adsorption of oneoxygen molecule perpendicular to the tube axis, the shortest O-Si distance, adsorption energy and HOMO-LUMO gap.

Initial site	Final site	D_{O-Si} (Å)	D_{O-O} (Å)	Adsorption energy (eV)	HOMO-LUMO gap (eV)	Radial buckling (Å)
Normal B.	NB+ZB	1.65/1.68	2.80	9.64	1.01	0.309
Zigzag B.	NB+ZB	1.71/1.72	3.53	9.26	1.00	0.278
Hollow	NB+ZB	1.71/1.72	3.69	9.27	0.95	0.292
On-top	Top+Top	1.74/1.74	1.58	5.18	0.87	0.340

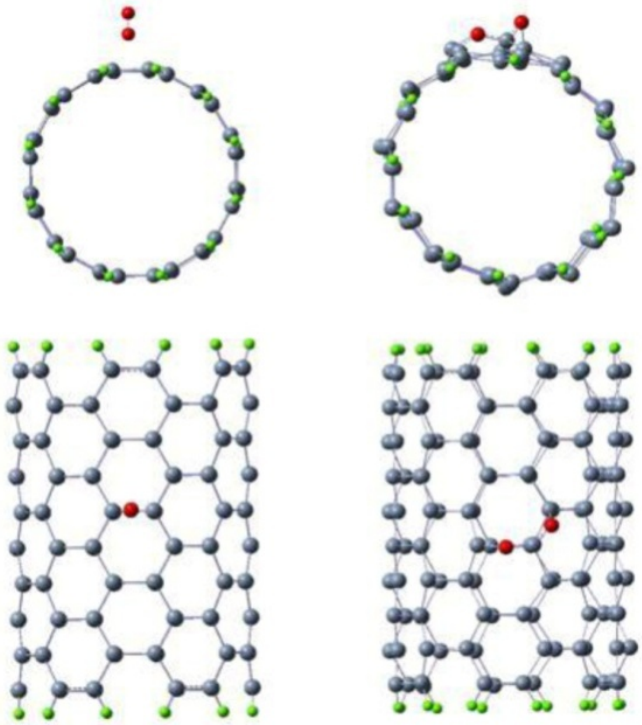

(a) (b)

Figure 4.8 Perpendicular adsorption of O_2 from outside of the nanotube: (a) Initial site: normal bridge; (b) Final site: normal bridge & zigzag bridge.

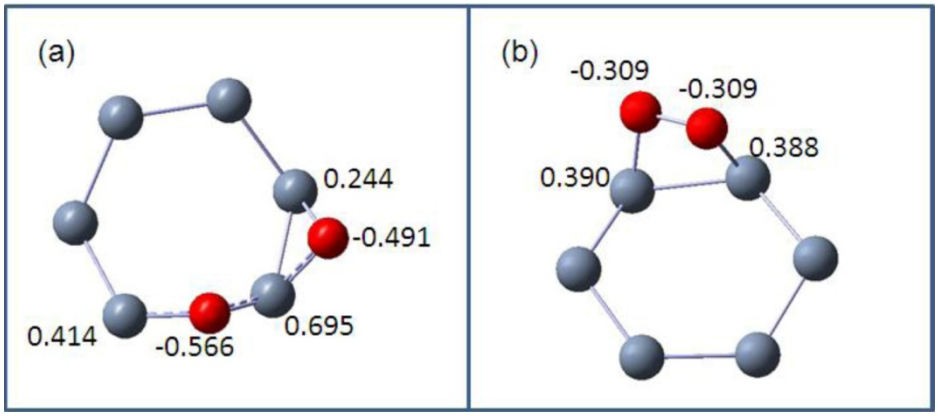

Figure 4.9 Local adsorption configurations and Mulliken charge of O_2 on the sidewall of SiNTs. ((a) the external adsorption with both oxygen atoms on bridge sites and (b) the external adsorption with the oxygen molecule parallel to the bridge)

In the case of parallel adsorption, the oxygen molecule dissociated only in one case and the two oxygen atoms are all in normal bridge site (Fig.4.10) with adsorption energy of 9.57eV (Table 4.6). In other three cases the oxygen molecules did not dissociate and they have a slightly stretched bond length. Combined with the observation from the perpendicular adsorption, we noticed that when the oxygen molecule did not dissociate, it only stayed on top of the silicon bridge with the O-O bond parallel to the Si-Si bond bridge underneath. And when the nanotubes have similar radial buckling, the adsorption energies and the HOMO-LUMO gaps are also very close (in the case when the molecule did not dissociate). Therefore the radial buckling provides a qualitative view of the geometry deformation along with the stability of the nanotube.

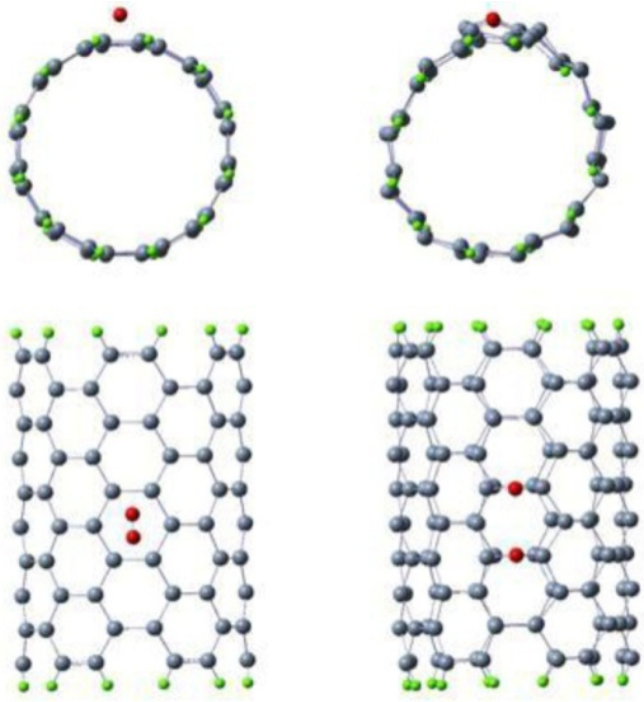

(a) (b)

Figure 4.10 Parallel adsorption of O_2 from outside of the nanotube: (a) Initial site: hollow site; (b) Final site: normal bridge & normal bridge.

Table 4.6 Initial and final sites for external adsorption of oneoxygen molecule parallel to the tube axis, the shortest O-Si distance, adsorption energy and HOMO-LUMO gap.

Initial site	Final site	D_{O-Si} (Å)	D_{O-O} (Å)	Adsorption energy (eV)	HOMO-LUMO gap (eV)	Radial buckling (Å)
Normal B.	Top+Top	1.74/1.72	1.57	5.68	1.02	0.308
Zigzag B.	Top+Top	1.74/1.74	1.58	5.19	0.87	0.339
Hollow	NB+NB	1.65/1.64	3.68	9.57	0.80	0.340
On-top	Top+Top	1.73/1.75	1.58	5.66	1.02	0.298

In general, molecular chemisorptions of O_2 on the SiNT sidewall is stronger than H_2, as indicated by larger adsorption energies. The bond length measurement shows an increase from 2.240 Å to 2.268 Å and the hybridization of the silicon atoms increased to around $sp^{2.31}$ on average after adsorption of oxygen. Alternative pyramidal and planar configurations due to geometrical frustration effect are also observed on the nanotube. Fig. 4.11 shows the NBO analysis for external oxygen adsorption.

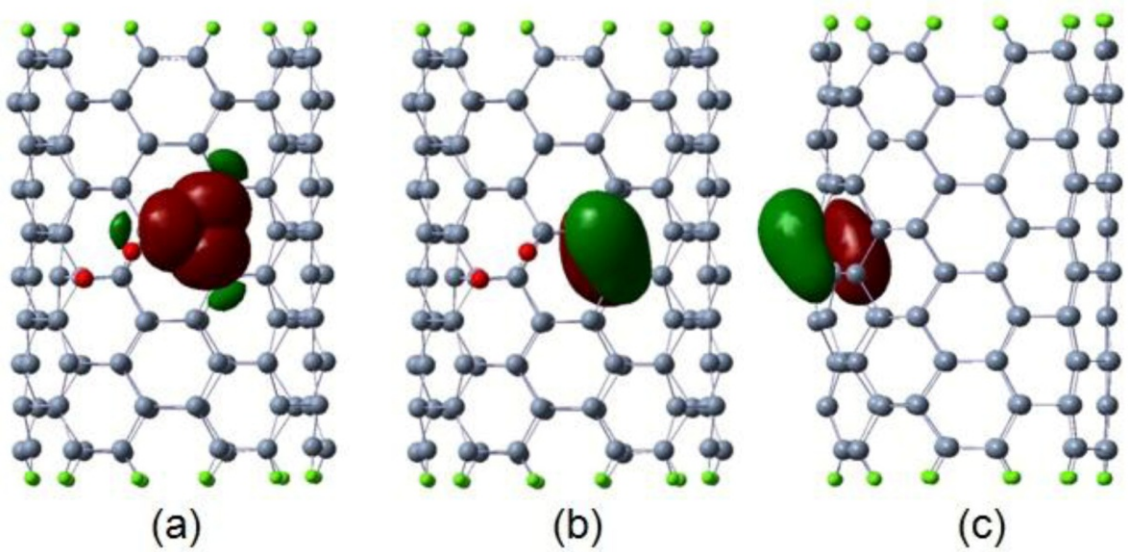

Figure 4.11 NBO plot of a Si atom on Si (6, 6) after external adsorption of single oxygen molecule (a) the three sp^2-sp^2 like bonding, (b) and (c) the π bond. Red atoms are oxygen atoms.

When the oxygen molecule is adsorbed from inside of the nanotube, the molecule also dissociated into two atoms in most cases. For example, in perpendicular adsorption, the two oxygen atoms all moved to zigzag bridge sites (Fig.4.12) with adsorption energy of 9.61eV(Table 4.7) when we placed the oxygen molecule in zigzag bridge site initially. The dissociated oxygen atoms could also be adsorbed in two normal bridge sites with smaller adsorption energy. The radial buckling for the internal adsorption is larger than the external adsorption indicating there is greater surface deformation. This is reasonable because when the oxygen molecule is placed inside of nanotube it could interact with more silicon atoms. The interaction of the oxygen with more silicon atoms induces greater deformation. When the oxygen molecule was placed in on-top site initially it did not dissociate with slightly increased bond length of 1.56 Å. And the O-O bond is parallel to the Si-Si bond bridge.

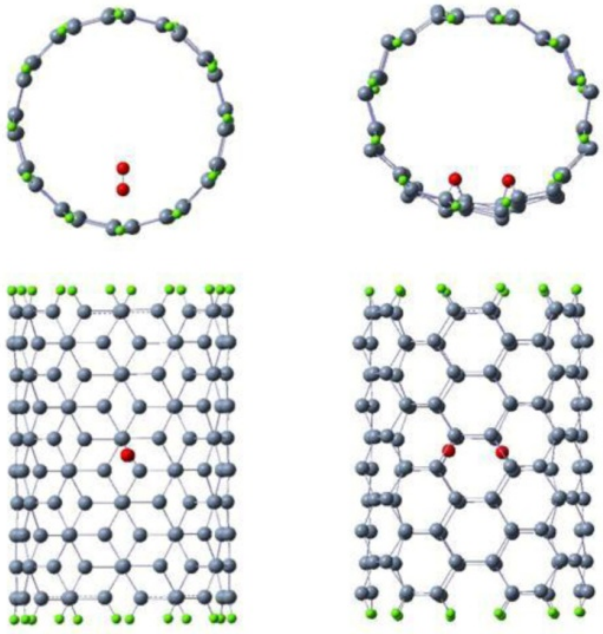

Figure 4.12 Perpendicular adsorption of O_2 from inside of the nanotube: (a) Initial site: zigzag bridge; (b) Final site: zigzag bridge & zigzag bridge.

Table 4.7 Initial and final sites for internal adsorption of oneoxygen molecule perpendicular to the tube axis, the shortest O-Si distance, adsorption energy and HOMO-LUMO gap.

Initial site	Final site	D_{O-Si} (Å)	D_{O-O} (Å)	Adsorption energy (eV)	HOMO-LUMO gap (eV)	Radial buckling (Å)
Normal B.	NB+NB	1.72/1.72	3.81	8.93	0.66	0.367
Zigzag B.	ZB+ZB	1.65/1.76	3.96	9.62	0.69	0.382
Hollow	ZB+ZB	1.7/1.72	3.26	9.00	0.97	0.383
On-top	Top+Top	1.71/1.73	1.56	5.60	0.79	0.398

In the case of parallel adsorption, the dissociated oxygen atoms moved to two normal bridge sites with an adsorption energy of 8.73eV when the initial site is hollow site, or two zigzag bridge sites (Fig. 4.13) with an adsorption energy of 9.93eV when the oxygen molecule was placed in on-top site initially. And when the oxygen molecule was placed in normal bridge or zigzag bridge site it did not dissociate and the oxygen molecule has a stretched bond length (Table 4.8). The oxygen molecule also forms a Si-O-O-Si structure with the neighboring silicon atoms accompanied by large charge transfer. We note that, the oxygen molecule is more likely to form the charge-transfer complex when it was placed parallel to the tube axis either for external or internal adsorption. This structure is also reported to have been observed in the initial stage of Si oxidation.[136]However, it is also reported that the Si-O-O-Si structure is energetically very unstable. Here, the clusters with the Si-O-O-Si structure all have a higher energy than the clusters with dissociative oxygen atoms indicating a less stable structure of Si-O-O-Si.

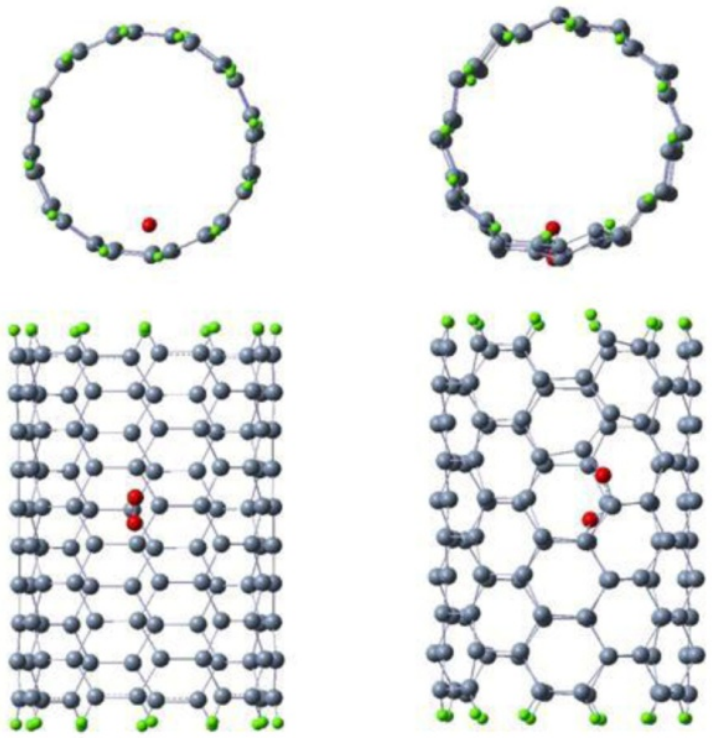

(a) (b)

Figure 4.13 Parallel adsorption of O_2 from inside of the nanotube: (a) Initial site: on-top site; (b) Final site: zigzag bridge & zigzag bridge.

Table 4.8 Initial and final sites for internal adsorption of oneoxygen molecule parallel to the tube axis, the shortest O-Si distance, adsorption energy and HOMO-LUMO gap.

Initial site	Final site	$D_{O\text{-}Si}$ (Å)	$D_{O\text{-}O}$ (Å)	Adsorption energy (eV)	HOMO-LUMO gap (eV)	Radial buckling (Å)
Normal B.	Top+Top	1.74/1.73	1.58	5.24	0.85	0.346
Zigzag B.	Top+Top	1.76/1.76	1.57	5.17	0.88	0.290
Hollow	NB+NB	1.73/1.72	3.69	8.73	0.61	0.287
On-top	ZB+ZB	1.64/1.72	2.77	9.93	1.23	0.311

When the oxygen molecule dissociates, the two oxygen atoms prefer to be adsorbed in bridge sites - two normal bridge sites, or two zigzag bridge sites, or one normal bridge site and one zigzag bridge site. The binding energy of Si-O dimer is 3.922 eV/atom and the binding energy of O-O dimer is 2.196 eV/atom with B3LYP functional and 3-21G* basis set. Therefore, it

is energetically more favorable for O molecules to dissociate and break Si-Si bond then form Si-O-Si structure. Highly reactive oxygen and silicon has a large difference in electronegativity (1.90 for silicon and 3.44 for oxygen) and thus it is comparatively easy to form Si-O-Si structure. The formation of the Si-O-Si has been observed on Si surface.[58] There are two types of Si-O-Si in our study of SiNTs. One type is that although the oxygen atom is interacting with both Si atoms, the two Si atoms also interact with each other. In the other case, the oxygen atom is breaking the Si-Si bond and bridging the two Si atoms. Hoshino[71] has studied adsorption of atomic and molecular oxygen on Si (111) surface. The Si-O-Si structure without the elimination of Si-Si bond is a transition state in his study and the bridging structure has a much lower potential energy. In silicon oxides, the Si-O-Si bond angles are not as rigid as the O-Si-O angles which are close to the value of standard sp^3 hybridization (109.5°) and can vary widely in different phases. In Fig.4.9(a), the oxygen atom with Mulliken charge -0.566e is breaking the Si-Si bond and forming a Si-O-Si chain structure, in which the Si-O bond length is 1.67 Å and 1.65 Å, respectively and the Si-O-Si angle is 137.6° . The oxygen atom with Mulliken charge of -0.491e is forming a Si-O-Si ring structure with two Si atoms, in which the Si-O bond length is 1.68 Å and 1.75 Å, the Si-Si bond length is 2.24 Å and the Si-O-Si angle is 81.2° . This is important in that it indicates in the Si-O-Si ring structure the Si-Si bond is a stable covalent bond and the other Si-O-Si bond formed by oxygen interstitially in silicon is very similar to that of SiO_2.

In general, hydrogen adsorption with the molecular axis aligned parallel to the surface of the nanotube is less favorable. Hydrogen molecule does not dissociate while oxygen molecule dissociates after optimization. The on-top site is the preferred site for hydrogen molecule with an adsorption energy of 3.71eV and an optimized distance of 3.31 A for external adsorption whereas the on-top site is the most preferred site with adsorption energy of 3.70eV for internal adsorption and an optimized distance of around 3.2 A. The adsorption of hydrogen in silicon nanotube which takes place near the surface would induce surface deformation and

frustration. The deformation or the frustration is accompanied by the transition of the hybridization of Si atoms on SiNTs from sp^2 to sp^3. For oxygen, the molecule dissociates and the most preferred sites are the two bridge sites with an adsorption energy of 9.64eV, the optimized distance being 1.65/1.68Å when it is adsorbed from outside of the tube. When oxygen molecule is originally placed at on-top site it will hold as a molecule after adsorption with a slightly increased bond length. For the internal adsorption of oxygen, the molecule also dissociates in most cases and the zigzag bridge site is the most preferred site with an adsorption energy of 9.93eV. The oxygen molecule could also be adsorbed parallel to the silicon bridge on the surface to form a Si-O-O-Si structure. But this structure is less stable than the dissociative adsorption. The oxygen molecule could also be adsorbed parallel to the silicon bridge on the surface to form a Si-O-O-Si structure. But this structure is less stable than the dissociative adsorption. After molecular adsorption for both hydrogen and oxygen, the buckling of the nanotubes increased.

Co-adsorptions of two hydrogen molecules

In co-adsorption of two hydrogen molecules, there are three initial configurations of the two hydrogen molecules. One is to place both of them outside of the nanotube, the second way is to place both of them inside of the nanotube and the third way is to place one hydrogen molecule inside and the other outside the nanotube. When two hydrogen molecules are adsorbed from outside of the nanotube, in all cases the optimized structure of the nanotube and the hydrogen molecule has a H-H distance of 0.75 Å. The optimized H_2distance without the nanotube was also 0.75 Å, the experimental bond length being 0.74Å; therefore, it is reasonable to assume that the hydrogen molecule did not dissociate and, in fact, maintained the original diatomic linear structure. This is consistent with our observation for single hydrogen molecule adsorption on silicon nanotube in which the hydrogen molecule also maintained the original diatomic structure.Hydrogen molecules oriented themselves perpendicular to the tubes if adsorbed in an on-top site and the most preferred site was the on-top site for single hydrogen

molecule adsorption. For co-adsorption, the most preferred site is still the on-top site in which two hydrogen molecules prefer to stay in two different on-top sites (Table4.9). After comparing the adsorption energy from co-adsorpion with single molecule adsorption, we found that the adsorption energy per hydrogen molecule has decreased when we increase the number of adsorbed hydrogen molecules. For example, the adsorption energy for single hydrogen molecule in on-top site was 3.710 eV, whereas in this study with the two hydrogen molecules both being in on-top sites the adsorption energy per hydrogen molecule is 1.857 eV.

Table 4.9 Initial and final sites for external adsorption of two hydrogen molecules, the shortest H-Si distance, adsorption energy and HOMO-LUMO gap.

Initial site (H_{out} and H_{out})	Final site (H_{out} and H_{out})	$D_{H\text{-}Si}$ (Å)	E_{ad}(eV)	E_{gap}(eV)
NB and NB	NB and Top	3.25	1.739	0.81
NB and ZB	Top and Top	3.32	1.854	1.26
NB and Hol	NB and ZB	3.73	1.323	0.99
NB and Top	Top and Top	4.02	1.757	1.26
ZB and ZB	Top and Top	3.30	1.857	1.26
ZB and Hol	Top and Top	3.28	1.854	1.26
ZB and Top	Top and Top	3.29	1.856	1.01
Hol and Hol	Top and Top	3.27	1.837	1.26
Hol and Top	Top and Top	3.31	1.854	1.26
Top and Top	Top and Top	3.30	1.856	1.26

As far as the distances are concerned, the distance from the two hydrogen molecules to the nearest Si atom are 3.31Å and 3.30 Å respectively, which is close to the result from single molecule adsorption of 3.31 Å. The "frustration" effect has been observed for single hydrogen molecule adsorption on silicon nanotube, in which the surface of the nanotube has been deformed from a smooth surface to a puckered surface. In that study, there are two kinds of local geometrical configurations for the Si atoms after adsorption, pyramidal and planar. Moreover, there is an alternation of these two kinds of structures on the nanotube, meaning every pyramidal structure is surrounded by three planar structures, and vice versa. This same

effect has also been noted for co-adsorption of two hydrogen molecules. We performed a NBO (Natural Bond Orbital) analysis for the clusters representing the bare Si (6, 6) nanotube and combinations of the Si (6, 6) tube and the hydrogen molecules. The hybridization of the silicon atoms on Si (6, 6) is around $sp^{2.01}$ on average, with basically sp^2-like bonds. After adsorption of hydrogen molecule from outside of the nanotube, the hybridization of silicon atoms increased to around $sp^{2.51}$ on average throughout the nanotube. It is evident that the transition from sp^2-like to an approximate sp^3-like hybridization among silicon atoms occurred after hydrogen adsorption. It should be noted that although there is a tendency for the sp^2-to-sp^3 transition, we do not see pure sp^3 hybridization of the Si atoms on the tube. The effect is consistent with the results on single hydrogen molecule adsorption on silicon nanotube in which the hybridization of the silicon atoms increased to around $sp^{2.41}$ on an average. At this stage of the calculation, we cannot predict the effect of the number of hydrogen molecules on the sp^2 to sp^3 bonding.

Mulliken charge analysis indicates strong charge polarization on the nanotube after adsorption. Fig.4.14 shows the Mulliken charge distribution on Si (6, 6) and the hydrogen molecules when two hydrogen molecules were placed in two separate zigzag bridge sites initially. The Mulliken charges on the hydrogen molecules are very small and they are barely polarized (Fig. 4.15). Each negatively charged Si atom is surrounded by three positively charged Si atoms and vice versa. In addition, the negatively charged Si atoms are displaced away from the surface extruding out thus forming the tip of a pyramidal structure. The positively charged hydrogen atom in the slightly polarized hydrogen molecule is attracted to the negatively charged silicon atom. Fig. 4.16 shows the HOMO (highest occupied molecular orbital) and the LUMO (lowest unoccupied molecular orbital), the orbitals most likely to be involved in any chemical reactions. The orbitals are spread throughout the whole tube. In general the more delocalized the orbitals are, more stable is the tube. Hybridization (sp^2-sp^3 transition) shifts the HOMO and LUMO and thus broadens the gap. Also, the bare Si (6, 6) nanotube before adsorption has an average bond length of 2.240 Å. After adsorption, the average bond length

increased to 2.267 Å. The bond-length measurement showed that the bond frustration effect is caused mainly by the local strain because a change in bond lengths occurs only for Si-Si bonds.

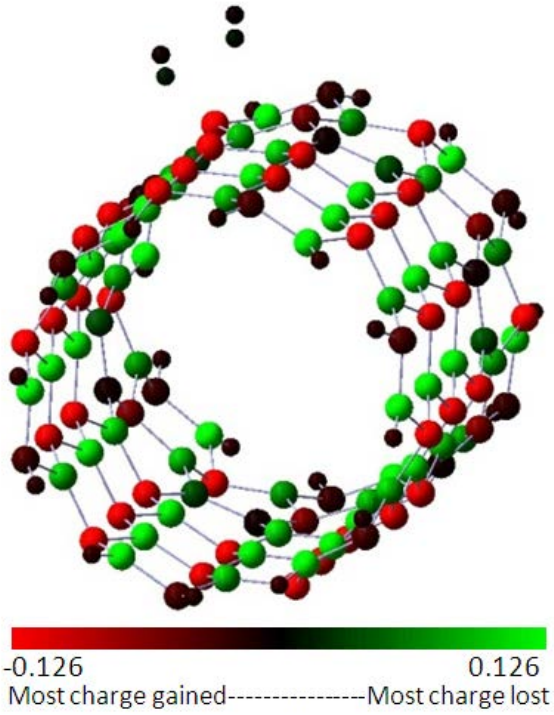

Figure 4.14 Mulliken charge distribution on the silicon nanotube when two hydrogen molecules are initially in zigzag bridge sites.

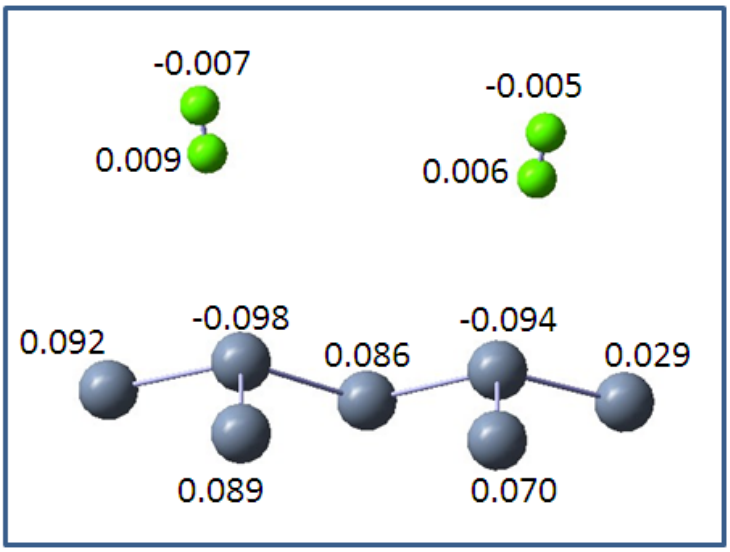

Figure 4.15 Mulliken charge distribution for co-adsorption of two hydrogen molecules when two hydrogen molecules are initially in zigzag bridge sites.

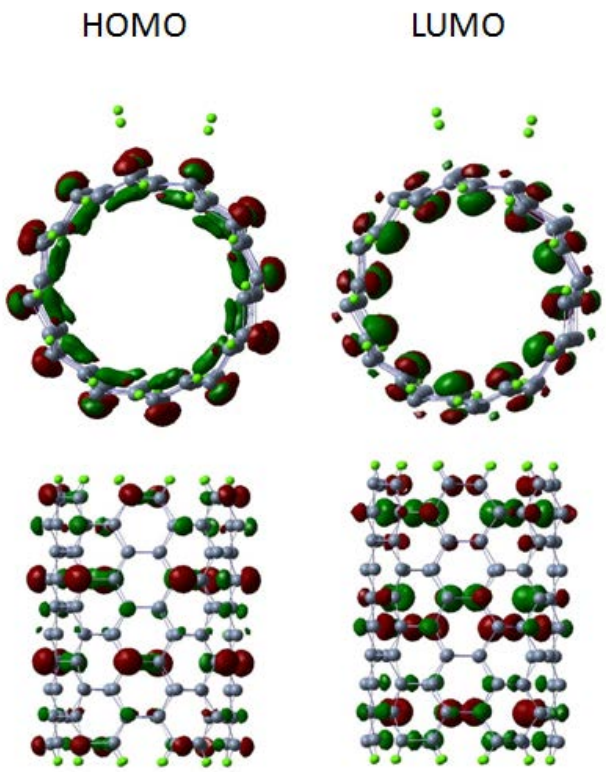

Figure 4.16 HOMO and LUMO for hydrogen adsorption when two hydrogen molecules are initially in zigzag bridge sites.

Table 4.10 Initial and final sites for internal adsorption of two hydrogen molecules, the shortest H-Si distance, adsorption energy and the HOMO-LUMO gap.

Initial site (H_{in} and H_{in})	Final site (H_{in} and H_{in})	$D_{H\text{-}Si}$ (Å)	E_{ad}(eV)	E_{gap}(eV)
NB and NB	NB and (Q)Top	3.36	1.327	0.96
NB and ZB	(Q)Top and (Q)Hol	3.55	1.347	1.26
NB and Hol	(Q)Top and (Q)Top	3.29	1.852	1.26
NB and Top	(Q)Hol and (Q)Top	3.77	1.325	0.96
ZB and ZB	Top and (Q)Top	3.16	1.333	0.95
ZB and Hol	Top and (Q)Top	3.14	1.328	0.96
ZB and Top	(Q)Top and Top	3.43	1.850	1.26
Hol and Hol	Top and (Q)Top	3.29	1.834	0.99
Hol and Top	(Q)Top and Top	3.15	1.853	0.97
Top and Top	Top and (Q)Top	3.14	1.853	0.99

When two hydrogen molecules are both adsorbed inside the nanotube, we observe a similar trend as external adsorption. The most preferred sites are still on-top sites (Table 4.10). For example, when one hydrogen molecules was placed in a hollow site and the other hydrogen molecule is placed in an on-top site, after optimization, the former one moved to an on-top site and the latter one stayed in the on-top site. However, in some cases, although the hydrogen molecule is on top of Si atom, it changes its orientation slightly, which is not strictly perpendicular to the tube axis. These on-top sites are called quasi on-top sites, which in the tables are written as (Q)Top. This effect could be caused by the interactions between the hydrogen molecules and the confinement of the tube wall. The highest adsorption per hydrogen molecule is 1.863 eV. When one hydrogen molecule is adsorbed from outside the nanotube while the other hydrogen molecule is adsorbed from inside the nanotube, the adsorption energy is close to the energies for the external and internal adsorptions discussed above. For example, when one hydrogen molecules was initially placed in zigzag bridge site and the other hydrogen molecule was in normal bridge site, after optimization they moved to two different quasi on-top sites, with an adsorption energy of 1.852 eV and a HOMO-LUMO gap of 1.26eV (Table 4.11).

Table 4.11 Initial and final sites for external/internal adsorptions of two hydrogen molecules, the shortest H-Si distance, adsorption energy and the HOMO-LUMO gap.

Initial site (H_{out} and H_{in})	Final site (H_{out} and H_{in})	D_{H-Si} (Å)	E_{ad}(eV)	E_{gap} (eV)
NB and NB	(Q)Top and (Q)Top	3.42	1.852	1.26
NB and ZB	(Q)Top and (Q)Top	3.40	1.854	1.26
NB and Hol	Top and (Q)Top	3.16	1.852	1.26
NB and Top	(Q)NB and (Q)Top	3.76	1.848	1.26
ZB and NB	(Q)Top and (Q)Top	3.22	1.852	1.26
ZB and ZB	ZB and (Q)ZB	3.46	1.847	0.99
ZB and Hol	(Q)ZB and (Q)Hol	3.33	1.827	0.99
ZB and Top	(Q)ZB and Top	3.27	1.848	1.26
Hol and NB	(Q)Hol and (Q)Hol	3.66	1.824	0.96
Hol and ZB	(Q)Hol and ZB	3.45	1.848	1.00
Hol and Hol	(Q)Hol and (Q)Hol	3.59	1.843	0.99
Hol and Top	(Q)Hol and (Q)Hol	3.35	1.848	0.97
Top and NB	(Q)NB and NB	3.67	1.782	0.97
Top and ZB	Top and ZB	3.54	1.828	0.98
Top and Hol	(Q)Top and (Q)Hol	3.13	1.852	1.26
Top and Top	Top and Top	3.26	1.851	0.98

Hydrogen is the simplest adsorbate but the adsorption of hydrogen on Si material is complex. The adsorption and desorption of hydrogen molecules on silicon is a subject of countless research, the phenomenon of hydrogen adsorption and desorption from Si surface has been reported by many groups. Therefore it is reasonable to assume this mechanism could also happen on SiNTs. In a previous study on atomic adsorption on SiNTs, the hydrogen atom plays a role of inducing a puckered structure on the tube wall of SiNTs. In the case of hydrogen molecule adsorption on the nanotube, the hydrogen molecule *may* have dissociated first onto the tube wall and induced the puckered structure, then desorbed and form a molecular form through recombination. However, H_2 does not dissociate spontaneously on silicon nanotube. Moreover, in this study, the hydrogen molecules could adopt different orientations other than being strictly perpendicular to the tube axis. This could be caused by the interaction between

the two hydrogen molecules. The HOMO-LUMO gaps generally increased after the adsorption of two H_2 molecules.

Co-adsorptions of two oxygen molecules

Similar to hydrogen, oxygen has the capacity to passivate silicon dangling bonds. However, unlike hydrogen, each oxygen atom would passivate two silicon bonds, as in silicon dioxide. The interaction of oxygen with silicon plays a very important role in both the bulk- and surface- governed electronic properties of semiconductors[62-64]. Plans *et al.*[68] have studied how oxygen breaks the covalent Si-Si bond forming a local configuration similar to that of SiO_2. Theoretical studies have shown that oxygen molecule is not stable in the Si lattice. Zhao *et al.*[72] have studied surface structures and electronic states of silicon nanotubes stabilized by oxygen atoms. Moreover, in silicon oxides, the Si-O-Si bond angles can vary widely in different phases. For example, the Si-O-Si bond angles in α cristobalite are 146° but become 180° in β cristobalite. Surface relaxations *may* modify the electronic state hybridization and the electrical and optical properties of nanotubes.

The adsorption of two O_2 molecules has been studied at the same arrangement of the adsorption sites as the two H_2 molecules to allow for comparative studies. However, different final configurations can result from the nature of oxygen interactions with silicon as compared to hydrogen interactions. When two O_2 molecules were adsorbed from outside the nanotube, complete dissociation (both O_2 molecules are dissociated), partial dissociation (one O_2 molecule is dissociated), and non-dissociation have been noted (Table 4.12). Fig.4.17a shows the complete dissociation of O_2molecules when one O_2 molecule was placed in NB site and the other O_2 molecule was placed in top site initially. Fig. 4.17b shows the partial dissociation of O_2 molecules when one O_2 molecule was placed in NB site and the other O_2 molecules was placed in ZB site. Fig. 4.17c shows the non-dissociation of O_2 molecules when one O_2 molecule was placed in hollow site and the other O_2 molecule was placed in top site.

Table 4.12 Initial and final sites for external adsorptions of two oxygen molecules, the shortest O-Si distance, adsorption energy and the HOMO-LUMO gap.

Initial Site (O_{out} and O_{out})	Final local config.	D_{O-Si}	E_{ad}(eV)	E_{gap}(eV)
NB and Top	4 O	1.63	7.592	1.12
NB and NB	4 O	1.65	7.277	1.02
ZB and ZB	4 O	1.64	7.276	0.99
NB and ZB	$1O_2$+2O	1.63	6.399	1.07
NB and Hol	$1O_2$+2O	1.65	6.318	1.02
ZB and Hol	$1O_2$+2O	1.69	6.065	0.96
ZB and Top	$1O_2$+2O	1.63	5.544	1.01
Hol and Top	$2O_2$	1.72	3.509	0.66
Hol and Hol	$2O_2$	1.72	3.325	0.66
Top and Top	$2O_2$	1.72	2.956	0.66

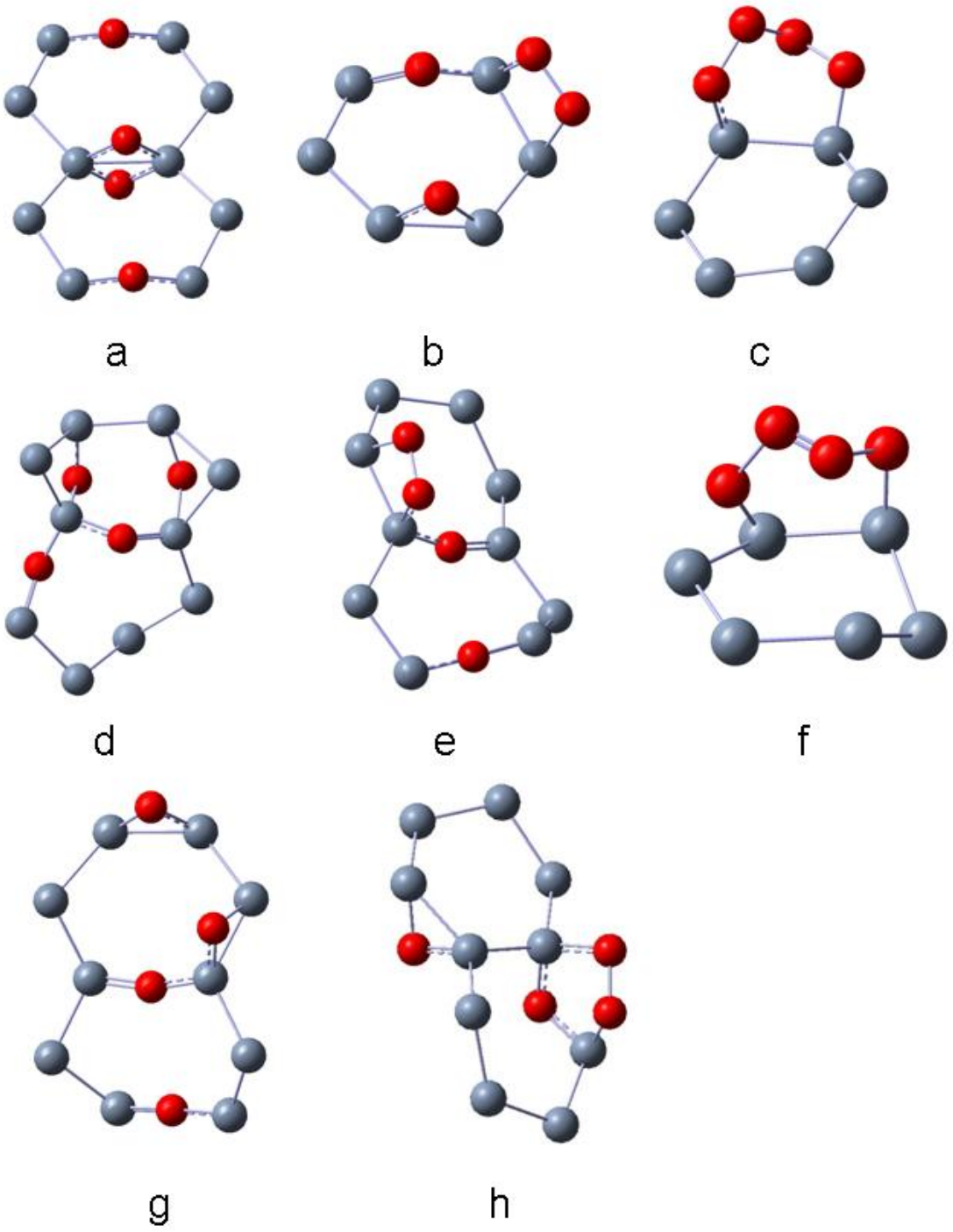

Figure 4.17 Local atomic geometry for co-adsorption of two oxygen molecules, a, b and c are the local configurations for two oxygen molecules adsorbed from outside of the nanotube; d, e, and f are the local configurations for two oxygen molecules adsorbed from inside of the nanotube; g and h are local configurations for one oxygen molecule adsorbed from outside and the other oxygen molecule from inside of the nanotube.

In Fig. 4.17a, two O atoms share a same normal bridge site and the other two O atoms are located in two different normal bridge sites. When the two O atoms share the same bridge site, the Si-O-Si angle is around 92.5°, but for O atoms located in separate bridge sites, the Si-O-Si angle is around 160°. The electronegativity of O atom is 3.44 and our calculations indeed indicate that there is a transfer of electron charge primarily from its two nearest-neighbor Si atoms. Fig.4.18 shows the Mulliken charge distribution on O atoms and neighboring Si atoms in Fig. 4.17a. In Fig. 4.17b, two O atoms are located in two bridge sites while the other two O atoms are forming a Si-O-O-Si structure with two Si atoms. The bond lengths of two Si-O bonds in the Si-O-O-Si structure are 1.68 Å and 1.76 Å respectively. The Mulliken charge (Fig. 4.19) on the two Si atoms are 0.766e and 0.215e, the Mulliken charge on two O atoms are -0.298e and -0.281e in the Si-O-O-Si ring structure indicating charge transfer from Si atoms to O atoms. In order to determine the bonding between the two O atoms, we performed NBO analysis on the two O atoms. Fig.4.20 shows the natural bond orbital plot between the two O atoms. The distance between the two O atoms is 1.58 Å, which means it is a stretched bond when compared to the bond length 1.30 Å of an O_2 molecule. In Figure 5c, we do not see any oxygen atom located in bridge site. Four O atoms form a Si-O-O-O-O-Si structure with two Si atoms. Fig.4.21 shows the Mulliken charge distribution on this ring structure. We see significant charge transfer from the Si atoms to the O atoms. However, the two O atoms in the middle have less charge (-0.024e and -0.005e) than the other two O atoms (-0.271e and -0.282e) that are bonded directly to Si atoms. Structure of Fig. 4.17c could be a "precursor state" in which the four O atoms form a charge transfer complex with the nanotube. The resulting electrostatic attraction provides a stabilizing force for the complex. The nature of the attraction in a charge-transfer complex is not a stable chemical bond, and is thus much weaker than covalent forces. Kim *et al.*[136] reported the identification of the precursor state in the initial stages of Si (111)-(7X7) oxidation and concluded that lifetime of molecular oxygen precursors are much short. It is possible that this precursor state could also take place in SiNTs.

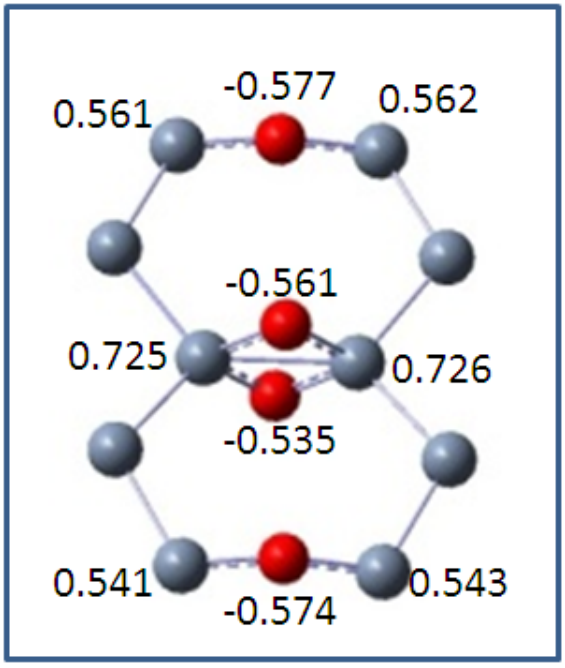

Figure 4.18 Mulliken charge distribution for Fig. 4.17a.

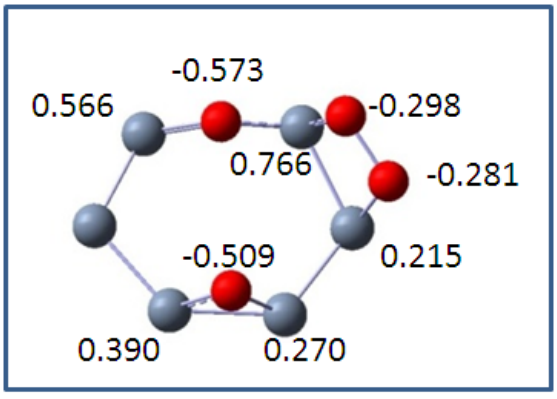

Figure 4.19 Mulliken charge distribution for Fig. 4.17b.

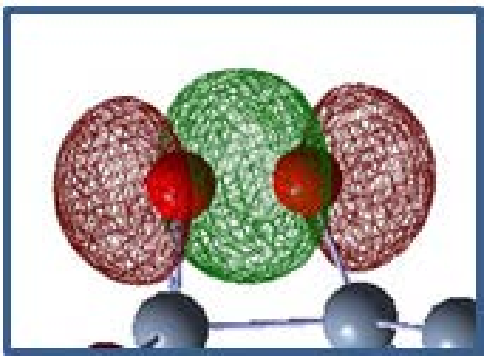

Figure 4.20 NBO of two oxygen atoms in peroxide of Fig. 4.17b.

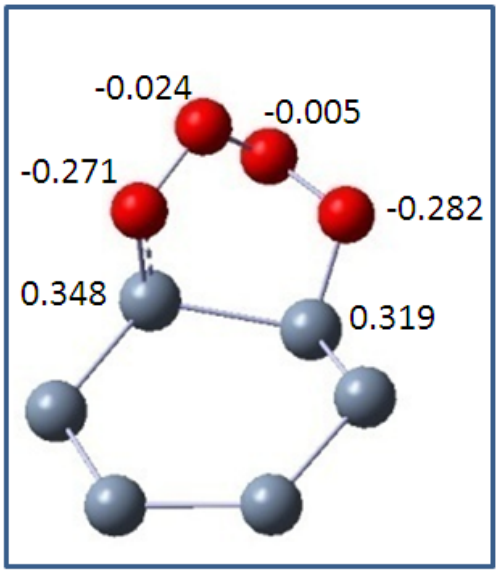

Figure 4.21 Mulliken charge distribution of Fig. 4.17c.

When two O_2 molecules are adsorbed both inside the nanotube, complete dissociation, partial dissociation and non-dissociation are also noted. Fig. 4.17d shows that two O atoms are bridging two non-neighboring silicon atoms while two other O atoms are occupying two separate bridge sites, when the two O_2 molecules were placed in two separate ZB sites initially. Fig. 4.17eshows two O atoms are in bridge sites and the other two O atoms are forming a Si-O-O-Si ring structure with the two Si atoms, when the two O_2 molecules were placed in two separate hollow sites. Due to the confinement of the tube wall, oxygen molecules inside the nanotube have a possibility to interact with more Si atoms than outside the nanotube. Fig. 4.17f shows the

Si-O-O-O-O-Si structure can also be formed when one O_2 molecule was placed in NB site and the other O_2 molecule was placed in top site. When we place one O_2 molecule outside of the nanotube and the other O_2 molecule inside of the nanotube, only complete dissociation and partial dissociation were noted. Fig. 4.17g shows the complete dissociation of O_2 molecules and Fig. 4.17h shows the partial dissociation. In this case, one oxygen molecule is outside and the other oxygen molecule is inside the nanotube and thus there is barely any interaction between the two O_2 molecules indicating the absence of any possible Si-O-O-O-O-Si structure. The highest adsorption energies are 7.592, 7.261, and 7.659 eV, respectively for the three cases with corresponding gaps of 1.12, 0.96, and 0.94 eV (Tables 4.12, 4.13, and 4.14).

Table 4.13 Summary of adsorption of two oxygen molecules, both from inside of SiNT, including the final configuration, adsorption energy and HOMO-LUMO gap.

Initial Site (O_{in} and O_{in})	Final local config.	D_{O-Si}	E_{ad}(eV)	E_{gap}(eV)
ZB and ZB	4 O	1.63	7.261	0.96
ZB and Hol	4 O	1.63	7.015	0.99
NB and ZB	4 O	1.62	6.903	1.10
NB and NB	4 O	1.64	6.551	0.98
Hol and Hol	$1O_2$+2O	1.73	6.824	1.05
ZB and Top	$1O_2$+2O	1.68	6.609	1.20
NB and Hol	$1O_2$+2O	1.66	6.501	1.12
Hol and Top	$1O_2$+2O	1.71	5.979	0.96
Top and Top	$1O_2$+2O	1.69	4.915	0.93
NB and Top	$2O_2$	1.74	2.826	0.53

Table 4.14 Summary of adsorption of two oxygen molecules, one from outside and one from inside of SiNT, including the final configuration, adsorption energy and HOMO-LUMO gap.

Initial Site (O_{out} and O_{in})	Final local config.	D_{O-Si}	E_{ad}(eV)	E_{gap}(eV)
ZB and Hol	4 O	1.64	7.659	0.94
NB and ZB	4 O	1.67	7.323	1.13
Hol and NB	4 O	1.63	7.114	0.94
ZB and ZB	4 O	1.65	7.074	0.93
Top and ZB	4 O	1.64	6.935	1.14
NB and NB	4 O	1.70	6.819	1.03
NB and Top	4 O	1.70	6.732	0.93
ZB and NB	4 O	1.68	6.461	0.97
Hol and Top	$1O_2$+2O	1.68	6.667	0.93
Hol and ZB	$1O_2$+2O	1.65	6.645	0.93
Top and Top	$1O_2$+2O	1.67	6.553	0.98
Top and Hol	$1O_2$+2O	1.64	6.259	0.87
Hol and Hol	$1O_2$+2O	1.70	6.239	1.16
NB and Hol	$1O_2$+2O	1.70	6.216	0.94
Top and NB	$1O_2$+2O	1.65	6.154	1.00
ZB and Top	$1O_2$+2O	1.69	4.768	0.85

By comparing the present results with previous findings, we conclude that oxygen prefers to be adsorbed in the bridge site on the tube wall of Si nanotube. With the exposure to oxygen at both sides of the silicon nanotube, oxygen bonds in bridge sites may cause adatom disorder. The result yields a novel picture of O_2 dissociation on Si nanotube, which emphasizes the importance of Si-O atom coordination, and of the three-dimensional nature of the dissociation process. Fig. 4.22 shows the HOMO and LUMO plots for adsorption of O_2 molecules of structure (Fig.4.17a). The HOMO and LUMO are localized on one half of the nanotube. Investigations of oxidation of tube wall of SiNTs elucidate the mechanisms by which oxygen combines with SiNTs. Substances based on single O-O bonds are known as peroxides. In adsorption of O_2 molecules the peroxide bridge of Si-O-O-Si has been formed in the form of ring structure. However, this Si-O-O-Si structure is less energetically favorable than other structures. Therefore, a probable dissociation mechanism could be as follows. First, some

electron charge from the tube wall reaches the highly electronegative O_2, then the double O=O bond of the physisorbed O_2 changes into a weaker O-O bond forming peroxide structure with Si atoms. Second, the single O-O bond is broken and the molecule dissociates moving to bridge sites on SiNTs. The HOMO-LUMO gaps for adsorption of two O_2 molecules vary from case to case. For complete dissociation, the two O_2 molecules are all dissociated and moved to bridge sites, reduced the electrical activity of the nanotube, thus increasing the HOMO-LUMO gap of the nanotube. For partial dissociation, the increase of the HOMO-LUMO gaps was also noted. However, for non-dissociation, the HOMO-LUMO gaps decrease.

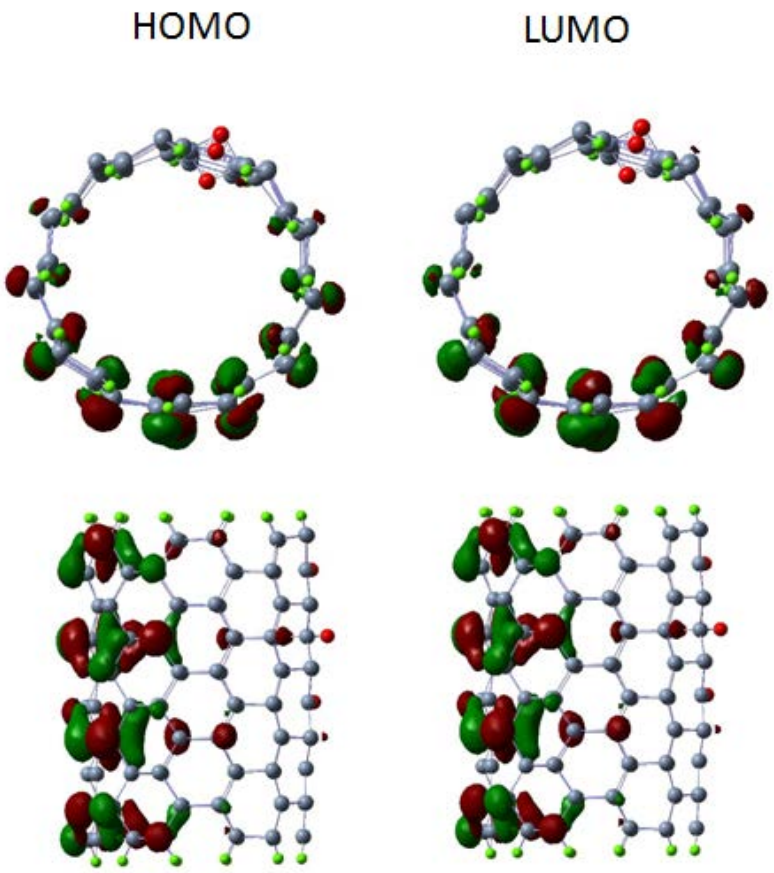

Figure 4.22 HOMO and LUMO for adsorption of two oxygen molecules.

Co-adsorptions of one hydrogen molecule and one oxygen molecule

Many groups have studied the adsorptions of hydrogen and oxygen on silicon surface and their interaction [137,138]. Markevich and co-worker [138] reported that hydrogen molecules located at tetrahedral interstitial site of Si interact with interstitial oxygen atoms and form O_i-H_2 complex. In this study, we have adopted the same arrangement for the adsorption sites of one H_2 molecule and one O_2 molecule as was done above for two hydrogen or two oxygen molecules. When we place both H_2 and O_2 molecules outside the nanotube, we found that the most preferred configuration is that the O_2 molecule dissociated into bridge sites while the H_2 molecule stayed on top of one O atom. Fig.4.23 shows several local atomic structures for external adsorption of hydrogen and oxygen. Fig. 4.23a shows two O atoms in two separate NB sites and H_2 molecule is on top of one O atom, when initially the H_2 and O_2 molecules are in two separate NB sites. Fig.4.23b shows one O atom is in NB site and the other O atom is in ZB site, the H_2 molecule is on top of one silicon atom, when initially the O_2 molecule was in hollow site and the H_2 molecule is in ZB site. Fig. 4.23c shows two O atoms form a Si-O-O-Si ring structure with two Si atoms and the H_2 molecule is on top of one O atom, when initially the O_2 molecule was in NB site and the H_2 molecule was in ZB site. Fig. 4.23d shows a similar structure as Fig. 4.23c but the H_2 molecule is on top of Si atom. Comparing Fig. 4.23a with Fig. 4.23b, the difference is in the position of the H molecule, it is either on top of an O atom or a Si atom, but the top site of O is more preferred. Comparing structure Fig. 4.23c with Fig. 4.23d, the difference is also in the position of the H molecule, it is either on top of an O atom or a Si atom, but the top site of O is more preferred. The H_2 molecule is thought to be one of the most stable and abundant species and is believed to be electrically inactive in Si. Our results show a complex of a bond-centered O atom with a weakly bound H_2 molecule in the vicinity. The arguments presented above leads us to conclude that the H_2 molecule is trapped adjacent to an O atom or a Si atom, but there is an energetic preference of O atom over Si atom. Fig. 4.24 shows Mulliken charge distribution on O atoms and the H_2 molecule in Fig.4.23a. There is a

large charge transfer from Si atoms to O atoms, and the H_2 molecule is slightly polarized. The H atom with Mulliken charge 0.010|e| is closer to the O atom with charge of -0.573e in Fig.4.27. The electrostatic attraction provides a stabilizing force for the hydrogen molecule and the nanotube. Fig.4.25 shows Mulliken charge distribution on the O atoms and the H_2 molecule in Fig. 4.23c, the Mulliken charge on two O atoms are -0.308|e| and -0.307|e|, and the H_2 molecules is also slightly polarized. The H atom with positive Mulliken charge is also closer to O atom, which means the electrostatic attraction plays an important role of stabilizing the force between H_2 and SiNT.

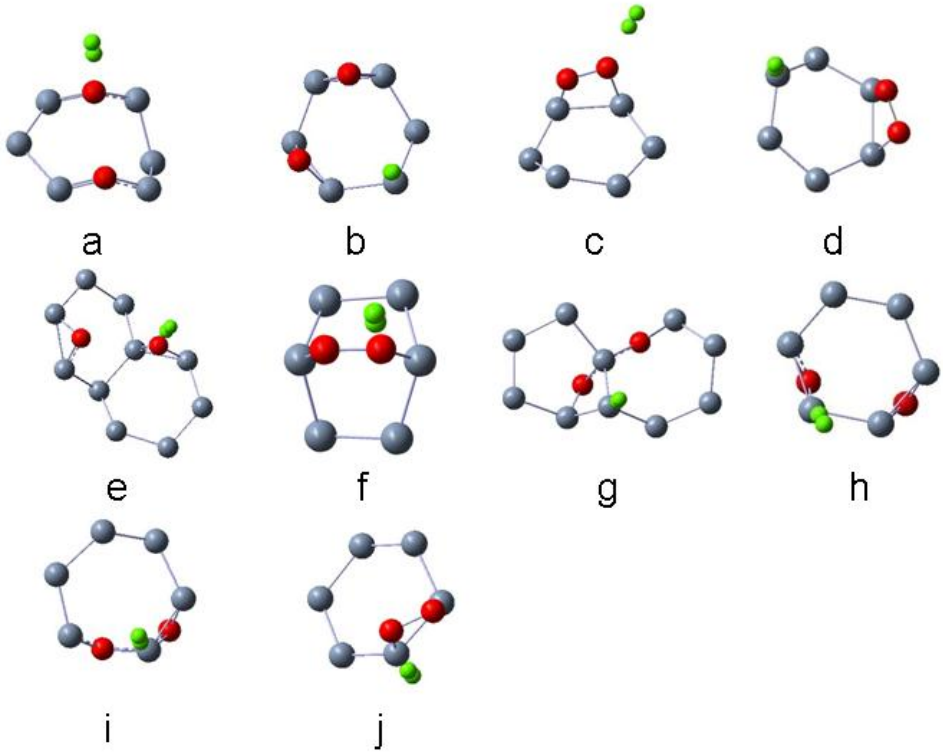

Figure 4.23 Local atomic geometry for co-adsorption of two oxygen molecules, a, b, c and d are the local configurations for two hydrogen molecules adsorbed from outside of the nanotube; e and f are the local configurations for two hydrogen molecules adsorbed from inside of the nanotube; g and h are local configurations for one hydrogen molecule adsorbed from outside and one oxygen molecule from inside of the nanotube; i and j are the local configurations for one hydrogen molecule adsorbed from inside and one oxygen molecule from outside of the nanotube.

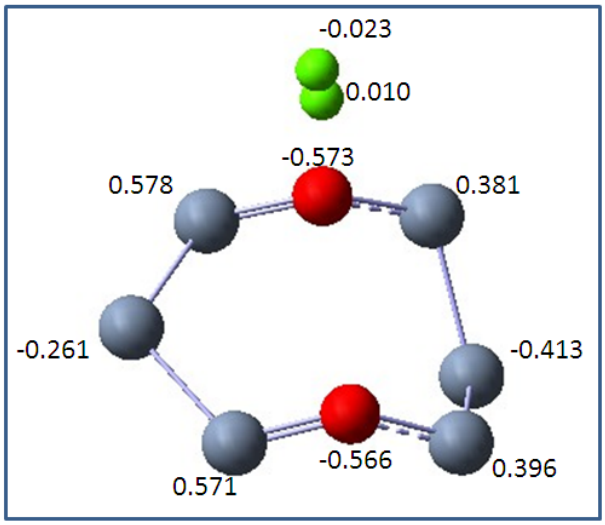

Figure 4.24 Mulliken charge distribution for Fig. 4.23a.

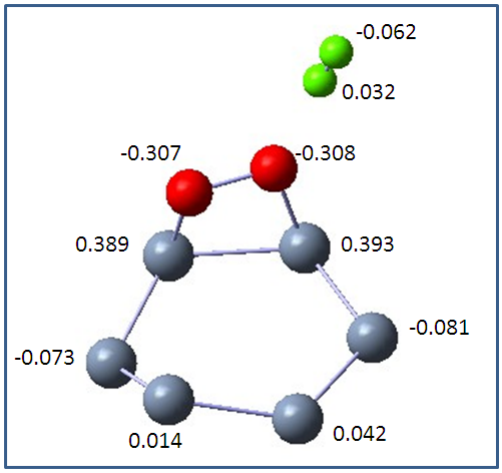

Figure 4.25 Mulliken charge distribution for Fig. 4.23c.

When the H_2 and O_2 molecules are adsorbed both inside of the nanotube, the dissociation and non-dissociation of O_2 molecule were both noted. In Fig. 4.23e, two O atoms which are in two separate bridge sites, and the H_2 molecule is on top of one O atom, when initially the O_2 and H_2 molecules were in two separate ZB sites. In Fig. 4.23f, a Si-O-O-Si ring

structure has been formed and the H_2 molecule is on top of one O atom, when initially the O_2 molecule was in NB site and the H_2 molecule was in ZB site.

When we place one H_2 molecule outside and another O_2 molecule inside of the nanotube, the oxygen molecule dissociated. In Fig. 4.23g, one O atom is bridging two neighboring Si atoms while the other O atom is bridging two non-neighboring Si atoms, and the H_2 molecule is on top of one Si atom. Fig. 4.23h shows that two oxygen atoms are in two separate bridge sites and the H_2 molecule is on top of one Si atom. When we place one H_2 molecule inside and another O_2 molecule outside of the nanotube, Fig. 4.23i and 4.23j show the other two local geometries. Fig. 4.23i shows that two O atoms are in bridge sites and the H_2 molecule is on top of one Si atom, when initially the O_2 molecule was outside the nanotube in hollow site and the H_2 molecule was inside the nanotube in top site. In Fig. 4.23j, A Si-O-O-Si ring structure is formed and the hydrogen molecule is on top of one Si atom, when initially the O_2molecule was outside of the nanotube in ZB site and the H_2 molecule was inside of the nanotube in NB site.

For the co-adsorption of H_2 and O_2 molecule from the same side of SiNT, the interaction between oxygen and hydrogen is very important. However, when one molecule is inside and the other molecule is outside, the interaction between two molecules is very weak, because the tube wall plays a role of separating the two molecules. “Precursor states” and peroxide structure are also observed for co-adsorption of one hydrogen molecule and one oxygen molecule. It is clear from these examples that the interactions between hydrogen, oxygen in silicon lead to important and complicated behavior.

Oxygen molecules tend to dissociate and occupy bridge sites on SiNTs, while hydrogen molecules tend to keep diatomic structure. Hydrogen molecules tend to be adsorbed in on-top site, but it may adopt different orientations other than perpendicular to the tube axis. Peroxide structure has been observed in adsorption of two oxygen molecules as well as co-adsorption of one hydrogen and oxygen molecule. For the co-adsorption of one hydrogen and oxygen

molecule, the hydrogen molecules prefer to stay as molecular form in the on-top site of oxygen atom which is in the bridge site on the nanotube.

Table 4.15 Summary of adsorption of one oxygen molecule and one hydrogen molecule from outside of SiNT, including the final configuration, adsorption energy and HOMO-LUMO gap.

Initial Site (O_{out} and H_{out})	Final local config.	D_{O-Si}	E_{ad}(eV)	E_{gap}(eV)
NB and NB	$2O+1H_2$	1.64	5.268	0.95
NB and Hol	$2O+1H_2$	1.65	5.013	1.01
Hol and ZB	$2O+1H_2$	1.71	4.716	0.86
ZB and NB	$2O+1H_2$	1.71	4.715	0.86
Top and ZB	$2O+1H_2$	1.67	4.649	0.91
NB and ZB	$1O_2+1H_2$	1.73	3.537	1.01
ZB and Hol	$1O_2+1H_2$	1.73	3.535	1.01
Top and Hol	$1O_2+1H_2$	1.73	3.529	1.01
Hol and NB	$1O_2+1H_2$	1.72	3.485	1.09
Top and Top	$1O_2+1H_2$	1.72	3.243	1.07
ZB and Top	$1O_2+1H_2$	1.74	3.095	0.75
Top and NB	$1O_2+1H_2$	1.74	3.044	0.87
Hol and Top	$1O_2+1H_2$	1.70	2.989	0.70
ZB and ZB	$1O_2+1H_2$	1.74	2.894	0.81
Hol and Hol	$1O_2+1H_2$	1.73	2.746	0.85
NB and Top	$1O_2+1H_2$	1.75	2.385	0.75

Table 4.16 Summary of adsorption of one oxygen molecule and one hydrogen molecule from inside of SiNT, including the final configuration, adsorption energy and HOMO-LUMO gap.

Initial Site (O_{in} and H_{in})	Final local config.	D_{O-Si}	E_{ad}(eV)	E_{gap}(eV)
ZB and ZB	$2O+1H_2$	1.64	5.244	1.03
Hol and NB	$2O+1H_2$	1.65	5.232	1.09
ZB and Hol	$2O+1H_2$	1.64	5.197	0.93
ZB and Top	$2O+1H_2$	1.69	5.055	0.96
ZB and NB	$2O+1H_2$	1.68	4.902	0.99
Top and NB	$2O+1H_2$	1.66	4.902	0.99
Top and ZB	$2O+1H_2$	1.66	4.902	0.99
Hol and Hol	$2O+1H_2$	1.70	4.872	1.09
Hol and ZB	$2O+1H_2$	1.68	4.836	1.12
Hol and Top	$2O+1H_2$	1.69	4.797	0.94
Top and Top	$2O+1H_2$	1.66	4.782	0.98
NB and NB	$2O+1H_2$	1.69	4.582	1.09
NB and ZB	$1O2+1H_2$	1.88	3.186	1.08
NB and Hol	$1O2+1H_2$	1.89	3.186	1.18
NB and Top	$1O2+1H_2$	1.88	3.186	1.18
Top and Hol	$1O2+1H_2$	1.72	3.066	0.93

Table 4.17 Summary of adsorption of one oxygen molecule from inside and one hydrogen molecule from outside of SiNT, including the final configuration, adsorption energy and HOMO-LUMO gap.

Initial Site (H_{out} and O_{in})	Final local config.	D_{O-Si}	E_{ad}(eV)	E_{gap}(eV)
Hol and Top	$2O+1H_2$	1.69	5.653	0.97
NB and Top	$2O+1H_2$	1.63	5.128	0.91
ZB and Hol	$2O+1H_2$	1.63	5.109	0.87
Top and ZB	$2O+1H_2$	1.63	5.101	0.91
Hol and NB	$2O+1H_2$	1.64	5.097	1.08
NB and Hol	$2O+1H_2$	1.64	5.029	0.98
Hol and ZB	$2O+1H_2$	1.69	4.929	1.01
Hol and Hol	$2O+1H_2$	1.64	4.918	0.94
ZB and Top	$2O+1H_2$	1.68	4.826	1.14
NB and ZB	$2O+1H_2$	1.68	4.825	1.12
ZB and ZB	$2O+1H_2$	1.68	4.825	1.14
NB and NB	$2O+1H_2$	1.69	4.743	1.09
ZB and NB	$2O+1H_2$	1.71	4.723	1.14
Top and NB	$2O+1H_2$	1.70	4.712	1.12
Top and Hol	$2O+1H_2$	1.69	4.551	1.01
Top and Top	$2O+1H_2$	1.70	4.544	0.98

Table 4.18 Summary of adsorption of one oxygen molecule from outside and one hydrogen molecule from inside of SiNT, including the final configuration, adsorption energy and HOMO-LUMO gap.

Initial Site (O_{out} and H_{in})	Final local config.	D_{O-Si}	E_{ad}(eV)	E_{gap}(eV)
Hol and Top	$2O+1H_2$	1.65	5.234	1.04
Hol and ZB	$2O+1H_2$	1.65	5.229	1.04
NB and NB	$2O+1H_2$	1.66	5.079	1.02
NB and Hol	$2O+1H_2$	1.66	5.075	1.02
ZB and Hol	$2O+1H_2$	1.71	4.771	1.16
ZB and Top	$2O+1H_2$	1.71	4.631	0.95
ZB and ZB	$2O+1H_2$	1.71	4.611	0.96
ZB and NB	$1O_2+1H_2$	1.72	3.978	0.83
Top and NB	$1O_2+1H_2$	1.72	3.489	1.03
NB and ZB	$1O_2+1H_2$	1.72	3.489	1.03
Hol and NB	$1O_2+1H_2$	1.72	3.489	1.03
Top and Top	$1O_2+1H_2$	1.73	3.433	0.91
Top and Hol	$1O_2+1H_2$	1.73	3.428	0.92
Top and ZB	$1O_2+1H_2$	1.73	3.010	0.94
NB and Top	$1O_2+1H_2$	1.73	3.002	0.73
Hol and Hol	$1O_2+1H_2$	1.72	3.001	0.72

4.2 Single Molecule and Co-Adsorptions of Hydrogen and Oxygen Molecules in Zigzag Silicon Nanotubes

In last section, we have discussed the adsorption of single molecule and co-adsorptions of hydrogen and oxygen molecules in armchair SiNTs. In this section we extend the discussion to single molecule adsorption and co-adsorptions of hydrogen and oxygen molecules in zigzag nanotube Si (10, 0).

Similar to the atomic hydrogen and oxygen adsorption in zigzag SiNTs, the molecule can be located at the top of Si atom, the center of Si-Si bond (parallel bridge site and zigzag bridge site), and the center of the Si hexagon (hollow site).We describe the interaction of molecules with SiNTs for (1) adsorption from outside of nanotube, (2) adsorption from inside of nanotube, (3) molecular axis perpendicular to the tube axis, (4) molecular axis parallel to the tube axis. The adsorption energy for each system can be calculated from:

E_a= {[E (SiNT) + E (X_2)]-E (SiNT+X_2)} , if the molecule does not dissociate

or

E_a= {[E (SiNT) + 2E (X)]-E (SiNT+2X)}/2 , if the molecule dissociates

where E(SiNT) is the ground state total energy of the bare silicon nanotube, E (X_2) and E (X) are the ground state energies of the X molecule and atom, respectively. E (SiNT+X_2) and E (SiNT+2X) are the total energies of the optimized clusters incorporating SiNT and the adsorbed molecule or atom.

Adsorption of single hydrogen molecule

The hydrogen molecule was initially placed in four adsorption sites with two orientations, one being perpendicular and the other being parallel to the tube axis. Also the hydrogen molecule can approach the tube wall from either outside or inside of the nanotube. For perpendicular adsorption, when the hydrogen approached the tube wall from outside of the nanotube, we found out that on-top site is the only preferred site. Whether the hydrogen molecule was placed in on-top site, hollow or bridge sites, after optimization the hydrogen

molecule moved to only on-top site. After adsorption, the hydrogen molecule has an H-H distance of 0.75 Á. Therefore, it is reasonable to assume that the hydrogen molecule did not dissociate. Fig. 4.26 shows that the hydrogen molecule was placed in zigzag bridge site, after optimization it moved to on-top site. The hydrogen molecule still retains its perpendicular orientation. The nearest distance between the nanotube and the hydrogen molecule is in the range from 3.26 to 3.36 Á. This distance is so large that it indicates the interaction between the hydrogen molecule and the nanotube is very weak. This can also be confirmed by the calculated adsorption energies (Table 4.19).The adsorption energies are in the range from 0.403 to 0.636 eV. Compared with the adsorption energies in armchair SiNTs (3.71 eV), the adsorption energies in zigzag SiNTs are significantly smaller. The HOMO-LUMO gaps are in the range from 0.53 to 0.56 eV. The bare nanotube Si (10, 0) has a HOMO-LUMO gap of 0.25 eV. Therefore there is a significant increase in the HOMO-LUMO gap after the adsorption of hydrogen molecule. When the hydrogen molecule approaches the nanotube from the inside with H-H bond perpendicular to the tube axis, the hydrogen molecule also maintains its molecular form. The on-top site is still the only preferred site. The HOMO-LUMO gaps are in the range from 0.410 to 0.638 eV. (Table 4.20)Generally, when the hydrogen molecule was initially placed perpendicular to the tube axis, on-top site is the only preferred site. The hydrogen molecule will retain its perpendicular orientation and molecular form. Also, adsorption of hydrogen molecule will increase the HOMO-LUMO gap of the nanotube, although the interaction is very weak considering the small adsorption energies. There is no significant difference for external and internal adsorptions of single hydrogen molecule perpendicular to the tube axis. The largest adsorption energy is 0.636 and 0.638 eV for external and internal adsorption, respectively, with HOMO-LUMO gap of 0.55 and 0.53 eV. Also the distance between the hydrogen molecule and the nanotube is 3.31 and 3.18 Å respectively, indicating the interaction is very weak.

The Mulliken charge analysis shows that the nanotube is polarized, every positively charged Si atoms is surrounded by three negatively charged Si atoms (Fig. 4.27). Since the bare nanotube Si (10, 0) shows a same charge polarization, we can assume adding hydrogen molecule to the nanotube will not affect the charge distribution on the nanotube. The Mulliken charge on the hydrogen molecule is very small (Fig. 4.28) but we can still notice there is a slight charge polarization on the hydrogen molecule. The hydrogen atom closer to the nanotube has charge of 0.007|e| and the closest Si atom has charge of -0.067|e|. Therefore the interaction between the hydrogen molecule and the nanotube is mainly stabilized by the electro static force. After a close look into the area near the adsorbed hydrogen molecule, it is noted that a local deformation has occurred on the Si atoms close to the hydrogen molecule. The four Si atoms forming a planar structure undergo a deformation to a pyramidal structure (Fig. 4.29). Considering sp^2 hybridization gives a planar structure and sp^3 hybridization give a tetrahedral structure, it is reasonable to assume there is a transition occurring on the Si atoms to go from sp^2 to sp^3 hybridization.

Table 4.19 External adsorption of one hydrogen molecule perpendicular to the tube axis.

Initial site	Final site	$D_{H\text{-}Si}$ (Å)	Adsorption energy (eV)	HOMO-LUMO gap (eV)
Para B.	On-top	3.36	0.403	0.54
Zigzag B.	On-top	3.31	0.636	0.55
Hollow	On-top	3.26	0.453	0.53
On-top	On-top	3.35	0.571	0.56

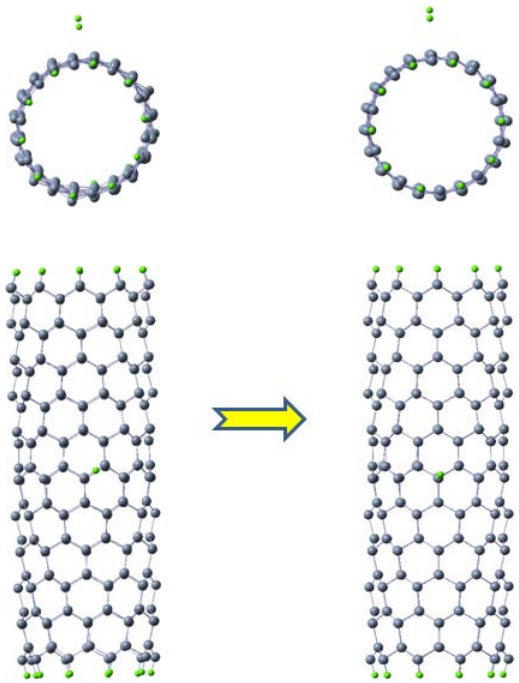

Figure 4.26 The hydrogen molecule migrated from initial zigzag bridge site to final on-top site.

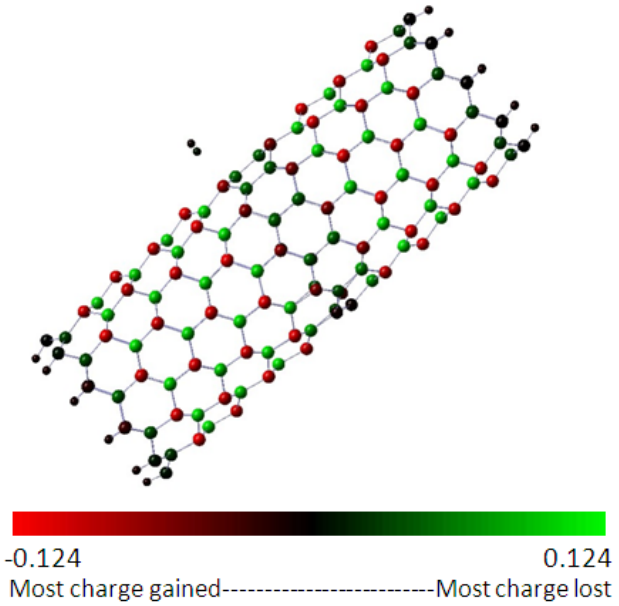

Figure 4.27 The Mulliken charge distribution on hydrogen adsorbed SiNT.

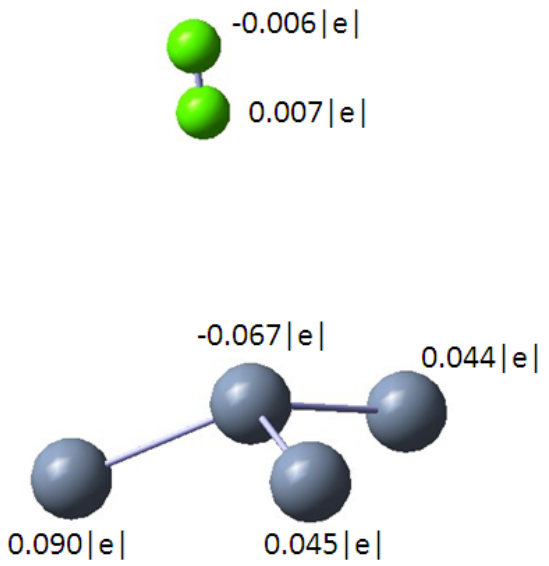

Figure 4.28 Mulliken charge on hydrogen molecule and the nearest Si atoms.

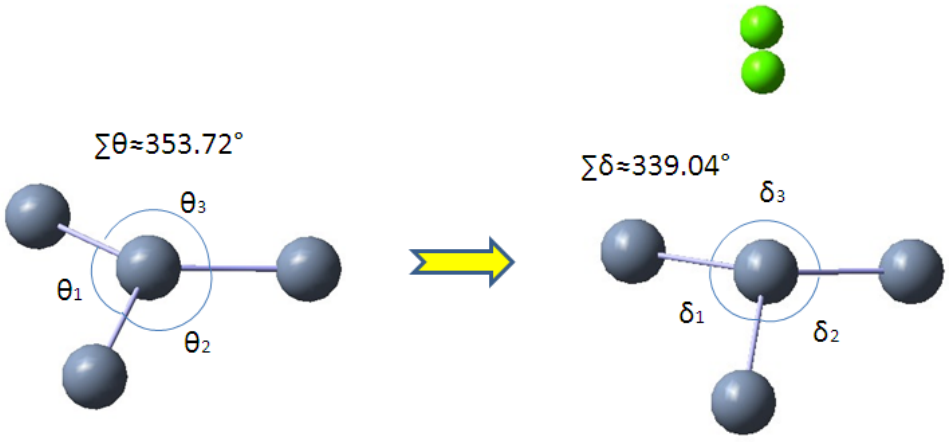

Figure 4.29 The local geometry near the hydrogen molecule changed from planar to pyramidal structure.

Table 4.20 Internal adsorption of one hydrogen molecule perpendicular to the tube axis.

Initial site	Final site	D_{H-Si} (Å)	Adsorption energy (eV)	HOMO-LUMO gap (eV)
Para B.	On-Top	3.14	0.607	0.55
Zigzag B.	On-Top	3.18	0.638	0.53
Hollow	On-Top	3.13	0.410	0.55
On-top	On-Top	3.18	0.573	0.56

In the case of parallel adsorption, the H-H bond of the hydrogen molecule was placed parallel to the tube axis. Similar to perpendicular adsorption, the hydrogen molecule did not dissociate. The on-top site is the only preferred site. The adsorption energies are in the range from 0.305 to 0.587 eV. After adsorption of hydrogen molecule, the HOMO-LUMO gaps also increased. (Table 4.21 and 4.22) The hydrogen molecule tried to align the H-H bond perpendicular to the tube axis. When the hydrogen molecule was placed parallel to the tube axis, after optimization the hydrogen molecule aligned itself perpendicular to the tube axis (Fig. 4.30). The adsorption energy (the largest one is 0.576 eV) is smaller than perpendicular adsorption (the largest one is 0.636 eV) because here the hydrogen molecule is not strictly perpendicular to the tube axis after adsorption. Therefore perpendicular adsorption is more favorable for single hydrogen molecule adsorption in nanotube Si (10, 0). The Mulliken charge analysis indicates that the hydrogen molecule is slightly polarized. The hydrogen molecule and the nanotube are stabilized by the electro static force. For internal adsorption, on-top site (quasi on-top site) is the only preferred site. Similar to external adsorption, the hydrogen molecule tried to align itself perpendicular to the tube axis. The largest adsorption here is 0.587 eV, slightly larger than that of external adsorption, which is 0.576 eV. Therefore for internal adsorption the interaction between the hydrogen molecule and the nanotube is stronger. For both external and internal adsorption, the HOMO-LUMO gap all increased. The HOMO-LUMO gap is in the range from 0.50 to 0.56 eV.

From the discussion above, we can conclude that the interaction between hydrogen molecule and nanotube Si (10, 0) is very weak because the adsorption energies are very small. The HOMO-LUMO gap of the nanotube will increase after adsorption of single hydrogen molecule. Also the internal adsorption is slightly stronger than external adsorption.

Table 4.21 External adsorption of one hydrogen molecule parallel to the tube axis.

Initial site	Final site	D_{H-Si} (Å)	Adsorption energy (eV)	HOMO-LUMO gap (eV)
Para B.	Q-top	4.03	0.305	0.50
Zigzag B.	Q-top	4.10	0.325	0.53
Hollow	Q-top	3.30	0.576	0.54
On-top	Q-top	3.91	0.491	0.52

Table 4.22 Internal adsorption of one hydrogen molecule parallel to the tube axis.

Initial site	Final site	D_{H-Si} (Å)	Adsorption energy (eV)	HOMO-LUMO gap (eV)
Para B.	Q-top	3.44	0.490	0.54
Zigzag B.	Q-top	3.69	0.489	0.55
Hollow	Q-top	3.11	0.587	0.54
On-top	Q-top	3.52	0.498	0.56

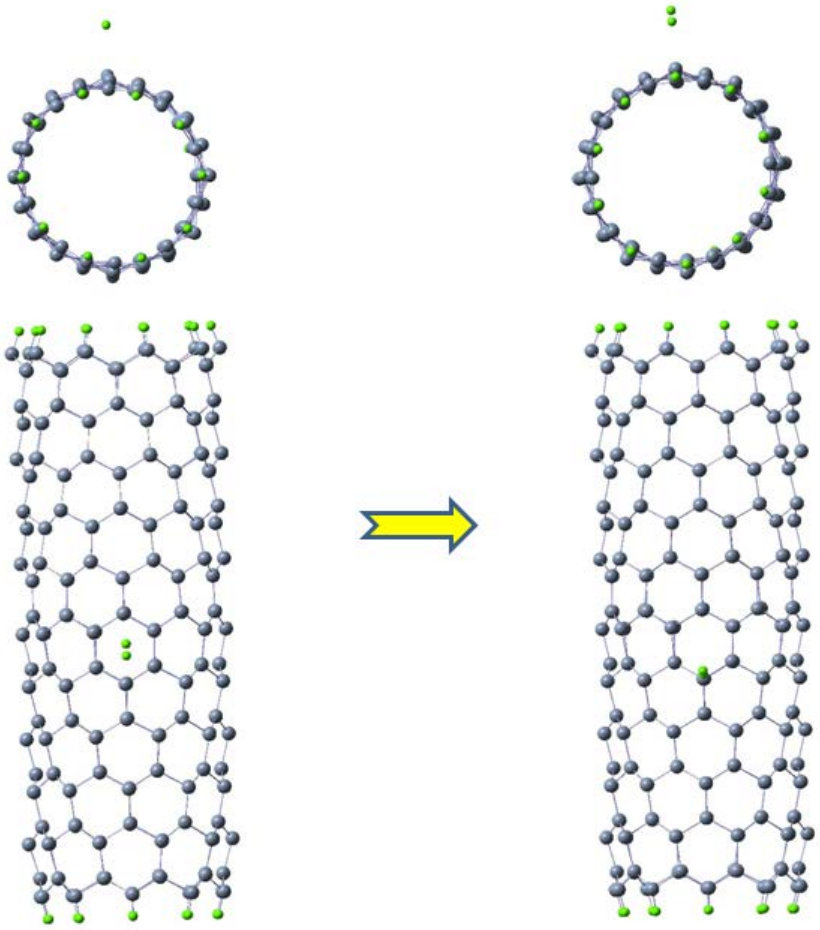

Figure 4.30 The hydrogen molecule moved from hollow site to quasi-top site, with its orientation changed from parallel to perpendicular to the tube axis.

Adsorption of single oxygen molecule

The oxygen molecule was placed at the same adsorption sites with two orientations, from outside or inside of the nanotube. Unlike hydrogen molecule adsorption in zigzag SiNTs, dissociation is noted in the adsorption of oxygen molecule. When the oxygen was initially placed perpendicular to the tube axis, for external adsorption it is noted that the oxygen molecule tended to maintain its molecular form after adsorption. When the oxygen molecule was placed in parallel bridge, hollow and on-top site, the oxygen molecule did not dissociate and the adsorption energies are very small. Fig. 4.31shows that the oxygen molecule was initially

placed in on-top site with the O-O bond perpendicular to the tube axis, after optimization it moved to a hollow site with adsorption energy of 0.879 eV. However, when the oxygen molecule was placed in zigzag bridge site, after adsorption the molecule dissociated (Fig. 4.32), and two oxygen atoms moved to different zigzag bridge sites with adsorption energy of 6.466 eV (Table 4.23).The Mulliken charge in Fig. 4.31 on two oxygen atoms is 0.003|e| and 0.016|e| indicating there is slight charge transfer from the oxygen molecule to the nanotube (Fig. 4.33). The Mulliken charge on the two oxygen atom in Fig. 4.32 is -0.537|e| and -0.536|e| indicating there is a large charge transfer from nearby Si atoms to oxygen atoms (Fig. 4.34). The HOMO-LUMO gap is in the range from 0.54 to 0.55 eV. The HOMO-LUMO gaps increased after the adsorption of oxygen molecule significantly. For internal adsorption, we do not see the existence of molecular oxygen after adsorption. The oxygen molecule all dissociated and move to different bridge sites after adsorption. The adsorption energies are in the range from 6.054 to 6.466 eV. The HOMO-LUMO gaps also increased significantly after the internal adsorption of oxygen molecule. For internal adsorption, the oxygen molecules all dissociated (Table 4.24). Also, there is large charge transfer from the Si atoms to the O atoms due to the electronegativity difference between Si and O. With the dissociation of the oxygen molecule, the oxygen atoms moved only to two bridge sites. The difference between external and internal adsorptions is that in internal adsorption, the oxygen molecules all dissociated regardless of their initial sites. The reason for this is that the oxygen molecules inside of the nanotubes can interact with Si atoms on tube wall stronger due the curvature effect of the tube wall.

Table 4.23 External adsorption of oneoxygen molecule perpendicular to the tube axis.

Initial site	Final site	$D_{O\text{-}Si}$ (Å)	Adsorption energy (eV)	HOMO-LUMO gap (eV)
Para B.	Q-top	3.13	0.763	0.55
Zigzag B.	ZB/ZB	1.70	6.466	0.54
Hollow	Hollow	2.99	0.876	0.55
On-top	Hollow	3.00	0.879	0.55

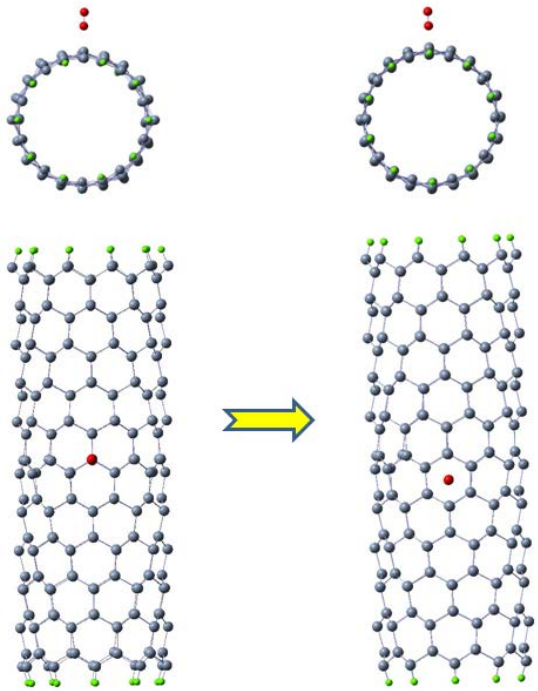

Figure 4.31 The oxygen molecule moved from on-top site to hollow site.

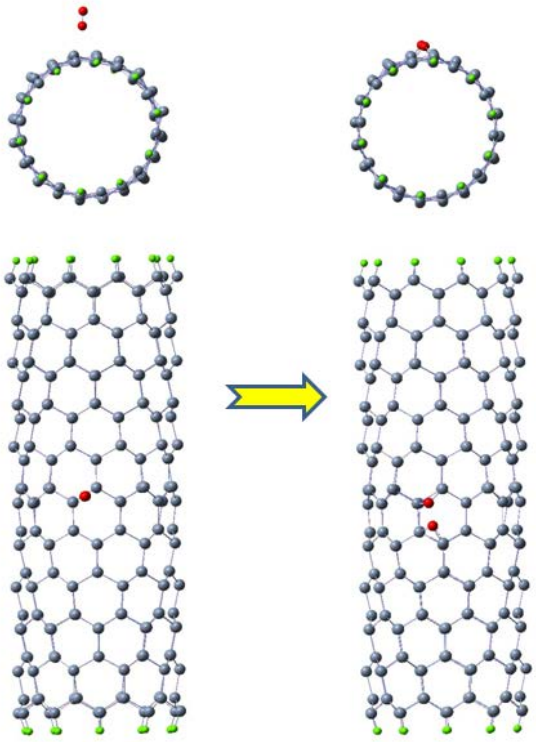

Figure 4.32 The oxygen molecule dissociated and moved from zigzag bridge site to two different zigzag bridge sites.

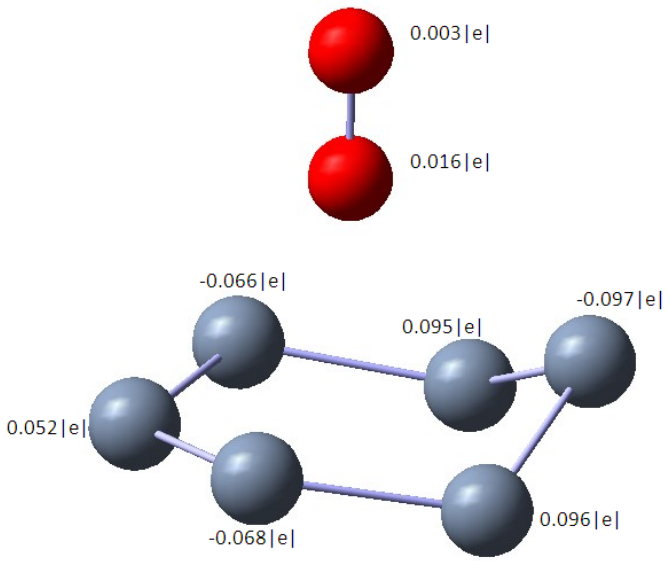

Figure 4.33 Mulliken charge on oxygen molecule and nearby Si atoms (non-dissociation).

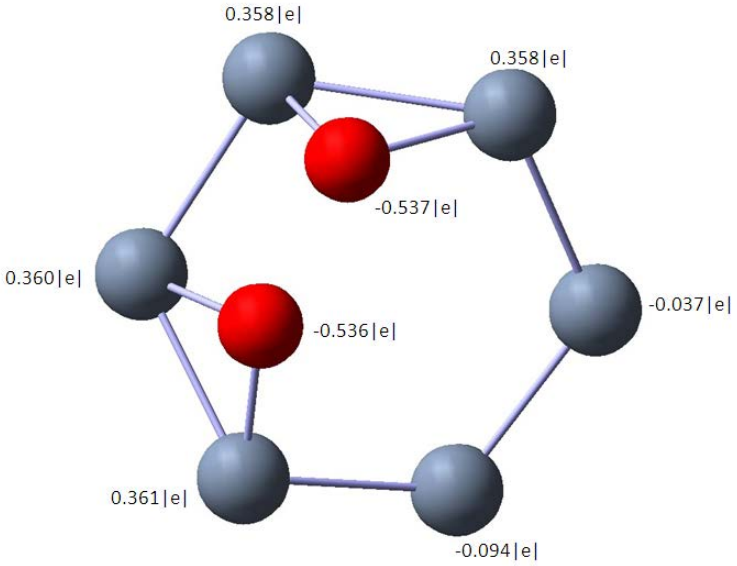

Figure 4.34 Mulliken charge on oxygen atoms and Si atoms (dissociation).

Table 4.24 Internal adsorption of oneoxygen molecule perpendicular to the tube axis.

Initial site	Final site	D_{O-Si} (Å)	Adsorption energy (eV)	HOMO-LUMO gap (eV)
Para B.	ZB/ZB	1.70	6.466	0.54
Zigzag B.	ZB/NB	1.70	6.352	0.55
Hollow	PB/PB	1.71	6.054	0.54
On-top	PB/PB	1.70	6.427	0.53

When the oxygen molecule was placed initially parallel to the tube axis, for the external adsorption, the molecule all dissociated and moved to different bridge sites. Compared with the perpendicular adsorption, it is noted that the oxygen molecule has a tendency to dissociate when the O-O bond is parallel to the tube axis (Table 4.25).The oxygen molecules all dissociated in both external and internal adsorption. Fig. 4.35 shows that the oxygen molecule was initially placed in an on-top site with O-O bond parallel to the tube axis, after optimization it dissociated and the two O atoms moved to two different bridge sites. For internal adsorption, the interaction between the oxygen molecule and the nanotube is stronger. The oxygen can "see" more silicon atoms when it is placed inside of the nanotube. Therefore, the oxygen molecule inside of the nanotube can interact with more silicon atoms. The oxygen molecule did not move to any of the four pre-defined adsorption sites. For example, in Fig. 4.36, the two O atoms are interacting with two non-neighboring Si atom, which is not any of the two bridge sites. Because in the two pre-defined bridge sites, the O atom should be at the center of two neighboring Si atoms. This effect should be caused by the curvature effect and the orientation of oxygen molecule. The parallel orientation of the oxygen molecule enables the two oxygen atoms to interact with the Si atoms on the tube wall simultaneously. It is reasonable to assume that when oxygen molecule is initially placed perpendicular to the tube axis, it will align itself parallel to the tube axis first. Compared with the adsorption energy of external adsorption (the largest one is 6.436 eV), the adsorption energy of internal adsorption is slightly higher (the

largest one is 6.608 eV).The HOMO-LUMO gaps also increase after the internal adsorption of oxygen molecule (Table 4.26).

Table 4.25 External adsorption of oneoxygen molecule parallel to the tube axis.

Initial site	Final site	D_{O-Si} (Å)	Adsorption energy (eV)	HOMO-LUMO gap (eV)
Para B.	PB/ZB	1.73	6.168	0.60
Zigzag B.	ZB/ZB	1.76	6.198	0.51
Hollow	ZB/ZB	1.72	6.052	0.55
On-top	PB/ZB	1.66	6.436	0.62

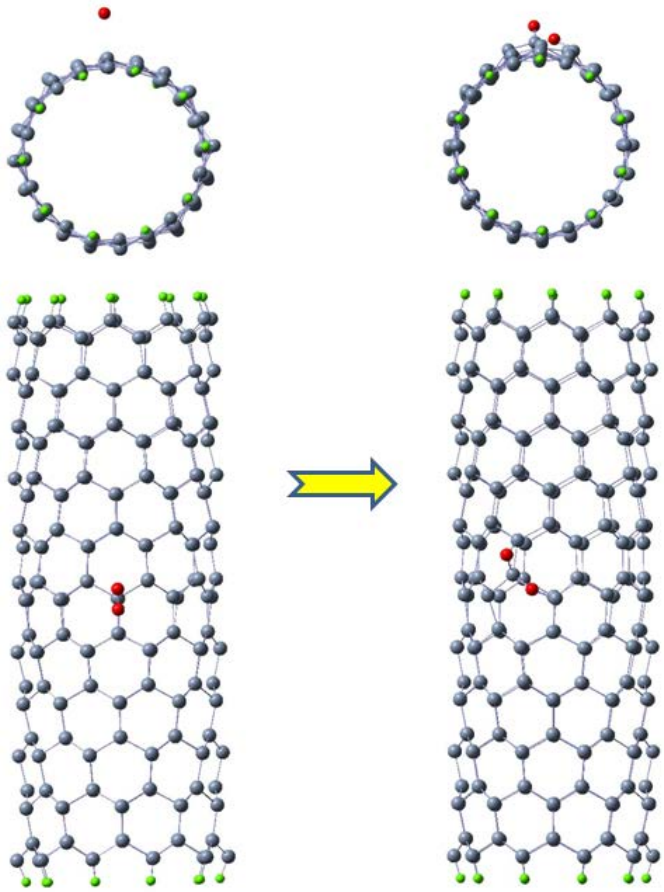

Figure 4.35 The oxygen molecule dissociated and moved from on-top site to two different bridge sites. The oxygen molecule was placed parallel to the tube axis

Table 4.26 Internal adsorption of one oxygen molecule parallel to the tube axis.

Initial site	Final site	$D_{O\text{-}Si}$ (Å)	Adsorption energy (eV)	HOMO-LUMO gap (eV)
Para B.	Undefined	1.71	6.015	0.38
Zigzag B.	Undefined	1.75	5.738	0.45
Hollow	Undefined	1.71	5.864	0.50
On-top	Undefined	1.62	6.608	0.49

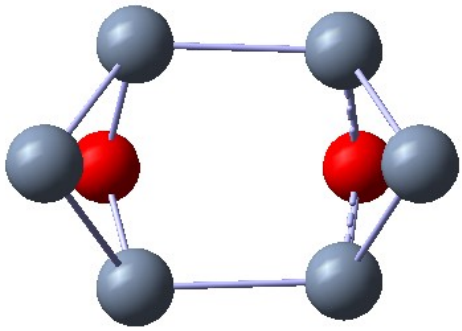

Figure 4.36 The oxygen atoms are bridging two non-neighboring Si atoms.

Co-adsorption of hydrogen molecules

In the co-adsorption of hydrogen molecules, there are three initial arrangements of the two hydrogen molecules. One is to place both of them outside of the nanotube, the second way is to place both of them inside of the nanotube and the third way is to place one hydrogen molecule inside and the other outside of the nanotube. The hydrogen molecules are only placed with the H-H bond perpendicular to the axis. When two hydrogen molecules are adsorbed from outside of the nanotube, in all cases the optimized structure of the nanotube and the hydrogen molecule has H-H distance of 0.75 Å. it is reasonable to assume that the hydrogen molecule did not dissociate and, in fact, maintained the original diatomic linear structure. In our previous study, hydrogen molecules oriented themselves perpendicular to the tubes if adsorbed in an on-

top site and the most preferred site was the on-top site for single hydrogen molecule adsorption. For co-adsorption, the most preferred site is still the on-top site in which two hydrogen molecules prefer to stay in two different on-top sites. In Fig. 4.37, two hydrogen molecule were placed in two PB sites, after optimization, they moved to two on-top sites. Similar to single hydrogen adsorption, the Mulliken charge distribution shows that the charge on H_2 is very small but slightly polarized. Fig.4.38shows the Mulliken charge distribution on the hydrogen molecules were adsorbed in two separate on-top sites. The Mulliken charge on first hydrogen molecule is -0.005|e|, 0.006|e| and the Mulliken charge on second is -0.005|e|, 0.007|e|. The positively charged hydrogen atom in the slightly polarized hydrogen molecule is attracted to the negatively charged silicon atoms, which all have Mulliken charge of -0.093|e|.

We found that the adsorption energy per hydrogen molecule has decreased when we increased the number of adsorbed hydrogen molecules. The adsorption energy for single hydrogen molecule in on-top site was 0.636 eV, whereas in this study with the two hydrogen molecules both being in on-top sites the adsorption energy per hydrogen molecule is 0.240 eV. As far as the distances are concerned, the closest distance from the two hydrogen molecules to the nearest Si atom is3.28 Å, which is close to the result from single molecule adsorption of 3.26 Å. It is reasonable to assume that adding more hydrogen molecules to the nanotube Si (10, 0) will further make the adsorption energy decrease. The HOMO-LUMO gaps are in the range from 0.50 to 0.56 eV indicating a significant increase from the bare nanotube Si (10, 0). However, compared with the HOMO-LUMO gaps after adsorption of single hydrogen molecule (which is also in the range from 0.50 to 0.56 eV), there is no change on the HOMO-LUMO gap when we add an extra hydrogen molecule. Therefore adding more hydrogen molecules may not change the HOMO-LUMO gap of the nanotube.

When two hydrogen molecules are both adsorbed from inside of the nanotube, we observe a similar trend. The most preferred sites are still on-top sites. However, in some cases, although the hydrogen molecule is on top of Si atom, it changes its orientation slightly, which is

not strictly perpendicular to the tube axis. This effect could be caused by the interactions between the hydrogen molecules and the confinement of the tube wall. When one hydrogen molecule is adsorbed from outside the nanotube while the other hydrogen molecule is adsorbed from inside the nanotube, the adsorption energy is close to the energies for the external and internal adsorptions discussed above. Also the on-top site is the most preferred site.

The adsorption energies for co-adsorption of hydrogen molecules are in the range from 0.061 to 0.317 eV. The adsorption energies vary from case to case due to the change of the orientation of the hydrogen molecules and the distance from the hydrogen molecules to the nanotube. The HOMO-LUMO gaps are in the range from 0.48 to 0.58 eV.

Table 4.27 Initial and final sites for external adsorption of two hydrogen molecules, the shortest H-Si distance, adsorption energy and HOMO-LUMO gap.

Initial site (H_{out} and H_{out})	Final site (H_{out} and H_{out})	$D_{H\text{-}Si}$ (Å)	E_{ad}(eV)	E_{gap}(eV)
PB and PB	Top and Top	3.31	0.240	0.51
PB and Hol	(Q)top and Top	3.35	0.235	0.52
Hol and Hol	(Q)top and (Q)top	3.28	0.225	0.51
PB and ZB	(Q)top and (Q)top	3.33	0.197	0.53
PB and Top	(Q)top and (Q)top	3.31	0.195	0.54
Hol and Top	Hol and Top	3.31	0.110	0.50
ZB and ZB	ZB and Top	3.48	0.110	0.50
Top and Top	Top and Top	3.57	0.106	0.52
ZB and Hol	(Q)top and Hol	3.85	0.096	0.56
ZB and Top	(Q)top and Top	3.89	0.094	0.55

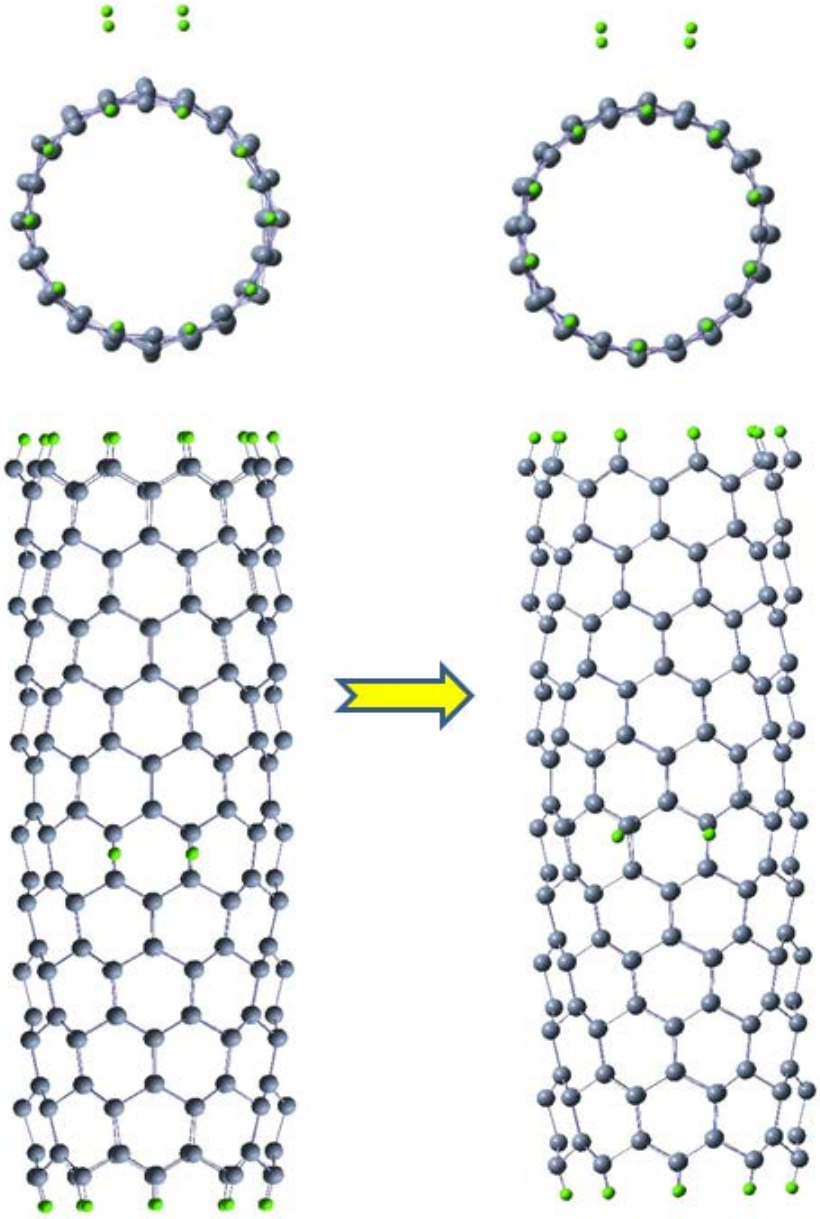

Figure 4.37 Two hydrogen molecules moved from PB/PB site to Top/Top site

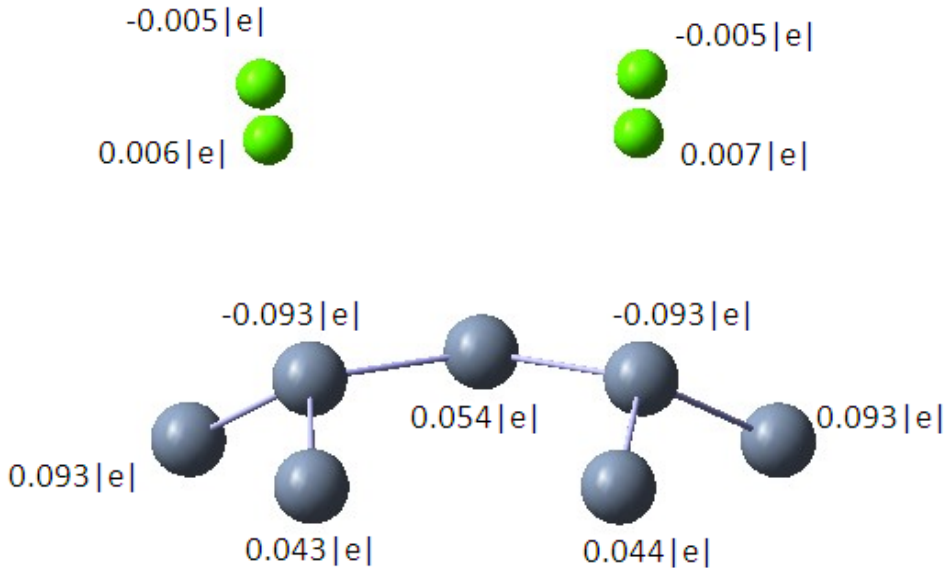

Figure 4.38 Mulliken charge on two hydrogen moelcules

Table 4.28 Initial and final sites for internal adsorptions of two hydrogen molecules, the shortest H-Si distance, adsorption energy and the HOMO-LUMO gap.

Initial site (H_{in} and H_{in})	Final site (H_{in} and H_{in})	$D_{H\text{-}Si}$ (Å)	E_{ad}(eV)	E_{gap}(eV)
ZB and ZB	Top and Top	3.20	0.291	0.55
Hol and Hol	(Q)top and Top	3.20	0.289	0.51
Hol and Top	(Q)top and (Q)top	3.30	0.283	0.50
PB and PB	(Q)top and (Q)top	3.14	0.210	0.54
Top and Top	(Q)top and (Q)top	3.36	0.164	0.56
PB and ZB	(Q)top and (Q)top	3.40	0.142	0.52
PB and Hol	PB and (Q)PB	3.21	0.085	0.55
ZB and Hol	(Q)top and (Q)hol	3.59	0.072	0.54
PB and Top	(Q)top and Top	3.32	0.065	0.53
ZB and Top	ZB and Top	3.32	0.061	0.51

Table 4.29 Initial and final sites for external/internal adsorptions of two hydrogen molecules, the shortest H-Si distance, adsorption energy and the HOMO-LUMO gap.

Initial site (H_{out} and H_{in})	Final site (H_{out} and H_{in})	$D_{H\text{-}Si}$ (Å)	E_{ad}(eV)	E_{gap}(eV)
ZB and ZB	Top and Top	3.24	0.317	0.57
PB and ZB	Top and Top	3.21	0.303	0.56
ZB and Top	ZB and Top	3.21	0.291	0.58
Hol and Top	Hol and Top	3.21	0.276	0.53
Top and PB	Top and (Q)top	3.20	0.247	0.55
Hol and Hol	(Q)Hol and (Q)top	3.15	0.214	0.50
Top and ZB	Top and Top	3.19	0.213	0.52
Top and Hol	Top and Hol	3.50	0.205	0.51
PB and Top	(Q)top and Top	3.21	0.200	0.54
ZB and PB	Top and Top	3.28	0.185	0.58
Top and Top	Top and Top	3.20	0.172	0.48
PB and PB	Top and Top	3.20	0.139	0.49
PB and Hol	PB and Hol	3.50	0.117	0.59
ZB and Hol	(Q)ZB and Hol	3.36	0.105	0.50
Hol and ZB	Hol and (Q)ZB	3.26	0.094	0.52
Hol and PB	Hol and (Q)PB	3.24	0.093	0.52

Co-adsorption of oxygen molecules

The adsorption of two O_2 molecules has been studied at the same arrangement of the adsorption sites as the two H_2 molecules to allow for comparative studies. However, different final configurations can result from the nature of oxygen interactions with silicon as compared to hydrogen interactions. When two O_2 molecules were adsorbed from outside the nanotube, we do not see the complete dissociation (both O_2 molecules are dissociated) of the O_2 molecules. However, it is noted that the Si-O-O-Si peroxide and Si-O-O structure have formed in some cases (Fig. 4.39).In all cases at least one oxygen molecule is not bonded to the nanotube. When one oxygen molecule forms Si-O-O-Si peroxide structure with Si atoms and one oxygen molecule does not dissociate, the adsorption energies are in the range from 1.954 to 2.209 eV.

When one oxygen molecule forms Si-O-O structure and one oxygen molecule does not dissociates, the adsorption energies are in the range from 0.634 to 1.188 eV. When both oxygen molecules do not dissociate, the adsorption energies are in the range from 0.297 to 0.566 eV. Comparing these adsorption energies, it is reasonable to assume that energetically Si-O-O-Si is the more favorable than Si-O-O structure, and O_2 is the least favorable. However, we do not see the complete dissociation of both oxygen molecules, which possibly means there may exist some competition or correlation between two oxygen molecules. Also the preference of the oxygen molecule on parallel orientation may also cause this partial dissociation to happen. After adsorption, the HOMO-LUMO gaps of the nanotubes all increased.

The Mulliken charge on the two O atoms in the peroxide structure(Fig. 4.40)are -0.300|e| and -0.299|e|, the Mulliken charge on the two neighboring Si atoms are 0.399|e| and 0.397|e| indicating charge transfer from Si atoms to O atoms. The distance between the two O atoms is 1.56 Å, which means it is a stretched bond when compared to the bond length 1.30 Å of an O_2 molecule. However, the Mulliken charge on the isolated oxygen molecule is 0.006|e| and 0.010|e| indicating very weak interaction between the oxygen molecule and the nanotube. In Fig. 4.41, the O-O bond length in the Si-O-O structure is 1.44 Å. The Mulliken charge on the two O atoms is -0.259|e| and -0.074|e|, respectively, which also means there is charge transfer from Si atoms to oxygen atoms.

When two O_2 molecules are adsorbed both inside the nanotube, complete dissociation, partial dissociation and non-dissociation are noted. When the two oxygen molecules were placed in two different hollow sites, after optimization they both dissociated, and moved to four different bridge sites. The adsorption energy is 5.875 eV which is the largest for internal adsorption, indicating complete dissociation is the most favorable. However, this is the only case for complete dissociation. Partial dissociation was also observed. When two oxygen molecules were placed in two different parallel bridge sites, after optimization the oxygen molecule inside the nanotube dissociated and moved to two different bridge sites, the oxygen

molecule outside of the nanotube formed Si-O-O-Si peroxide structure with the neighboring Si atoms. Due to the confinement of the tube wall, oxygen molecules inside the nanotube have a possibility to interact with more Si atoms than outside the nanotube. Generally the adsorption energies of internal adsorption are higher than external adsorption. Therefore the interaction between the oxygen molecule inside of the nanotube and the tube wall is much stronger resulting in the dissociation of the oxygen molecule. Similar to external adsorption, the HOMO-LUMO gaps also increased after internal adsorption.

When we place one O_2 molecule outside of the nanotube and the other O_2 molecule inside of the nanotube, we do not see complete dissociation. Similar to the external adsorption, only partial and non-dissociation were found. The most favorable condition is that two oxygen molecules are both forming Si-O-O-Si peroxide structures. When the two oxygen molecules were placed in two different parallel bridge sites, after optimization they both formed Si-O-O-Si peroxide structures with nearby Si atoms, with the largest adsorption energy of 3.816 eV. The partial dissociation were also observed. For example, when one oxygen molecule was placed in parallel bridge site outside of the nanotube and the other oxygen molecule was placed in hollow site inside of the nanotube, after optimization, the oxygen molecule outside of the nanotube did not dissociate but the other oxygen molecule dissociated and moved to two different bridge sites. The cases with partial dissociation of oxygen molecules have slightly lower adsorption energies ranging from 3.109 to 3.328 eV. The Si-O-O-Si and Si-O-O structures were also observed. After adsorption, the HOMO-LUMO gaps all increased.

The HOMO-LUMO gaps for adsorption of two O_2molecules vary from case to case. However, either for complete dissociation, partial or non-dissociation, the HOMO-LUMO gap of the nanotube all increased. Energetically from the most favorable to least favorable, the structures for oxygen molecules are as follows: 2O>Si-O-O-Si>Si-O-O>O_2. Similar to single oxygen molecule adsorption, oxygen molecules still prefer to dissociate. However, complete dissociation was only observed in one case. The formation of Si-O-O-Si and Si-O-O structures

maybe caused by the competition and correlation of two oxygen molecules. Also these two structures could be precursor state for complete dissociation.

Table 4.30 Initial and final sites for external adsorption of two oxygen molecules, the shortest O-Si distance, adsorption energy and HOMO-LUMO gap.

Initial site (O_{out} and O_{out})	Final local config.	D_{O-Si} (Å)	E_{ad}(eV)	E_{gap}(eV)
PB and PB	Si-O-O-Si and O_2	1.74	2.290	0.69
Top and Top	Si-O-O-Si and O_2	1.74	2.012	0.65
ZB and ZB	Si-O-O-Si and O_2	1.74	1.954	0.68
PB and Top	Si-O-O and O_2	1.75	1.188	0.43
ZB and Hol	Si-O-O and O_2	1.75	1.113	0.50
PB and Hol	Si-O-O and O_2	1.77	0.992	0.53
Hol and Top	Si-O-O and O_2	1.82	0.634	0.49
Hol and Hol	$2O_2$	2.95	0.566	0.56
PB and ZB	$2O_2$	3.21	0.311	0.51
ZB and Top	$2O_2$	3.15	0.297	0.47

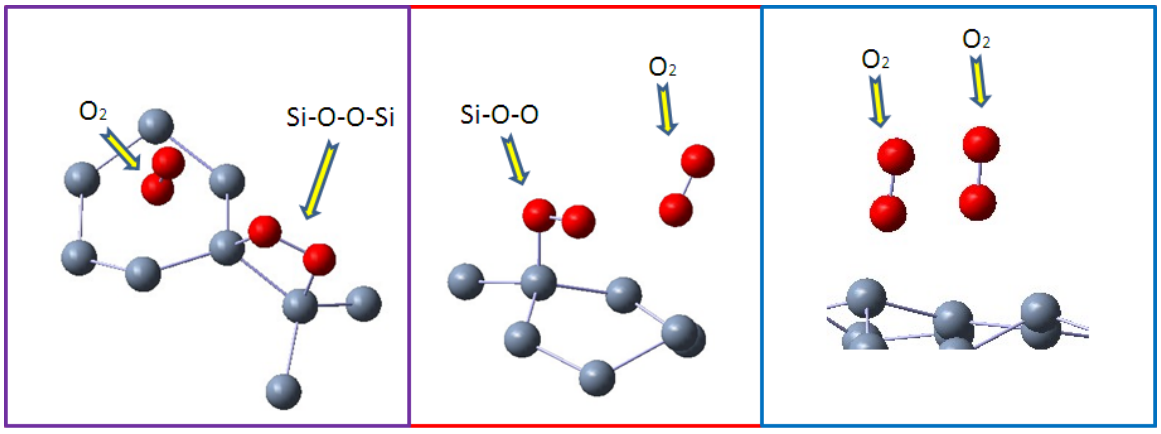

Figure 4.39 Three types of local configurations for co-adsorption of oxygen molecules.

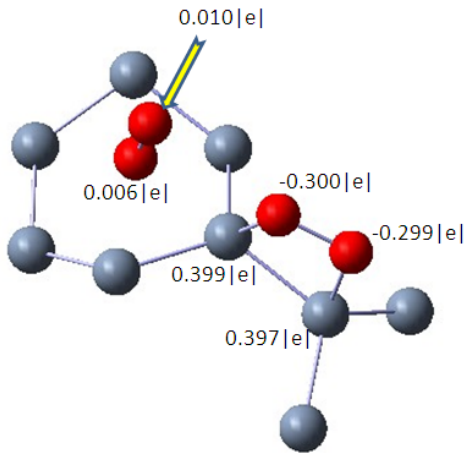

Figure 4.40 Mulliken charge on the Si-O-O-Si structure.

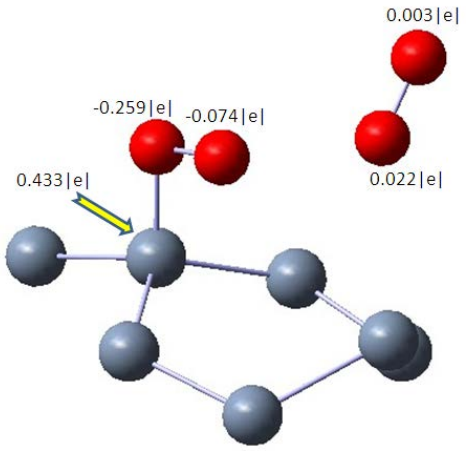

Figure 4.41 Mulliken charge on the Si-O-O structure.

Table 4.31 Initial and final sites for internal adsorptions of two oxygen molecules, the shortest O-Si distance, adsorption energy and the HOMO-LUMO gap.

Initial site (O_{in} and O_{in})	Final local config.	$D_{O\text{-}Si}$ (Å)	E_{ad}(eV)	E_{gap}(eV)
Hol and Hol	4O	1.71	5.875	0.52
PB and PB	Si-O-O-Si and 2O	1.74	5.305	0.49
Hol and Top	Si-O-O-Si and 2O	1.72	5.151	0.46
ZB and Top	2(Si-O-O-Si)	1.72	3.730	0.57
PB and ZB	Si-O-O-Si and Si-O-O	1.72	2.806	0.40
PB and Hol	Si-O-Oand O_2	1.71	1.958	0.52
ZB and Hol	$2O_2$	2.92	0.624	0.48
ZB and ZB	$2O_2$	2.12	0.411	0.50
PB and PB	$2O_2$	2.56	0.365	0.56
Top and Top	$2O_2$	2.88	0.350	0.47

Table 4.32 Initial and final sites for external/internal adsorptions of two oxygen molecules, the shortest O-Si distance, adsorption energy and the HOMO-LUMO gap.

Initial site (O_{out} and O_{in})	Final local config.	$D_{O\text{-}Si}$ (Å)	E_{ad}(eV)	E_{gap}(eV)
PB and PB	2(Si-O-O-Si)	1.72	3.816	0.40
ZB and Hol	O_2+2O	1.70	3.328	0.52
Hol and PB	O_2+2O	1.70	3.243	0.45
ZB and Top	O_2+2O	1.68	3.109	0.46
ZB and ZB	O_2 and Si-O-O-Si	1.72	1.646	0.41
PB and ZB	O_2 and Si-O-O-Si	1.71	1.577	0.46
ZB and PB	O_2 and Si-O-O	1.77	1.087	0.39
Hol and ZB	O_2 and Si-O-O	1.72	1.065	0.55
Hol and Hol	O_2 and Si-O-O	1.76	0.984	0.51
Hol and Top	O_2 and Si-O-O	1.72	0.956	0.55
PB and Hol	O_2 and Si-O-O	1.71	0.931	0.41
Top and Hol	O_2 and Si-O-O	1.73	0.893	0.53
Top and PB	O_2 and Si-O-O	1.70	0.758	0.48
Top and Top	$2O_2$	3.56	0.601	0.43
Top and ZB	$2O_2$	3.21	0.590	0.46
PB and Top	$2O_2$	3.11	0.565	0.51

Co-adsorption of one hydrogen molecule and one oxygen molecule

We have adopted the same arrangement for the adsorption sites of one H_2 molecule and one O_2 molecule as was done above for two hydrogen or two oxygen molecules. When we placed both H_2 and O_2 molecules outside the nanotube, we found that the most preferred configuration is that the O_2 molecule formed Si-O-O-Si structure with Si atoms while the H_2 molecule stayed molecular. The H_2 molecule is thought to be one of the most stable and abundant species and is believed to be electrically inactive in Si. Our results show that oxygen molecules did not dissociate but they tended to form Si-O-O-Si peroxide or Si-O-O structure. The HOMO-LUMO gaps all increased after adsorption. However, the increments of the HOMO-LUMO gaps are very small compared to adsorption of one hydrogen molecule or oxygen molecule. The HOMO-LUMO gaps after adsorption are in the range from 0.25 to 0.32 eV. Therefore there could be a suppression effect on the HOMO-LUMO gap for co-existence of hydrogen and oxygen molecules.

When the H_2 and O_2 molecules are adsorbed both inside of the nanotube, in only one case the oxygen molecule dissociated. When the oxygen molecule was placed in on-top site and the hydrogen molecule was in zigzag bridge site, after optimization the oxygen molecule dissociated and moved to two different bridge sites with adsorption energy of 3.464 eV. The formation of Si-O-O-Si and Si-O-O structures was also observed. The adsorption energies are in the range from 0.29 to 0.45 eV. There still exists suppression effect on the HOMO-LUMO gaps after adsorption.

When we place one H_2 molecule outside and another O_2 molecule inside of the nanotube, the oxygen molecule tends to form Si-O-O-Si structure. When we place one H_2 molecule inside and another O_2 molecule outside of the nanotube, the oxygen molecule tends to form Si-O-O structure. The interaction between the oxygen molecules and the nanotube is stronger for internal adsorption. Also energetically Si-O-O bonding is weaker than Si-O-O-Si bonding so for internal adsorption Si-O-O-Si tended to be formed and for external adsorption Si-

O-O tended to be formed. The HOMO-LUMO gaps are in the range from 0.38 to 0.59 eV. Compared to the adsorption of hydrogen and oxygen molecules from the same side of the nanotube, the suppression effect on the HOMO-LUMO gap is much less pronounced.

For the co-adsorption of H_2 and O_2 molecule from the same side of SiNT, the interaction between oxygen and hydrogen is very important because we can study the interaction between H_2 and O_2 molecules. This interaction between hydrogen and oxygen molecule can also be demonstrated by the suppression effect on the HOMO-LUMO gap when they are adsorbed from the same side of the nanotube. However, when one molecule is inside and the other molecule is outside, the interaction between two molecules is very weak, because the tube wall plays a role of separating the two molecules.

Table 4.33 Summary of adsorptions of one oxygen molecule and one hydrogen molecule from outside of SiNT, including the final configuration, adsorption energy and HOMO-LUMO gap.

Initial Site (O_{out} and H_{out})	Final local config.	D_{O-Si}	E_{ad}(eV)	E_{gap}(eV)
Top and PB	Si-O-O-Si and H_2	1.73	2.070	0.29
PB and Hol	Si-O-O-Si and H_2	1.75	1.845	0.31
Hol and PB	Si-O-O-Si and H_2	1.69	1.632	0.29
Hol and Top	Si-O-O-Si and H_2	1.62	1.383	0.30
PB and ZB	Si-O-O and H_2	1.85	0.883	0.27
PB and Top	Si-O-O and H_2	1.75	0.840	0.28
Top and Hol	Si-O-O and H_2	1.76	0.757	0.29
ZB and PB	Si-O-O and H_2	1.73	0.607	0.29
PB and PB	Si-O-O and H_2	1.78	0.391	0.31
ZB and Hol	Si-O-O and H_2	1.97	0.374	0.32
Top and Top	Si-O-O and H_2	1.87	0.355	0.27
Hol and Hol	O_2 and H_2	3.20	0.343	0.27
Hol and ZB	O_2 and H_2	2.89	0.290	0.25
Top and ZB	O_2 and H_2	3.16	0.233	0.29
ZB and ZB	O_2 and H_2	3.38	0.210	0.30
ZB and Top	O_2 and H_2	2.96	0.198	0.28

Table 4.34 Summary of adsorptions of one oxygen molecule and one hydrogen molecule from inside of SiNT, including the final configuration, adsorption energy and HOMO-LUMO gap.

Initial Site (O_{in} and H_{in})	Final local config.	D_{O-Si}	E_{ad}(eV)	E_{gap}(eV)
Top and ZB	2O and H_2	1.61	3.464	0.35
ZB and Top	Si-O-O-Si and H_2	1.73	3.025	0.38
PB and Hol	Si-O-O-Si and H_2	1.75	2.825	0.29
Top and Hol	Si-O-O-Si and H_2	1.77	2.631	0.30
ZB and PB	Si-O-O and H_2	1.89	0.785	0.25
ZB and ZB	Si-O-O and H_2	1.75	0.769	0.43
Hol and ZB	Si-O-O and H_2	1.79	0.744	0.41
PB and ZB	Si-O-O and H_2	1.79	0.713	0.29
PB and PB	Si-O-O and H_2	1.78	0.698	0.32
Top and PB	Si-O-O and H_2	1.78	0.687	0.36
Hol and Top	O_2 and H_2	2.76	0.307	0.41
PB and Top	O_2 and H_2	2.64	0.213	0.39
Hol and Hol	O_2 and H_2	2.50	0.182	0.45
ZB and Hol	O_2 and H_2	2.54	0.137	0.40
Hol and PB	O_2 and H_2	3.02	0.124	0.38
Top and Top	O_2 and H_2	2.88	0.120	0.29

Table 4.35 Summary of adsorptions of one oxygen molecule from inside and one hydrogen molecule from outside of SiNT, including the final configuration, adsorption energy and HOMO-LUMO gap.

Initial Site (H_{out} and O_{in})	Final local config.	D_{O-Si}	E_{ad}(eV)	E_{gap}(eV)
ZB and ZB	H_2 and Si-O-O-Si	1.73	2.035	0.54
ZB and Hol	H_2 and Si-O-O-Si	1.72	1.962	0.55
Hol and Hol	H_2 and Si-O-O-Si	1.78	1.938	0.48
Hol and PB	H_2 and Si-O-O-Si	1.74	1.921	0.52
PB and Top	H_2 and Si-O-O-Si	1.76	1.906	0.56
PB and ZB	H_2 and Si-O-O-Si	1.75	1.893	0.50
Top and Top	H_2 and O_2	2.26	1.826	0.51
Top and PB	H_2 and O_2	2.90	0.347	0.50
Hol and Top	H_2 and O_2	3.31	0.341	0.51
PB and Hol	H_2 and O_2	2.82	0.329	0.55
Hol and ZB	H_2 and O_2	2.98	0.325	0.54
PB and PB	H_2 and O_2	2.85	0.318	0.56
Top and Hol	H_2 and O_2	2.95	0.316	0.49
Top and ZB	H_2 and O_2	3.01	0.310	0.52
ZB and Top	H_2 and O_2	2.79	0.294	0.53
ZB and PB	H_2 and O_2	2.87	0.256	0.54

Table 4.36 Summary of adsorptions of one oxygen molecule from outside and one hydrogen molecule from inside of SiNT, including the final configuration, adsorption energy and HOMO-LUMO gap.

Initial Site (O_{out} and H_{in})	Final local config.	D_{O-Si}	E_{ad}(eV)	E_{gap}(eV)
PB and Top	Si-O-O and H_2	1.72	1.402	0.52
PB and ZB	Si-O-O and H_2	1.73	1.196	0.48
Top and PB	Si-O-O and H_2	1.76	1.092	0.47
PB and Hol	Si-O-O and H_2	1.72	0.961	0.49
Top and Top	Si-O-O and H_2	1.76	0.888	0.47
ZB and Hol	Si-O-O and H_2	1.76	0.792	0.52
PB and PB	Si-O-O and H_2	1.77	0.520	0.40
ZB and ZB	Si-O-O and H_2	1.72	0.509	0.48
ZB and PB	Si-O-O and H_2	1.77	0.487	0.43
Hol and ZB	O_2 and H_2	2.60	0.424	0.59
Top and Hol	O_2 and H_2	2.17	0.401	0.44
Hol and PB	O_2 and H_2	2.33	0.256	0.51
Hol and Top	O_2 and H_2	2.65	0.213	0.49
Hol and Hol	O_2 and H_2	2.56	0.201	0.38
ZB and Top	O_2 and H_2	2.48	0.194	0.46
Top and ZB	O_2 and H_2	2.88	0.185	0.52

CHAPTER 5

ALKALI METAL ADSORPTIONS IN SILICON NANOTUBES

Unlike carbon that can form sp, sp^2 and sp^3bonded structures which provide the richness of carbon chemistry, silicon prefers sp^3 bonding and does not exist in sp^2 bonded form by itself. An alternative approach in stabilizing the sp^2 bond in silicon and also to form nanotubes could be by doping Si with metal atoms. The presence of metal atoms could facilitate sp^2 bonding in silicon and lead to the formation of nanotubes with metal atom encapsulation.

It has been reported that very long Si nanotubes stabilized by metal doping have metallic character [36] while the finite nanotubes are semiconducting. Also the metal-doped Si clusters [139] and nanotubes [140] have attracted much attention due to the possibility of applications for magnetic devices.

5.1 Alkali Metal Adsorptions in Armchair Silicon Nanotubes

The adsorption of alkali metal atoms Li, K, Na have been performed in Si (6, 6) nanotube. Similar to the adsorption of hydrogen atom, the alkali metal atom can be placed at four different adsorption sites: normal bridge, zigzag bridge, hollow and on-top site.

The adsorption energy of alkali metal with the silicon nanotubes are calculated by,

$$E_{ad} = E(AM) + E(SiNT) - E(AM + SiNT) \quad (5.1)$$

where, $E(AM)$is the ground state energy of alkali metal atom, $E(SiNT)$ is the ground state energy of bare silicon nanotube, and $E(AM + SiNT)$ is the ground state energy of the doped silicon nanotube.From this definition, the positive value of E_{ad} is needed for a silicon nanotube to adsorb an alkali metal atom. The alkali metal atoms put at the initial adsorption site migrate to more stable site after optimization.

When the Li atom approaches the nanotube Si(6, 6) from the outside, after optimization the Li atoms only moved to hollow site for the four different initial adsorption sites (Table 5.1). Fig. 5.1 shows that when the Li atom was initially placed in zigzag bridge site, after optimization it moved to hollow site. The largest adsorption here is 5.449 eV, with a HOMO-LUMO gap of 0.42 eV. Although the final sites are all hollow sites, the adsorption energies and HOMO-LUMO gaps vary from case to case. This is because they are not exactly the same hollow site. The adsorption energies are in the range from 4.888 to 5.449 eV indicating a strong binding between the Li atom and the nanotube. The HOMO-LUMO gaps are in the range from 0.42 to 0.67 eV indicating a decrease of the bang gap after adsorption of Li atom from outside of the nanotube (Si(6, 6) has a HOMO-LUMO gap of 0.98 eV).Fig. 5.2 plots the Mulliken charge distribution for external adsorption of Li atom. It is noted that there is charge polarization of the Si atoms, which is similar to the effect induced by adsorption of H and O atoms.The Mulliken charge on the Li atom is 0.560|e| which means there is large charge transfer from the Li atom to the nanotube. The electronegativity of Li is 0.98 and Si is 1.9 so the Si atom has larger attraction to the electrons.

Table 5.1 Adsorption energy for different external adsorption sites and the corresponding optimized distance from the adsorbed Li atom to the nearest silicon atom, HOMO-LUMO gap.

Initial site	Final site	D_{Li-Si} (Å)	Adsorption energy (eV)	HOMO-LUMO gap (eV)
Normal B.	Q-hollow	2.77	4.938	0.67
Zigzag B.	Hollow	2.73	4.888	0.58
Hollow	Hollow	2.83	4.616	0.49
On-top	Hollow	2.69	5.449	0.42

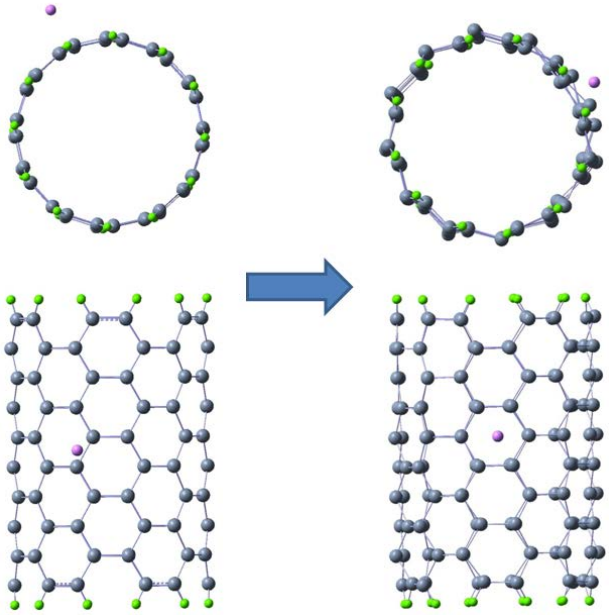

Figure 5.1 Li atom moved from zigzag bridge site to hollow site after optimization.

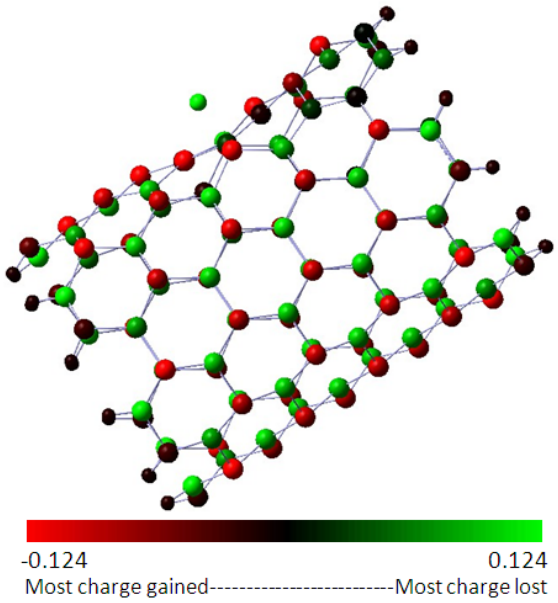

Figure 5.2 Mulliken charge distribution for external adsorption of Li atom.

Similar to the external adsorption of Li atom, in internal adsorption the interaction between the Li and the nanotube is strong with adsorption energies ranging from 5.652 to 5.680

eV (Table 5.2). Also the HOMO-LUMO gaps decreased after adsorption. The hollow site is still the only preferred site. The largest adsorption energy for internal adsorption is 5.680 eV and the largest adsorption energy for external adsorption is 5.449 eV. Therefore the interaction between Li atom and the nanotube is stronger for internal adsorption.

Table 5.2 Adsorption energy for different internal adsorption sites and the corresponding optimized distance from the adsorbed Li atom to the nearest silicon atom, HOMO-LUMO gap.

Initial site	Final site	D_{Li-Si} (Å)	Adsorption energy (eV)	HOMO-LUMO gap (eV)
Normal B.	Hollow	2.71	5.652	0.77
Zigzag B.	Hollow	2.70	5.680	0.64
Hollow	Hollow	2.70	5.680	0.64
On-top	Hollow	2.71	5.652	0.77

Table 5.3 and 5.4 show the data for external adsorption and internal adsorption of Na atom in Si (6, 6), respectively. Similar to adsorption of Li atom, the only preferred site for Na adsorption is also hollow site. The HOMO-LUMO gaps also decrease after adsorption of Na atom. Fig. 5.3 shows that there is also charge polarization in the SiNT. The largest adsorption energy for external and internal adsorption of Na atom is 5.403 and 5.622 eV, respectively. Compared with the adsorption energies for Li atom (5.449 and 5.680 eV), the adsorption energies for Na atom are slightly lower.

Table 5.3 Adsorption energy for different external adsorption sites and the corresponding optimized distance from the adsorbed Na atom to the nearest silicon atom, HOMO-LUMO gap.

Initial site	Final site	D_{Na-Si} (Å)	Adsorption energy (eV)	HOMO-LUMO gap (eV)
Normal B.	Hollow	2.91	4.572	0.52
Zigzag B.	Hollow	2.91	5.403	0.50
Hollow	Hollow	2.91	4.572	0.50
On-top	Hollow	2.91	5.403	0.50

Table 5.4 Adsorption energy for different internal adsorption sites and the corresponding optimized distance from the adsorbed Na atom to the nearest silicon atom, HOMO-LUMO gap.

Initial site	Final site	D_{Na-Si} (Å)	Adsorption energy (eV)	HOMO-LUMO gap (eV)
Normal B.	Hollow	2.94	5.622	0.52
Zigzag B.	Q-hollow	3.00	4.809	0.53
Hollow	Hollow	3.09	4.822	0.47
On-top	Hollow	3.10	4.927	0.49

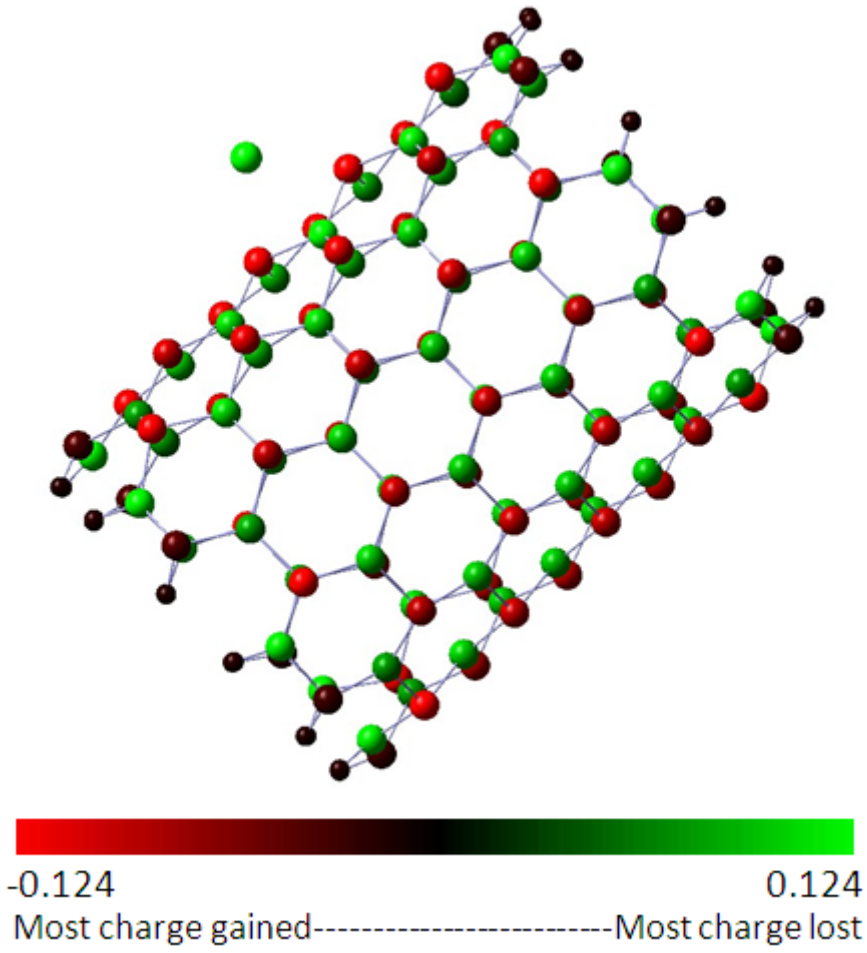

Figure 5.3 Mulliken charge distribution when H atom is in NB site

Similar to Li and Na adsorption in SiNT, the adsorption of K atom shows a same trend. In general, for alkali metal atoms Li, Na and K, the adsorption energies for internal adsorption are greater than external adsorption. As we go from Li to K, the distance between the alkali metal and the nanotube increase, and the adsorption energies are generally decreasing. Adsorption of alkali metal atoms will make the HOMO-LUMO gap of the nanotube Si (6, 6) decrease.

Table 5.5 Adsorption energy for different external adsorption sites and the corresponding optimized distance from the adsorbed K atom to the nearest silicon atom, HOMO-LUMO gap.

Initial site	Final site	$D_{K\text{-}Si}$ (Å)	Adsorption energy (eV)	HOMO-LUMO gap (eV)
Normal B.	Hollow	3.48	4.548	0.49
Zigzag B.	Hollow	3.55	4.692	0.51
Hollow	Hollow	3.55	4.402	0.46
On-top	Hollow	3.45	4.462	0.46

Table 5.6 Adsorption energy for different internal adsorption sites and the corresponding optimized distance from the adsorbed K atom to the nearest silicon atom, HOMO-LUMO gap.

Initial site	Final site	$D_{K\text{-}Si}$ (Å)	Adsorption energy (eV)	HOMO-LUMO gap (eV)
Normal B.	Hollow	3.54	5.008	0.45
Zigzag B.	Hollow	3.58	4.957	0.43
Hollow	Hollow	3.59	5.099	0.48
On-top	Q-hollow	3.51	5.564	0.55

5.2 Atomic Hydrogen Adsorption in Alkali Metal Doped Silicon Nanotubes

In order to study the adsorption of H atom on SiNTs in the presence of alkali metals, we also investigated briefly the adsorption of H atom in Li doped silicon nanotube (6, 6). Since in Section 5.1 we know that the hollow site is the only preferred adsorption site for alkali metals, in this study we only placed the Li atom in hollow site. There are still four different adsorption sites

for H atom. Both the external (H and Li are both outside of the nanotube)and internal adsorptions are studied.

The adsorption energy of H atom with doped silicon nanotubes are calculated by,

$$E_{ad} = E(Li + SiNT) + E(H) - E(Li + SiNT + H) \quad (5.2)$$

Where, $E(Li + SiNT)$is the ground state energy of Li doped SiNT, $E(H)$ is the ground state energy of H atom, and $E(Li + SiNT + H)$ is the ground state energy of the doped silicon nanotube and the H atom.

It is noted that after optimization, the Li atoms sill stay in hollow sites. However, the H atoms only moved to the top site of silicon atoms. For external adsorption, the adsorption energies are in the range from 3.408 to 3.414 eV and the HOMO-LUMO gaps are around 1.00 eV (Table 5.7).Fig. 5.4 shows that the H atom moved from normal bridge site to the top site of Si atom. The adsorption of H atom increases the HOMO-LUMO gaps of the Li doped SiNTs.

It is noted that the adsorption of H atom in nanotube Si (6, 6) in the presence of Li atom is lower than the adsorption of H without Li atom. However, we also notice that the adsorption energy of H without Li atom incorporate deformation energy of the nanotube, because after adsorption of H atom the Si (6, 6) changed from a smooth tube to a "wrinkled" tube. Therefore it is impulsive to say right now that the presence of Li atom will suppress the adsorption of H atom. It requires further study on minimizing the influence of structural deformation on the adsorption energy to understand the behavior of H adsorption in presence of alkali metal atoms.

Table 5.7 The external adsorption of H atom in Li doped SiNT

Initial site(H)	Final site(H)	Final site(Li)	$D_{H\text{-}Si}$ (Å)	$D_{H\text{-}Li}$ (Å)	Adsorption energy (eV)	HOMO-LUMO gap (eV)
Normal B.	Top-Si	Hollow	1.54	2.36	3.410	1.01
Zigzag B.	Top-Si	Hollow	1.54	2.37	3.414	1.03
Hollow	Top-Si	Hollow	1.54	2.37	3.408	0.99
On-top	Top-Si	Hollow	1.54	2.38	3.409	1.01

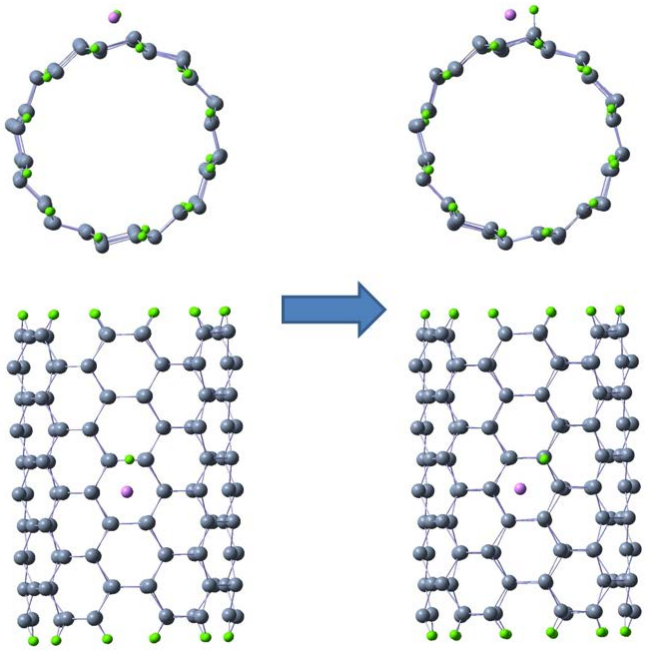

Figure 5.4 The H atom moved from normal bridge site to on-top site

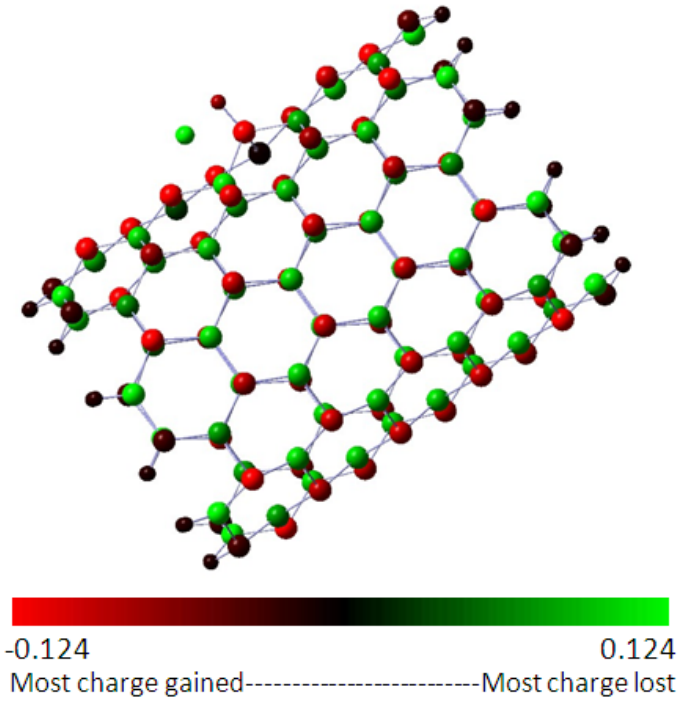

Figure 5.5 Mulliken charge distribution of H adsorption in Li doped SiNT

Table 5.8 The internal adsorption of H atom in Li doped SiNT

Initial site(H)	Final site(H)	Final site(Li)	D_{H-Si} (Å)	D_{H-Li} (Å)	Adsorption energy (eV)	HOMO-LUMO gap (eV)
Normal B.	Top-Si	Hollow	1.54	1.99	2.940	1.20
Zigzag B.	Top-Si	Hollow	1.54	1.99	2.940	1.20
Hollow	Top-Si	Hollow	1.50	1.98	2.905	1.13
On-top	Top-Si	Hollow	1.54	1.99	2.940	1.20

CHAPTER 6

CONCLUSIONS AND SUGGESTIONS FOR FUTURE RESEARCH

Carbon nanotubes have aroused scientific interest in various areas due to their great potential of applications. The nanotubes have novel electronic properties attributed to their quasi-one-dimensional tubular structure, which can be metal or semiconductor depending on the diameters and chiralities. Silicon atoms have similar electronic configurations with carbon atom. However, the possibility of silicon forming nanotubular structures has usually been considered doubtful. Silicon tends to form sp^3 bonds and avoids the creation of sp^2-like bonds. Also the possible metallic nature of SiNTs is still an open question.

The structure of MWSiNTs is a matter of some critical debate and one of the underlying tender problems is that it strongly depends on the method of preparation. Though MWSiNTs are useful because they are stabilized by a large number of layers and available in relatively large quantities, SWSiNTs are more ideal for understanding electronic structure and transport phenomenon. They also lend themselves to nanoscopic applications because they have exceptionally quasi-one-dimensional structure, a nanoscale diameter and they are not affected by inter-layer interaction.

Nanotubes are important due to their fascinating chemical and physical properties and huge potential applications in the electronics industries. Our study focuses on the electronic and structural properties of silicon nanotubes from single-walled to multi-walled. We have presented a detailed *ab initio* study of the evolution of electronic properties with the size of silicon nanotubes. Results have shown that the binding energy per atom increases as the tube diameter increases and tends to saturate for both armchair and zigzag single-walled silicon nanotubes. The calculation of the HOMO-LUMO gaps indicates that neither armchair nor zigzag single-walled silicon nanotubes have metallic behavior. Energetically zigzag silicon nanotubes

are more favorable than armchair silicon nanotubes. The buckling of zigzag silicon nanotubes is significantly larger than armchair silicon nanotubes. Also armchair silicon nanotubes have smooth tubular structure but all zigzag silicon nanotubes have “wrinkled” tubular structure. It is reasonable to assume that zigzag silicon nanotubes have sp^3-like character and armchair silicon nanotubes have sp^2-like character.

One can imagine using them for nanoscale devices, or taking a single SiNT as an electric wire. This would be the ultimate level of miniaturization in microchip technology. It is also possible to connect two SiNT junctions which exhibit different electronic behaviors. Such devices can act as a molecular diode, which allows electrical current to flow in one direction, from a semiconductor to a metal, but not in the opposite direction.

Our studies on double-walled armchair silicon nanotubes have confirmed that all double-walled silicon nanotubes are semiconducting like their single-walled constituents. However comparison of band gaps of single-walled nanotube and those of double-walled nanotubes indicates that the band gap of a double-walled nanotube is always smaller than that of the individual single-walled components. Also nanotubes with small interlayer separations, called “meshed” tubes, do not hold the coaxial cylindrical structure. However, these so-called “meshed” nanotubes have a resemblance to the already fabricated silicon nanotubes. Therefore, study of these double-walled silicon nanotubes including meshed tubes can help us better understand the synthesis of silicon nanotubes. Multi-walled nanotubes may have been more complex behavior, because each layer in the tube has a slightly different geometry. If we could tailor their composition individually, we might one day make multi-walled tubes that are self-insulating or that carry multiple signals at once, like nanoscopic coaxial cables.

The electronic properties of single-walled nanotubes can be appreciably altered by the presence of other adsorbed atoms or molecules. This has important ramifications for device applications involving SWNTs, and it has led to considerable interest in the possible use of SWNTs as the basis of chemical sensors. Also, sp^2 bonding in silicon can be stabilized by

doping Si with metal atoms. The properties of such nanotubes are controlled by the metal atoms and it has been possible to develop metallic, semiconducting, and magnetic nanotubes.

Our study of atomic H and O adsorption has shown that H atom can only be adsorbed in on-top site of silicon atoms. O atom tends to be adsorbed in bridge sites. Adsorption of H atom in armchair silicon nanotubes will make the band gap decrease. However, adsorption of H atom in zigzag silicon nanotubes will make the band gap increase. The adsorption energies for armchair silicon nanotubes are higher than zigzag silicon nanotubes. After adsorption of H atom, armchair silicon nanotubes became more puckered but zigzag nanotubes did not have much change in their structure. Therefore the adsorption energies for armchair silicon nanotubes include large deformation energy. Adsorption of O atom will also cause band gap to increase. The adsorption of hydrogen on armchair silicon nanotubes can induce the charge polarization of Si atoms. Point charges upon the material's surface can improve the storage capacity since they increase the binding energy of hydrogen. The binding energy of the hydrogen molecules would be enhanced due to charge induced dipole interactions. The charge induced dipole interaction characterizes the H_2 physisorption on SiNTs and is responsible for the higher hydrogen uptake of the tubes. Among different adsorption orientations, hydrogen adsorbing on the on-top site with the H-H bond vertical to the tube surface is the most favorable adsorption mode for both inside and outside of the tube wall. This phenomenon mainly stems from the dense electron cloud around the SiNT surface, which produce a strong VDW attraction to hydrogen. Single-walled silicon nanotubes have shown some promise to be a viable adsorbent for hydrogen storage. However, many fundamentally important issues have remained unanswered.

Also, study of interaction of various gases like O_2, H_2 etc. with silicon nanotube might help develop detection techniques for these gases up to the precision of single molecule. Such gases can also be detected by studying the variation in electronic properties of nanotubes when the molecule is absorbed in the tube surface. Our study on adsorption of hydrogen and oxygen

molecules has shown that hydrogen molecule will stay molecular after adsorption but oxygen molecule will dissociate. The most preferred site for single hydrogen molecule adsorption is on-top site for both armchair and zigzag silicon nanotubes. Also adsorption of single hydrogen molecule will increase the band gap of both armchair and zigzag silicon nanotubes. Si-O-O-Si peroxide structure has been observed in adsorption of two oxygen molecules in silicon nanotubes. It is noted that there is a suppression effect on the HOMO-LUMO gap when hydrogen and oxygen molecules are adsorbed from the same side of the tube wall.

The functionalization of silicon nanotubes by alkali metal atoms is an interesting area of research. Understanding nature of interaction between alkali metal and the nanotubes might help us design novel hybrid nanostructures applicable in nanoelectronics. Our study shows that the interaction of alkali metal with silicon nanotubes is more pronounced when adsorbed internally. As an extension of the work, functionalization of double-walled nanotube and associated electronic and magnetic structure properties need to be investigated in detail. In future, it would be of great relevance to be able to eventually enhance the intrinsic conductivity of SiNTs. In this respect, the development in alkali metal doped SiNTs look rather promising. Also, study of interaction of silicon nanotubes with alkali metals might lead us to the possibilities of increasing the adsorption capability of silicon nanotubes for hydrogen molecules. To further explore the possible applications of silicon nanotubes, study of a wide range of chemicals encapsulated silicon nanotubes should be pursued.

Study of electron transport properties of nanotubes is important to understand the behavior of the nanotubes used in nano-electronic circuits. Silicon nanotubes are very promising material for nanoelectronics. To understand and control the electronic properties of nanotubes for implementation in such applications, a detailed study of transport properties of these nanotubes is required. An accurate and comprehensive analysis of such electronic transport properties of silicon nanotubes has not received enough attention and would be an interesting area of research. The computational methods which are already being used

successfully to investigate transport properties of other nano-scale systems can be used in case of silicon nanotubes also.

Unfortunately, before all these potential applications for SiNTs could be transferred from the research laboratory to industry, it is crucial to increase the yield in the synthesis technique. A large effort in the understanding of growth mechanisms has to be made in order to be able to produce SiNT by significant amount as required for most industrial processes. Studies on SiNTs have been flourishing in recent years. However, it seems great difficulties remain for commercialization for two reasons, manipulation and selection of SiNTs. Explicit control of the chirality, diameter, length and electronic structure of SiNTs is required for pragmatic usage.

To conclude, despite great challenges and difficulties in fabricating silicon nanotubes in experiments, much can be learned from computer experiments of these structures which would not only find possible future applications of silicon nanotubes in various fields but also encourage experimental research by providing possible synthesis pathways. Hopefully, our study so far on silicon nanotubes raises more questions than answers and further detailed experimental and theoretical studies will continue to provide answers to a relatively unexplored field in nanoscience and nanotechnology.

REFERENCES

1. S. Iijima, Helical microtubes of graphitic carbon. Nature 354 (1991) 56-58. doi: 10.1038/354056a0

2. S. Iijima and T. Ichihashi, Single-shell carbon nanotubes of 1-nm diameter. Nature 363 (1993) 603-605. doi: 10.1038/363603a0

3. D.S. Bethune, C.H. Kiang, M.S. de Vries, G. Gorman, R. Savoy, J. Vazquez, and R. Beyers, Cobalt-catalysed growth of carbon nanotubes with single-atomic-layer walls. Nature 363 (1993) 605-607

4. J. Cumings and A. Zettl, Mass-production of boron nitride double-wall nanotubes and nanococoons. Chemical Physics Letters 316 (2000) 211-206. doi: 10.1016/S0009-2614(99)01277-4

5. Q. Wu, Z. Hu, X. Wang, Y. Lu, X. Chen, H. Xu, and Y. Chen, Synthesis and characterization of hexagonal aluminum nitride nanotubes. Journal of the American Chemical Society 125 (2003) 10176-10177.

6. J. Goldberger, R. He, Y. Zhang, S. Lee, H. Yan, H. Chol, and P. Yang, Single-crystal gallium nitride nanotubes. Nature 422 (2003) 599-602. doi: 10.1038/nature01551

7. P. Pradhan and A.K. Ray, A hybrid density functional study of armchair Si and Ge nanotubes. Journal of Computational and Theoretical Nanoscience 3 (2006) 128-133. doi: 10.1166/jctn.2006.011

8. M.N. Huda, L. Kleinman, and A.K. Ray, Silicon-carbide nanostructures to nanotubes. Journal of Computational and Theoretical Nanoscience 4 (2007) 739-744. doi:10.1166/jctn.2007.003

9. K. Alam and A.K. Ray, Hybrid density functional study of armchair SiC nanotubes. Physical Review B 77 (2008) 035436-035445. doi: 10.1103/PhysRevB.77.035436

10. S. J. Rathi and A.K. Ray, On the electronic and geometric structures of armchair GeC nanotubes: a hybrid density functional study. Nanotechnology 19 (2008) 335706-335716. doi: 10.1088/0957-4484/19/33/335706

11. Nanoparticles and Nanostructured Surfaces, Ed. A. K. Ray (American Scientific Publishing, 2010)

12. N. Wang, Y.H. Tang, Y.F. Zhang, C.S. Lee, and S.T. Lee, Nucleation and growth of Si nanowires from silicon oxide. Physical Review B58 (1998) R16024-R16026. doi: 10.1103/PhysRevB.58.R16024

13. J. Hu, M. Ouyang, P. Yang, and C. M. Lieber, Controlled growth and electrical properties of heterojunctions of carbon nanotubes and silicon nanowires.Nature 399 (1999) 48-51. doi: 10.1038/19941

14. M. Menon and E. Richter, Are quasi-one dimensional structures of Si stable? Physical Review Letters 83 (1999) 792-795. doi: 10.1103/PhysRevLett.83.792

15. B. Marsen and K. Sattler, Fullerene-structured nanowires of silicon. Physical Review B60 (1999) 11593-11600. doi: 10.1103/PhysRevB.60.11593

16. U. Landman, R.N. Barnett, A.G. Scherbakov, and Ph. Avouris, Metal-semiconductor nanocontacts: silicon nanowires. Physical Review Letters 85 (2000) 1958-1961. doi: 10.1103/PhysRevLett.85.1958

17. R.Q. Zhang, S.T. Lee, C.K. Law, W.K. Li, and B.K. Teo, Silicon nanotubes: Why not? Chemical Physics Letters 364 (2002) 251-258. doi: 10.1016/S0009-2614(02)01334-9

18. Carbon Nanotubes-Synthesis, Structure, Properties and Applications, Topics in Applied Physics Vol. 80, edited by M.S. Dresselhaus, G. Dresselhaus, and Ph. Avouris (Springer, Berlin, 2001)

19. J. Sha, J. Niu, X. Ma, J. Xu, X. Zhang, Q. Yang, and D. Yang, Silicon nanotubes. Advanced Materials 14 (2002) 1219-1221. doi: 10.1002/1521-4095(20020903)14:17<1219::AID-ADMA1219>3.0.CO;2-T

20. S. Y. Jeong, J. Y. Kim, H. D. Yang, B. N. Yoon, S. Choi, H. K. Kang, C. W. Yang, and Y. H. Lee, Synthesis of silicon nanotubes on porous alumina using molecular beam epitaxy. Advanced Materials 15 (2003) 1172-1176. doi: 10.1002/adma.200304898

21. M. De Crescenzi, P. Castrucci, M. Scarselli, M. Diociaiuti, P.S. Chaudhari, C. Balasubramanian, T.M. Bhave, and S.V. Bhoraskar, Experimental imaging of silicon nanotubes. Applied Physics Letters 86 (2005) 231901-231903. doi: 10.1063/1.1943497

22. G. Seifert, Th. Kohler, H.M. Urbassek, E. Hernandez, and Th. Frauenheim, Tubular structures of silicon. Physical Review B63 (2001) 193409. doi: 10.1103/PhysRevB.63.193409

23. S.B. Fagan, R. Mota, R.J. Baierle, G. Paiva, A.J.R. da Silva, and A. Fazzio, Stability investigation and thermal behavior of a hypothetical silicon nanotube. Journal of Molecular Structure 539 (2001) 101-106. doi: 10.1016/S0166-1280(00)00777-6

24. V. Kumar, C. Majumder, and Y. Kawazoe, M@Si_{16}, M=Ti, Zr, Hf: π conjugation, ionization potentials and electron affinities. Chemical Physics Letters 363 (2002) 319-322. doi: 10.1016/S0009-2614(02)01184-3

25. R.Q. Zhang, H. Lee, W. Li, and B.K. Teo, Investigation of possible structures of silicon nanotubes via density-functional tight-binding molecular dynamics simulations and ab initio calculations. Journal of Physical Chemistry B 109 (2005) 8605-8612. doi: 10.1021/jp045682h

26. B. Yan, G. Zhou, J. Wu, W. Duan, and B. Gu, Bonding modes and electronic properties of single-crystalline silicon nanotubes. Physical Review B73 (2006) 155432. doi: 10.1103/PhysRevB.73.155432

27. S.J. Rathi and A.K. Ray, A hybrid density functional study of zigzag and chiral Si nanotubes. Journal of Computational and Theoretical Nanoscience 5 (2008) 464-475. doi: 10.1166/jctn.2008.004

28. S.B. Fagan, R.J. Baierle, R. Mota, A.J.R. da Silva, and A. Fazzio, Ab initio calculations for a hypothetical material: Silicon nanotubes. Physical Review B61 (2000) 9994-9996.doi: 10.1103/PhysRevB.61.9994

29. M. Zhang, Y.H. Kan, Q.J. Zang, Z.M. Su, and R.S. Wang, Why silicon nanotubes stably exist in armchair structure? Chemical Physics Letters 379 (2003) 81-86. doi: 10.1016/j.cplett.2003.08.030

30. E. Durgun, S. Tongay, and S. Ciraci, Silicon and III-V compound nanotubes: structural and electronic properties. Physical Review B72 (2005) 075420. doi: 10.1103/PhysRevB.72.075420

31. A.S. Barnard and S.P. Russo, Structure and energetics of single-walled armchair and zigzag silicon nanotubes. Journal of Physical Chemistry B 107 (2003) 7577-7581. doi: 10.1021/jp0347421

32. O. Ponomarenko, M.W. Radny, and P.V. Smith, Energetics of finite, clean and hydrogenated silicon nanotubes. Surface Science 562 (2004) 257-268. doi: 10.1016/j.susc.2004.06.105

33. J.W. Kang, J.J. Seo, and H.J. Hwang, Molecular dynamics study of hypothetical silicon nanotubes using the Tersoff potential. Journal of Nanoscience and Nanotechnology 2 (2002) 687-691. doi: 10.1166/jnn.2002.146

34. J.W. Kang and H.J. Hwang, Hypothetical silicon nanotubes under axial compression. Nanotechnology 12 (2003) 402-408. doi: 10.1088/0957-4484/14/3/309

35. A.N. Andriotis, G. Mpourmpakis, G.E. Froudakis, and M. Menon, Stabilization of Si-based cage clusters and nanotubes by encapsulation of transition metal atoms. New Journal of Physics 4 (2002) 78.1-78.14. doi: 10.1088/1367-2630/4/1/378

36. M. Menon, A.N. Andriotis, and G. Froudakis, Structure and stability of Ni-encapsulated Si nanotube. Nano Letters 2 (2002) 301-304. doi: 10.1021/nl015695w

37. A.K. Singh, T.M. Briere, V. Kumar, and Y. Kawazoe, Magnetism in transition-metal-doped silicon nanotubes. Physical Review Letters 91 (2003) 146802. doi: 10.1103/PhysRevLett.91.146802

38. G.C. Shan and W. Huang, Energy band and band-gap properties of deformed single-walled silicon nanotubes. Frontiersof Physics in China 5 (2010) 183-187. doi: 10.1007/s11467-010-0017-7

39. M. Zhao, R.Q. Zhang, Y. Xia, C. Song, and S.T. Lee, Faceted silicon nanotubes: structure, energetic, and passivation effects.Journal of Physical Chemistry C 111 (2007) 1234-1238. doi: 10.1021/jp066177i

40. K. Tada, S. Furuya, and K. Watanabe, *Ab inito* study of hydrogen adsorption to single-walled carbon nanotubes. Physical Review B63 (2001) 155405-155408. doi: 10.1103/PhysRevB.63.155405

41. W. An, X. Wu, J.L. Yang, and X.C. Zeng, Adsorption and surface reactivity on single-walled boron nitride nanotubes containing Stone-Wales defects. Journal of Physical Chemistry C 111 (2007) 14105-14112. doi: 10.1021/jp072443w

42. R.J. Baierle, S.B. Fagan, R. Mota, A.J.R. da Silva, and A. Fazzio, Electronic and structural properties of silicon-doped carbon nanotubes. Physical Review B64 (2001) 085413-085416. doi: 10.1103/PhysRevB.64.085413

43. Y. Ye, C.C. Ahn, C. Witham, B. Fultz, J. Liu, A.G. Rinzler, D. Colbert, K.A. Smith, and R.E. Smalley, Hydrogen adsorption and cohesive energy of single-walled carbon nanotubes. Applied Physics Letters 74 (1999) 2307-2310. doi: 10.1063/1.123833

44. X. Zhang, D. Cao, and J. Chen, Hydrogen adsorption storage on single-walled carbon nanotube arrays by a combination of classical potential and density functional theory. Journal of Physical Chemistry B 107 (2003) 4942-4950. doi: 10.1021/jp034110e

45. S. Banerjee, S. Nigam, C.G.S. Pillai, and C. Majumder, Hydrogen storage on Ti decoratd SiC nanostructures: A first principles study. International Journal of Hydrogen Energy 37 (2012) 3733-3710. doi: 10.1016/j.ijhydene.2011.05.078

46. R. StrÖbel, L. JÖrissen, T. Schliermann, V. Trapp, W. Schutz, K. Bohmhammel, G. Wolf, and J. Garche, Hydrogen adsorption on carbon materials. Journal of Power Sources 84 (1999) 221. doi: 10.1016/S0378-7753(99)00320-1

47. F.E. Pinkerton, B.G. Wicke, C.H. Olk, G.G. Tibbetts, G.P. Meisner, M.S. Meyer, and J.F. Herbst, Thermogravimetric measurement of hydrogen absorption in alkali-modified carbon materials. Journal of Physical Chemistry B 104 (2000) 9460-9467. doi: 10.1021/jp000957o

48. R.T. Yang, Hydrogen storage by alkali-doped carbon nanotubes-revisited. Carbon 38 (2000) 623-626.

49. H.G. Schimmel, G.J. Kearley, M.G. Nijkamp, C.T. Visser, K.P. de Jong, and F.M. Mulder, Hydrogen adsorption in carbon nanostructures: comparison of nanotubes, fibers, and coals. Chemistry-A European Journal 9 (2003) 4764-4770. doi: 10.1002/chem.200304845

50. The Department of Energy Hydrogen and Fuel Cells Program Plan, 2011, (http://www.hydrogen.energy.gov/pdfs/program_plan2011.pdf)

51. A.C. Dillion, T. Gennett, J.L. Alleman, K.M. Jones, P.A. Parilla, M.J. Heben, in Proceedings of the 2000 DOE/NREL Hydrogen Program Review, 2000. (http://www1.eere.energy.gov/hydrogenandfuelcells/pdfs/28890kkk.pdf)

52. F. Darkrim and D. Levesque, Monte Carlo simulations of hydrogen adsorption in single-walled carbon nanotubes. Journal of Chemical Physics 109 (1998) 4981-4984. doi: 10.1063/1.477109

53. S.M. Lee, K.S. Park, Y.C. Choi, Y.S. Park, J.M. Bok, D.J. Bae, K.S. Nahm, Y.G. Choi, S.C. Yu, N. Kim, T. Frauenheim, and Y.H. Lee, Hydrogen adsorption and storage in carbon nanotubes. Synthetic Metals 113 (2000) 209-216. doi: 10.1016/S0379-6779(99)00257-1

54. A.C. Dillion, K.M. Jones, T.A. Bekkedahl, C.H. Kiang, D.S. Bethune, and M.J. Heben, Storage of hydrogen in single-walled carbon nanotubes. Nature 386 (1997) 377-379. doi: 10.1038/386377a0

55. S. Mukherjee and A.K. Ray, An *ab initio* study of molecular hydrogen interaction with SiC nanotube-a precursor to hydrogen storage. Journal of Computational and Theoretical Nanoscience 5 (2008) 1210-1219.

56. H. Xu, X.B. Yang, C.S. Guo, and R.Q. Zhang, An energetic stability predictor of hydrogen-terminated Si nanostructures. Applied Physics Letters 95 (2009) 253106. doi: 10.1063/1.3276554

57. D.W. Boukhvalov, M.I. Katsnelson, and A.I. Lichtenstein, Hydrogen on graphene: electronic structure, total energy, structural distortions and magnetism from first-principles calculations. Physical Review B77 (2008) 035427. doi: 10.1103/PhysRevB.77.035427

58. P. Ruffieux, Q. Groning, P. Schwaller, L. Schlapbach, and P. Groning, Hydrogen atoms cause long-range electronic effects on graphite. Physical Review Letters 84 (2000) 4910-4913. doi: 10.1103/PhysRevLett.84.4910

59. K.G. Nakamura, K. Ishioka, M. Kitajima, and K. Murakami, *Ab initio* calculation of the hydrogen molecule in silicon. Solid State Communications 101 (1997) 735-738. doi: 10.1016/S0038-1098(96)00694-1

60. B. Hourahine, R. Jones, S. Oberg, R.C. Newman, P.R. Briddon, and E. Roduner, Hydrogen molecules in silicon located at interstitial sites and trapped in voids. Physical Review B57 (1998) R12666-R12669. doi:10.1103/PhysRevB.57.R12666

61. K. Oura, V.G. Lifshits, A.A. Saranin, A.V. Zotov, and M. Katayama, Hydrogen interaction with clean and modified silicon surfaces. Surface Science Reports 35 (1999) 1-69. doi: 10.1016/S0167-5729(99)00005-9

62. K. Sinniah, M.G. Sherman, L.B. Lewis, W.H. Weinberg, J.T. Yates, and K.C. Janda, New mechanism for hydrogen desorption from covalent surfaces: the monohydride phase on Si (100). Physical Review B62 (1989) 567-570. doi: 10.1103/PhysRevLett.62.567

63. C.G. Van de Walle, P.J.H. Denteneer, Y. Bar-Yam, and S.T. Pantelides, Theory of hydrogen diffusion and reactions in crystalline silicon. Physical Review B39 (1989) 10791-10808. doi:10.1103/PhysRevB.39.10791

64. P. Bratu, W. Brenig, A. Grob, M. Hartmann, U. Hofer, P. Kratzer, and R. Russ, Reaction dynamics of molecular hydrogen on silicon surfaces. Physical Review B54 (1996) 5978-5991. doi: 10.1103/PhysRevB.54.5978

65. P.G. Collins, K. Bradley, M. Ishigami, and A. Zettl, Extreme oxygen sensitivity of electronic properties of carbon nanotubes. Science 287 (2000) 1801-1804. doi: 10.1126/science.287.5459.1801

66. J. Kong, N.R. Franklin, C. Zhou, M.G. Chapline, S. Peng, K. Cho, and H. Dai, nanotube molecular wires as chemical sensors. Science 287 (2000) 622-625. doi: 10.1126/science.287.5453.622

67. K. Bradley, S.H. Jhi, P.G. Collins, J. Hone, M.L. Cohen, S.G. Louie, and A. Zettl, Is the intrinsic thermoelectric power of carbon nanotubes positive? Physical Review Letters 85 (2000) 4361-4364. doi: 10.1103/PhysRevLett.85.4361

68. J. Plans, G. Diaz, E. Martinez, and F. Yndurain, Theoretical study of oxygen in silicon: breaking of the Si-Si bond. Physical Review B35 (1987) 788-791. doi: 10.1103/PhysRevB.35.788

69. L.I. Murin, T. Hallberg, V.P. Markevich, and J.L. Lindstorm, Experimental evidence of the oxygen dimer in silicon. Physical Review B80 (1998) 93-96. doi: 10.1103/PhysRevLett.80.93

70. S. Oberg, C.P. Ewels, R. Jones, T. Hallberg, J.L. Lindstorm, L.I. Murin, and P.R. Briddon, First stage of oxygen aggregation in silicon: the oxygen dimer. Physical Review Letters 81 (1998) 29302933. doi: 10.1103/PhysRevLett.81.2930

71. T. Hoshino, Adsorption of atomic and molecular oxygen and desorption of silicon monixide on Si(111) surfaces. Physical Review B59 (1999) 2332-2340. doi: 10.1103/PhysRevB.59.2332

72. M. Zhao, R.Q. Zhang, and Y. Xia, Surface structures and electronic states of silicon nanotubes stabilized by oxygen atoms. Journal of Applied Physics 102 (2007) 024313. doi: 10.1063/1.2752115

73. M. Zhao, J.Z. Zhu, Y. Xia, and M. Lu, Stabilizing zigzag single-walled silicon nanotubes and tailoring the electronic structures by oxygen atoms: first-principles studies. Journal of Physical Chemistry C 111 (2007) 2942-2946. doi: 10.1021/jp067434

74. R.G. Parr andW. Yang, Density functional theory of atoms and molecules. Oxford University Press, New York, (1989).

75. L.H. Thomas, The calculation of atomic fields. Proceedings of the Cambridge Philosophical Society 23, 542-548 (1927). doi: 10.1017/S0305004100011683.

76. E. Fermi, Eine statistische Methode zur Bestimmung einiger Eigenschaften des Atoms und ihre Anwendung auf die Theorie des periodischen Systems der Elemente (A statistical method for the determination of some properties of the atom and its application to the theory of the periodic table of elements), Zeitschrift für Physik 48 (1928)73-79. doi:10.1007/BF01351576.

77. E.Teller, On the stability of molecules in the Thomas-Fermi theory. Reviews of Modern Physics 34 (1962)627-631. doi:10.1103/RevModPhys.34.627

78. P.A.M. Dirac, Note on Exchange Phenomena in the Thomas Atom. Mathematical Proceedings of the Cambridge Philosophical Society 26 (1930)376-385. doi:10.1017/S0305004100016108.

79. P. Hohenberg and W. Kohn, Inhomogeneous electron gas.Physical Review 136 (1964) B864-B871. doi: 10.1103/PhysRev.136.B864

80. W. Kohn and L.J. Sham, Self-consistent equations including exchange and correlation effects. Physical Review 140 (1965)A1133-A1138. doi:10.1103/PhysRev.140.A1133.

81. R.M. Dreizler, E.K.U. Gross, Density functional theory: an approach to the quantum many-body problem, Springer-Verlag Berlin Heidelberg (1990).

82. J. P. Perdew, Electronic structure of solids '91, edited by P. Ziesche and H. Eschig, Akademie Verlag, Berlin (1991).

83. E. Helmut, The fundamental of density functional theory, B.G. Teubner Verlagsgesellschaft, Stuttgart- Leipzig (1996).

84. J.F. Dobson, G. Vignale, and M.P. Das (Eds.), Electronic density functional theory: recent progress and new directions, Plenum Press, New York and London (1998).

85. W. Koch and M.C. Holthausen, A chemist's guide to density functional theory, second edition, Wiley, Weinheim (Federal Republic of Germany) (2001).

86. C.Fiolhais, F. Nogueira, and M. Marques (Eds.) A primer in density functional theory, Springer-Verlag Berlin Heidelberg (2003).

87. E. Engel and R.M. Dreizler, Density functinal theory: an advanced course, Springer-Verlag Berlin Heidelberg (2011).

88. D.R. Hartree, The wave mechanics of an atom with a non-coulomb central field. part i. theory and methods. Mathematical Proceedings of the Cambridge Philosophical Society 24 (1928) 89-110. doi:10.1017/S0305004100011919

89. V. Fock, Näherungsmethode zur Lösung des quantenmechanischen Mehrkörperproblems. Zeitschrift für Physik 61(1930)126-148. doi:10.1007/BF01340294

90. C. Coulson, present state of molecular structure calculations. Reviews of Modern Physics 32(1960) 170-177. doi:10.1103/RevModPhys.32.170

91. W.J. Carr and A.A. Maradudin, Ground-state energy of a high-density electron gas, Physical Review 133(1964) A371-A374. doi: 10.1103/PhysRev.133.A371

92. M. Gell-Mann and K.A. Brueckner, Correlation energy of an electron gas at high density.Physical Review 106 (1957) 364-368. doi: 10.1103/PhysRev.106.364

93. U.von Barth and L. Hedin, A local exchange-correlation potential for the spin polarized case. Journal of Physics C: Solid State Physics 5(1972)1629-1642.doi:10.1088/0022-3719/5/13/012

94. O. Gunnarsson and B.I. Lundqvist, Exchange and correlation in atoms, molecules, and solids by the spin-density-functional formalism.Physical Review B 13 (1976) 4274-4298. doi: 10.1103/PhysRevB.13.4274

95. S.H. Vosko, L. Wilk and M. Nusair, Accurate spin-dependent electron liquid correlation energies for local spin density calculations: a critical analysis. Canadian Journal of Physics 58(1980)1200-1211. doi: 10.1139/p80-159.

96. L.A. Cole and J.P. Perdew, Calculated electron affinities of the elements. Physical Review A 25(1982) 1265-1271.doi:10.1103/PhysRevA.25.1265.

97. J.P. Perdew and A. Zunger, Self-interaction correction to density-functional approximations for many-electron systems. Physical Review B 23(1981)5048-5079. doi:10.1103/PhysRevB.23.5048.

98. J.P. Perdew and Y. Wang, Accurate and simple analytic representation of the electron-gas correlation energy. Physical Review B 45, (1992)13244-13249.doi:10.1103/PhysRevB.45.13244.

99. O.Gunnarsson, M. Jonson, and B.I. Lundqvist,Exchange and correlation in inhomogeneous electron systems.Solid State Communications 24(1977)765-768. doi:10.1016/0038-1098(77)91185-1

100. T. Ziegler, A. Rauk, and E.J. Baerends,On the calculation of multiple energies by the Hartree-Fock-Slater method. Theoretical chemistry accounts: theory, computation, and modeling (Theoretica chimica acta) 43 (1977) 261-271. doi: 10.1007/BF00551551

101. K.Burke, J.P. Perdew, and M. Ernzerhof, Why semilocal functionals work: accuracy of the on-top pair density and importance of system averaging. Journal of Chemical Physics 109, (1998)3760-3771. doi: 10.1063/1.476976.

102. D.C. Langreth and J. P. Perdew, Theory of nonuniform electronic systems. I. Analysis of the gradient approximation and a generalization that works. Physical Review B 21(1980) 5469-5493. doi: 10.1103/PhysRevB.21.5469

103. J. P. Perdew, Accurate density functional for the energy: real-space cutoff of the gradient expansion for the exchange hole. Physical Review Letters 55 (1985) 1665-1668. doi: 10.1103/PhysRevLett.55.1665.

104. J. P. Perdew, Density-functional approximation for the correlation energy of the inhomogeneous electron gas. Physical Review B 33(1986)8822-8824. doi: 10.1103/PhysRevB.33.8822.

105. A.D. Becke, Density-functional thermochemistry. III. The role of exact exchange.Journal of Chemical Physics 98 (1993) 5648-5652. doi:10.1063/1.464913.

106. A. D. Becke, A new mixing of Hartree-Fock and local density-functional theories. Journal of Chemical Physics 98(1993)1372-1377. doi: 10.1063/1.464304

107. C. Lee, W. Yang, and R.G. Parr, Development of the Colle-Salvetti correlation-energy formula into a functional of the electron density. Physical Review B 37 (1988)785-789. doi:10.1103/PhysRevB.37.785.

108. J.P. Perdew, J.A. Chevary, S.H. Vosko, K.A. Jackson, M.R. Pederson, D.J. Singh, and C. Fiolhais, Atoms, molecules, solids, and surfaces: applications of the generalized gradient approximation for exchange and correlation. Physical Review B 48(1992) 6671-6687. doi: 10.1103/PhysRevB.46.6671.

109. K. Burke, J.P. Perdew, and Y. Wang, in Electronic Density Functional Theory: Recent Progress and New Directions, Ed. J. F. Dobson, G. Vignale, and M. P. Das (Plenum, New York, 1998).

110. J.P. Perdew, K. Burke, and M. Ernzerhof, Generalized gradient approximation made simple. Physical Review Letters 77 (1996) 3865-3868. doi: 10.1103/PhysRevLett.77.3865

111. S.F. Boys, Electronic wave functions. A general method of calculation for the stationary states of any molecular system, Proceedings of the Royal Society of London. Series A, mathematical and Physical Sciences 200 (1950) 542-554. doi: 10.1098/rspa.1950.0036

112. W.J. Hehre, L. Radom, P.R. Schleyer, and J.A. Pople, *Ab initio* molecular orbital theory, first ed., Wiley, New York, 1986

113. E.G. Lewars, Computational chemistry: introduction to the theory and applications of molecular and quantum mechanics, second ed., Springer, 2011.

114. K.I. Ramachandran, G. Deepa, and K. Namboori, Computational chemistry and molecular modeling: principles and applications, Springer, 2008.

115. J. Muscat, A. Wander, N.M. Harrison, On the prediction of band gaps from hybrid functional theory, Chemical Physics Letters 342(2001)397-401. doi:10.1016/S0009-2614(01)00616-9

116. J.Heyd, G. Scuseria, Efficient hybrid density functional calculations in solids: assessment of the Heyd-Scuseria-Ernzerhof screened Coulomb hybrid functional. Journal of Chemical Physics 121(2004)1187-1192. doi:10.1063/1.1760074

117. C.W. Bauschlicher, A comparison of the accuracy of different functional. Chemical Physics Letters 246 (1995) 40-44. doi: 10.1016/0009-2614(95)01089-R

118. S. Tomic, B. Montanari, N.M. Harrison, The group III–V's semiconductor energy gaps predicted using the B3LYP hybrid functional. Physica E 40(2008) 2125-2127. doi:10.1016/j.physe.2007.10.022

119. S. Tomic, N.M. Harrison, Electronic structure of III-V's semiconductors from B3LYP and PBE0 functionals. AIP Conference Proceedings 65 (2010) 65-66. doi: 10.1063/1.3295556

120. F.D. Proft, P. Geerlings, Calculation of ionization energies, electron affinities, electronegativities, and hardnesses using density functional methods. Journal of Chemical Physics 106(1997) 3270-3279. doi:10.1063/1.473796

121. M.W. Wong, Vibrational frequency prediction using density functional theory. Chemical Physics Letters 256(1996)391-399. doi:10.1016/0009-2614(96)00483-6.

122. M.J. Frisch et al. Gaussian 03, Revision C. 02, Gaussian Inc., Wallingford CT, (2003)

123. M.J. Frisch et al. Gaussian 09, Revision A.1, Gaussian Inc., Wallingford CT, (2009)

124. P.J. Hay and W.R. Wadt, Ab initio effective core potentials for molecular calculations. Potentials for the transition metal atoms Sc to Hg. Journal of Chemical Physics 82 (1985) 270-283. doi: 10.1063/1.448799

125. A.D. Mclean and G.S. Chandler, Contracted Gaussian basis sets for molecular calculations. I. Second row atoms, Z=11-18. Journal of Chemical Physics 72 (1980) 56395648. doi: 10.1063/1.438980

126. S.F. Boys and F. Bernardi, The calculation of small molecular interactions by the differences of separate total energies. Some procedures with reduced errors. Molecular Physics. 19 (1970) 553-566. doi: 10.1080/00268977000101561

127. F.B. van Dujineveldt, J.G.C.M. van Dujineveldt-van de Rijdt, and J.H. van Lenthe, State of the art in counterpoise theory. Chemical Reviews 94 (1994) 1873-1885. doi: 10.1021/cr00031a007

128. S. Simon, M. Duran, and J.J. Dannenberg, How does basis set superposition error change the potential surfaces for hydrogen-bonded dimers? Journal of Chemical Physics 105 (1996) 11024-11031. doi: 10.1063/1/472902

129. K. Adhikari and A.K. Ray, On the existence and stability of double-walled armchair silicon carbide nanotubes. Solid State Communications 151 (2001) 430-435. doi: 10.1016/j.ssc.2011.01.004

130. K. Adhikari and A.K. Ray, Cluster modeling of three types of double-walled armchair silicon carbide nanotubes. European Physical Journal D 64 (2011) 353-363. doi: 10.1140/epjd/e2011-20280-3

131. Y.H. Tang, L.Z. Pei, Y.W. Chen, and C. Guo, Self-assembled silicon nanotubes under supercritically hydrothermal conditions. Physical Review Letters 95 (2005) 116102. doi: 10.1103/PhysRevLett.95.116102

132. NBO Version 3.1, E. D. Glendening, A.E. Reed, J. E. Carpenter, F. Weinhold.

133. J. Sadoc and R. Mosseri, Geometrical Frustration, Cambridge University Press, Cambridge, 2006.

134. E. Roduner, Nanoscopic Materials: Size-Dependent Phenomena, The Royal Society of Chemistry, Cambridge, 2006.

135. C.S. Smith, Piezoresistance effect in germanium and silicon. Physical Review 94 (1954) 42-49. doi: 10.1103/PhysRev.94.42

136. K.Y. Kim, T.H. Shin, S.J. Han, and H. Kang, Identification of the precursor state in the initial stages of Si(111)-(7X7) oxidation. Physical Review Letters 82 (1999) 1329-1332. doi: 10.1103/PhysRevLett.82.1329

137. L. Zhong and F. Shimura, Hydrogen enhanced out-diffusion of oxygen in Czochralski silicon. Journal of Applied Physics 73 (1993) 707-710. doi: 10.1063/1.353326

138. V.P. Markevich and M. Suezawa, Hydrogen-oxygen interaction in silicon at around 50°C. Journal of Applied Physics 83 (1998) 2988-2993. doi: 10.1063/1.367054

139. J. Lu and S. Nagase, Structural and electronic properties of metal-encapsulated silicon clusters in a large size range. Physical Review Letters 90 (2003) 115506. doi: 10.1103/PhysRevLett.90.115506

140. A.K. Singh, V. Kumar, T.M. Briere, and Y. Kawazoe, Cluster assembled metal encapsulated thin nanotubes of silicon. Nano Letters 2 (2002) 1243-1248. doi: 10.1021/nl0257891

BIOGRAPHICAL INFORMATION

Haoliang Chen received his bachelor's degree on automation and control from Hefei University of Technology in China. He received his master's degree in physics from Texas A&M University at Commerce. His research during his master's studies was on telerobotics. After receiving his master's degree he joined the University of Texas at Arlington (UTA) in the fall of 2009. His current research interest is in theoretical and computational condensed matter physics. In the department of physics at UTA, he worked under the supervision of Dr. Asok K Ray.